ISRES Publishing

The Eurasia Proceedings of Science, Technology, Engineering & Mathematics

EPSTEM

VOLUME 16 IConTES CONFERENCE

ISSN: 2602-3199

ISBN: 978-605-71165-5-0

IConTES 2021: International Conference on Technology, Engineering and Science (IConTES)
November 04 - 07, 2021
Antalya, Turkey

Edited by: Mehmet Ozaslan (Chair), Gaziantep University, Turkey

The Eurasia Proceedings of
Science, Technology, Engineering & Mathematics (EPSTEM)
ISSN: 2602-3199

IConTES 2021 DECEMBER

Volume 16, Pages 1-247 (December 2021)

The Eurasia Proceedings of Science, Technology, Engineering & Mathematics (EPSTEM)

e-ISSN: 2602-3199

Address: Istanbul C. Cengaver S. No 2 Karatay/Konya/TURKEY

Website: www.isres.org

Contact: isrespublishing@gmail.com

Conference: IConTES 2021: International Conference on Technology, Engineering and Science (IConTES)
Conference website: https://www.2021.icontes.net
Dates: November 04 – 07, 2021
Location: Antalya, Turkey
Edited by: Mehmet Ozaslan

About Editor(s)
Prof Dr. Mehmet Ozaslan
Department of Biology, Gaziantep University, Turkey
Website: http://mehmetozaslan.com/
Email: ozaslanmd@gantep.edu.tr

Language Editor(s)
Assoc. Prof. Dr. Kagan Buyukkarci
Department of English Language Education, Suleyman Demirel University, Turkey
Email: kaganbuyukkarci@sdu.edu.tr

ORGANIZING COMMITTEE

Editorial Policies

ISRES Publishing follows the steps below in the procedings book publishing process.
In the first stage, the papers sent to the conferences organized by ISRES are subject to editorial oversight. In the second stage, the papers that pass the first step are reviewed by at least two international field experts in the conference committee in terms of suitability for the content and subject area. In the third stage, it is reviewed by at least one member of the organizing committee

ISSN: 2602-3199

for the suitability of references. In the fourth step, the language editor reviews the language for clarity.

Review Process

Abstracts and full-text reports uploaded to the conference system undergo a review procedure. Authors will be notified of the application results in three weeks. Submitted abstracts will be evaluated on the basis of abstracts/proposals. The conference system allows you to submit the full text if your abstract is accepted. Please upload the abstract of your article to the conference system and wait for the results of the evaluation. If your abstract is accepted, you can upload your full text. Your full text will then be sent to at least two reviewers for review. **The conference has a double-blind peer-review process.** Any paper submitted for the conference is reviewed by at least two international reviewers with expertise in the relevant subject area. Based on the reviewers' comments, papers are accepted, rejected or accepted with revision. If the comments are not addressed well in the improved paper, then the paper is sent back to the authors to make further revisions. The accepted papers are formatted by the conference for publication in the proceedings.

Aims & Scope

Engineering, technology and basic sciences are closely related fields. Developments and innovations in one of them affect the others. Therefore, **the focus of the conference** is on studies related to these three fields. Studies in the fields of engineering, technology and basic science are accepted to the conference even if they are not associated with other fields. The conference committee thinks that a study in only one field (for example, mathematics, physics, etc.) will contribute to other fields (for example, engineering, technology, etc.) in future studies, even if it is not associated with the presentation at the conference. In line with this perspective, studies in the following fields are accepted to the conference: *Biology, Chemistry, Engineering, Mathematics, Physics and Technology*.
The aim of the conference is to bring together researchers and administrators from different countries, and to discuss theoretical and practical issues in all fields of Engineering, Technology and Basic Sciences.

Articles: 1-33

CONTENTS

The Eurasia Proceedings of
Science, Technology, Engineering & Mathematics (EPSTEM)
ISSN: 2602-3199

The Eurasia Proceedings of
Science, Technology, Engineering & Mathematics (EPSTEM)
ISSN: 2602-3199

The Eurasia Proceedings of
Science, Technology, Engineering & Mathematics (EPSTEM)
ISSN: 2602-3199

The New Designed Mechanical Systems and Protypes for Z-Scan and Nonlinear Measurements

Pages: 240-247

Ferit ARTKIN

The Eurasia Proceedings of Science, Technology, Engineering & Mathematics (EPSTEM)
ISSN: 2602-3199

The Eurasia Proceedings of Science, Technology, Engineering & Mathematics (EPSTEM), 2021

Volume 16, Pages 1-7

IConTES 2021: International Conference on Technology, Engineering and Science

DFT Analysis of Ions Conductivity of Proline in Certain Solvents: Calculation of Association Parameters

Fanar M. AL-HEALY
University of Mosul

Shaymaa H. ABDULRAHMAN
University of Mosul

Abstract: Proline (Pro.) is non-essential amino acid, and it is from the amino acids which the human's body can synthesize it, from L-glutamate. It is studied in the temp. range from 288.16 to 313.16 K at 5 K by conductivities in H_2O, and methanol. The Kohlrausch equations was used to find out pattern of electrolyte, the curve indicate pro. was weakly associated in various temperatures and solvents. The Lee-Wheaton equation was us to calculation the Equivalent conductance at infinite dilution (Λo), The association constant (Ka) and distance parameter (R). The values of (Λo), (Ka), and (R) differ from solvent to another depending on the interactions in solution. The molecular modeling, geometry optimization and characterization of pro. has been performed using semi empirical method, and all theoretical parameters was calculated by using Austin Model 1 (AM1), and used density functional theory (DFT) B3LYP method by using 6-311G bases set.

Keywords: Proline, Kohlrausch equations, Lee-Wheaton equation, AM1, DFT

Introduction

Proline, which is an amino acid, in fact is one of the twenty amino acids found most frequently in animal proteins. Only the L version (L-prol.) may be found in mammalian proteins. It is not an essential amino acid because it can be produced in the human body. İt is one of the most popular in the cellular milieu, accounting for roughly 25% of residues in collagen, the primary protein in the extracellular matrix, along with hydroxyproline (Liu et. al., 2012).

Using a literature search, we discovered numerous previously published methods for determining pro. in biological fluids. Pro. in human serum detection using a robust LC-MS/MS which is a classic method for determining it in human serum (Su et. al., 2015). Other methods were developed employing Fluorometric measurement of pro. in honey by high-performance liquid chromatography after pre-column derivatization with 7-fluoro-4-nitrobenzo-2-oxa-1,3-diazole (NBD-F), with a detection limit of 3.00 mg kg1 and recoveries of more than 90%. (Li et. al., 2015). Amino acid and antioxidant installation of three medicinal plants from the uttarakhand himalayas (Pithoragarh). Also the simultaneous analysis of 26 physiological amino acids in plasma along with total cysteine and homocysteine by high-performance liquid chromatography (HPLC) employing 6-aminoquinolyl-N-hydroxysuccinimidyl carbamate (AQC) as precolumn derivatizing reagent (Gaurav et. al., 2014). The equivalent conductivities of pro-Mn (II) Complex in H_2O, MeOH, and mixes of MeOH and water at proportions from hundreds of 10, 20, 30, 40, and 50 of MeOH were examined at 310.16K in the temperature range of 288.16 to 313.16 K at 5 K intervals (Al-Healy et. al., 2021). LiClO4 in propylenecarbonate is a nonassociated electrolyte, according to the Lee-Wheaton equation of conductivity. The results of conductometric examinations of solutions of numerous 1-1 electrolytes in propylene carbonate at temperatures ranging from 298 to 398 K are reported to account for the dynamics of ionic solvation (Chernozhak, et. al., 2016)

The electrical conductivities of tyrosine in aqueous solutions was measured by using Kohlrausch equation and Lee-Wheaton equation at 310.16K then They prepared complexes of tyrosine with Co(II) , Mn(II) , Ni(II) , Fe(II) , to form $[Ni(tyr)_3]Cl_2$, $[Co(tyr)_3]Cl_2$, $[Fe(tyr)_3]Cl_2$, $[Mn(tyr)_3]Cl_2$ this complexes are measured using in the temperature range from (288.16–313.16K) from the conductivity result they calculation of the thermodynamic quantities (ΔH°, ΔG°, ΔS°) (Al-Healy et. al., 2019). The electrical conductivities of glutamic acid in the water, MeOH, and EtOH are measured at 310.16 K and the main interest is to find an accurate yet efficient solvation model for semiempirical quantum-mechanical and Density Function Theory (DFT) methods applicable to amino acids (glutamic acid) in the context of computer-aided conductivity studying (Abdulrahmana et. al., 2021).

Kohlrausch equations was used to discover types of electrolyte through plot the relation between equivalent conductivity against the square root of molar concentration of pro. The plot indicate that amino acid was weakly associated in water and MeOH (Al-Healy et. al., 2021). In the domains of chemical, biological, and material sciences, computational chemistry is becoming increasingly relevant. (Mourik, et. al., 2012). It aids in the knowledge of molecular structure in organic chemistry, providing insight into reaction pathways and chemical reactions through the assessment of geometrical features of molecules. (Art et. al., 2016; Miriding et. al., 2017).

Conceptual Density Functional Theory (DFT) or Chemical Reactivity Theory (as it is also known) is a strong tool for predicting, analysing, and interpreting the outcome of chemical interactions. In this study, a series of molecular descriptors and attributes of their optimal geometries were calculated using density functional theory (DFT) and thermodynamics modelling (Dehdab et al, 2016). Theoretical studies provide insights into this kind of study in conductivity and have been making a great contribution to support experimental results. Comparing experimental results and theoretical studies indicates that some density functional theory calculations (DFT) consistently underestimate band gaps (Lu et al, 2019).

Experimental Methodology

Computational Details

All calculations were done with the Gaussian '09 program package and semi-empirical methods. Semi-empirical approaches are based on what is commonly referred to as empirical methods. After energy minimization and geometry optimization, the DFT approach was utilized with the hybrid B3LYP model (Becke's three-parameter hybrid exchange functional with the Lee-Yang–Parr correlation functional) and basis set 6-311G for equilibrium geometry at ground state in water and MeOH. The properties of the thermodynamic, electronic, and other descriptors were calculated.

Expermental Details

For measuring the conductance of the fluids, a general approach was utilized in which the conductivity cell was cleaned, dried, weighed empty, and kept at a constant temperature (0.1oC) using a water circulation ultra thermostat. The conductivity of the sample was observed using a WTW Inolab 740 computerized conductometer after a particular amount of solution was introduced into the conductivity cell. A 1ml syringe was used to inject another known volume of fluid, and the measurement was repeated. By weighing the amount for each one, approximately (15) additions have been made.

Results and Discussion

The relationship between equivalent conductivity and the square root of the molar concentration of pro. was shown using Kohlrausch equations to identify types of electrolytes. The amino acid was poorly linked in water and MeOH, according to the plot which had from the results. The pro. solution promised symmetrical electrolytes of type (1:1) if the positive ion is denoted by (M+) and negative ion (X-) when using the equation for these solution can be explaining as follows (Al-Healy et. al., 2019).

$$M + aq. + X\text{-}aq \rightarrow . Ka \rightarrow (M.aq + n\ X)$$

Ka: association constant K

Figure (1) demonstrates this behavior

Table 1. Molar concentration (M) and Equivalent conductance of Proline in water at 310.16K

Conc.*10^{-7} M	√Conc. *10^{3} M	Λ (Ohm^{-1}. $equive^{-1}$ .cm^{2})
5.2573	0.6609	142.6582
10.2259	0.9096	97.79028
14.9181	1.1019	83.79053
19.9200	1.2654	75.30096
24.6343	1.4150	71.03902
29.6084	1.5435	67.54828
34.2994	1.6665	58.30994
39.1146	1.7941	51.13183
43.6948	1.8976	46.64819
48.2334	1.9816	45.77197

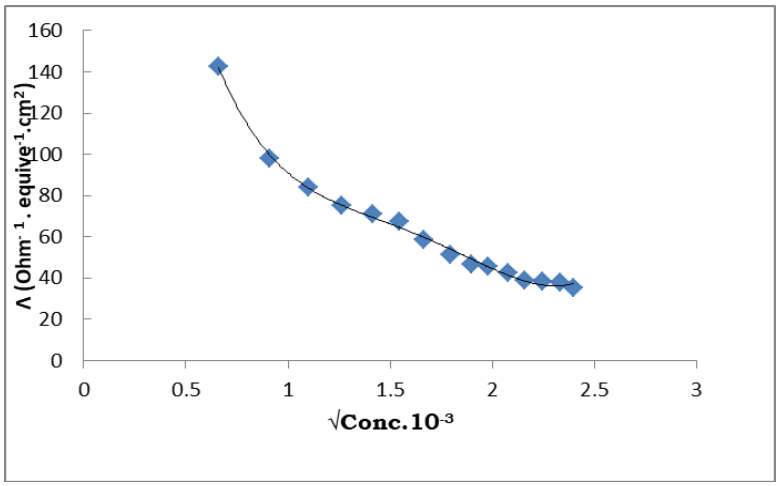

Figure 1. Equivalent conductance of Proline in water at 310.16K

Table 2. Molar concentration (M) and Equivalent conductance of Proline in methanol at 310.16K

Conc.*10^{-7} M	√Conc. *10^{3} M	Λ (Ohm^{-1}. $equive^{-1}$ .cm^{2})
5.3767	0.6609	92.9926
10.5242	0.9096	47.5091
15.2765	1.1019	32.7300
20.0511	1.2654	24.9362
24.8952	1.4150	20.0841
29.8601	1.5435	16.7447
34.6992	1.6665	15.4051
39.2040	1.7941	14.4095
44.4990	1.8976	14.0208
48.6850	1.9816	12.9178

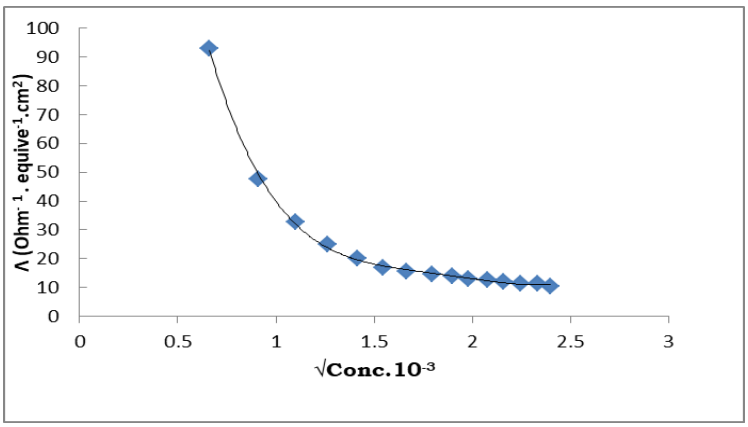

Figure 2. Equivalent conductance of Proline in methanol at 310.16K

The Lee-Wheaton equation is applicable to complete analysis of any sample symmetrical and asymmetrical electrolyte at different temperatures. the intent used is then to calculated the equivalent concentration for pro. solution using a special calculation program to extract the equivalent continuity after entering the conductivity information, physical parameter, temperature and weights of the additives, as it was shown that amino acid under study the behavior of the weak electrolytes was demonstrated by the relationship between the square root of the different conc. of the pro. solution versus the equivalent continuation calculated through the calculation program(Al-Healy et. al., 2019). Figure (1) demonstrates this behavior.

Tables (3) show the results of the analysis complexes at different temperatures. where each table show the association constant (KA) and the equivalent conductance (Λ), the(R) values (distance parameter) and the best fit data standard deviation σs(Λ).

Table 3. Ka, Λ, R and σΛ of Proline in water and methanol

Solvents	Ka	Λ	R(A°)	бΛ
Water	10.6	379.6	$1*10^{-6}$	5.358
Methanol	49.73	110.012	$1*10^{-6}$	16.309

Optimizing of Molecular Geometry

The goal of geome optimization was to discover the optimal atomic arrangement that would make the molecule more stable. Topo-geometrical properties of the pro. molecule, such as bond lengths, bond angles, and dihedral angles, were optimized using semi-empirical approaches and subsequently DFT. Figure 3 shows the optimized structures of Iron bimetallic complexes with atom and number labeling.

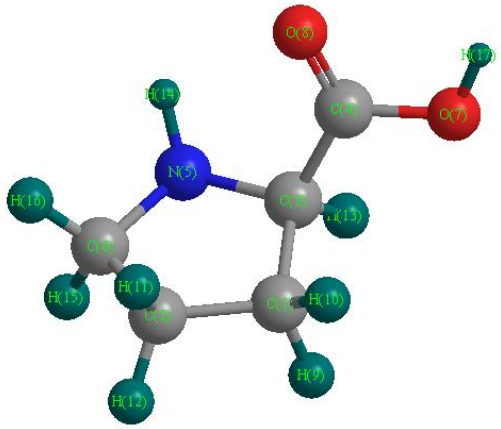

Figure 3. 3D-structure of Proline

Table 4: The 3D structures of Proline molecule in water and methanol by different approach

Type of Approach	Water	Methanol
AM1	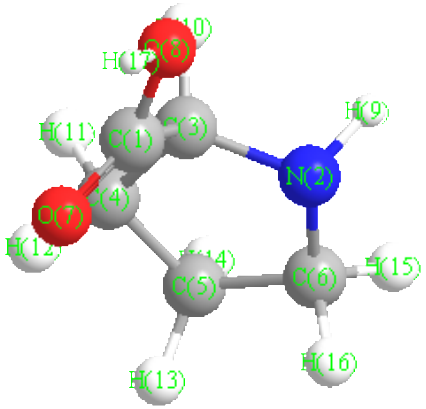	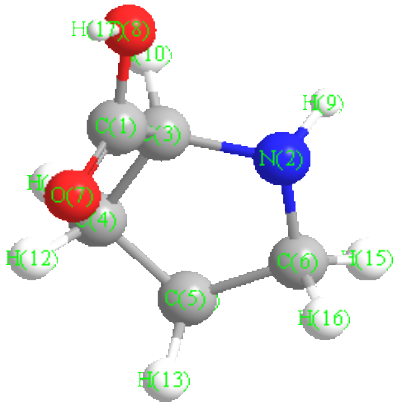
	Finished Energy = -98.19 Kcal/Mol	Finished Energy = -103.92 Kcal/Mol

DFT (6-311G)	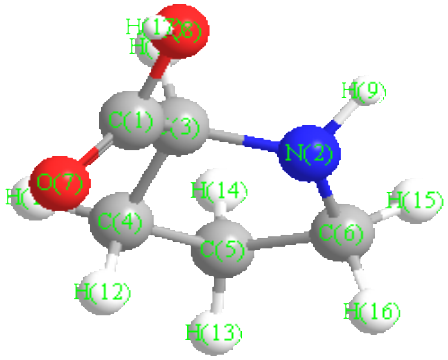	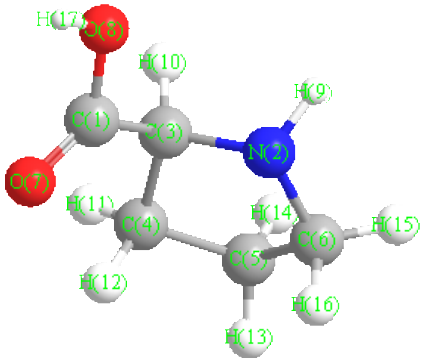
	Finished Energy = -250171.43 Kcal/Mol	Finished Energy = -250119.79 Kcal/Mol

Table 5 shows the HOMO and LUMO orbital energies (in eV), as well as other descriptors. We formerly prepared many descriptors that tie the results acquired by HOMO and LUMO calculations to the experimental data.

Table 5: Parameters of Proline molecule in water and methanol were calculated by DFT method

Parameters	Water	Methanol
HOMO (eV)	-0.37843	-0.3648
LUMO (eV)	0.14339	0.1470
Gap (eV)	-0.52182	-0.5119
RMS Force: Kcal/Mole	0.0017	0.0035
SCF Energy: Kcal/Mole	-250290.11	-250288.96
Connolly Accessible Area: $(A°)^2$	277.449	272.687
Connolly Molecular Area: $(A°)^2$	126.886	123.486
Connolly Solvent Excluded Volume: $(A°)^3$	100.075	98.926
Dipole: Debye	1.8993	2.3779
Molecular Volume: bohr**3/mol	1025.511	915.473
Entropy: Cal/Mol-Kelvin	80.699	77.266
Thermodynamic Energy: Kcal/Mol	100.48	101.782
Zero-Point Energy: Kcal/Mol	96.889564	98.2333

The values of HOMO and LUMO were in a small deferent between them in MeOH and water. From the energies values the molecule of pro. is stable in the water than the MeOH, and the volume of space bounded by the solvent accessible molecular surface, which is Connolly Solvent Excluded Volume that refer to the volume in the water bigger than in the MeOH, in addition the Molecular Volume have the same indicators. Also the entropy value (S) in water more than in MeOH, which shows that the pro. molecule has more freedom of movement in water than MeOH and this is confirmed by the practical results through the value of the equivalent conduction in water is higher than in MeOH.

Conclusion

The calculations were made on the most stable conformer, after geometry optimizations, then compare the theoretical result with the experimental results which is in a similar evaluation that the conductivity of pro. in water more than MeOH. The molecular volume calculated by DFT analysis was big in the MeOH which has less mobility, which leads to a lower conductivity due to the lack of freedom of movement in the solution, and the reason is also due to the fact that the polarity of water and its dielectric constant is higher than MeOH.

Recommendations

The lee-wheaton equation is very important, it be used to determination of any ionic compound at very low concentration, with any solvent at different temperatures and give information about association constant KA, equivalent conductivity at infinity dilution $\Lambda°$ and the distance parameter R, which is very important constant in Thermodynamic.

Acknowledgements

This work was financially supported by the University of Mosul, College of Science, Department of Chemistry.

Scientific Ethics Declaration

The authors declare that the scientific ethical and legal responsibility of this article published in EPSTEM journal belongs to the authors.

References

Abdulrahman Sh. H. & Khalil R.A.(2020), S*tatistical treatment for study the relationship between the chemical structure and activity of some biologically active isatin derivatives using quantum mechanics methods*, [Ph.D Thesisi]. University of Mosul.

Abdulrahman, S. H., & Alhealy, F. M. (2021). Electrical Conductance And Theoretical Study Of Glutamic Acid In Different Solvents at 310.16 k. *Egyptian Journal of Chemistry*, *64*(8), 4359-4367.

Al-Healy, F. M., Abdulrahman, S. H., & Mahmoud, A. R. (2021, May). Conductometric Study of Proline-Mn (II) Complex in Some Solvents at Various Temperatures, with Computational Factors Calculation. In *Journal of Physics: Conference Series* 1879(2), 022068. IOP Publishing.

Al-Healy, F. M. & Hameed, Y. O. (2019). Electrochemical and thermodinamic study of tyrosine and its complexes in aqueous solution by conductivity measurement. *The Eurasia Proceedings of Science Technology Engineering and Mathematics*, *7*, 48-57.

Art, D. B., Mark, A. W. & Jeremy, R. G. (2016), Density functional teory-based pKa prediction in application to large, fexible organic molecules with diverse functional groups. *J. Chem. Teory Comput. 12*, 6001–6019.

Chernozhak, T. Kalugin,O., (2016), Conductivity and interparticle interactions in the solutions of 1-1 electrolytes in propylene carbonate in the wide range of temperatures. *Chemistry & Chemical Technologe ,10*.

Dehdab, M., Shahraki, M., & Habibi-Khorassani, S. M. (2016). Theoretical study of inhibition efficiencies of some amino acids on corrosion of carbon steel in acidic media: green corrosion inhibitors. *Amino acids*, *48*(1), 291-306. 10.1007/s00726-015-2090-2.

Sharma, G., Attri, S. V., Behra, B., Bhisikar, S., Kumar, P., Tageja, M., ... & Singhi, S. (2014). Analysis of 26 amino acids in human plasma by HPLC using AQC as derivatizing agent and its application in metabolic laboratory. *Amino Acids*, *46*(5), 1253-1263.

Liu, W., Glunde, K., Bhujwalla, Z. M., Raman, V., Sharma, A., & Phang, J. M. (2012). Proline oxidase promotes tumor cell survival in hypoxic tumor microenvironments. *Cancer research*, *72*(14), 3677-3686. doi: 10.1158/0008-5472.CAN-12-0080.

Lu, J., Meng, D., Li, F., Guo, M., & Li, Y. (2020). Theoretical study of the structure and ionization potentials of proline. *Russian Journal of Physical Chemistry A*, *94*(7), 1427-1432.

Mutailipu, M., Xie, Z., Su, X., Zhang, M., Wang, Y., Yang, Z., ... & Pan, S. (2017). Chemical cosubstitution-oriented design of rare-earth borates as potential ultraviolet nonlinear optical materials. *Journal of the American Chemical Society*, *139*(50), 18397-18405.

Van Mourik, T., Bühl, M., & Gaigeot, M. P. (2014). Density functional theory across chemistry, physics and biology. *Philosophical Transactions of the Royal Society A: Mathematical, Physical and Engineering Sciences*, *372*(2011), 20120488.

Liang, S., Sanchez-Espiridion, B., Xie, H., Ma, J., Wu, X., & Liang, D. (2015). Determination of proline in human serum by a robust LC- MS/MS method: application to identification of human metabolites as candidate biomarkers for esophageal cancer early detection and risk stratification. *Biomedical Chromatography*, *29*(4), 570-577.

Li, Y., Zhou, J., Xue, X., Wu, L., Chen, L., Zhang, J., & Yang, S. (2015). Fluorometric determination of proline in honey by high-performance liquid chromatography after pre-column derivatization with 7-fluoro-4-nitrobenzo-2-oxa-1, 3-diazole (NBD-F). *Analytical Methods*, *7*(18), 7625-7630.

Author Information

Fanar M. AL-HEALY
Department of Chemistry
College of Science, Mosul University
Mosul/Iraq
Contact E-mail:*Fm.alhealy@gmail.com*

Shaymaa H. ABDULRAHMAN
Department of Chemistry
College of Science,Mosul University
Mosul/Iraq

To cite this article:

Al-Healy, F. & Abdulrahman, S.H. (2021). DFT analysis of ions conductivity of proline in certain solvents: Calculation of association parameters. *The Eurasia Proceedings of Science, Technology, Engineering & Mathematics (EPSTEM), 16*, 1-9.

The Eurasia Proceedings of Science, Technology, Engineering & Mathematics (EPSTEM)
ISSN: 2602-3199

The Eurasia Proceedings of Science, Technology, Engineering & Mathematics (EPSTEM), 2021

Volume 16, Pages 8-13

IConTES 2021: International Conference on Technology, Engineering and Science

Effect of Alloying on the Microstructure and Strength of the Ni Bronzes

Ibrahim CELIKYUREK
Eskişehir Osmangazi University

Bedri BAKSAN
Eskişehir Osmangazi University

Adem TASDEMIR
Eskişehir Osmangazi University

Abstract: In this study, Al was added to the Cu15Ni8Sn Ni-bronze alloy. The effects of the added amount of Al on the microstructure and strength of the alloy were investigated. As an approach, the Sn element has been replaced by Al. The element Al was added at 2, 4, 6, and 8 wt. %. Alloys were melted in a graphite crucible by induction melting and poured into a graphite mold. No heat treatment was applied to the cast alloys. The microstructure of the alloys was studied under a light optical microscope (LOM) and scanning electron microscope (SEM). Mechanical characterizations were made by hardness measurement and tensile tests. Metallographic studies showed that the microstructure was not changed with the amount of Al added. Chemical composition changes in the phases were reflected in the mechanical properties. It was determined that the composition with the highest hardness and strength among the alloys was the composition containing 15Ni, 4Sn, and 4Al wt.%. The alloy with the highest ductility and toughness is Cu15Ni8Al.

Keywords: Ni-bronze, High strength, Alloying, Hardness

Introduction

Copper and copper alloys, which have the best conductivity after silver, are the oldest metals used by humanity. Copper can form solid solutions with many elements, so many copper alloys are homogeneous. Copper alloys attract the attention of researchers due to their very good properties such as electrical and thermal conductivity, corrosion resistance, strength, ductility and wear resistance (Yin et al. 2011).

It is known that the change in the microstructure has a great effect on the mechanical properties of the alloy. Microstructure also primarily depends on the chemical composition. In Cu-Ni-Sn alloys that can decompose spinodally, the mechanical properties can also be changed by microstructure (İlangovan et al. 2016, Zhao et al. 1998).

Cu15Ni8Sn alloy, commercially known as C72900, is an alloy that hardens spinodally and exhibits very good bearing properties in dry and lubricated environments. These alloys are widely used as bearing materials especially in aviation and mining applications due to their very good properties. (Singh et al. 2007). In addition, due to its high strength and electrical conductivity, it also provides opportunities for use in the machinery and electrical/electronic industries (Peng et al. 207, Hoang et al. 2018).

The properties of Cu-Ni-Sn alloys can also be changed by heat treatment. These alloys are alloys in which the aging process can be applied. (Ilangovan et al. 2016, Peng et al. 2017, Sato et al. 1988, Lopez et al. 1999). There are also studies on the use of these alloys as coatings (Huia et al. 2010, Hunnik et al. 1992).

The effects of alloying elements are investigated to improve the mechanical and physical properties of these alloys. Luo et al. (2019) reported that by adding 0.5 Si to Cu-Ni-Sn alloy with low tin content, the strength of the alloy decreased slightly while its ductility increased. On the other hand, Lei et al. (2013) studied the effects of Aluminum on the microstructure and properties of Cu-Ni-Si alloys. A slight increase in yield and tensile strengths was achieved with the addition of a small amount of Al.

When the studies in the literature are examined, no study has been found on how the properties of Cu-Ni-Sn spinodal alloys change with the systematic addition of a second alloying element. In this study, the effects of Al added by systematically increasing amounts of Al to Cu15Ni8Sn spinodal alloy on the microstructure, hardness and tensile strength of the alloy were investigated. As an approximation, Al has been added instead of Sn element.

Method

Elements with the purity of 99.9%Cu, 99.65%Ni, 99.7%Al, 99.8%Sn were used in the preparation of alloys. The elements prepared according to the alloy composition were melted in a graphite crucible by an induction melting furnace. After melting, the alloys were poured into a graphite mold and allowed to cool in the air. Thus, 10mm diameter rods were produced.

Commercial Cu15Ni8Sn alloy was taken as the basis for alloy selection. In this alloy, Aluminum element has been systematically added instead of Tin at increasing rates. For this purpose, Cu15Ni2Al6Sn, Cu15Ni4Al4Sn, Cu15Ni6Al2Sn, and Cu15Ni8Al alloys were cast. No treatment (thermal/mechanical) was applied to the alloys after casting.

Sections were taken from the cast alloys and the surfaces were sanded and polished with a 3-micron diamond paste. The microstructures of the alloys were studied under optical light microscope (LOM) and scanning electron microscope (SEM).

The hardness of the alloys was measured by Vickers hardness measurement by applying 0.5kgf load for 15 seconds. The tensile test samples were prepared from the bars by machining. Tensile tests were carried out in a universal testing device at room temperature and with a jaw speed of 5mmmin^{-1}. The effects of the change in alloy composition on alloy hardness, ductility, tensile strength, and toughness were revealed.

Results and Discussion

The optical microstructure images of the alloys at low magnifications are given in Figure 1. From the microstructure images, Cu15Ni8Sn alloy has a microstructure consisting of long dendrites. Dendrites are randomly oriented. It is considered that this structure is a result of rapid cooling as a result of casting into a cold graphite mold. There is no significant change in the microstructure of the alloys with Al added either. It can be said that the dendrites are shortened and expanded with the addition of Al. In the alloy containing no Tin (Fig. 1e), the detrites were formed in an even longer form.

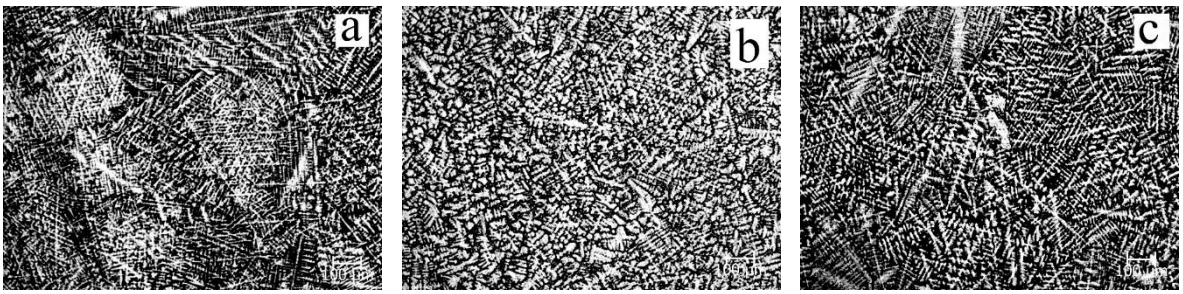

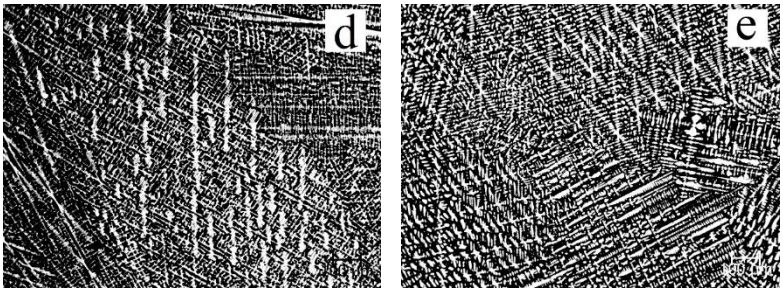

Figure 1. The light optical microstructure of the alloys at low magnification. a) Cu15Ni8Sn, b) Cu15Ni2Al6Sn, c) Cu15Ni4Al4Sn, d) Cu15Ni6Al2Sn, and e) Cu15Ni8Al

Microstructure images at high magnifications (Fig. 2) show that the structures usually contain 3 phases. It is seen in Figure 2a that the phase, which appears as a precipitate in the form of very small grains, grows with the addition of Al. The Cu15Ni8Al alloy, which does not contain any Tin, is seen as two-phase (Figure 2e)

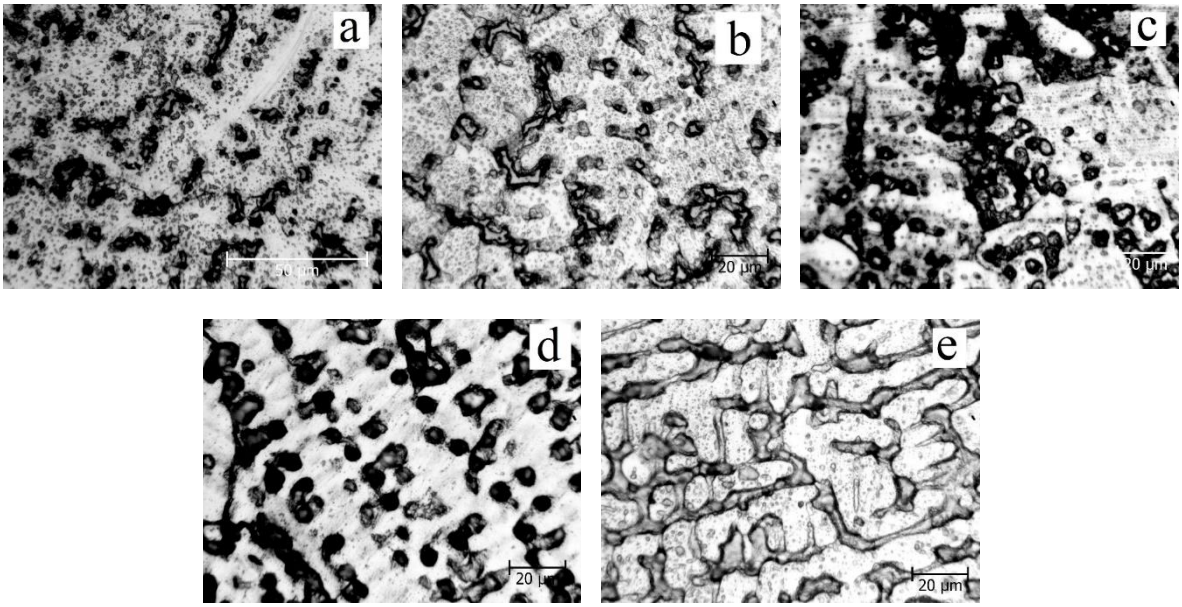

Figure 2. The light optical microstructure of the alloys at high magnification. a) Cu15Ni8Sn, b) Cu15Ni2Al6Sn, c) Cu15Ni4Al4Sn, d) Cu15Ni6Al2Sn, and e) Cu15Ni8Al

In Figure 3, SEM microstructure images of alloys and SEM energy dispersive spectroscopy (EDS) composition analyzes taken from certain points are given. From the general composition analyzes made, it is seen that the alloys have compositions very close to their nominal compositions. The Cu15Ni8Sn alloy, determined as the base alloy, contains the tin-rich-phase and the Cu-Ni matrix phases. The Sn content of the matrix phase is much less than that of the precipitate particles. The tin content increases at the boundary between the matrix phase and the precipitate phase (Figure 3a). With the addition of Al to the alloy, Aluminum also entered the precipitate phase, and while the Tin ratio in this phase decreased, the Aluminum and Nickel ratios increased (Figure 3b,c,d).

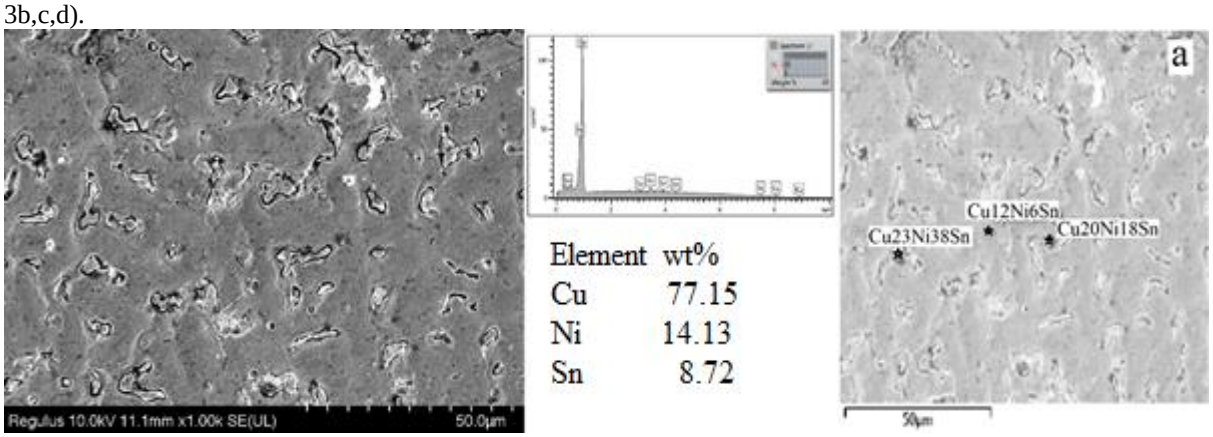

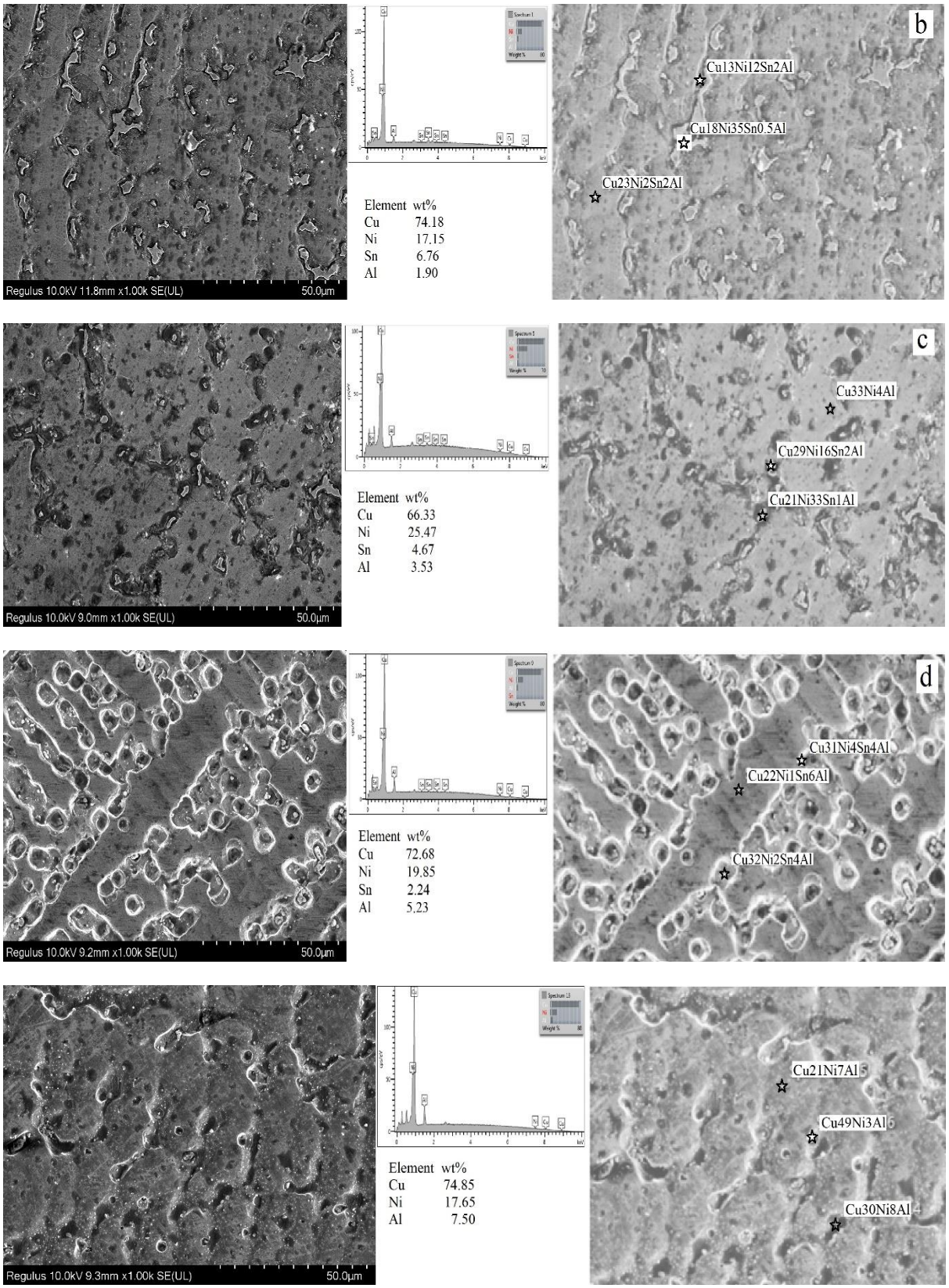

Figure 3 shows the tensile curves of cast alloys. It is clearly seen from the curves that Cu15Ni4Al4Sn alloy has the highest strength, on the other hand, Cu15Ni8Al alloy exhibits the highest ductility and toughness.

In the tin-free alloy, the precipitate phase is in the nickel-rich Cu-Ni composition (Figure 3e). Tin content in the matrix phase decreased with the addition of Al. No Tin was found in the matrix phase of the alloy where the Tin and Aluminum contents were equal. This composition is the composition with the highest hardness and strength.

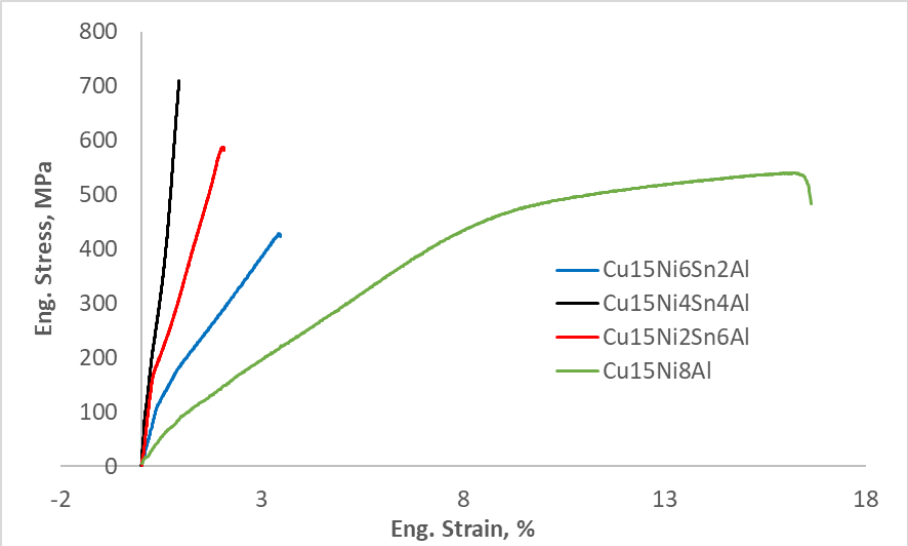

Figure 4. Tensile diagrams of the alloys.

Table 1 summarizes the mechanical properties of cast alloys. Al-containing alloys have higher hardness than Cu15Ni8Sn alloy. When the Al and Sn content of the alloy are equal, the hardness and strength take the maximum value. If the amount of Al is more than Sn, there is a decrease in strength but an increase in ductility.

Table 1. Mechanical properties of the alloys

Alloy	Hardness, HV0.5	Ductility, %	Tensile Strength, MPa	Toughness, $Nmmmm^{-3}$
Cu15Ni8Sn	140			
Cu15Ni2Al6Sn	214	3.46	424	8.7
Cu15Ni4Al4Sn	310	0.94	711	3.13
Cu15Ni6Al2Sn	229	2.06	581	6.83
Cu15Ni8Al	195	16.63	541	62.9

Conclusion

The cast microstructure of the Cu15Ni8Sn alloy chosen as the base alloy has a dendritic structure as a result of rapid cooling. Adding aluminum to the alloy at increasing rates did not cause a significant change in the casting microstructure of the alloy. While the change in the composition did not cause a change in the phase structure of the alloys, it created differentiation in the composition of the phases, which was reflected in the mechanical properties of the alloy. The highest hardness and strength were observed in the composition containing 4% Al and Sn. In this composition, the composition of the precipitate particles is similar to other alloys, while the matrix phase does not contain any Tin. In the alloy containing no Tin, the composition of the precipitate and matrix phases is similar. It has been determined that the strength is high in the alloys containing tin, but the strength decreases slightly in the alloy containing only Al, but the ductility and toughness increase significantly. It has been evaluated that the most responsible for this effect is the composition of the matrix phase.

Recommendations

1. The alloys should be heat treated including aging to determine the microstructural evaluations and mechanical properties.
2. The friction and wear behavior of the Al added alloys should be investigated.

Scientific Ethics Declaration

The authors declare that the scientific ethical and legal responsibility of this article published in EPSTEM journal belongs to the authors.

References

Hoang, A. T., Nguyen, L. H., & Nguyen, D. N. (2018). A study of mechanical properties and conductivity capability of CU-9NI-3SN ALLOY. *Int. J. Appl. Eng. Res*, *13*(7), 5120-5126.

Hui, Z., Yizhu, H., Xiaomin, Y., & Ye, P. (2010). Microstructure and age characterization of Cu–15Ni–8Sn alloy coatings by laser cladding. *Applied surface science*, *256*(20), 5837-5842.

Van Hunnik, E. W. J., Colijn, J., & Schade van Westrum, J. A. F. M. (1992). Heat treatment and phase inter-relationships of the spray cast Cu-15 wt% Ni-8 wt% Sn alloy. In *Materials Science Forum* (pp. 115-124). Trans Tech Publications Ltd.

Ilangovan, S., & Sellamuthu, R. (2016). Measurement of the variation of mechanical properties with aging temperatures for sand cast Cu-5Ni-5Sn alloy. *Journal of Engineering Science and Technology*, *11*(11), 1609-1619.

Lei, Q., Li, Z., Dai, C., Wang, J., Chen, X., Xie, J. M., ... & Chen, D. L. (2013). Effect of aluminum on microstructure and property of Cu–Ni–Si alloys. *Materials Science and Engineering: A*, *572*, 65-74.

López-Hirata, V. M., Arias-Pérez, Á. D. J., & Saucedo-Muñoz, M. L. (1999). A study of precipitation in a Cu-15 wt% Ni-8 wt% Sn alloy. *Journal of materials science letters*, *18*(20), 1697-1699.

Luo, B., Li, D., Zhao, C., Wang, Z., Luo, Z., & Zhang, W. (2019). A low Sn content Cu-Ni-Sn alloy with high strength and good ductility. *Materials Science and Engineering: A*, *746*, 154-161.

Peng, G., Gan, X., Jiang, Y., Li, Z., & Zhou, K. (2017). Effect of dynamic strain aging on the deformation behavior and microstructure of Cu-15Ni-8Sn alloy. *Journal of Alloys and Compounds*, *718*, 182-187.

Sato, A., Katsuta, S. I., & Kato, M. (1988). Stress aging of a Cu-10Ni-6Sn spinodal alloy. *Acta Metallurgica*, *36*(3), 633-640.

Singh, J. B., Cai, W., & Bellon, P. (2007). Dry sliding of Cu–15 wt% Ni–8 wt% Sn bronze: Wear behaviour and microstructures. *Wear*, *263*(1-6), 830-841.

Yin, B., Yin, Y., Lei, Y., Dong, L., & Zhang, Y. (2011). Experimental and density functional studies on the corrosion behavior of the copper-nickel-tin alloy. *Chemical Physics Letters*, *509*(4-6), 192-197.

Zhao, J. C., & Notis, M. R. (1998). Spinodal decomposition, ordering transformation, and discontinuous precipitation in a Cu–15Ni–8Sn alloy. *Acta materialia*, *46*(12), 4203-4218.

Author Information

Ibrahim CELIKYUREK
Eskişehir Osmangazi University
Eng. and Arch. Faculty, Metallurgical and Materials Eng. Dept. Eskişehir, Turkey
Contact e-mail: cibrahim@ogu.edu.tr

Bedri BAKSAN
Eskişehir Osmangazi University
Eng. and Arch. Faculty, Metallurgical and Materials Eng. Dept. Eskişehir, Turkey

Adem TASDEMIR
Eskişehir Osmangazi University
Eng. and Arch. Faculty, Mining Eng. Dept.
Eskişehir, Turkey

To cite this article:

Celikyurek, I., Baksan, B. & Tasdemir, A. (2021). Effect of alloying on the microstructure and strength of the Ni bronzes. *The Eurasia Proceedings of Science, Technology, Engineering & Mathematics (EPSTEM)*, *16*, 8-13.

The Eurasia Proceedings of Science, Technology, Engineering & Mathematics (EPSTEM)
ISSN: 2602-3199

The Eurasia Proceedings of Science, Technology, Engineering & Mathematics (EPSTEM), 2021

Volume 16, Pages 14-19

IConTES 2021: International Conference on Technology, Engineering and Science

Cryogenic Process Optimization for Medium Carbon Spring Steels

Resat Can OZDEN
Eskişehir Osmangazi University

Ersu LOKCU
Eskişehir Osmangazi University

Mustafa ANIK
Eskişehir Osmangazi University

Abstract: Spring steels are extensively used in load bearing elements of road and railway vehicles. The basic microstructure of these parts, which are subjected to high cycle fatigue, is tempered martensite. The improvement of the mechanical properties of these steels can only be achieved by modifying the material microstructure. In the microstructure of steel parts produced in different diameters, the formation of retained austenite and residual stresses is inevitable. For spring steels operating under heavy load, it is very important to remove the residual austenite form. Although the cryogenic treatment process is applied as a standard process for high alloyed and high carbon steels, it is not optimized for low alloy and medium carbon steels. In this study, different types of cryogenic treatment (Deep Cryogenic Treatment (DCT) / Shallow Cryogenic Treatment (SCT)) and tempering applications were carried out on spring steels with different alloying levels. With the outputs obtained from these experiments, optimization of cryogenic process parameters for medium carbon spring steels is aimed.

Keywords: Steels, Cryogenic treatment, Alloying

Introduction

Spring steels classified as medium carbon steels, with carbon contents ranging from 0.25 percent to 0.60 percent. Conventional heat treatment (CHT) can improve the mechanical properties of certain alloyed steels (austenitizing, quenching and tempering). However, using CHT, converting the full austenite structure to martensite may not always be achieved, and remaining austenite can reduce the steel's mechanical properties (Özden et al., 2020a). The austenite structure is entirely or partially transformed into martensite, cousing hardness and strength improvement throughout the cryogenic procedure (D. Das et al., 2009; Özbek et al., 2014). The cryogenic technique has been claimed to boost wear resistance by up to 270 percent (Senthilkumar et. al., 2012).

The idea of subzero cooling, which was introduced in the mid-1920s, was extensively studied in the 1940s, and thanks to these studies, the foundation for the complementary process known as the cryogenic process was laid (Villa et al., 2017). Cryogenic treatment is an effective method used to increase hardness, toughness, wear and fatigue resistance similar to CHT and has been used commercially for years to increase the service life of many metal materials.

The application of the method is usually in two temperature zones. These temperatures are -145°C for shallow cryogenic treatment (SCT); for deep cryogenic treatment (DCT) it is -190°C. In commercial applications, there

- Selection and peer-review under responsibility of the Organizing Committee of the Conference

are cold working (CW) applications around -80°C. The material is subjected to cryogenic treatment at the temperature and time determined according to the process, and then it is brought to room temperature at a certain rate. This is usually followed by a tempering process with a temperature of 150 – 500 °C (Das, 2011).

Cryogenic treatment is used as a very common method for high-carbon and high-alloy steels that contain a heavy retained austenite structure. However, studies are ongoing to clearly demonstrate the relationship of cryogenic treatment in the strengthening of lower alloy steels (Özden et al., 2020b). Although the structure-property relationship of the cryogenic treatment process applied in medium carbon steels has not been clearly revealed but it has been reported that the cryogenic process, which triggers mechanisms such as residual stress relief and grain homogenization, provides an increase in toughness properties without compromising strength values (Özden et. al., 2020). In this study, different cryogenic conditions were applied to three different spring steels and the cryogenic process was tried to be optimized by considering the tensile strength and toughness values.

Method

In the study, medium carbon spring steels 55Cr3, 51CrV4, 52CrMoV4 alloyed with different alloying elements were used. The steels were produced by ÇEMTAŞ (Bursa) in 55 mm diameter by continuous casting method. After obtaining the casting products, they were reduced to 19 mm in diameter by hot rolling and cut into 20 cm in length. Optical emission spectrometry analysis results of steels are presented in Table 1.

Table 1. Optical emission spectrometry analysis results of steels

Weight %	C	Si	Mn	Cr	Mo	V	P	S
55Cr3	0,57	0,30	0,85	0,91	-	-	0,010	0,005
51CrV4	0,52	0,28	0,84	0,93	-	0,13	0,008	0,004
52CrMoV4	0,54	0,26	0,87	1,12	0,19	0,11	0,009	0,003

Tensile tests were used to examine the effect of cryogenic treatment on strength and toughness. For this purpose, cryogenic treatment was applied to the samples at different temperatures (-196 °C, -145 °C) and times (12 – 24 - 36 hours). Following this process, the several samples were tempered at two different tempering conditions. Variables of applied heat treatments are presented in Table 2. Tensile tests were carried out in accordance with ASTM E8 / E8M-13 standard with a 250kN capacity Shimadzu tensile device.

Table 2. Heat treatment variables

Procedure	Code
Quenching *(850°C (Oil))*	Conventional Heat Treatment (CHT)
Tempering *(500°C;1 Hour)*	
Quenching *(850°C (Oil))*	Shallow Cryogenic Treatment (SCT)
Cryogenic Process *(-145°C; 24 Hours)*	
Tempering *(500°C;1 Hour)*	
Quenching *(850°C (Oil))*	Deep Cryogenic Treatment (DCT)
Cryogenic Process *(-196°C;12-24-36 Hours)*	
Tempering *(500°C;1 Hour)*	

Results and Discussion

In order to monitor the effect of cryogenic treatment temperature on these steel groups, firstly, shallow (-145°C) and deep (-196°C) cryogenic treatment was applied to 51CrV4 steel for 24 hours and the tensile test results were compared. No significant change was observed in the shallow cryogenic treated sample compared to

conventional heat treatment. On the other hand, an increase in tensile and strain values were observed after deep cryogenic treatment, and an increase in static toughness of approximately 18% was observed. According to the results, it was concluded that the shallow cryogenic process could not produce a significant level of carbide in this steel group. The strain-strain diagrams of the tensile tests are presented in Figure 1 and the numerical data of the tests are presented in Table 3.

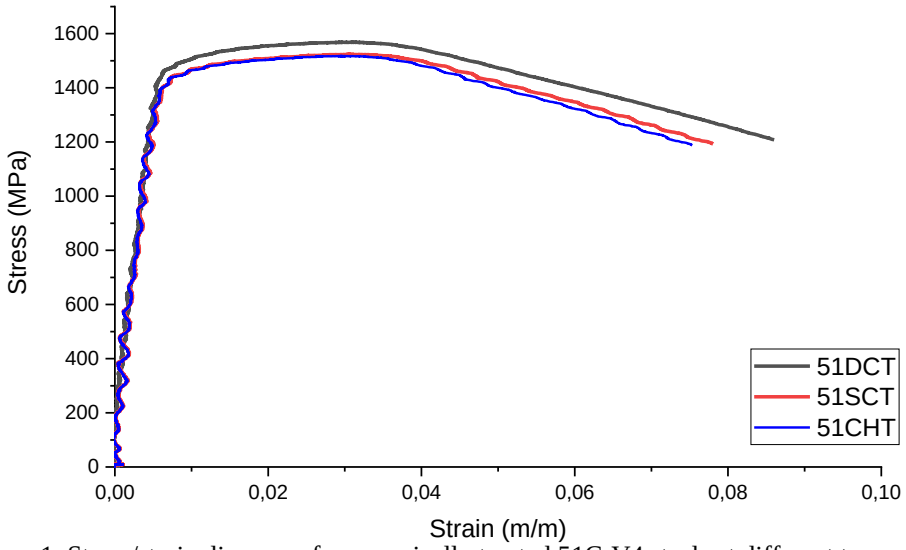

Figure 1. Stress/strain diagram of cryogenically treated 51CrV4 steels at different temperatures

Table 3. Tensile strength and strain comparison of cryogenic treated 51CrV4 steel at different temperatures

Sample	Tensile Strength (MPa)	Strain (m/m) (%)
51CHT	1517	7,53366
51SCT (-145°C, 24h)	1523	7,80379
51DCT (-196°C, 24h)	1568	8,60249

Afterwards, the effect of cryogenic treatment time was investigated by applying cryogenic treatment to 55Cr3 samples in three different time periods (12 – 24 – 36 hours). The tensile strengths of the samples after cryogenic treatment are given in Figure 2.

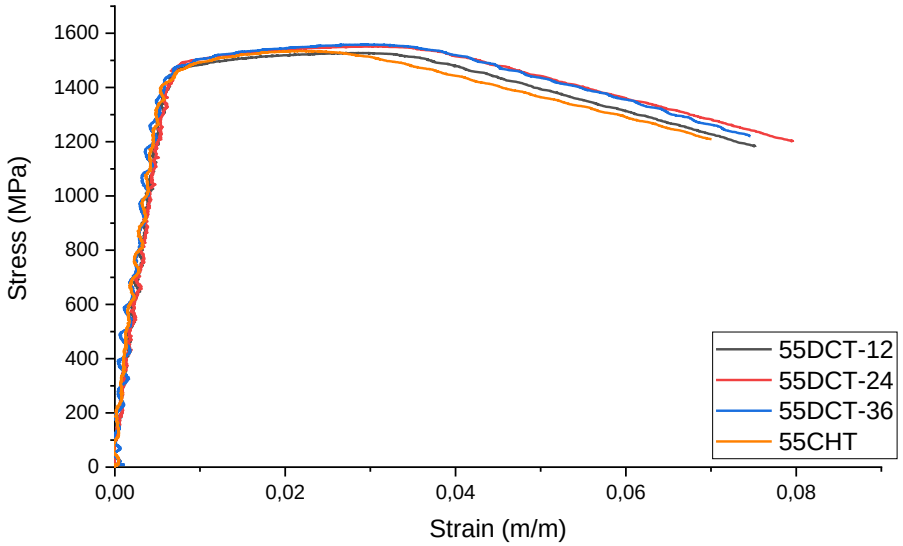

Figure 2. Stress/strain diagram of cryogenically treated 55Cr3 steels at different time periods

Consistent with the existing literature, it has been experimentally verified that the effect of cryogenic treatment on the tensile strength of the medium carbon low alloy steel group increases with the holding time, but the extension of the time does not provide a visible gain (Vahdat et al., 2013). Although the specimens had the highest tensile strength after 36 hours, no significant improvement in strain values was observed. The 12-hour cryogenic treatment increased the strain of the material but did not lead to an improvement in strength. A 24-hour immersion time seems ideal for this steel group. Numerical data on tensile tests are given in Table 4.

Table 4. Tensile strength and strain comparison of cryogenic treated 55Cr3 steel at different time periods

Sample	Tensile Strength (MPa)	Strain(m/m) (%)
55CHT	1534	7,00546
55DCT-12 (-196°C, 12h)	1527	7,52053
55DCT-24 (-196°C, 24h)	1551	7,96199
55DCT-36 (-196°C, 36h)	1558	7,46351

Spring steels are a steel group that is used extensively in the automotive industry. Line designs are available depending on intense automation in the production of these steels. Performing the cryogenic treatment as a complementary process, typically post-hardening, prior to tempering, requires a restructuring of the manufacturing process. In order to evaluate the possibility of ease of application, the applicability of cryogenic treatment to structures already hardened for these steel groups was also investigated. For this reason, 52CrMoV4 steels were subjected to conventional heat treatment followed by cryogenic treatment and then tempering heat treatment. The stress-strain graphs of the samples are presented in Figure 3.

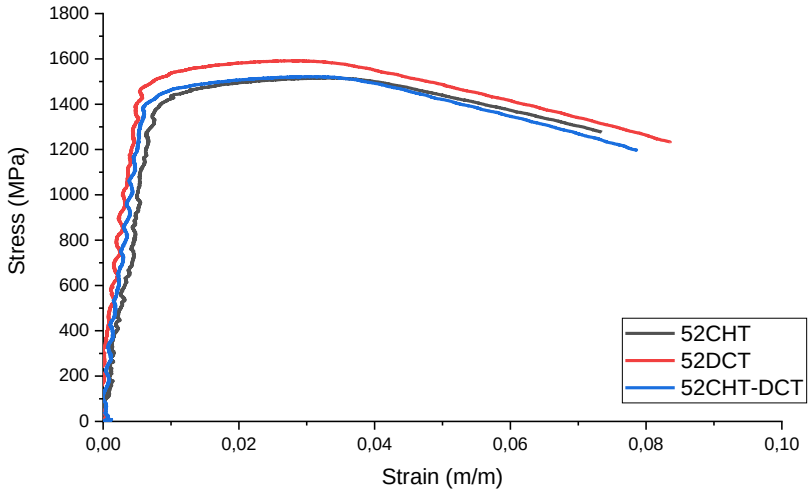

Figure 3. Stress/strain diagram of cryogenically treated 52CrMoV4 steels in different tempering conditions

52CHT-DCT samples have the lowest strength value with the effect of increasing tempering number. After the second tempering, the tetragonality and dislocation density of martensite decreased relatively, resulting in an increase in the strain value. In contrast, the typical cryogenic process continued to have the highest stress-strain value. The numerical data of the experiment are presented in Table 5.

Table 5. Tensile strength and strain comparison of cryogenic treated 52CrMoV4 steel at different tempering conditions

Sample	Tensile Strength (MPa)	Strain(m/m) (%)
52CHT	1515	7,34687
52DCT	1591	8,35312
52CHT-DCT	1521	7,86562

Conclusion

In our research, cryogenic process optimization was performed for low alloy medium carbon spring steels using three steels with different alloy levels. Accordingly, it was observed that SCT treatment had a strengthening

effect compared to CHT, but this effect was significantly lower than the effect created by DCT treatment. In addition, it has been observed that the increased time of DCT process performed over 24 hours has limited strength-increasing properties for this steel group. In this context, it was found significant that the cryogenic process time was limited to 24 hours, due to the importance of the toughness value.

Finally, the applicability of the cryogenic process to the already produced parts was investigated, but the desired values were not observed in the toughness and tensile strength values. As a result of these studies, it was concluded that the optimized cryogenic treatment process for medium carbon spring steels is a typical 24-hour deep (-196°C) cryogenic treatment.

Acknowledgements or Notes

Financial assistance from Eskisehir Osmangazi University Research Fund is gratefully acknowledged (Project No: 201615A230). The authors wish to thank ÇEMTAŞ (Bursa) and MMD Mechanical and Materials Technologies R&D Consulting Engineering Services Industry and Trade Limited Company (Eskişehir).

Scientific Ethics Declaration

The authors declare that the scientific ethical and legal responsibility of this article published in EPSTEM journal belongs to the authors

References

D Das, D., Ray, K. K., & Dutta, A. K. (2009). Influence of temperature of sub-zero treatments on the wear behaviour of die steel. *Wear*, *267*(9-10), 1361-1370.

D Das, D., Dutta, A. K., & Ray, K. K. (2010). Structure-property correlation of cryotreated AISI D2 steel. In *Advanced Materials Research* (pp. 49-54). Trans Tech Publications Ltd.

Özbek, N. A., Çiçek, A., Gülesin, M., & Özbek, O. (2014). Investigation of the effects of cryogenic treatment applied at different holding times to cemented carbide inserts on tool wear. *International Journal of Machine Tools and Manufacture*, *86*, 34-43. https://doi.org/10.1016/j.ijmachtools.2014.06.007

Özden, R. C., & Anik, M. (2020). Enhancement of the mechanical properties of EN52CrMoV4 spring steel by deep cryogenic treatment. *Materialwissenschaft Und Werkstofftechnik*, *51*(4), 422-431. https://doi.org/10.1002/mawe.201900122

Özden, R. C., Lökçü, E., & Anik, M. (2020). Effects of Deep Cryogenic Treatment on the Mechanical Properties of Medium Carbon Spring Steels. *The Eurasia Proceedings of Science Technology Engineering and Mathematics*, *11*, 48-52.

Senthilkumar, D., & Rajendran, I. (2012). Optimization of deep cryogenic treatment to reduce wear loss of 4140 steel. *Materials and Manufacturing Processes*, *27*(5), 567-572. https://doi.org/10.1080/10426914.2011.593237

Vahdat, S. E., Nategh, S., & Mirdamadi, S. (2013). Microstructure and tensile properties of 45WCrV7 tool steel after deep cryogenic treatment. *Materials Science and Engineering: A*, *585*, 444-454. https://doi.org/10.1016/j.msea.2013.07.057

Villa, M., Hansen, M. F., & Somers, M. A. (2017). Martensite formation in Fe-C alloys at cryogenic temperatures. *Scripta Materialia*, *141*, 129-132. https://doi.org/10.1016/j.scriptamat.2017.08.005

Author Information

Resat Can OZDEN
Department of Metallurgical and Materials Engineering, Eskisehir Osmangazi University, 26040, Eskisehir, Turkey
Contact e-mail: *rcanozden@ogu.edu.tr*

Ersu LOKCU
Department of Metallurgical and Materials Engineering, Eskisehir Osmangazi University, 26040, Eskisehir, Turkey

Mustafa ANIK
Department of Metallurgical and Materials Engineering, Eskisehir Osmangazi University, 26040, Eskisehir, Turkey

To cite this article:

Ozdan, R.C., Lokcu, E. & Anik, M. (2021). Cryogenic process optimization for medium carbon spring steels. *The Eurasia Proceedings of Science, Technology, Engineering & Mathematics (EPSTEM), 16,* 14-19.

The Eurasia Proceedings of Science, Technology, Engineering & Mathematics (EPSTEM)
ISSN: 2602-3199

The Eurasia Proceedings of Science, Technology, Engineering & Mathematics (EPSTEM), 2021

Volume 16, Pages 20-25

IConTES 2021: International Conference on Technology, Engineering and Science

Effect of Secondary Aging of AA7075 Aluminum Alloy to Hardness

Bedri BAKSAN
Eskisehir Osmangazi University

Adem TASDEMIR
Eskisehir Osmangazi University

Ibrahim CELIKYUREK
Eskisehir Osmangazi University

Abstract: In this study, one of the major aluminum alloys AA7075 was held to obtain the maximum benefit for structural parts. Nowadays for the energy efficiency of vehicles like electric cars or aerospace vehicles weight reducing efforts are needed. To obtain lighter structures specific strengths are gaining importance. In our study, AA 7075 aluminum alloy was processed with additional heat treatment rather than T6 condition to obtain high strength. According to our previous studies, statistical methods seemed very useful to predict probable strength very precisely, for this reason, Box-Behnken Surface Response Method was used. By applying statistical methods, the artificial aging temperature and time were optimized. According to optimized temperature and time, the secondary aging heat treatment was done. In this study three T6 conditions 150, 200, and 250 ^{o}C with four treatment times, 1,2,4 and 6 hours were chosen and applied. The secondary aging temperature and time were obtained from Box-Behnken optimization study results and found as 182 ^{o}C and 2 hours were applied to all samples. As a result, after secondary aging heat treatment maximum hardness of 151 Hv was obtained from samples that aged at 150 ^{o}C, and 250 °C for 1 hour, which is almost doubled because the T6 aged sample has a hardness value of 86 Hv. This is obvious that the strength almost doubled, therefore it is possible to use sections almost half of the T6 condition samples.

Keywords: 7075 Aluminum alloy, Aging, Microhardness, Optical microscopy

Introduction

The 7xxx series of aluminum alloys have been in service for several years in the aerospace industry for structural parts because of their superior properties i.e. low density, high strength, ductility, toughness, and fatigue resistance (Leacock et al., 2013; Li et al., 2008; Panigrahi et al., 2011). Nowadays, it has become more and more important for the electric car industry. AA7075 aluminum alloys have been preferred due to their high mechanical properties such as 505 MPa yield strength and 11% elongation. Besides its high mechanical properties, AA7075 aluminum has many excellent properties such as low density, good corrosion resistance, machinability, and electrical conductivity.

Aging is the most important heat treatment used for hardening in non-ferrous metals, mainly aluminum, as well as in high-strength stainless steel. Aluminum, which is used in various industries, such as aviation, is strengthened by the aging process. The aging process, also known as the precipitation hardening process, is the precipitation of the second phase by distributing it finely in the matrix phase, obtaining a hard structure. (Pankade et al., 2018; Zou et. al., 2017).

For today's manufacturers of automotive and aerospace vehicles, the replacement of aluminum alloys with conventional alloys or steels in engineering applications is the major design concept for increasing fuel prices (Başer, 2013). Aluminum and magnesium alloys are the main candidate materials for reducing the weight of vehicles, especially battery-operated cars (Hofer et al., 2012) main structural parts need to have high specific strength. Among these; age-hardenable aluminum alloys are becoming primary materials to reduce the weights (Kear et al., 1993). Another point to be taken care of because of huge mass production rates is the production costs (Roth et al., 2001). The 2XXX and 7XXX series age-hardenable alloys are gaining importance for their relatively high mechanical strength concerning their cost (Abd El-Rehim et al., 2013). The studies about lowering the weight of vehicles go back to the '80s (Century et al., 1993; et al., 1982). Some studies have been carried out to reduce the weight of military or logistics vehicles by replacing iron-based alloys with aluminum-based alloys. (N.R.C., 2003). There are numerous studies on the secondary aging procedure for aluminum alloys. One of the studies concerned the wear resistance of the AlSi10Mg alloy (Gül, 2014), An overview of the aging heat treatment of AlSi10Mg alloy was made by Vatansever et.al (Vatansever et al., 2018). There are some studies about the effects of secondary aging and interrupted aging to aluminum alloys indicating that the secondary aging heat treatment have increasing the mechanical properties (Baksan et al., 2020; Buha et al., 2006; Hai et al., 2005; Koch et al., 1979; Lumley et al., 2003; Lumley et al., 2005). The goal of this study is to achieve superior properties from a cheaper aluminum alloy to substitute and compete with iron-based alloys as well as 2xxx, and 7xxx series aluminum alloys by secondary aging heat treatment following a T6 treatment.

Materials and Method

Stock AA7075 aluminum alloy samples were supplied locally for this study. The samples were solutionized at 500 ^{o}C for 4 hours and aged at 150, 200, and 250 ^{o}C for 1, 2, 4, and 6 hours, following this T6 heat treatment, a secondary aging heat treatment was done for as 182 ^{o}C and 2 hours. The secondary aging heat treatment conditions of 182 ^{o}C and 2 hours were obtained from our previous study results of Box-Behnken statistical studies (Baksan et al., 2018) (Figure 1). Microhardness tests were performed for each experiment. Microstructures were obtained from an optical microscope to observe microstructural changes.

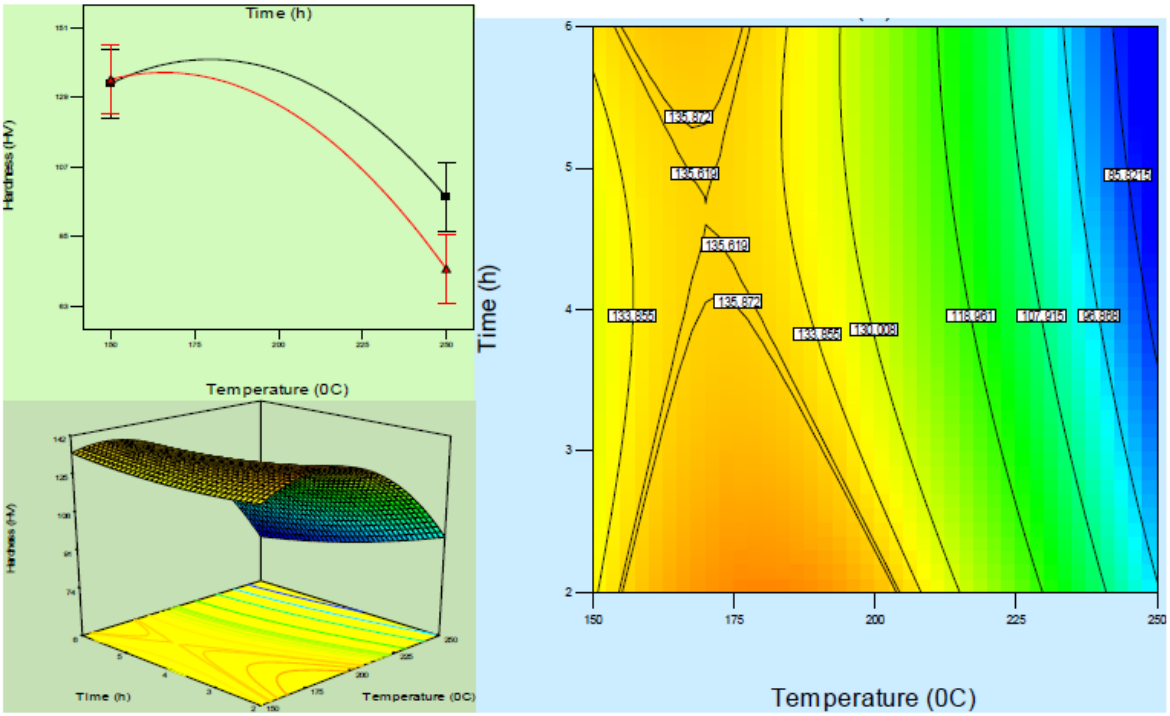

Figure 1. Box-Behnken optimization plots, (a) Aging time versus hardness (up-left), (b) 3D surface aging time-temperature and hardness plot (down-left), (c) isopleth of aging time and temperature plot (Baksan et al., 2018)

The samples were homogenized at 500 °C for 96 hours. The samples were solutionized at 500 °C for 4 hours and quenched in water at room temperature. The aging heat treatment was carried out at 150, 200, and 250 ^{o}C for 1, 2, 4, and 6 hours and quenched in water. Secondary aging heat treatment was carried out at 182 °C for 2 hours.

After completing the heat treatment procedure, the samples were polished and etched with Keller etchant.The microhardness testing was done by Futuretech make FV-800 instrument with 300 g load for 10 seconds.

Results and Discussion

The microhardness testing results showed that the secondary aging heat treatment improved the hardness. The hardness of secondarily aged samples decreases with the aging time. The maximum hardness value was obtained from samples that were aged at 150 °C, and 250 °C for 1 hour and secondarily aged at 182 °C for 2 hours, giving 151 H_v. This hardness value is 75% higher than the samples aged only at 150 °C for 6 hours which was obtained as 86 H_v. The change in hardnesses of secondarily aged samples was given in Figure 2.

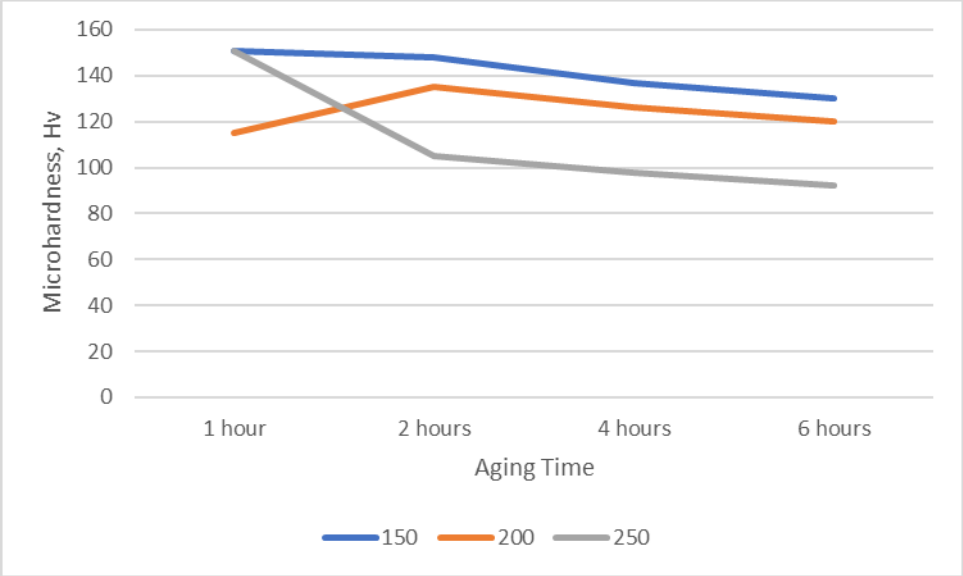

Figure 2. Microhardness change of samples secondarily aged at 182 °C for two hours at various T6 conditions

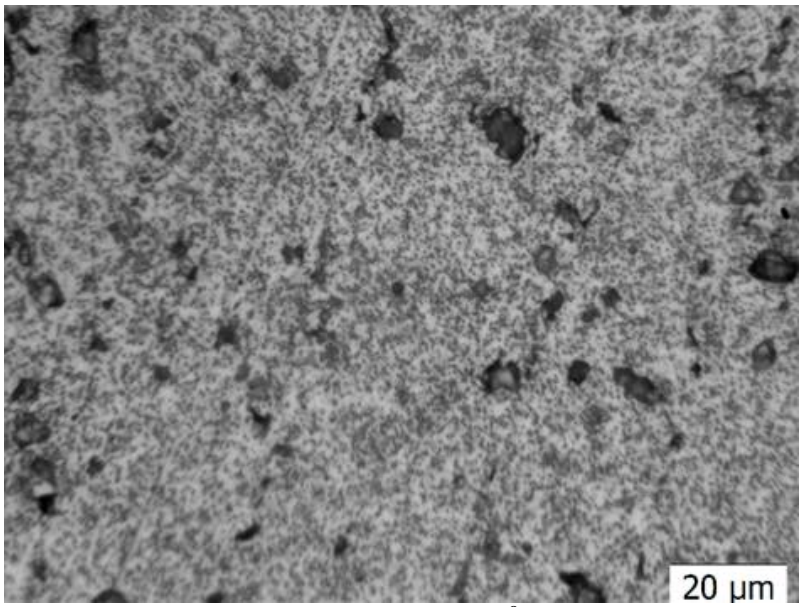

AA 7075 aluminum alloy Solutionized at 500 ^{o}C for 4 hours and aged at 150 ^{o}C for 1 hour

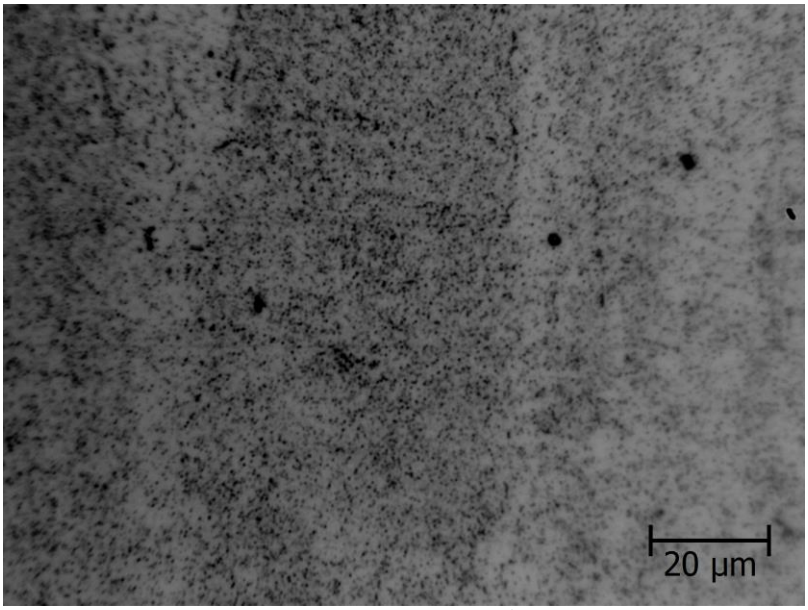

AA 7075 aluminum alloy Solutionized at 500 ^{o}C for 4 hours, aged at 150 ^{o}C for 1 hour, and additionally aged at 182 ^{o}C for 2 hours

Figure 3. Microstructures of AA7075 aluminum alloy aged at 150 ^{o}C for 1 hour, and secondarily aged at 182 ^{o}C for 2 hours.

The microstructures of aged and secondarily aged samples are given in Figure 3. The microstructures revealed that the grains were coarsening by increasing time in secondarily aged samples. During aging, with the effect of temperature, the precipitates dispersed through the matrix, as the aging continues, these clusters begin to form β precipitates compatible with the α matrix phase. These precipitates play a role in increasing hardness. As the aging continues, the precipitates grow further and reach a critical height, it is seen from the trend of the graph in Fig.2 but the time and hardness limit could not be detected because the experiments are limited to 6 hours. At higher magnifications, the fine precipitates were seen. As the aging time increases the fine precipitates dispersed very fine all over the matrix.

These results showed that it would be possible to produce materials with higher strengths since the hardness value of almost 75% higher than the stock alloy was obtained in this study. This means that it is possible to reduce aluminum weights in at least half of the current applications, especially in vehicle production.

Conclusion

The secondary aging heat treatment would be a weight reduction route for increasing the strength of age-hardenable alloys. This may also increase the service life of age-hardened parts. The increase in hardness in this study obtained more than at least 10% which is higher than ordinary aged ones. Our other studies revealed almost two-fold hardness values (Baksan et al., 2018)

In this study, the secondary aging heat treatment at 150 ^{o}C, and 250 ^{o}C for 1 hour also resulted in a peak hardness of 151 H_v this value is higher than T6 condition. This phenomenon may be related to reduced mobility of vacancies, and the growth of partially dissolved η' precipitates, the re-nucleation of precipitates, or the transformation to the stable η phase (Esmailian et al., 2015). It has been determined that two different aging temperatures give the same result, and it is obvious that it is preferable to use lower temperatures to save energy on the industrial production route. Therefore, 150 ^{o}C will be a more economical way to obtain high-strength materials.

Scientific Ethics Declaration

The authors declare that the scientific ethical and legal responsibility of this article published in EPSTEM journal belongs to the authors.

References

Abd El-Rehim, A. F., & Mahmoud, M. A. (2013). Transient and steady state creep of age-hardenable Al-5 wt% Mg alloy during superimposed torsional oscillations. *Journal of Materials Science, 48*(6), 2659-2669. doi:10.1007/s10853-012-7059-x

Baksan, B., Çelikyürek, İ., & Kılıç, Y. (2020). Effect of secondary aging of EN AC 43200 Aluminum alloy to mechanical properties. *The International Journal of Materials and Engineering Technology, 3*(1), 16-20.

Baksan, B., Çelikyürek, İ., Taşdemir A., Torun O. (2018). *Determination of parameters affecting hardness of aa7075 aluminum alloy by response surface method* [Conference presentation]. 4th International Conference on Engineering and Natural Science, Kyiv, Ukraine.

Başer, T. (2013). Alüminyum alaşımları ve otomotiv endüstrisinde kullanımı. *Mühendis ve Makina, 53*(635), 51-58.

Buha, J., Lumley, R., & Crosky, A. (2006). Microstructural development and mechanical properties of interrupted aged Al-Mg-Si-Cu alloy. *J Metallurgical Materials Transactions A, 37*(10), 3119-3130.

Kear, B. H., & National Research Council. (1993). *Materials research agenda for the automotive and aircraft industries: report*. National Academies Press.

Esmailian, M., Shakouri, M., Mottahedi, A., & Shabestari, S. G. (2015). Effect of T6 and re-aging heat treatment on mechanical properties of 7055 aluminum alloy. *International Journal of Materials and Metallurgical Engineering, 9*(11), 1303-1306. doi:doi.org/10.5281/zenodo.1110057

Vatansever, F., Ertürk, A. T., & Karabay, S. (2018). Alüminyum-Silisyum Alaşımlarının Mikroyapısal ve Mekanik Özelliklerinin T6 Isıl İşlemi ile İyileştirilmesi. *Dokuz Eylül Üniversitesi Mühendislik Fakültesi Fen ve Mühendislik Dergisi, 20*(60), 797-803. doi:DOI: 10.21205/deufmd. 2018206062

Gül, F. (2014). AlSi10Mg Döküm Alaşımlarının Bazı Mekanik Özellikleri Üzerine İkincil Yaşlandırma İşleminin Etkisi. *Süleyman Demirel Üniversitesi Fen Bilimleri Enstitüsü Dergisi, 18*(1). doi:10.19113/sdufbed.97535

Hai, L., Ziqiao, Z., & Zhixiu, W. (2005). Investigation of secondary ageing characteristics of 7055 aluminum alloy—(II) microstructures and fractography [J]. *Rare Metal Materials and Engineering, 8*.

Hofer, J., Wilhelm, E., & Schenler, W. (2012). Optimal lightweighting in battery electric vehicles. *World Electric Vehicle Journal, 5*(3), 751-762. doi:10.3390/wevj5030751

Koch, G., & Kolijn, D. (1979). The heat treatment of the commercial aluminum alloy 7075. *J Journal of Heat Treating, 1*(2), 3-14.

Leacock, A. G., Howe, C., Brown, D., Lademo, O.-G., & Deering, A. (2013). Evolution of mechanical properties in a 7075 Al-alloy subject to natural ageing. *Materials & Design, 49*, 160-167. doi:10.1016/j.matdes.2013.02.023

Li, J.-f., Peng, Z.-w., Li, C.-x., Jia, Z.-q., Chen, W.-j., & Zheng, Z.-q. (2008). Mechanical properties, corrosion behaviors and microstructures of 7075 aluminium alloy with various aging treatments. *Transactions of Nonferrous Metals Society of China, 18*(4), 755-762. doi:10.1016/s1003-6326(08)60130-2

Lumley, R., Polmear, I., & Morton, A. J. (2003). Interrupted aging and secondary precipitation in aluminium alloys. *J Materials Science Technology, 19*(11), 1483-1490.

Lumley, R., Polmear, I., & Morton, A. J. (2005). Development of mechanical properties during secondary aging in aluminium alloys. *J Materials Science Technology, 21*(9), 1025-1032.

Panigrahi, S. K., & Jayaganthan, R. (2011). Effect of ageing on microstructure and mechanical properties of bulk, cryorolled, and room temperature rolled Al 7075 alloy. *Journal of Alloys and Compounds, 509*(40), 9609-9616. doi:10.1016/j.jallcom.2011.07.028

Pankade, S. B., Khedekar, D. S., & Gogte, C. L. (2018). The influence of heat treatments on electrical conductivity and corrosion performance of AA 7075-T6 aluminium alloy. *Procedia Manufacturing, 20*, 53-58. doi:10.1016/j.promfg.2018.02.007

Roth, R., Clark, J., & Kelkar, A. (2001). Automobile bodies: Can aluminum be an economical alternative to steel? *Jom, 53*(8), 28-32. doi:10.1007/s11837-001-0131-7

National Research Council. (2003). *Use of Lightweight Materials in 21st Century Army Trucks*. National Academies Press.Vehicles, N. R. C. C. o. M. f. L. M., & Board, N. R. C. N. M. A. (1982). *Materials for Lightweight Military Combat Vehicles: Report*: National Academy Press.

Zou, X.-l., Yan, H., & Chen, X.-h. (2017). Evolution of second phases and mechanical properties of 7075 Al alloy processed by solution heat treatment. *Transactions of Nonferrous Metals Society of China, 27*(10), 2146-2155. doi:10.1016/s1003-6326(17)60240-1

Author Information

Bedri BAKSAN
Eskisehir Osmangazi University
Metalurji ve Malzeme Muh.Bolumu, Eskisehir, Turkey
Contact e-mail: *baksan@ogu.edu.tr*

Ibrahim CELIKYUREK
Eskisehir Osmangazi University
Metalurji ve Malzeme Muh.Bolumu, Eskisehir, Turkey

Adem TASDEMIR
Eskisehir Osmangazi University
Maden Muh.Bolumu, Eskisehir, Turkey

To cite this article:

Baksan, B., Celikyurek, I., & Tasdemir, A. (2021). Effect of secondary aging of AA7075 aluminum alloy to hardness. *The Eurasia Proceedings of Science, Technology, Engineering & Mathematics (EPSTEM), 16*, 20-25.

The Eurasia Proceedings of Science, Technology, Engineering & Mathematics (EPSTEM)
ISSN: 2602-3199

The Eurasia Proceedings of Science, Technology, Engineering & Mathematics (EPSTEM), 2021

Volume 16, Pages 26-30

IConTES 2021: International Conference on Technology, Engineering and Science

Interactive Simulation Program for Autonomous Vehicles

Claudiu Radu POZNA
Transilvania University of Brasov
Széchenyi István University

Csaba ANTONYA
Transilvania University of Brasov

Abstract: The paper presents an interactive simulation program dedicated to autonomous vehicles. The program, developed in the form of an app and written in the Matlab programming language, is a didactic tool, which aims to better understand the phenomena that occur during locomotion. To achieve this goal, the user can easily perform interactive simulations by changing the model parameters. In addition to the mentioned flexibility, the user can perform case studies and scenarios. The structure of the program is obtained by aggregating seven objects (modules), dedicated to studying the contributions of each to the simulation. These modules are for different types of trajectories, for controllers, three types of locomotion models, sensors, different filters, environment models, and for simultaneous localization and mapping. The connection between them is possible through a database. This framework ensures the continuity of the simulations. At the end of the interactive visual simulation, the user is obtaining a holistic report with the results.

Keywords: Autonomous vehicle, Simulation, Program, Interactive, Modeling.

Introduction

Autonomous vehicles represent a hot research topic in the last years. Real-world data acquisition and testing are difficult but computer modeling and simulation represent an efficient way to analyze and design such vehicles. Modern computer hardware and the advancement of artificial intelligence made possible the development of efficient tools for algorithm testing and simulation in virtual environments.

An autonomous vehicle is reacting to the feedback received from sensors. A typical vehicle simulator needs to incorporate a vehicle model as well as models for the sensors and decision algorithms. The most important part of a virtual environment is the simulator that realistically represents the physics of the vehicle (Rosique et al. 2019). Testing of an autonomous vehicle is critical before deployment. A simulator eliminates the difficulties of the road test and allows the understanding of driving behavior, testing driver assistant systems, and for traffic research. The simulation environment must provide reproducible testing methods to accelerate the development (Huang et al. 2016). The most important autonomous vehicle simulators are AirSim, DeepDrive, Udacity, Constellation, Carcraft/Waymo, SIMLidar, Helios, GLIDAR, and CARLA (Dosovitskiy et al. 2017; Chen et al. 2018).

Autonomous vehicle testing is difficult because of its diversity and complexity. A pipeline that generates various scenarios for autonomous vehicle simulations is proposed in (Wen et al. 2020). An architecture for vehicle control is proposed in (Pozna et al. 2016), through a methodology that involves identifying primitives, combining them, abstracting them, and finally identifying patterns (Pozna et al. 2021).

The Simulation Program

Computer modeling and simulation is a process of in-depth knowing a physical phenomenon. In general, the computer simulation of a robotic system results in a set of differential equations. Obtaining these equations is not the result but rather an intermediate step. These equations have to be transformed into algorithms and computational programs. The objective of knowledge is a priori, i.e. the possibility to anticipate the results of the causal relationship before the experiment. This goal can be achieved using computer programs through simulation. The quality of the simulation, the difference between the anticipated and the real results, depends on the quality of the model and that of the numerical methods used in solving the mentioned differential equations.

The various aspects and algorithms that are related to mobile robots and autonomous vehicles modeling led to the idea of their development in a unitary framework, which would allow a better understanding of the locomotion phenomenon of the autonomous vehicle. Consequently, the several models were brought together in the form of a complex simulation program.

The program is made in the form of an app is written in Matlab (www.mathworks.com) language. It is a didactic application aiming to better understand the phenomena that occur during locomotion. To achieve this goal, the user can easily undertake simulations by changing the model parameters. In addition to the mentioned flexibility, the user can perform case studies, scenarios, which allow the inheritance and addition of data in the program's database. In addition, the application contains the theoretical elements thus providing a unitary information and simulation environment.

The Architecture of the Simulator

The simulator has a structure obtained by aggregating seven objects. Figure 1 shows the block diagram of the mentioned architecture, the seven objects and their connection to the database. The architecture is modular, new modules (objects) can be imagined and can be added to enriched the program with new simulation methods.

Each of the objects is a module dedicated to studying its contributions to the simulation. These modules are for studying the effects on the autonomous vehicle of the trajectories, controller, locomotion models, sensors, filters, environment models, and for simultaneous localization and mapping (SLAM). The connection between them is possible through a database, this framework ensures the continuity of the simulations. The user can benefit from the data introduced in previous simulations or can add new data to the database. At the end of the interactive visual simulation, the user is obtaining a holistic report with the results.

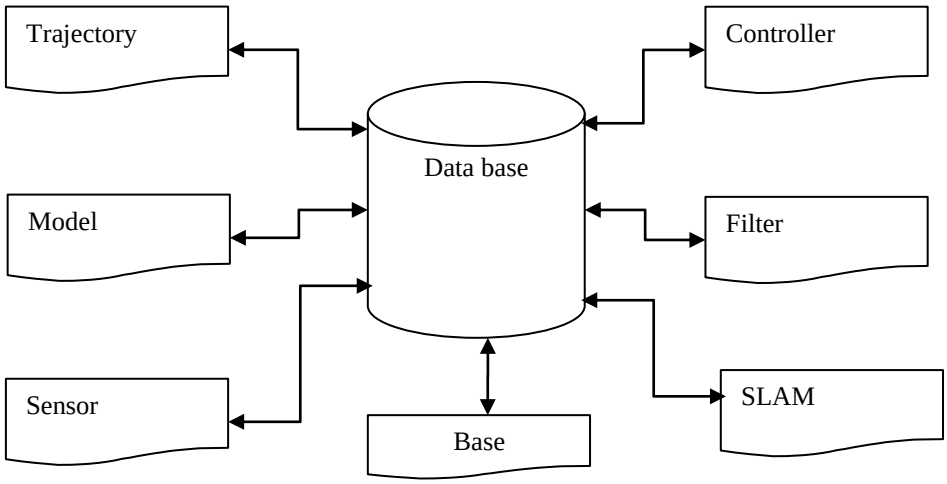

Figure 1. The autonomous vehicle simulator's architecture

The Modules of the Simulator

The modules and their features are presented in Table 1. Each of the modules can be used for testing and comparing different algorithms in the same area. Also, the user can change the parameters of the algorithm and visualize the results with plots and animations.

Table 1. The modules of the interactive simulation program

Module	Components	Observations
Trajectories	The domain of locomotion	It allows the definition of the locomotion environment by specifying multiple obstacles in the form of polylines. Here the environment discretion can be set.
	A* trajectory	The locomotion environment can be imported; starting position and destination points can be defined; one can calculate the trajectory between these points using the A* algorithm. The obtained trajectory avoids the obstacles that are in the field of locomotion.
	Clothoid trajectory	The locomotion environment can be imported. Limit points and guiding points can be specified, as well as the vehicle's speed. These allow the computation of the trajectory with clothoid segments and of the steering angle as a function of time.
Models	Geometric Model	The geometric model of the autonomous vehicle can be defined. The visualization can take several forms of the geometric model associated with the vehicle: a reference system; a triangle; a rectangle and a box shape. Here the posture can be changed.
	Cinematic Model	It allows the definition of the steering angle, as the control value, which in the end will lead to the representation of the trajectory and of the associated kinematic quantities.
		It allows the import of the steering angle of the trajectory with clothoid segments and the simulation of the vehicle's kinematics.
	Dynamic Model	Allows the definition of the steering angle, the control parameter and the inertial properties (mass, rolling inertia), which will ultimately lead to the presentation of the vehicle's trajectory. Here the over and understeering effects are highlighted.
		It allows the import of the steering angle of the trajectory with clothoid segments and the simulation of the vehicle's dynamics.
Sensors	LIDAR	It allows the import of the locomotion environment and the trajectory of the vehicle. The LIDAR parameters can be changed. It simulates the measurement of obstacles, the definition of the map and the occupancy grid.
	Odometer	Using the dynamic model with slip, the trajectory of the vehicle, obtained with odometric measurements is simulated.
Controllers	PID trajectory	Allows the import of the locomotion environment of the autonomous vehicle, the trajectory, the LIDAR sensor, the particle filter and simulates the controlled trajectory of the vehicle.
	Lateral dynamics	It permits the import or definition of the command parameter to control the vehicle for the elimination of the effects of lateral dynamics. Also, permits the tracking of the desired trajectory. The dynamic and desired controlled trajectories are illustrated.
Filters	Bayesian	The control values and measurements are defined, the probability distribution of the vehicle's position is shown.
	Extended Kalman Filter	The control quantities are defined, the probability distributions of the vehicle's position are calculated for various parameters of the sensors.
	Particle filter	
SLAM	Extended Kalman Filter method	The control quantities are defined, the probability distributions of the vehicle's position are calculated for various parameters of the sensors.
	Particle filter method	
Environment model		The general physical parameters are defined: absolute reference frame, friction, gravity, etc.

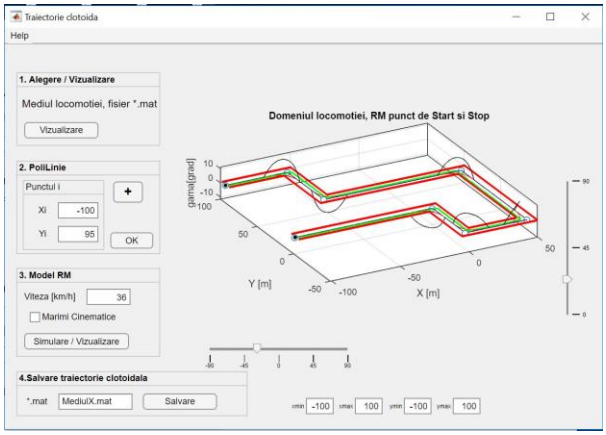

a

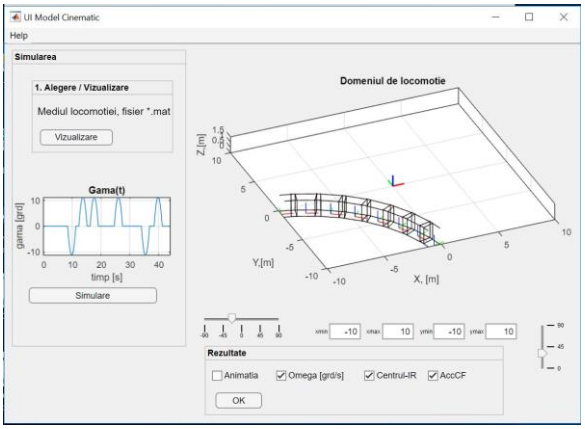

b

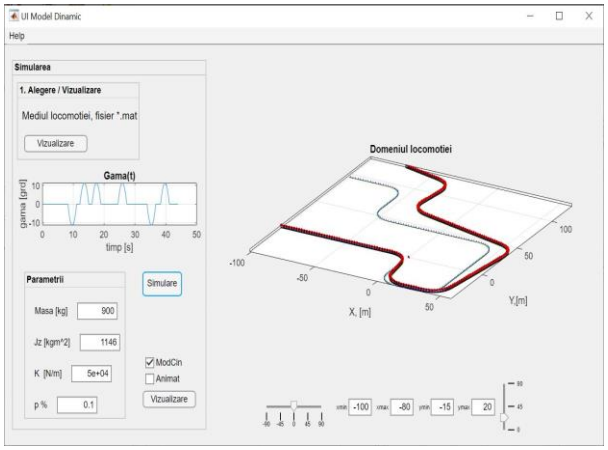

c

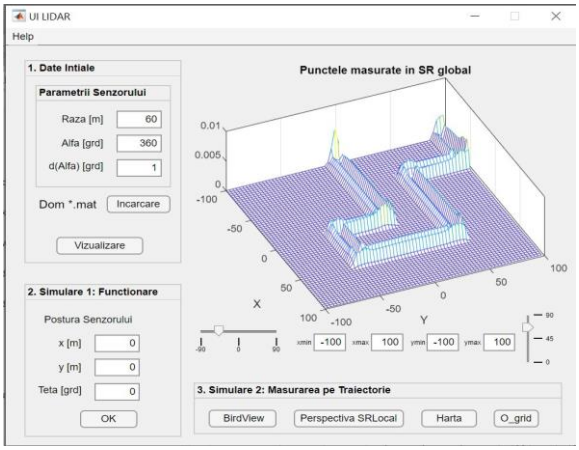

d

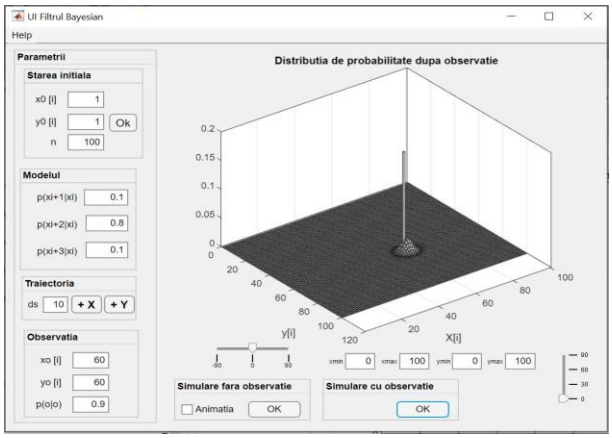

e

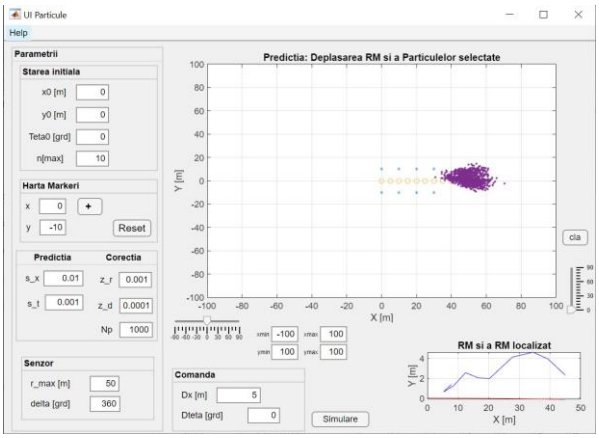

f

Figure 2. The interface of the simulation program

Some screenshots of the user interface of the simulator are shown in Figure 2. These are for the (a) trajectory with clothoid segments, (b) the kinematic model, (c) the dynamic model, (d) LIDAR model, (e) Bayes filter, and (f) particle filter.

With the simulator, the user has the possibility to study a certain phenomenon (filters, kinematic, dynamic, control, etc.) by modifying the model parameters (length, mass, resolution, tuning parameters, etc.) and the control values (linear speed, angular velocity, etc.) which, in the end, will allow the visualization of their influence.

In order to understand the holistic phenomenon of locomotion, the simulator also allows case studies. It is about linking the mentioned phenomena with the help of a database that takes over the effects of one phenomenon and transforms them into the causes of other phenomena.

Conclusion

The program is dedicated to autonomous vehicles (a mobile robot with four wheels) and allows the visualization of different locomotion scenarios. It is made in the form of an app is written in Matlab language. It is a didactic application aiming to better understand the phenomena that occur during locomotion, data processing, and decision making. The user can easily undertake simulations by changing the model parameters, can perform case studies, scenarios, which allow the inheritance and addition of data in the program's database. In addition, the application contains the theoretical elements thus providing a unitary information and simulation environment.

Acknowledgements

This work was supported by a grant of the Romanian Ministry of Research, Innovation and Digitization, CNCS/CCCDI – UEFISCDI, project number PN-III-P2-2.1-PED-2019-4366 within PNCDI III (431PED).

Scientific Ethics Declaration

The authors declare that the scientific ethical and legal responsibility of this article published in EPSTEM journal belongs to the authors.

References

Chen, Y., Chen, S., Zhang, T., Zhang, S., & Zheng, N. (2018, June). Autonomous vehicle testing and validation platform: Integrated simulation system with hardware in the loop. In *2018 IEEE Intelligent Vehicles Symposium (IV)* (pp. 949-956). IEEE.

Dosovitskiy, A., Ros, G., Codevilla, F., Lopez, A., & Koltun, V. (2017). CARLA: An open urban driving simulator. In *Conference on robot learning* (pp. 1-16). PMLR.

Huang, W., Wang, K., Lv, Y., & Zhu, F. (2016). Autonomous vehicles testing methods review. In *2016 IEEE 19th International Conference on Intelligent Transportation Systems (ITSC)* (pp. 163-168). IEEE.

The MathWorks Inc (2020). MATLAB version 9.8.0. Natick.

Pozna, C. R., & Antonya, C. (2016). Issues about autonomous cars. In *2016 IEEE 11th International Symposium on Applied Computational Intelligence and Informatics (SACI)* (pp. 13-18). IEEE.

Pozna, C. R., & Antonya, C. (2021). Proposal of an autonomous vehicle control architecture. In *2021 IEEE 25th International Conference on Intelligent Engineering Systems (INES)* (pp. 37-42). IEEE.

Rosique, F., Navarro, P. J., Fernández, C., & Padilla, A. (2019). A systematic review of perception system and simulators for autonomous vehicles research. *Sensors*, *19*(3), 648.

Wen, M., Park, J., & Cho, K. (2020). A scenario generation pipeline for autonomous vehicle simulators. *Human-centric Computing and Information Sciences*, *10*, 1-15.

Author Information

Claudiu Radu POZNA
Transilvania University of Brasov
Department of Automation and Information Technology
29 Eroilor Blvd, 500036 Brasov, Romania
Széchenyi István University
Department of Computer Science
Egyetem tér 1, 9026 Győr, Hungary

Csaba ANTONYA
Transilvania University of Brasov
Department of Automotive and Transport Engineering
29 Eroilor Blvd
500036 Brasov, Romania
Contact e-mail: *antonya@unitbv.ro*

To cite this article:

Pozna, C.R. & Antonya, C. (2021). Interactive simulation program for autonomous vehicles. *The Eurasia Proceedings of Science, Technology, Engineering & Mathematics (EPSTEM), 16*, 26-30.

The Eurasia Proceedings of Science, Technology, Engineering & Mathematics (EPSTEM)
ISSN: 2602-3199

The Eurasia Proceedings of Science, Technology, Engineering & Mathematics (EPSTEM), 2021

Volume 16, Pages 31-38

IConTES 2021: International Conference on Technology, Engineering and Science

Gissmo Failure Modelling for Crashworthiness Analysis Using Different Test Specimens

M. Emin TAMER
Borçelik Çelik Sanayii Ticaret A.Ş.

Almila Gulfem OZGULTEKIN
Borçelik Çelik Sanayii Ticaret A.Ş.

Beyzanur AYDIN
Borçelik Çelik Sanayii Ticaret A.Ş.

Abstract: The demand for lightweight products to reduce CO2 emissions and high safety requirements is an increasing trend, especially in the vehicle and electrical appliance industry. The use of high-strength steels instead of conventional mild steels by using predictive modeling methods in finite element analysis plays a major role. Moreover, physical full-scale crash tests are time-consuming as well as expensive. Crash tolerance analysis in the finite element environment depends on the accuracy of the damage and the definition of the material model parameters. This study examines the damage model GISSMO-Generalized Increasing Stress State-induced damage model and the onset of fracture was calculated by sample optimization via finite element analysis in this study. This research presents the modeling of a specific region of the material fracture curve using the different geometric samples. The results of the numerical simulations are validated by comparing the experimental data of the optimized test samples with their measurements.

Keywords: Gissmo, Damage, Mechanical characterization, Crashworthiness

Introduction

Nowadays, the demand on advanced high strength steels (AHSS) is significantly raising due to its industrial applications especially in automotive and defence industry which includes lightweight design. Brilliant mechanical properties of dual-phase (DP) or multiphase steels with elevated strength as well as improved ductility are chosen rather than other steels. The complexity in microstructure design of AHSS has been an enhanced and superior method to develop the mechanical properties in various grades of steels, such as DP steels (Liu et al., 2019). According to safety legislation the crash avoidance, mitigation the severity of an accident, crash mitigation and reducing injury is significant to address the pedestrian health. Numerical analysis for crashworthiness improves the safety of the cars and hence it considers the human safety. The priority policy of safety legislation of European commission are reducing serious and fatal casualties identified by research are a standardized test method for car-to-car compatibility and truck to car compatibility and improved methods for front and side, improving frontal protection for vulnerable road users, and implementation of Intelligent Speed Adaptation systems, seat belt reminders in all seating positions, alcohol interlocks for fleet drivers, event and journey data recorders and identification of further systems with large potential for casualty savings (Road Safety Annual Report, 2018). Almost all the cars which have 73% CO2 emitted should lower its weight done by different safety components (Hörling, 2015). Crashworthiness simulations are used to develop safety

- Selection and peer-review under responsibility of the Organizing Committee of the Conference

components in the automotive industry (Roth et al., 2016). The simulations may also give valuable information and understanding about different phenomena in a car crash (Bao et al., 2004). Moreover, crash tests of the cars are significantly expensive, and it is not reproducible due to variations in manufacturing (Mohr et al., 2007). Since the development time to launch a new car has been shortened and the demand for better crashworthiness and passive safety the manufacturers must rely more on crashworthiness simulations than before (Gholami et al., 1970). The milestones of related studies in deformation and fracture mechanism of metals have been summarized in literature (Mohr et al., 2004). Different deformation states can be executed by conducting several combinations of loading to test specimens such as butterfly specimen under biaxial loading with a combination of tension/shear and compression/shear (Peirs et al., 2012). The desires stress state is not exactly acquired by these experimental methods, involving biaxial loading setup, separate driving systems (displacement or force controlled) for the horizontal and vertical axes, and complexity in the sample manufacturing process. Another study includes different specimen geometries for a tensile testing device positioned in-plane notches or the out-of-plane notches between two central holes to obtain the shear stress state (Driemeier et al., 2010). The specimen geometry gives better chance to obtain the stress states, but it doesn't give an opportunity to acquire the proportional loading condition at the critical deformation in other words at the onset of necking during the damage tests.

In this study, the mechanical characterization test data were evaluated and optimized with finite element analysis by a new geometrical design with finite element analysis environment. In this context, tensile and compression tests are performed in order to obtain flow curve using Swift and Hockett-Sherby combined material model. This study depends on quick data processing, generally when raw data obtained there several methods to process and prepare for simulations. In the first part of this study the raw data were measured form mechanical tests and the second part includes the optimization with finite element analysis program. The evaluation of finite element analysis is done at Ls-Dyna environment. The validation is done with the real measurement's force-displacement curve.

To obtain different stress states range, a set of damage specimens were produced according to the identical uniaxial tensile test setup. These specimens were investigated with different deformation states of sheet material. The specimen set similarly involves in literature such that shear, notched and sub size tensile specimens. The new design is based on a consistent to tensile specimen, to figure out mid part of material instability curve called smile shear test specimen. On the contrary, it should be noted that despite having the same test set up and specimen geometry, the deformation states may be affected by plastic deformation. The damage model GISSMO-Generalized Incremental Stress State dependent damage model has been investigated and the onset of fracture has been figured out with specimen optimization. According to the literature all the specimen dimensions are redesigned. At a certain region of the material failure curve is modelled using different geometric specimens. The results of the numerical simulations are verified through the comparison of the results with the measurements of experimental data of those optimized test specimens. For the future study, the onset of fracture will be investigated with fractographic experiments.

Method

Material

A DP steel of HDG CR330Y590T-DP with 1.09 mm thickness is considered for the experimental study of the specimen geometry. DP590 is commonly used in automotive industry especially in safety parts. The tests were performed with three repetitions in each direction (rolling, diagonal and transverse) with Euro norm testing speed. The average values with standard deviation of the test results in three directions are given in table 1.

Table 1. The average mechanical properties of CR330Y590T-DP.

t (mm)	Yield Stress(MPa)	Tensile Stress (MPa)	A80 (%)	n	r
1.09 ± 0.02	380 ± 4	694 ± 5	25.2 ± 0.2	0.22	1.02

To acquire the biaxial flow, curve the stack compression tests, which was first proposed by Pawelski (Pawelski, 1967), in which an alternative experiment for acquiring flow curve in a wide range of strain values due to its deformation state, were performed (Merklein et al., 2009). This method is not standardized, and different test investigations and researches are still being made (Hochholdinger et al., 2009).

GISSMO Model and Damage Parameters

The model GISSMO is peculiar to an incremental formulation for damage accumulation and based on a phenomenological background of crashworthiness and can be expressed as (Neukamm et al., 2009),

$$\Delta D = \frac{n}{\varepsilon_f} D^{(1-1/n)} \Delta\varepsilon_v \quad (1)$$

where n is the damage exponent which leads to nonlinear representation of damage accumulation which increases the accuracy of forming and crash analysis. Moreover, $\Delta\varepsilon_v$ and ε_f describe the notation for the incremental step in equivalent plastic strain and triaxiality dependent failure strain in other words equivalent plastic strain to failure, respectively. The triaxiality is a measure of stress state acquired in different deformation states and given as,

$$\eta = \frac{\sigma_H}{\sigma_V} \quad (2)$$

where σ_H and σ_V represent hydrostatic and equivalent von Mises stress, respectively. The damage threshold, D_{crit}, is defined either as a fixed value or as a function of the forming intensity at the actual

state of deformation. When the damage reaches this curve for the actual triaxiality the damage threshold will be stored for the actual element and the flow stress and the damage will be coupled and the effective stress tensor which is expressed as,

$$\sigma_r = \sigma_n \left[1 - \left(\frac{D - D_{crit}}{1 - D_{crit}}\right)^m\right] \quad (3)$$

where m is the fading exponent which alters the stress state and checks the energy dissipation depending on element size in the analysis.

In this study, the five different specimens convenient for testing on tensile testing device covering the triaxiality range between pure shear and biaxial strain are selected for the identification of damage model parameters. The flow curve of dual phase steel and the tensile & stack compression test specimens are shown in Figure 1 and Figure 2, respectively. The test specimens are cut on electric discharge machine in the rolling direction. Their force vs. displacement curves serve as experimental data for the inverse optimization process.

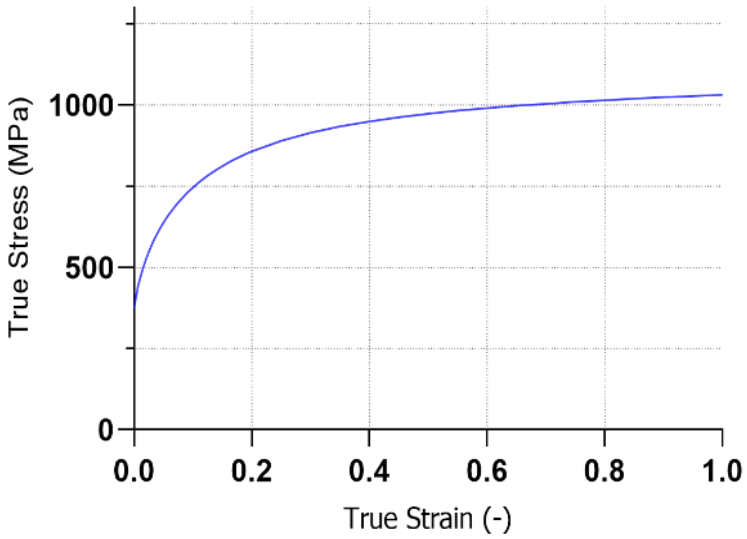

Figure 1. True stress-strain curve of CR330Y590T-DP with the thickness of 1.09 mm.

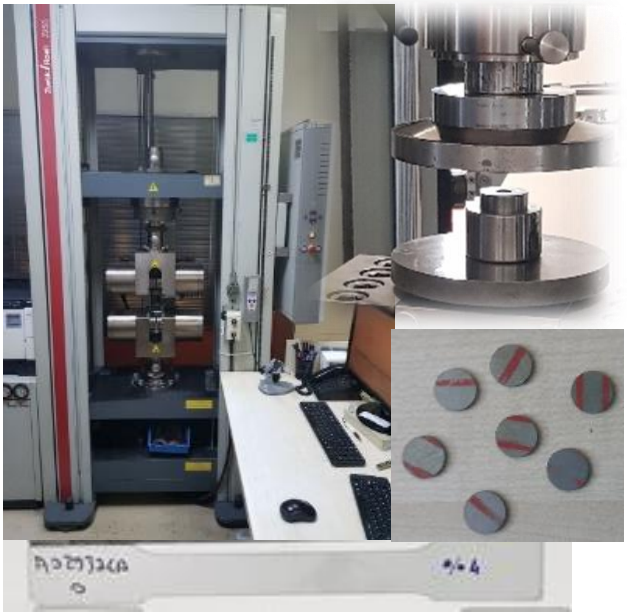

Figure 2. The test specimens for initial material characterization.

Numerical Analysis

Five different geometries are conducted to obtain different triaxiality paths. Numerical analysis of the test specimen is conducted to acquire insight into the deformation states details. Furthermore, the numerical analysis can also be used to reveal the effect of the design of the geometry on localization and distribution of strains at the beginning of necking. Regarding to this, Ls-Dyna is used as the simulation environment. The MAT-36 3 Parameter Barlat material model is used to model the test specimens. A mild steel is considered for optimizing the geometries, since it is found to be commonly used materials of its wide application range in automotive industry. The finite element analyses were conducted with Borcelik material cards. The initial mesh size was 0.5 mm, with 5 integration points. The triaxiality path are plotted using these geometries. In figure 3 and figure 4, the optimized geometries are illustrated both for FEA and experiments. In figure 5, the triaxiality paths are demonstrated and the critical points for determination of material failure and instability curves will be used according to this point.

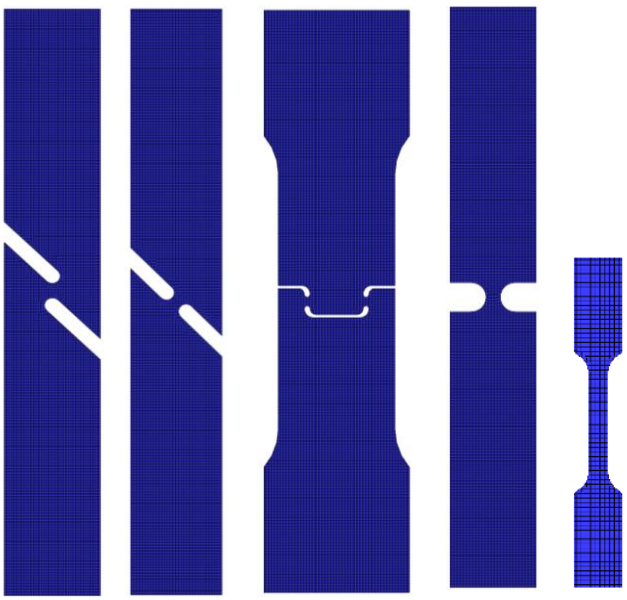

Figure 3. The undeformed test specimens used for modelling damage parameters

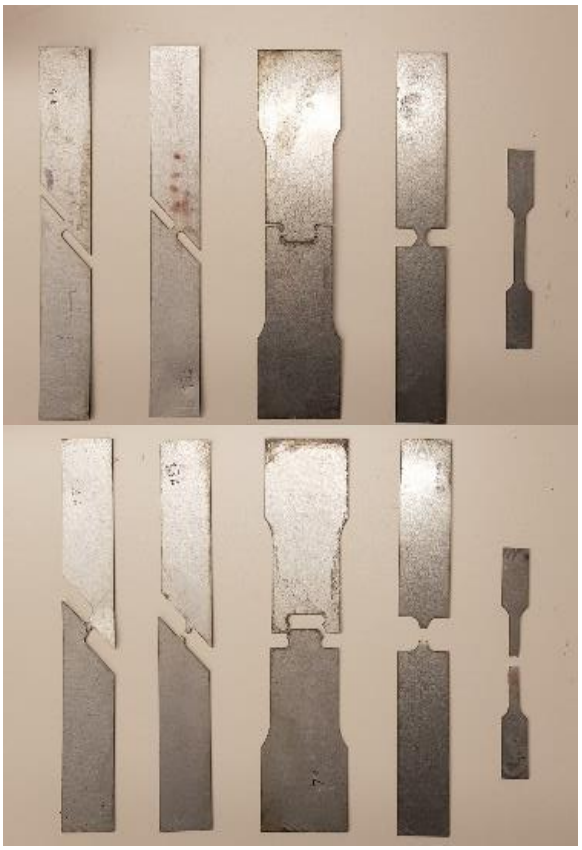

Figure 4. Deformed and undeformed test specimens for experimental study

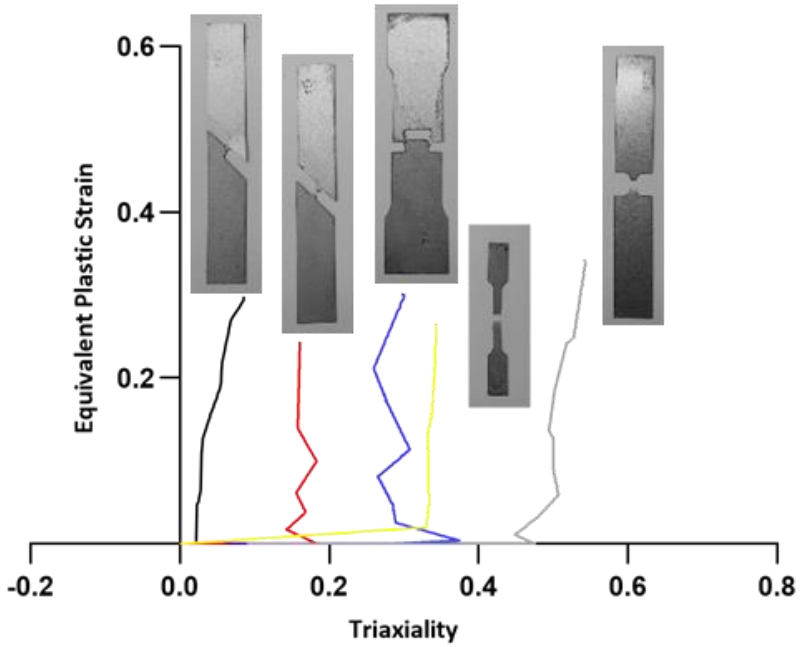

Figure 5. The triaxiality strain path of mild steel with 5 different geometries.

Results and Discussion

The simulations were executed with material model MAT_PIECEWISE_LINEAR_PLASTICITY, which is generally used in car crash simulations in order to reach the preliminary behaviour while identifying the GISSMO parameters.

Determination of Damage Parameters

To recognize the failure and failure behaviour of the test specimens, another material model is added, which is MAT_ADD_EROSION. This material includes the GISSMO parameters and curves that can be found via LS-OPT environment. The optimization is executed with respect to force displacement curves of experimentally achieved results. Along with optimization studies, transition models to enhance compatibility of finite element analysis vs. experimental results have been built. In this context, the force displacement curves of five specimens illustrated in figure 5 are used. 20 iterations have been established and for each iteration 50 simulations have been conducted in order to improve the accuracy of results. In figure 6, the material failure and instability curves are illustrated.

Determination of Parameters with Different Mesh Size

In crash simulations, much course meshes are used, so the characteristic element length differs in fading and regularization curves and necessitates to regularize those curves using larger mesh sizes. Regarding to this, uniaxial tensile test geometry is used beginning from 1 mm to 10 mm mesh size. The mesh size and the regularization curves are demonstrated. Since the parameters of these mesh dependent curve parameters, the optimization could be easily figured out via LS-OPT without having high computational cost.

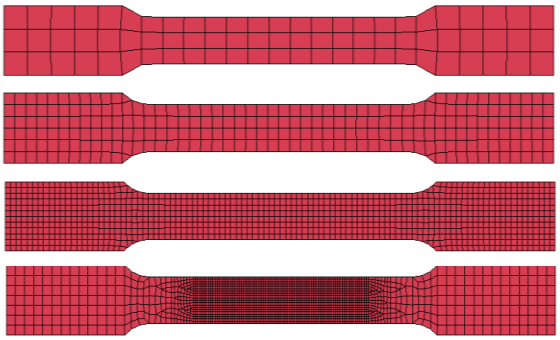

Figure 7. The undeformed test specimens used for mesh dependent modelling of GISSMO card.

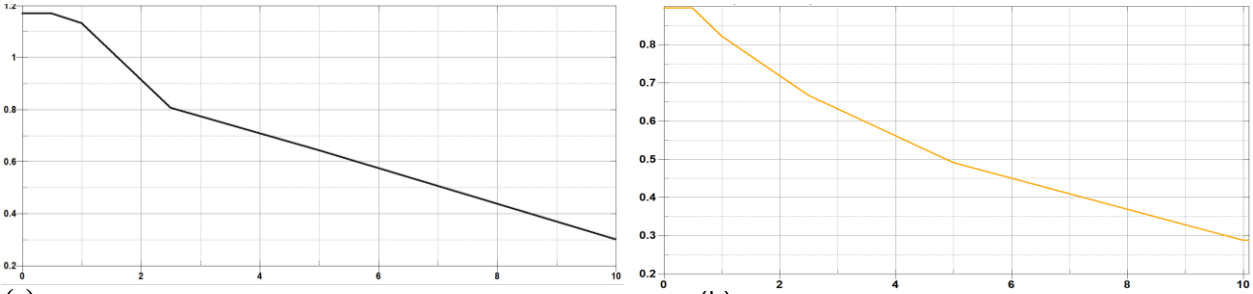

(a) (b)

Figure 8. Fading curve after meshing dependent optimization (a) and regularization curve (b)

Validation of Damage Parameters on a Physical Testing Specimen

To verify the applicability of the identified parameters and the regularization curves, the GISSMO model is used in a real tensile test specimen. The test specimen is modelled with 1 mm mesh size with 5 number of through shell thickness integration points. The mesh size and deformation result of galvanized sheet strip are illustrated in figure 9.

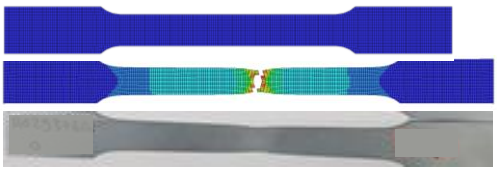

Figure 9. Equivalent plastic strain results at different localized necking regions.

According to the test results, the comparison of the force-displacement and engineering stress &strain curves show good agreement between the experiment and the simulations, figure 10. As can be seen in figure 10, the finite element test result of GISSMO material model after fine tuning operation is in the test results interval in all directions. The FEA result from both graphs matched well in diagonal test direction test specimen result.

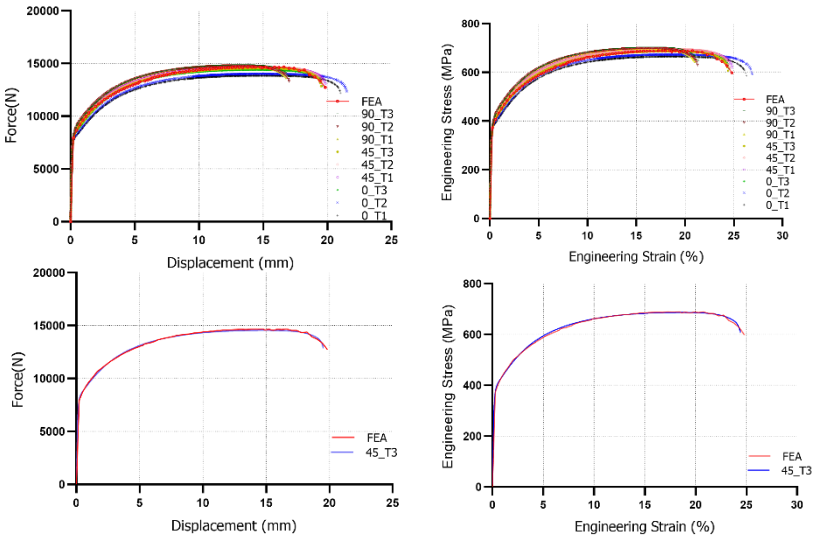

Figure 10. The comparison between FEA and experimental results after fine tuning of GISSMO material model.

Conclusion

In this study, an inverse identification method for the GISSMO damage model parameters has been considered and the damage model GISSMO-Generalized Incremental Stress State dependent damage model has been investigated and the onset of fracture has been figured out with specimen optimization. The use of high strength steels instead of conventional lightweight steels has a major role with predictive modelling methods in finite element analysis. Crashworthiness analysis in finite element environment depends on the accuracy of damage and material model parameters description. The onset of fracture has been shown via finite element analysis. At a certain region of the material failure curve is modelled using different geometric specimens. In regularization curves and fine tuning of damage parameters fine and homogeneous discretization with an element size of 0.5 mm has been used and the mesh dependent parameters have been regularized by using the uniaxial tensile test. It has been concluded that the experimental results have good agreement with finite element analysis results.

Recommendations

Especially in high formable deep drawing operations it is possible to decide which damage parameter could be offered to end-user with the execution of numerical analysis. As future work, fracture mechanism of optimized specimens should be investigated via fractography.

Acknowledgements or Notes

We would like to thank Ali Sulukoy, who is the supervisor of Metallurgy Quality Department in Borcelik Celik Sanayii Ticaret AS, for his valuable contributions in this study.

Scientific Ethics Declaration

The authors declare that the scientific ethical and legal responsibility of this article published in EPSTEM journal belongs to the authors.

References

Bao, Y., & Wierzbicki, T. (2004). On fracture locus in the equivalent strain and stress triaxiality space. *International Journal of Mechanical Sciences*, *46*(1), 81–98. https://doi.org/10.1016/j.ijmecsci.2004.02.006

Driemeier, L., Brünig, M., Micheli, G., & Alves, M. (2010). Experiments on stress-triaxiality dependence of material behavior of aluminum alloys. *Mechanics of Materials*, *42*(2), 207–217. https://doi.org/10.1016/j.mechmat.2009.11.012

Gholami, T., Lescheticky, J., & Paßmann, R. (2003, June). Crashworthiness simulation of automobiles with ABAQUS/Explicit. In *Journal of Abaqus User Conference*. BMW Group.

Hochholdinger, B., Grass, H., Lipp, A., Hora, P., & BMW AG, M. (2009). *Determination of flow curves by stack compression tests and inverse analysis for the simulation of hot forming.* 7th European LS-DYNA conference.

Hörling, D. (2015). *Parameter identification of GISSMO damage model for DOCOL 1200m: A study on crash simulation for high strength steel sheet components*. DIVA. http://kau.diva-portal.org/smash/record.jsf?pid=diva2%3A845116&dswid=-9443.

Liu, W., Lian, J., & Münstermann, S. (2019). Damage mechanism analysis of a high-strength dual-phase steel sheet with optimized fracture samples for various stress states and loading rates. *Engineering Failure Analysis*, *106*, 104–138. https://doi.org/10.1016/j.engfailanal.2019.08.004

Merklein, M., & Kuppert, A. (2009). A method for the layer compression test considering the anisotropic material behavior. *International Journal of Material Forming*, *2*(1), 483–486. https://doi.org/10.1007/s12289-009-0592-8

Mohr, D., & Doyoyo, M. (2004). Experimental investigation on the plasticity of hexagonal aluminum honeycomb under multiaxial loading. *Journal of Applied Mechanics*, *71*(3), 375–385. https://doi.org/10.1115/1.1683715

Mohr, D., & Henn, S. (2007). Calibration of stress-triaxiality dependent crack formation criteria: A new hybrid experimental–numerical method. *Experimental Mechanics*, *47*(6), 805–820. https://doi.org/10.1007/s11340-007-9039-7

Neukamm, F., Feucht, M., & Haufe A. (2009). The stamping to crash simulation process chain: A study of damage parameters with regard to element size dependency in the crashworthiness prediction.

Pawelski, O. (1967). Über das Stauchen von Hohlzylindern und seine Eignung zur Bestimmung der Formänderungsfestigkeit Dünner Bleche. *Archiv Für Das Eisenhüttenwesen*, *38*(6), 437–442. https://doi.org/10.1002/srin.196704204

Peirs, J., Verleysen, P., & Degrieck, J. (2012). Novel technique for static and dynamic shear testing of ti6al4v sheet. *Experimental Mechanics*, *52*(7), 729–741. https://doi.org/10.1007/s11340-011-9541-9

Road Safety Annual Report. (2018). *Road Safety Annual Report 2018*, 4–12. https://doi.org/10.1787/1c884dcb-en

Roth, C. C., & Mohr, D. (2016). Ductile fracture experiments with locally proportional loading histories. *International Journal of Plasticity*, *79*, 328–354. https://doi.org/10.1016/j.ijplas.2015.08.004

Author Information

M. Emin TAMER
Borcelik Celik Sanayii Ticaret AS
Ata, 125 Nolu Sokak No:1, 16601 Gemlik/Bursa, Turkey
Contact e-mail: *emint@borcelik.com*

Almila Gulfem OZGULTEKIN
Borcelik Celik Sanayii Ticaret AS
Ata, 125 Nolu Sokak No:1, 16601 Gemlik/Bursa, Turkey

Beyzanur AYDIN
Borcelik Celik Sanayii Ticaret AS
Ata, 125 Nolu Sokak No:1, 16601 Gemlik/Bursa, Turkey

To cite this article:

Tamer, M.E., Ozgultekin, A.G., & Aydin, B. (2021). Gissmo failure modelling for crashworthiness analysis using different test specimens. *The Eurasia Proceedings of Science, Technology, Engineering & Mathematics (EPSTEM), 16*, 31-38.

The Eurasia Proceedings of Science, Technology, Engineering & Mathematics (EPSTEM)
ISSN: 2602-3199

The Eurasia Proceedings of Science, Technology, Engineering & Mathematics (EPSTEM), 2021

Volume 16, Pages 39-46

IConTES 2021: International Conference on Technology, Engineering and Science

Determination ARIMA Model for the Discharge Acid Concentration in Pressure Oxidation Autoclave at A Gold Processing Plant

Adem TASDEMIR
Eskişehir Osmangazi University

Ibrahim CELIKYUREK
Eskişehir Osmangazi University

Bedri BAKSAN
Eskişehir Osmangazi University

Abstract: During industrial production, many quality parameters of products are measured to evaluate the quality of final products. These investigations are also applied for the machine parameters to control if they work properly. A huge amount of data is collected, recorded, and evaluated for these aims. Time series analyses are often a useful tool to evaluate the industrial data to analyze the products quality parameters or machine performances. The autoregressive integrated moving average (ARIMA) time series models are the most known and used method. One of the most important advantages of ARIMA models is its capability of near future estimation for the monitored process variable. For this aim, current research is carried out at a gold processing plant data. The plant gains the gold by applying the modern pressure oxide leaching in autoclave and cyanide leaching. Since the gold ore characteristics can be changed even, they are mined in the same mining area, monitoring the product quality and machine performances during production stages are needed. In this research, the data set, which was recorded at equal sampling time intervals and obtained in a month, is supplied from a gold processing plant in Turkey. During the gold production, the ground gold ore is subjected to the desulphurization process by pressure oxide (POX) in the autoclave. Discharge acid concentration is critical in this process and it is followed regularly by taking samples in 2 hours' time intervals in 24 hours. Using discharge acid concentration data set, the ARIMA (1,0,1) time series model was determined to monitor it. Also, near-future values of acid concentration were estimated by the ARIMA (1,0,1) model and compared with the real discharge acid concentrations. It was determined that there was a very good agreement between the estimated values obtained by the ARIMA (1,0,1) model and real values.

Keywords: Time series, ARIMA (1,0,1) model, Gold processing, Pressure oxidation, Acid concentration

Introduction

As of 2019, it is estimated that 197,596 tons of gold have been mined throughout history. Two thirds of this amount have been produced after 1950 (World Gold Council, 2021). In Turkey, gold production started in 2001 and the number of plants that started operating until 2020 was 18. Gold production, which started with 1.4 tons, reached 42 tons in 2020 and the total production reached 382 tons in 20 years (Altın Madencileri Derneği, 2021). As of 2019, Turkey has imported a total of 3215 tons of gold in the last 20 years. Turkey's gold reserve is 1500 tons and gold potential is 4618 tons (Altın Madencileri Derneği, 2021).

Despite the increasing gold production, Turkey ranks 5th among the countries that import the most gold in the world. Turkey's gold import, which was around 156 tons/year in last 20 years, reached 324 tons in 2018 (M. E.

N. R., 2021). It is clear that Turkey, which is an important gold importer, will make great contributions to the country's economy in many aspects if it evaluates its current gold reserves.

The properties that determine the selection and effectiveness of the gold recovery process are ore grade, mineralogy, determination of gold-bearing minerals, grain size distribution of gold, grain size distribution of main and gangue minerals, mineral metamorphoses, liberation properties of gold minerals, form of gold in the ore (Şen, 2007). In the enrichment of gold ores, while gravity, amalgamation and agglomeration methods are used for coarse-grained gold-bearing ores, for fine-grained and low-grade ores flotation and hydrometallurgical methods can be used (Bhappu, 1990). In general, if the gold particles are microscopically dispersed, solution technology is used with the of cyanide. Over 120 years, cyanidation technology has been used in 84% of the world's gold production. (Bhappu, 1990).

In the acidic environment under high pressure and temperature where oxygen is used as oxidizer, the sulphide minerals that make up the refractory ores can be separated. This process is carried out in specially designed reactors called as autoclave (Marsden et. a., 2006). This process is not applied to whole ores, it is a pre-concentration stage prior to cyanidation. At this stage, gold grains found in the inclusions are liberated, sulfide minerals are oxidized and the ore is made suitable for cyanide leaching (Rusanen et. al, 2013).

In literature, investigations of time series in gold production were mainly application for gold price forecasting. Many researchers have been successfully forecasted the gold price by using ARIMA models (Triphaty, 2017; Davis et al., 2014; Guha et. al., 2016; Sharma et. al., 2015; Khan, 2013; Ali et. al., 2016). However, there is any academic research of ARIMA models on the gold processing plant to forecast any parameters. In this research, the data of discharge acid concentration of POX autoclave were used to test if ARIMA time series models could be used as a useful tool for forecasting the discharged acid concentration

Method

In this study, we used discharged acid concentration data of a pressure oxidation (POX) autoclave at a gold processing plant in Turkey. General flowsheet of the gold processing plant is given in Figure 1. At this gold processing plant, the ground ore is subjected to desulphurization process by POX in the autoclave since the main gang mineral of ore is pyrite (FeS2) which is an iron sulphur mineral. The purpose of the autoclave and pressure oxidation (POX) operation in gold processing is to pretreat the gold ore to prepare it suitable for cyanidation. Sulphide minerals contain fine-grained gold particles. Oxidation of sulphide minerals, mostly pyrite to sulphates and oxides releases gold particles. Then using cyanide, gold is extracted into a solution in the downstream circuit. Therefore, the sulphur is oxidized by a pressure autoclave prior to cyanide tank leaching (Figure 1). Discharge acid concentration is critical in this process and this is controlled regularly by taking samples in 2 hours' time intervals (12 samples are taken and analyzed for acid concentration in 24 hours).

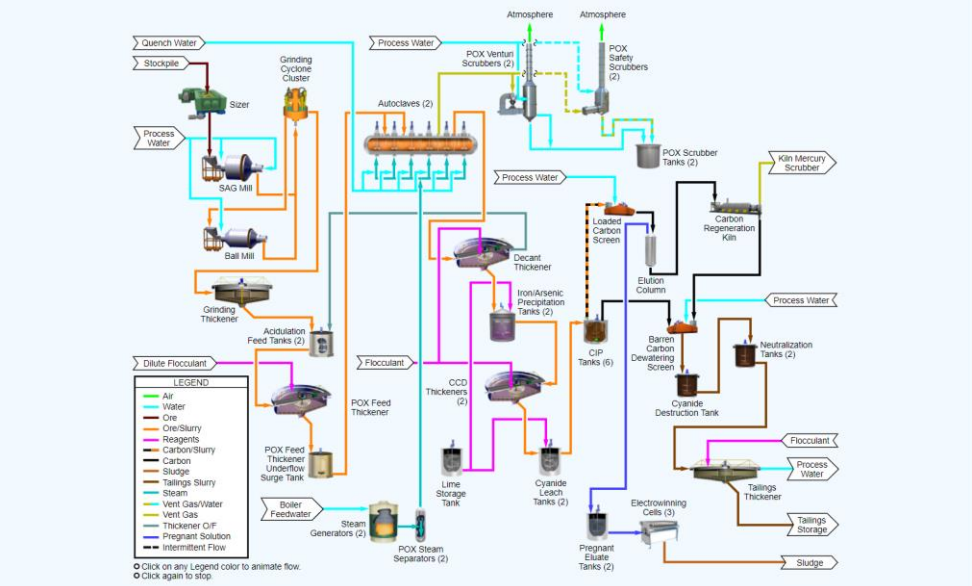

Figure 1. General flowsheet of gold processing plant

In order to evaluate the time dependent acid concentration data, totally 337 measured discharged acid data of POX circuit were obtained and used. Properties and ARIMA time series modelling studies of the data were carried out by using trial versions of Minitab 16.0 and Statgraphics XV softwares.

ARIMA (p,d,q) Time Series Model

There are many published textbooks available in the literature for time series analysis methods and models (Box et. al., 1976, Montgomery et al., 2008; Montgomery et. al., 2011). The readers can find detailed information in these books and the references cited in there. In short, time series analysis is used when observations are over 50 and they are obtained from equally spaced data periods (Datajobs, 2021). Time series analysis is used to forecast future patterns of events or to compare series of different kinds of events. The ARIMA, which is an acronym of **A**uto **R**egressive, **I**ntegrated, **M**oving **A**verage, model of a time series model is defined by three terms (*p*,*d*,*q*). The models are written as ARIMA(*p*,*d*,*q*). Identification of a time series is the process of finding values of *p*, *d* and *q*. The *p*, *d* and *q* describe the autoregressive (AR) part, integrated part (I) and moving average (MA) part of ARIMA models respectively. The *AR* denotes the function between current observation and previous observations, *I* represent if the investigated data values are used directly or they need to be differenced, *MA* explains if the current data depends the previous' error.

Autocorrelation and Determination of ARIMA Time Series Model

The correlation between consequence measurements (current observations of X_t and the observation from *p* periods before the current one, X_{t-p}) is defined as autocorrelation (Montgomery et al., 2008). The autocorrelation at given lag of *k* is calculated from the following formula:

$$r_k = \frac{\sum_{t=k+1}^{n}(y_t - \bar{y})(y_{t-k} - \bar{y})}{\sum_{t=1}^{n}(y_t - \bar{y})^2} \quad (1)$$

Results and Discussion

Data Properties of Discharged Acid Data

The normal probability plot with Anderson Darling (AD) normality test results (goodness of fit) is presented in Figure 2. As seen *p* value of test is 0,519 (>0,05) with AD value of 0,327. This result indicates that the data obey the normal distribution very well and there is no need any transformation. The mean value of 337 data is 21.82 g/L with standard deviation of 3,365.

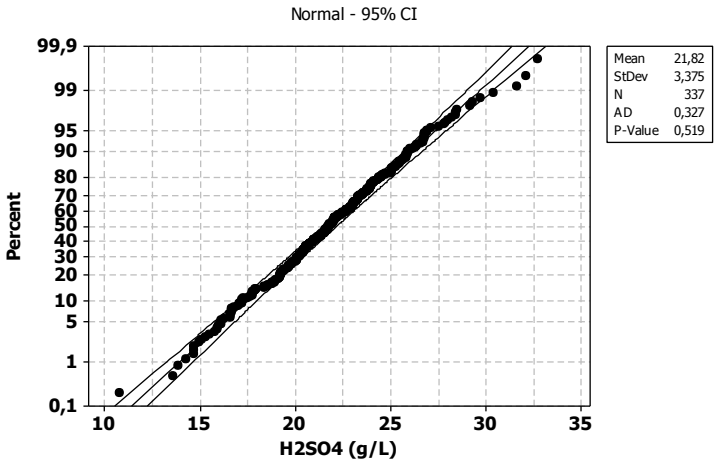

Figure 2. Probability plot of discharged acid concentration of POX

Time series plot in Figure 3 shows that the data used is stationary over time. This means that the data are not need to be differenced. Therefore, the integrated part (*d*) of ARIMA(*p*,*d*,*q*) model is 0 for the discharged acid concentration of POX autoclave.

Figure 4 gives the correlation relationship between the current observation (T) and the previous observation (t-1) at lag 1 for the acid concentration data. It seen clearly that consequent data observations of acid concentrations have an important correlation. They show symmetrical distribution around 1:1 line.

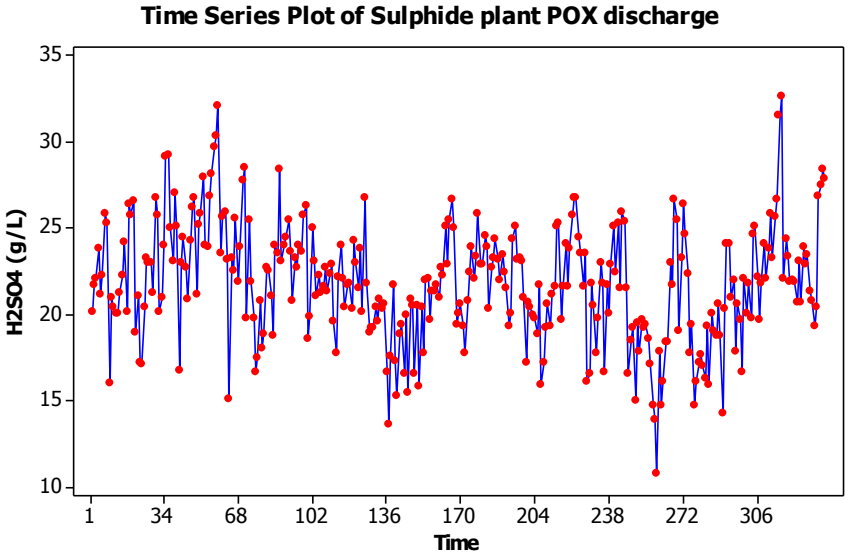

Figure 3. Time series plot of POX's discharged acid concentration

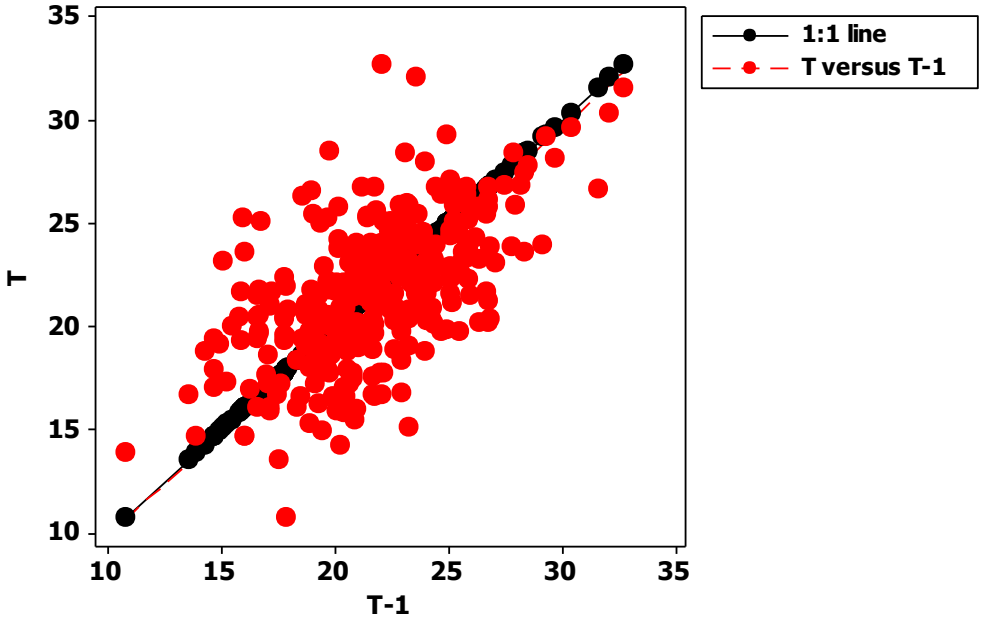

Figure 4. Scatter plot for *T* and *T-1*

In Figure 5, the autocorrelation function (ACF) and the partial autocorrelation (PACF) plots are presented. As seen, ACF decays quickly for the first five lags then almost constant within the 95% confidence limits and only one important spike exists in the first lag of PACF plot then decays immediately. This means that autocorrelation is explained efficiently by lag 1 autocorrelation. As shown in ACF plot, it was determined that coefficients of acid concentrations at lag 1 have a value of 0,585 and it is equal to 0,419 at lag 2.

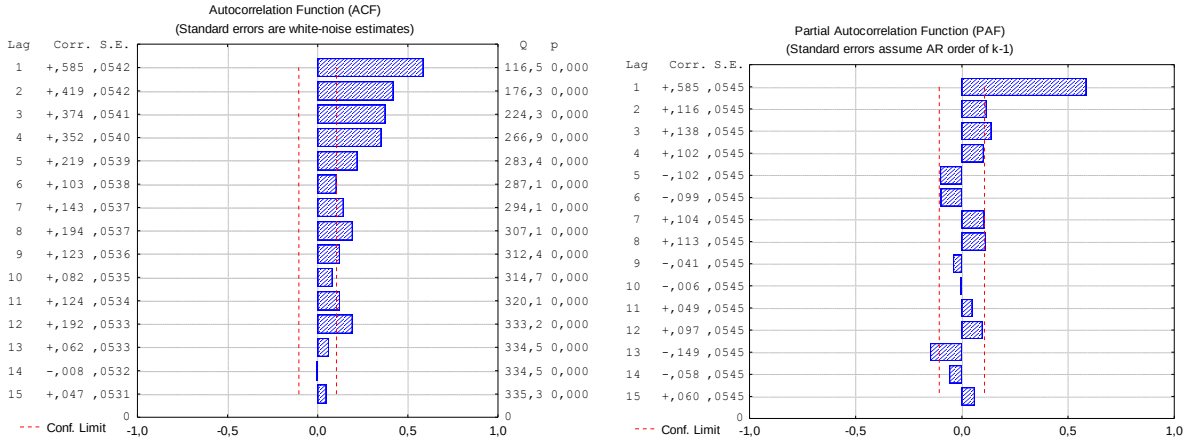

Figure 5. ACF and PACF plots for 15 lags of POX's discharge acid concentration

Table 1 compares the results of fitting some possible ARIMA time series models to the POX's discharged acid concentration data. Between the models, the model with the lowest value of the Akaike Information Criterion (*AIC*) is the ARIMA (1,0,1) model. Therefore, this model was chosen to generate the forecasts of discharged acid concentration.

Table 1. ARIMA models for the POX's acid discharge data

Model	*AIC*
ARIMA(1,0,1) with constant	2,005
ARIMA(1,0,2) with constant	2,00621
(ARIMA(1,1,2)	2,01398
ARIMA(2,0,2) with constant	2,01459
ARIMA(2,0,0) with constant	2,01672

The output presented in Table 2 summarizes the statistical significance of the ARIMA (1,0,1) model terms in the forecasting. ARIMA (1,0,1) model with constant, or ARMA(1,1)model, is described as following Equation 2 (Castagliola et. al., 2005):

$$X_t = \delta + \emptyset X_{t-1} + \theta a_{t-1} + a_t \qquad 2)$$

Here; δ is the constant of the model, $\emptyset$ is the constant of autoregressive (AR) term of the model, θ is the constant of moving average (MA) of the model, a_t is the error term, normal random shock (white noise) at time *t*. White noise is assumed to be independent and identically distributed normal (0, σ_a^2), σ_a^2 is the variance random noise (white noise variation).

In ARIMA (1,0,1) model, the AR (1) constant, i.e. δ, is equal to μ (1- $\emptyset$). Then it is equal to 21,8699*(1-0,793677) = 4,51226 (Table 2).

Terms with *p*-values less than 0,05 are statistically significantly different from zero at the 95,0% confidence level. The *p*-value for the AR (1) term is less than 0,05, so it is significantly different from 0. The *p*-value for the MA (1) term is less than 0,05, so it is significantly different from 0. The *p*-value for the constant term is less than 0,05, so it is significantly different from 0. The estimated standard deviation of the input white noise (σ_a) equals 2,70106.

Table 2. ARIMA (1,0,1) model summary

Parameter	*Estimate*	*Stnd. Error*	*t*	*P-value*
AR(1), $\emptyset$	0,793677	0,0559039	14,1972	0,000000
MA(1), θ	0,325924	0,0845613	3,85429	0,000139
Mean, μ	21,8699	0,469544	46,5769	0,000000
Constant, δ	4,51226			
White Noise Variance (σ_a^2)	7,29572			
White Noise Std. Dev. (σ_a)	2,70106			

The final time series equation obtained from the ARIMA(1,0,1) model is given in the following.

$$X_t = 4{,}51226 + 0{,}7937\,X_{t-1} + 0{,}3259\,a_{t-1} + a_t \quad (2)$$

a_t: Random noise or white noise at time =1, 2,…. which has a mean of zero (0) and standard deviation of σ_a i.e., $N(0; 2{,}70106)$

The diagnostic check results of ARIMA (1,0,1) model is given in Figure 6. The ACF plots of residuals (the difference between actual and estimated acid concentrations) shows that, the residuals are not autocorrelated (autocorrelation at lag 1 eliminated). In the right plot of Figure 5, the ARIMA (1,0,1) model residuals are distributed normally, has a mean of zero (0). The residuals are distributed homogeneously around zero, showing the adequacy of the model.

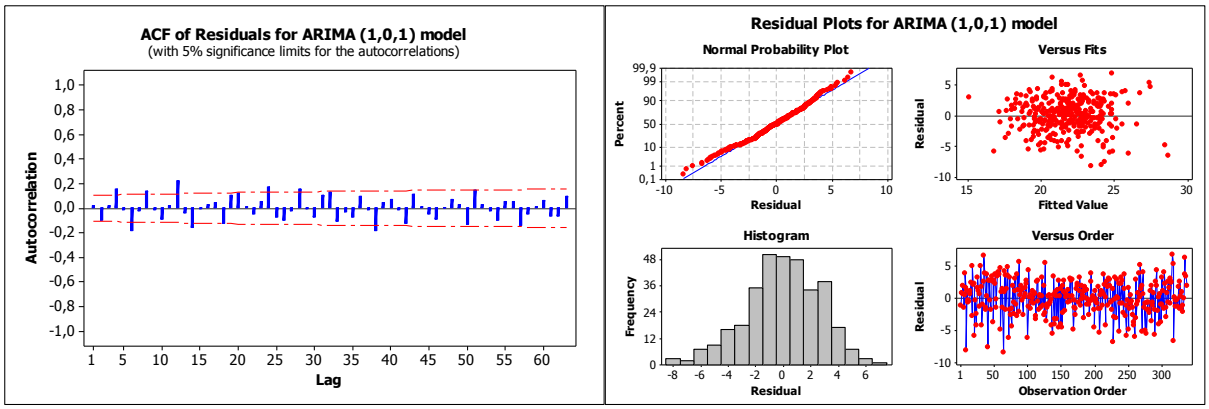

Figure 6. ACF of residuals and residual plots for fitted ARIMA (1,0,1) model

In Figure 7, the actual and estimated acid concentrations by Equation 2 are given in the same plot. It seems that the forecasting model of ARIMA (1,0,1) model has a high accuracy to estimating the discharges acid concentration of POX autoclave in gold processing plant.

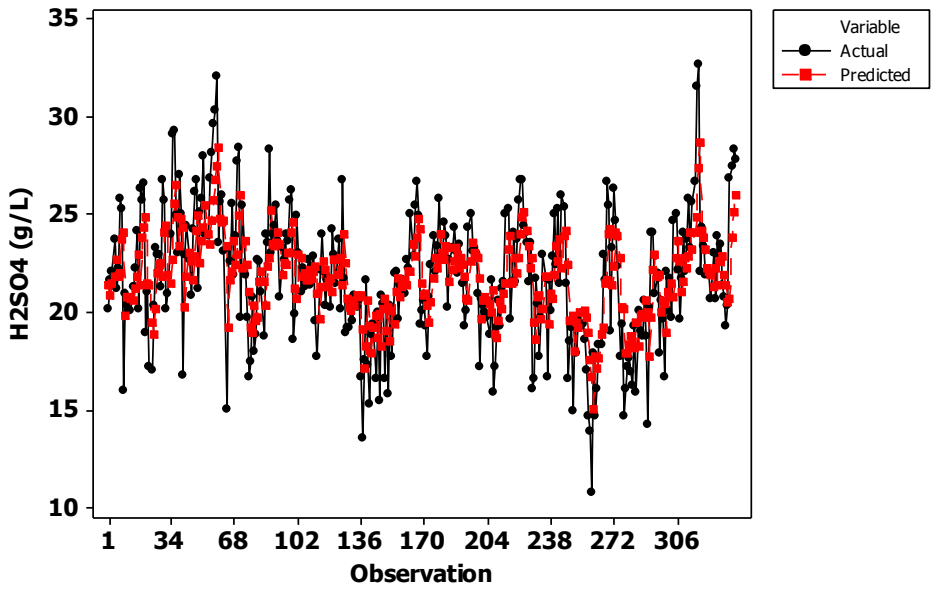

Figure 7. Actual versus predicted plot

Using the historical data, time series forecasting for near future observations can be done. For this aim, the performance of ARIMA (1,0,1) model was tested to forecast real data of the last 24 hours acid concentrations (measurements of 326-337 data). Actual and model fitted values are plotted within the 95% confidence limits and is presented in Figure 8. The ARIMA (1,0,1) model gives very good forecasting performance since all the actual data values forecasted are within the 95% confidence limits.

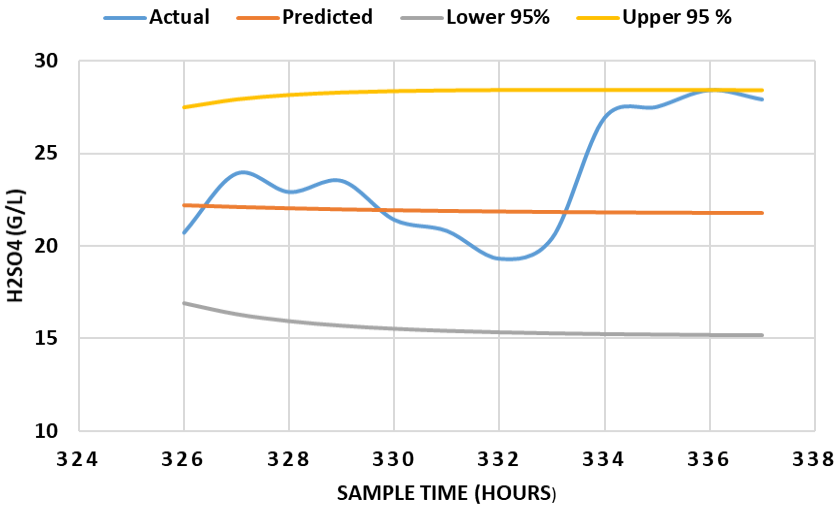

Figure 8. Actual versus predicted acid concentration of POX discharge for the last 12 hours by ARIMA (1,0,1) model

Figure 9 shows the near future forecasting of acid concentrations of POX autoclave for the next 24 hours (338-349 data).

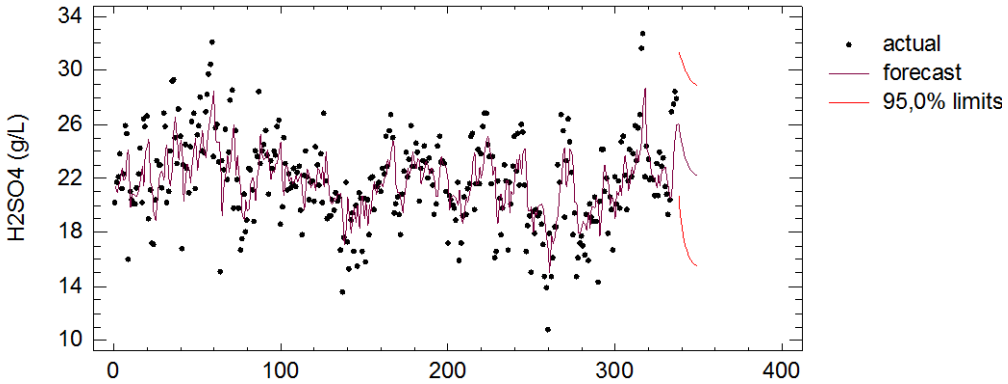

Figure 9. Actual points and forecasted discharge acid concentration. Near future estimation with 95% limits for the next 24 hours

Conclusion

In a gold processing plat, many critical parameters in different production stages should be controlled to reach a high production recovery. The parameter of discharged acid concentration from POX autoclave device is only one of these parameters. The results of this investigation indicate that forecasting is possible for discharge acid concentration by using historical data. It was determined that these data have important autocorrelation. This research showed that ARIMA (1,0,1) model can be used conveniently for forecasting the discharge acid concentration of POX autoclave in a gold processing plant. When the statistical process control (SPC) method is applied to control of quality parameter if the process is under control or not, the important autocorrelation determined in this study should be taken into account. Since wrong uncontrolled points are detected and the process control are interpreted wrong, the autocorrelation assumptions should be verified in SPC applications.

Scientific Ethics Declaration

The authors declare that the scientific ethical and legal responsibility of this article published in EPSTEM journal belongs to the authors.

References

Ali, A., Iqbal, C., M., Qamar, S., Akhtar, N., Mahmood, T., Hyder, M. & Jamshed, M. T. (2016). Forecasting of daily gold price by using Box-Jenkins methodology. *International Journal of Asian Social Science, 6(11),* 614-624.

Bhappu, B. R. (1990). Hydrometallurgical processing of precious metal ores. *Mineral Processing and Extractive Metallurgy Review, 6*(4), 67-80.

Box, G. E., Jenkins, G. M., Reinsel, G. C., & Ljung, G. M. (2015). *Time series analysis: forecasting and control*. John Wiley & Sons.

Castagliola, P. & Tsung., F. (2005). Autocorrelated SPC for non-normal situations. *Quality and Reliability Engineering Journal, 21*, 131-161.

Davis, R., Dedu, V. K. & Bonye, F. (2014). Modeling and forecasting of gold prices on financial markets. *American Journal of Contemporary Research, 4*(3), 107-113.

Guha, B. & Bandyopadhyay, G. (2016). Gold price forecasting using ARIMA model. *Journal of Advanced Management Science, 4*(2), 117-121.

Khan, M. M. A. (2013). Forecasting of gold prices (Box Jenkins approach). *International Journal of Emerging Technology and Advanced Engineering, 3*(3), 662-670.

Marsden, J. O., & House, C. I. (2006). The chemistry of gold extraction. In *Society for Mining, Metallurgy, and Exploration.* Littleton.

Montgomery, D. C., Jennings, C. L. & Kulahçı, M. (Eds.) (2008). *Introduction to time series analysis and forecasting*. John Wiley & Sons.

Montgomery, D. C., & Runger, G. C. (2010). *Applied statistics and probability for engineers*. John Wiley & Sons.

Rusanen, L., Aromaa, J. & Forsen, O. E. (2013). Pressure oxidation of pyrite-arsenopyrite refractory gold concentrate. *Physicochemical Problems of Mineral Processing, 49*, 101-109.

Sharma, A. M. & Baby, S. (2015). Gold price forecasting in India using ARIMA modelling. *GE-International Journal of Management Research, 3*(10), 14-33.

Şen, S. (2007). *Evaluation of coal-oil assisted gold flotation as a novel processing method for gold recovery*. [Unpublished doctoral dissertation]. Dokuz Eylül Üniversitesi.

Triphaty, N. (2017). Forecasting gold price with autoregressive integrated average model. *International Journal of Economics and Financial Issues. 7*(4), 324-329.

M. E. N. R. (2021, October 18). Altın. Ministry of Energy and Nature Reserves. https://enerji.gov.tr/bilgi-merkezi-tabi-kaynaklaraltin

Datajobs, (2021, October 19). Time series analysis. https://datajobs.com/data-science-repo/Time-Series-Analysis-Guide.pdf

Altın Madencileri Derneği, (2021, October 25). Türkiye'nin altın potansiyeli-Rezervi ve Üretimi, http://altinmadencileri.org.tr/turkiyenin-altin-potansiyeli/

Altın Madencileri Derneği, (2021, October 25). Türkiye'nin Altın üretimi. http://altinmadencileri.org.tr/turkiye-altin-uretimi-2/

World Gold Council, (2021, October 25). How much gold has been mined? https://www.gold.org/about-gold/gold-supply/gold-mining/how-much-gold/

Author Information

Adem TASDEMIR
Eskişehir Osmangazi University
Mining Engineering Department
26480, Batı Meşelik, Eskişehir, Turkey
Contact e-mail: *atasdem@ogu.edu.tr*

Ibrahim CELIKYUREK
Eskişehir Osmangazi University
Metallurgy and Materials Engineering Department
26480, Batı Meşelik, Eskişehir, Turkey

Bedri BAKSAN
Eskişehir Osmangazi University
Metallurgy and Materials Engineering Department
26480, Batı Meşelik, Eskişehir, Turkey

To cite this article:

Tasdemir, A., Celikyurek, I., & Baksan, B. (2021). Determination ARIMA model for the discharge acid concentration in pressure oxidation autoclave at a gold processing plant. *The Eurasia Proceedings of Science, Technology, Engineering & Mathematics (EPSTEM), 16*, 39-46.

The Eurasia Proceedings of Science, Technology, Engineering & Mathematics (EPSTEM)
ISSN: 2602-3199

The Eurasia Proceedings of Science, Technology, Engineering & Mathematics (EPSTEM), 2021

Volume 16, Pages 47-51

IConTES 2021: International Conference on Technology, Engineering and Science

Synthesis of rGO/g-C_3N_4 Composite Cathodes for Li – Ion – Oxygen Battery

Ersu LOKCU
Eskisehir Osmangazi University

Nilay KACAR
Eskisehir Osmangazi University

R. Can OZDEN
Eskisehir Osmangazi University

Mustafa ANIK
Eskisehir Osmangazi University

Abstract: The low-cost electro-catalysts are very crucial for the lithium-ion oxygen battery electrodes. In this work porous reduced graphene oxide (rGO) was synthesized by the chemical methods and mixed with melamine to obtain rGO/graphitic-C_3N_4 (g-C_3N_4) composite which compose of 50% rGO and 50% g-C_3N_4. SEM, XRD and FTIR characterizations showed that the synthesized composite structure reflected most of the features of the rGO structure. The synthesized rGO/g-C_3N_4 composite was prepared as the cathode for the Li-ion-oxygen battery and its discharge/charge performance was determined. The composite cathode demonstrated a distinctive performance since g-C_3N_4 catalyzed both the oxygen reduction and oxygen evolution reactions during the discharging and charging. This work showed that rGO/g-C_3N_4 composite electrode was quite promising as the cost-effective cathode for the Li-ion-oxygen batteries.

Keywords: Lithium oxygen battery, Reduced graphene oxide, g-C_3N_4

Introduction

The lithium (Li) ion oxygen batteries have higher energy density (2 – 3 kW kg^{-1}) than any other known batteries. The discharging and charging processes in the Li ion oxygen batteries involve oxygen reduction and oxygen evolutions reactions, respectively (Bruce et al., 2012). Therefore, the performances of the Li ion oxygen batteries are directly controlled by the porosity level and the loaded electro-catalysts of the cathode. The electro-catalysts are expected to have high stability, low cost and high efficiency. The most widely used electro-catalysts are carbon materials (Zhang et al., 2013), precious metals (Jung et al., 2013) and transition metal oxides (Han et al., 2014).

Graphitic carbon nitride (g-C_3N_4) can be simply synthesized from a convenient precursor via series of poly-condensation reactions and it can be used as electro-catalyst for the Li ion oxygen battery cathodes since it catalyzes both the oxygen reduction and oxygen evolution reactions (Niu et al., 2012). In this work g-C_3N_4 was chemically mixed with the porous reduced graphene oxide (rGO) to get efficient composite cathode for the Li ion oxygen battery. In the composite electrode, while g-C_3N_4 was expected to catalyze oxygen reactions, porous rGO provided large and highly conductive surface areas to the cathode.

Method

The mixture of acids, H_2SO_4:H_3PO_4 (360:40 mL), was slowly added into a mixture of $KMnO_4$ (18.0 g) and graphite flakes (3.0 g) to synthesize graphene oxide (GO). Then the reaction mixture was heated to 50°C and stirred at 300 rpm for 12 h. The reaction mixture was cooled down to RT normally and poured onto ice (400 mL) and at the same time H_2O_2 (3 mL) was added drop wise to the mixture. After this step, the mixture was filtered and washed. The initial washing step was performed with 30% HCl solution and this step was repeated as necessary until the supernatant becomes transparent. Then the washing process was continued with DI water and ethanol until achieving a neutral pH value. All the washing process was performed by the centrifugation at 6000 rpm for 30 min. The resulting solid was dispersed in DI water by ultrasonication at a concentration of 1.0 mg ml^{-1}.

Silica (SiO_2) nanoparticles were synthesized on the basis of hydrolysis of tetraethyl orthosilicate (TEOS) in pure water/ethanol medium in which ammonia acts as a catalyst. The range of 0.5 – 3 M for NH_3 and 0.1 – 0.5 M for TEOS was used. Pure water, ammonium hydroxide and ethanol were mixed at 50ºC for 5 min. Then, TEOS was added to the mixture and stirred for 6 h, and then the mixture was centrifuged in isopropyl alcohol (5000 rpm, 30 minutes). At the end of the washing process, the final solid content was left to dry at 80ºC under vacuum. The synthesized silica nanoparticles were dispersed in pure water with the help of sonication. Then, HCl, methyl group containing (-CH_3) Pluronic F108 and dimethoxydimethylsilane were added to the prepared silica solution and they were mixed for 24 h. Then the final suspension was brought to a neutral pH with the help of NH_4OH. The prepared GO suspension was mixed with the neutralized suspension for 24 h at RT, then the solid content of the obtained suspension was centrifuged at 6000 rpm for 1 h and then it was dried in a vacuum controlled atmosphere at RT.

For the synthesis of porous rGO, the synthesized GO/SiO_2 nanostructures were first heat treated at 900°C for 5 h in Ar atmosphere. Then, silica nanoparticles were etched with sodium hydroxide and then they kept in an Ar atmosphere at 900°C for 5 h. In order to prepare porous rGO/g-C_3N_4 composite, porous rGO was mixed with melamine in ethylene at 60°C and then mixture was stirred until getting dried solid structure. The solid mixture was then putted into sealed alumina crucible and it was heated up to 550°C at a rate of 3°C min^{-1} and kept at 550°C for 3 h under Ar atmosphere. After air cooling in Ar atmosphere, the rGO/g-C_3N_4 composite was obtained. The composition of mixture was arranged so that the final composite composed of 50% rGO and 50% g-C_3N_4 by weight.

The metallic lithium was used as the counter electrode in the battery cell. The cathodes were prepared by mixing composite and poly (vinylidene fluoride) (PVDF) (80:20 wt%) in the 1-methyl-2-pyrrolidone (NMP). Then the slurry was coated onto the gas diffusion layer (TGP-H-060). Before the battery assembly, the electrodes were dried in a vacuum oven at 100°C for overnight. An electrolyte solution of 1 M LiTFSI in DME solvent was used at all the discharge/charge tests conducted in this study. The air battery cell (EQ-STC-LI-AIR, MTI Corporation) was assembled in a glove box (H_2O and O_2 ≤0.1 ppm) and it tested galvanostatically by using Gamry Reference 3000 Potentiostat/Galvanostat/ZRA. The measurements were conducted in a dry pure oxygen atmosphere (1 atm). The mass loading of the cathode was about 0.5 mg cm^{-2}. The discharge and charge current density was used as 0.05 mA cm^{-2} (100 mA g^{-1} composite cathode).

X-ray diffraction (XRD) analyses were performed on a PANalytical Empyrean diffractometer with Cu K-alpha radiation at a scanning rate of 2° min^{-1}. The morphologies of the electrodes were examined with a ZEISS Ultraplus scanning electron microscope (SEM). FT-IR spectra was obtained using a PerkinElmer Spectrum Two.

Results and Discussion

Characterizations

Micrographs of g-C_3N_4 and porous rGO are provided in Figures 1a and 1b. The large particular appearance of g-C_3N_4 and the porous nature of rGO are observable clearly in the figures. The morphology of the 50% rGO and 50% g-C_3N_4 composite in Figure 1c is very similar to that porous rGO in Figure 1b since the expected density of the porous rGO is much lower than that of g-C_3N_4 and therefore, the volume percentage of the porous rGO is much higher in the composite. Similarly the XRD pattern of the composite reflects the pattern of rGO rather than that of g-C_3N_4 in Figure 2 where rGO shows a graphitic peak at at $2\theta = 26.2°$ (with an interlayer spacing of 0.34nm, indicating the existence of graphene atomic layers) and g-C_3N_4 shows one weak peak at $2\theta = 13.1°$

((100) crystal face indicating the interplanar distance between the nitride pores) and strong peak at 2θ = 27.4° (the characteristic feature of the (002) crystal face indicating the interlayer stacking of the conjugated aromatic systems).

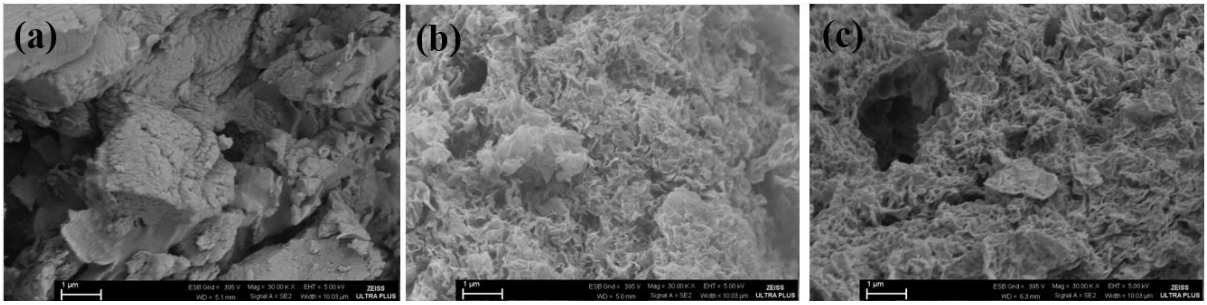

Figure 1. Micrographs of (a) g-C_3N_4 (b) porous rGO and (c) composite.

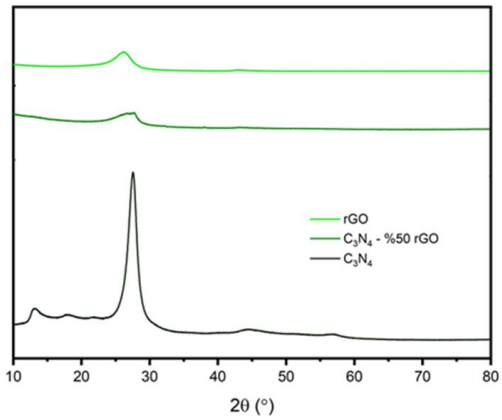

Figure 2. Comparison of the XRD patterns of g-C_3N_4, porous rGO and the composite.

The FT-IR spectra of g-C_3N_4, porous rGO and the composite are compared in Figure 3. The large absorption peak of g-C_3N_4 in a 3000 – 3200 cm^{-1} range belongs to the stretching vibration modes of N-H bonds and those at 1230, 1305, 1370, 1550 ve 1630 cm^{-1} belong to CN hetero-cyclic stretching vibration modes. The peak at 1705 cm^{-1} belongs to the stretching vibrations of C=O and that at 1595 cm^{-1} to the vibrations of sp2 hybrid C-C for rGO in Figure 3. Once again, the FT-IR spectra of the composite reflects most of the features of that of rGO.

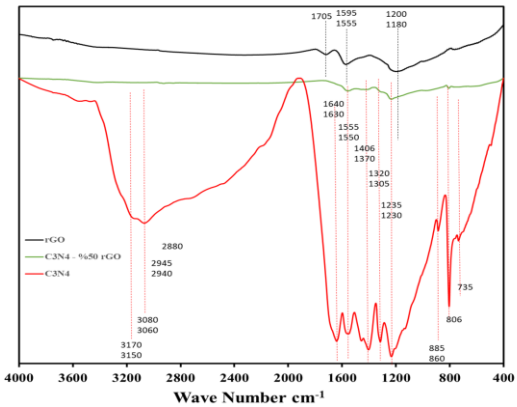

Figure 3. Comparison of the FT-IR spectra of g-C_3N_4, porous rGO and the composite.

Discharge - Charge Tests

The discharge - charge curves of the Li-ion oxygen battery contains rGO and composite cathodes are shown in Figures 4a and 4b, respectively, up to the 50th cycle. The discharge capacities depend on the discharge - charge

cycle number are provided in Figure 4c for both cathodes. Obviously despite the structural similarities of the composite to the rGO (in Figures 1, 2 and 3), it has much better electrode performance with respect to the rGO. The catalytic action of the g-C_3N_4 on the porous rGO surface towards both the oxygen reduction and evolution reactions are clearly observed in this work.

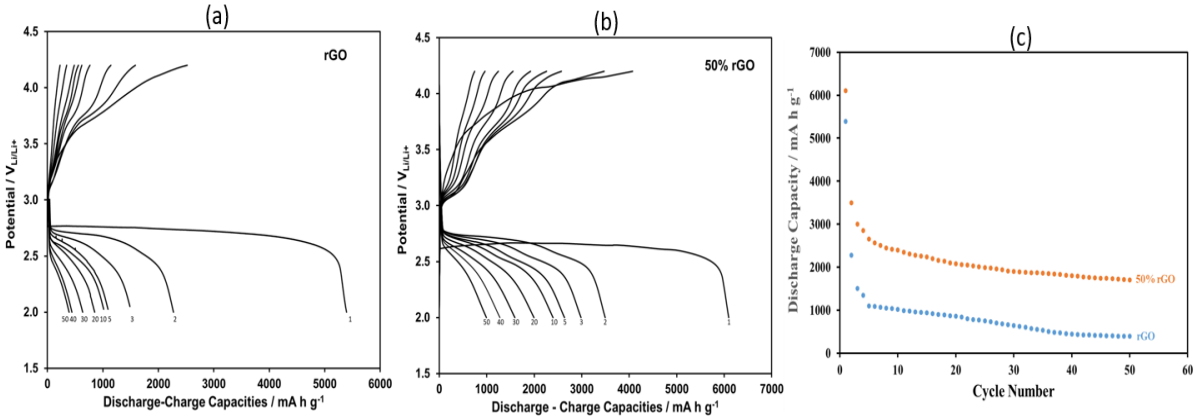

Figure 4. Discharge – charge curves of Li-ion oxygen battery contain (a) porous rGO and (b) composite cathodes, and (c) comparison of the discharge capacities depend on the cyclic number.

Conclusion

The porous reduced graphene oxide (rGO) - graphitic-C_3N_4 (g-C_3N_4) composite consisted of 50% rGO and 50% g-C_3N_4 was synthesized. SEM, XRD and FTIR characterizations showed that the synthesized composite structure reflected most of the features of the rGO structure. The composite had much better cathode performance as compared to the cathode performance of the porous rGO in the Li-ion-oxygen battery.

Acknowledgements

This work was supported by The Scientific and Technological Research Council of Turkey under the contract number 219M269.

Scientific Ethics Declaration

The authors declare that the scientific ethical and legal responsibility of this article published in EPSTEM journal belongs to the authors.

References

Bruce, P. G., Freunberger, S. A., Hardwick, L. J., & Tarascon, J. M. (2012). Li–O 2 and Li–S batteries with high energy storage. *Nature materials*, *11*(1), 19-29.

Han, X., Cheng, F., Chen, C., Hu, Y., & Chen, J. (2015). Uniform MnO 2 nanostructures supported on hierarchically porous carbon as efficient electrocatalysts for rechargeable Li-O 2 batteries. *Nano Research*, *8*(1), 156-164.

Jung, H. G., Jeong, Y. S., Park, J. B., Sun, Y. K., Scrosati, B., & Lee, Y. J. (2013). Ruthenium-based electrocatalysts supported on reduced graphene oxide for lithium-air batteries. *Acs Nano*, *7*(4), 3532-3539.

Niu, P., Zhang, L., Liu, G., & Cheng, H. M. (2012). Graphene- like carbon nitride nanosheets for improved photocatalytic activities. *Advanced Functional Materials*, *22*(22), 4763-4770.

Zhang, T., & Zhou, H. (2013). A reversible long-life lithium–air battery in ambient air. *Nature communications*, *4*(1), 1-7.

Author Information

Ersu LOKCU
Metallurgical and Materials Engineering
Eskisehir Osmangazi University
Contact e-mail: *elokcu@ogu.edu.tr*

Nilay KACAR
Metallurgical and Materials Engineering
Eskisehir Osmangazi University

R. Can OZDEN
Metallurgical and Materials Engineering
Eskisehir Osmangazi University

Mustafa ANIK
Metallurgical and Materials Engineering
Eskisehir Osmangazi University

To cite this article:

Lokcu, E., Kacar, N., Ozden, R.C., & Anik, M. (2021). Synthesis of rGO/g-C3N4 composite cathodes for Li – ion – oxygen battery. *The Eurasia Proceedings of Science, Technology, Engineering & Mathematics (EPSTEM), 16*, 47-51.

The Eurasia Proceedings of Science, Technology, Engineering & Mathematics (EPSTEM)
ISSN: 2602-3199

The Eurasia Proceedings of Science, Technology, Engineering & Mathematics (EPSTEM), 2021

Volume 16, Pages 52-56

IConTES 2021: International Conference on Technology, Engineering and Science

Synthesis of Some New Hydrazones from Quinazolinone Moiety

Hiba Ameen AL-ALAAF
University of Mosul

Mohammed Ahmed AL-IRAQI
College Al-Noor University

Abstract: Methyl α-[(4-oxoquinazolin-2-yl)thio]acetate (4) is one of the important heterocyclic compounds. It is used as a precursor to synthesis new derivatives of quinazolin-4-one moiety. The compound (4) was synthesized *via* a series of steps from anthranilic acid. The anthranilic acid was converted to its methyl ester (1) by esterification with methanol under acidic condition. The ester (1) was reacted with chloroacetyl chloride to produce methyl α-chloroacetamido benzoate (2). The chloro compound (2) was converted to the corresponding thiocyanato compound (3) by its reaction with ammonium thiocyanate. The thiocyanato compound (3) was cyclized to the target precursor (4) by boiling of compound (3) for 12 h. compound (4) was reacted with aromatic aldehydes under boiling condition to produce different hydrazones derivatives (5-12). The hydrazones compounds (5-12) were reacted with Chloroacetyl chloride to afforded the Azetedines compounds (13-20). The synthesized compounds were identified *via* the physical and spectral data.

Keyword: 2-Mercapto quinazolin-4-one, Methyl 2-chloroacetamido benzoate, Methyl anthranilate, Azetidene coumpounds, Hydrazones derivatives, Thiocyanato compound.

Introduction

Quinazolin-4(3)-one is one of most important nucleus in heterocyclic chemistry owing to its participation in building block enormous number of biologically active compounds, by incorporation of the quinazolin-4(3)-one nuclei with heterocyclic moieties, such as triazole, thiadiazole and oxadiazole moieties. These compounds have been enticing attention of medicinal chemists to find and design novel structures having pharmacological activity (Jaianand et al., 2009). Quinazolin-4(3H)-one derivatives showed diversity of biological activity such as analgesic, anti-inflammatory (Bhalla et al, 1993), anti-hypertensive, anti-histaminic, anti-cancer (Boyle et al, 1993), anti-tumor (Al-Omary et al, 2012), sedative, hypnotic and anti-microbial activity (Vogels, 1994), anti-leishmanial activity (Agarwal et al, 2009) and as anti-oxidant (Decker; 2008). So, the previous views encouraged us to synthesize novel compounds containing quinazolin-4(3H)-one nucleus incorporated with hydrazones moiety starting from methyl α-[(4-oxoquinazolin-2-yl)thio]acetate.

Experimental

Melting points were recorded on a Stuart melting point SMP30 apparatus and were uncorrected. IR spectra were recorded as neat using Bruker system 2000 FT.IR spectrophotometer. 1H NMR spectra on a Bruker DPX (400)

super conducting NMR Spectrometer (400 MHz) using CDCl3 or DMSO-d6 as solvents with TMS as internal standard.

Synthesis of Methyl Anthranilate

A solution of anthranilic acid (1mol, 14.7 g) in absolute methanol (250 ml) was cooled to 0-5 oC, then a concentrated sulfuric acid (20 ml) was added dropwise with stirring. After the addition was completed, the mixture was refluxed for 72 h. The volatile components were evaporated under reduced pressure. A cold water (100 ml) was added to the residue. The mixture was basified by dropwise addition of (5 %) sodium bicarbonate solution, then the resulted mixture extracted with (20 * 30 ml) dichloromethane. The organic layers were collected, dried over magnesium sulfate, then evaporated. The crude product was recrystallized from methanol to give red crystals in 85% yield: melting point 22-23 oC. IR spectrum (neat, ν Cm-1) 3369 (N-H), 1704 (C=O), 1604 (C=C), 1442 (CH3), 1245 (C-O). 1H NMR (DMSO-d6) (δ, ppm): 3.39 (s, 3H, CH3), 6.66 (s, 2H, NH2), 6.53 (t, 1H, H5), 6.79 (d, 1H, H3), 7.25 (t, 1H, H4), 7.71 (d, 1H, H6).

Methyl N-(α-chloroacetyl) Anthranilate

To a solution of methyl anthranilate (0.01mol, 1.52 g) in chloroform (50 ml), chloroacetyl chloride (0.012 mol, 1.36 g) and potassium carbonate (0.015 mol, 2.1 g) were added. The reaction mixture was refluxed for 12 h. the volatile material was evaporated under reduced pressure. The residue was washed thoroughly with water then with 5% sodium bicarbonate solution and finally with water. The resulted product was dried then recrystallized from ethanol to give white crystals, in 98% yield, m.p. 90-91 oC, IR (neat, ν, cm -1): 3194 (N-H), 1682, 1676 (2C=O), 1441 (CH3),1226 (C-O). 1H NMR (DMSO-d6): δ, ppm, 3.89 (s, 3H, CH3), 4.45 (s, 2H, CH2), 7.27 (t, 1H, H5) , 7.66 (t, 1H, H4), 7.99 (d, 1H, H3), 8.40 (d, 1H, H6), 11.33 (s,1H, NH).

Synthesis of Methyl α-[(4-oxoquinazolin-2-yl)thio]Acetate

To a solution of methyl 2-(α-chloroacetamino) benzoate (2) (0.01 mol, 2.27 g) in methanol (30 ml), ammonium thiocyanate (0.015 mol, 1.15 g) was added with stirring. The mixture was refluxed for 12h then cooled to room temperature. The resulted precipitate was filtered off, washed with water, dried then recrystallized from methanol to give pale yellow crystals in 98 % yield, m.p. 191-192 oC. IR (neat, ν/cm -1): 3170 (N-H), 1734, 1682 (2C=O), 1375 (CH3), 681 (C-S). 1H NMR (DMSO-d6): δ, ppm: 3.69 (s, 3H, CH3), 4.11 (s, 2H, CH2), 7.4 (t,1H, H6), 7.75 (t, 1H, H7), 7.98 (d, 1H, H5), 8.23 (d, 1H, H8), 11.14 (s,1H, NH).

Synthesis of α-[4-oxoquinazolin-2-yl) thio]Acetohydrazide

A solution of methyl α-(4-oxoquinazolin-2-yl) thio] acetate (3) (0.01mol, 2.64 g), hydrazine hydrate (99.5 %) (0.015 mol, 0.75 g) in absolute ethanol (30 ml) was refluxed with stirring for 12 h. The solid product was separated by filtration, washed with cold water, dried, then recrystallized from ethanol to give green crystals in 90 % yield, m.p. 248 oC. IR (neat, ν, cm-1): 3289, 3128 (NH2, N-H), 1662 (2 C=O), 682 (C-S). 1H NMR (DMSO-d6): δ, ppm: 4.41 (s, 2H, CH2), 5.43 (s, 2H, NH2) (D2O exchangeable), 5.88(s, 1H, NNH), 7.14 (t, 1H, H6), 7.31 (d,1H, H5), 7.70 (d, 1H, H8), 7.48 (t, 1H, H7), 8.23 (s, 1H, H3).

Synthesis of α-[(4`-oxoquinazolin-2`-yl) thio] Aceto-3-Substituted Phenyl Hydrazone

To a solution of the hydrazide (4), (0.01 mol, 2.5 g) in absolute ethanol (25 ml), an aromatic aldehyde (0.01 mol) was added with stirring, followed by addition of (1 ml) of glacial acetic acid. The mixture was refluxed for 4 hrs. The reaction mixture was cooled and left in refrigertor for 24 hrs, the resultant precipitate was separate by filtration, washed with cold ethanol then recrystallized from ethanol. The physical properties of compounds (5-12) are illustrated in Table (1), 1HNMR (DMSOd6): δ, ppm: 3.99(s,2H, CH_2), 6.85(d,2H, $H_{3:5}$), 7.42(t,1H, H_6), 7.61(d,1H,

H_8), 7.66(d,2H, $H_{2:6}$), 7.77(t,1H, H_7), 8.07(d,1H, H_5), 8.47(s,1H, CH), 9.68(b,1H, OH), 11.07(s,1H, NH), 12.65(s, 1H, NH) amide

Compd. No.	R	Yield %	m.p. °C	color	IR (neat, ν, Cm^{-1})		
					C=O	N-N	N-H
6	4-hydroxybenzaldehyde	98	244-245	green	1662	1066	3389
7	2-chlorobenzaldehyde	94	110-111	yellow	1676	1079	3368
8	2,4-dichlorobenzaldehyde	95	286-287	green	1670	1057	3358
9	2-piperenal	90	138-139	yellow	1691	1078	3362
10	3-nitrobenzaldehyde	93	212-213	green	1698	1054	3378
11	4-tolualdehyde	98	204-205	green	1681	1082	3362
12	4-N, N-dimethylaminobenzaldehyde	95	215-216	green	1685	1035	3304

Table 1. The physical and IR spectral data of compounds (5-12).

Synthesis of α-[(4`-oxoquinazolin-2`-yl) thio] Acetamido-β-[3``-chloro-4``-Substituted Phenyl Azetidene-2``-One

To a solution of the hydrazone (H95-H104) (0.01 mol) in dimethylformamide (30 ml, triethylamine (0.02 mole, 2.78 ml) was added with stirring followed by dropping wisely addition of chloroactyl chloride (0.02 mol, 1.6 ml) within a period of 30 min. the resulted mixture was refluxed for 10 hrs, then poured on to crushed ice (50 g) to give a precipitate. The precipitate was collected by filtration, washed with cold water, dried then recrystallized from ethyl acetate. The physical properties of compounds (13-20) are illustrated in Table (2). 1H NMR (DMSO-d6): δ, ppm: 3.84(s,2H, CH_2), 5.08(s,1H, NH), 5.44(s,1H, CH), 6.71(d,2H, $H_{3:5}$), 7.05(d,2H, $H_{2:6}$), 7.42(t,1H, H_6), 7.61 (d,1H, H_8), 7.77(t,1H, H_7), 8.07(d,1H, H_5), 9.06(b,1H, OH), 12.65(s,1H, NH) amide.

Table 2. The physical and chemical properties of compounds (12-18).

Compd. No.	R'-	Yield %	m.p. ℃	color	IR (neat) , ν (Cm^{-1})			
					C=N	C=O	C-Cl	N-H
13	4-hydroxybenzaldehyde	90	193-194	yellow	1566	1660	732	3365
14	2-chlorobenzaldehyde	88	280-281	yellow	1527	1654	745	3340
15	2,4-dichlorobenzaldehyde	90	209-210	yellow	1578	1686	700	3368
16	2-piperenal	86	246-247	grey	1534	1664	698	3300
17	3-nitrobenzaldehyde	87	235-236	grey	1544	1674	734	3379
18	4-tolualdehyde	91	272-273	grey	1567	1670	750	3354
19	4-N, N-dimethylaminobenzaldehyde	93	286-287	brown	1556	1683	722	3346
20	2-thiophenecarbaxaldehyde	89	256-257	brown	1598	1669	745	3367

Result and Discussion

The synthetic route of the quinazolin-4(3H)-one derivatives (5-7) was illustrated in Figure 1. The primal precursor for these heterocyclic compounds is α-[(4-oxo-3,4-dihydroquinazolin-2-yl)thio]acetohydrazide (4). This compound was synthesized from anthranilic acid via four steps. The anthranilic acid was converted to its methyl ester (1)

Present as thiol in the solution. The IR spectrum of the hydrazone compound (5) showed absorption bands at 3389 Cm^{-1} for the (N-H) bond stretching quinazolinone and oxadiazole moieties respectively, at 1662for the (C=O) bond stretching and at 1066for the (N-N) bond stretching1HNMR(DMSOd6):δ,ppm:3.99(s,2H,CH_2),6.85(d,2H,$H_{3:5}$) 7.42(t,1H,H_6),7.61(d,1H,H_8),7.66(d,2H,$H_{2:6}$),7.77(t,1H,H_7),8.07(d,1H,H_5),8.47(s,1H,CH),9.68(b,1H,OH),11.07(s,1H ,NH),12.65(s, 1H, NH)amide. Furthermore, two series of derivatives were prepared from the α-[(4`-oxoquinazolin-2`-yl) thio] acetamido-β-[3``-chloro-4``-substituted phenyl azetidene-2``-one. The ester (1) was reacted with chloroacetyl chloride in presence of potassium carbonate as a base to afford methyl 2-(α-chloroacetamino) benzoate (2).

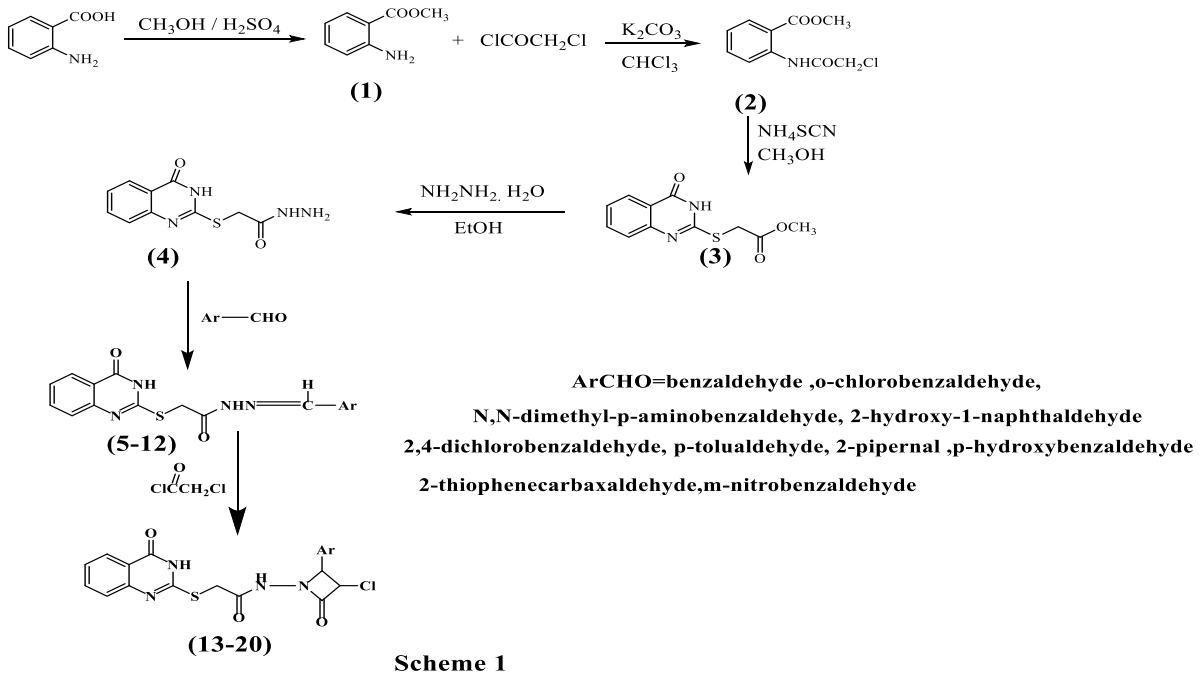

Scheme 1

Figure 1. Through the conventional acid catalyzed esterification method.

The ^{1}H NMR spectrum of compound (2) showed the following chemical shifts (δ, ppm): 3.89 (s, 3H, CH_3), 4.45 (s, 2H, CH_2), 7.27 (t, 1H, H5) , 7.66 (t, 1H, H4), 7.99 (d, 1H, H3), 8.40 (d, 1H, H6), 11.33 (s,1H, NH) [Crews et al, 1998].[16] The reaction of compound (2) with ammonium thiocyanate in absolute ethanol under reflux for 12 h afforded methyl α-[(4-oxoquinazolin-2-yl)thio]acetate (3) via the formation and cyclization of un-isolated methyl 2-(α-thiocyanato acetamino)benzoate (I) as an intermediate compound.

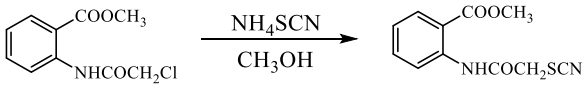

The IR spectrum of the quinazolinone compound (3) showed absorption bands at 3170 $Cm^{-1}$for the N-H bonds stretching of the quinazolinone nucleus, and two absorption bands at 1734, 1682 Cm^{-1} for the C=O bond stretching of the ester and the amide respectively. The proton NMR spectrum of compound (3) showed the following chemical shifts (δ, ppm): 3.69 (s, 3H, CH_3), 4.11 (s, 2H, CH_2), 7.4 (t,1H, H6) , 7.75 (t, 1H, H7), 7.98 (d, 1H, H5), 8.23 (d, 1H, H8), 11.14 (s,1H, NH). The ester (3) was converted to the corresponding hydrazide (4) by its refluxing with hydrazine hydrate in absolute ethanol. The absence of the C=O bond stretching of the ester at 1704 Cm^{-1} indicates the full conversion of the ester (3) to the hydrazide (4). The ^{1}H NMR spectrum of the hydrazide (4) (DMSO-d6) showed the following chemical shifts: δ, ppm: 4.41 (s, 2H, CH_2), 5.43 (s, 2H, NH_2) (D_2O exchangeable), 5.88(s, 1H, NNH), 7.14 (t, 1H,H6), 7.31 (d,1H, H5), 7.70 (d, 1H, H8), 7.48 (t, 1H, H7), 8.23 (s, 1H, H3). The hydrazide (4) was used as precursor to synthesize the posterior heterocyclic compounds (5-12). Firstly, the hydrazide (4) was reacted with substituted aldehydes in presence of ethanolic solution to give α-[(4`-oxoquinazolin-2`-yl) thio] aceto-3-substituted phenyl hydrazone (5-12). The first one involves the reaction of compound (5-12) with different aldehydes to synthesize the hydrazones derivatives (5-12). This reaction takes place *via* S_N2 mechanism. These compounds showed an absorption band in the IR spectra at 1662-1691Cm^{-1} for C=O bond stretching, in addition to absorption band at 1704 Cm^{-1} for the ketonic C=O bond stretching related to compound (5), and at 1035-1082 Cm^{-1} for N-N bond stretching. The ^{1}H NMR (DMSO-6d) spectrum of compound (12) showed the following chemical shifts: δ, ppm: 3.84(s,2H,CH_2),5.08(s,1H,NH)5.44(s,1H,CH),6.71(d,2H,$H_{3:5}$),7.05(d,2H,$H_{2:6}$),7.42(t,1H,H_6),7.61 (d,1H,H_8), 7.77(t,1H,H_7),8.07(d,1H,H_5),9.06(b,1H,OH),12.65(s,1H,NH)amide.The ^{1}H NMR (DMSO-6d) spectrum of compound (14) showed the following chemical shifts: δ, ppm: 1.24 (d, 2H, allelic CH_2), 3.90 (s, 2H, CH_2), 4.09 (d, 1H, vinylic CH), 6.1 (d, 2H, vinylic CH_2), 7.37 (t, 1H, H6), 7.48 (t,1H, H7), 7.47 (d, 1H, H5), 7.83 (d, 1H, H8), 8.19 (s, 1H, H3). The ^{1}H NMR (DMSO-6d) spectrum of compound (10) showed the following chemical shifts: δ,

ppm: 3.18 (s, 2H, benzylic CH_2), 3.86 (s, 2H, CH_2), 7.39 (t, 1H, H6), 7.46 (t, 1H, H7), 7.48 (d, 1H, H5), 7.71(d, 1H, H8), 7.81-8.21 (m, 5H, benzylic-H), 8.26 (d, 1H, H3). The second series involves the reaction of compound (5) with different aldehydes to synthesize the azetidenes derivatives (13-20). These compounds showed an absorption bands in their IR spectra at 1654-1689 Cm^{-1} for C=O bond stretching, at 1527-1598 Cm^{-1} for C=N bond stretching, at 698-750 Cm^{-1} related to C-Cl bond stretching and at 3300-3379 Cm^{-1} for the N-H bond stretching. The ^{1}H NMR (DMSO-6d) spectrum of compound (13) showed the following chemical shifts: δ, ppm:3.84(s,2H, CH_2), 5.08(s,1H, NH), 5.44(s,1H, CH), 6.71(d,2H, $H_{3:5}$), 7.05(d,2H, $H_{2:6}$), 7.42(t,1H, H_6), 7.61(d,1H, H_8), 7.77(t,1H, H_7), 8.07(d,1H, H_5), 9.06(b,1H, OH), 12.65(s,1H, NH) amide. The ^{1}H NMR (DMSO-6d) spectrum of compound (14) showed the following chemical shifts: δ, ppm: 3.84(s,2H, CH_2), 5.08(s,1H, NH), 5.44(s,1H, CH), 7.21(t,1H, H_5), 7.22(d,1H, H_6), 7.25 (t,1H, H_4), 7.42(t,1H, H_6), 7.61 (d,1H, H_8), 7.68 (d,1H, H_3), 7.77(t,1H, H_7), 8.07(d,1H, H_5), 12.65(s,1H, NH) amide. The ^{1}H NMR (DMSO-6d) spectrum of compound (17) showed the following chemical shifts: δ, ppm: 3.84(s,2H, CH_2), 5.08 (s,1H, NH), 5.44(s,1H, CH), 7.42(t,1H, H_6), 7.61(d,1H, H_8), 7.64(t,1H, H_5), 7.76(d,1H, H_6), 7.77(t,1H, H_7), 8.07(d,1H, H_5), 8.16(d,1H, H_4), 8.22(s,1H, H_2), 12.65(s,1H, NH) amide**.**

Scientific Ethics Declaration

The authors declare that the scientific ethical and legal responsibility of this article published in EPSTEM journal belongs to the authors.

References

Agarwal, K. C., Sharma, V., Shakya, N., & Gupta, S. (2009). Design and synthesis of novel substituted quinazoline derivatives as antileishmanial agents. *Bioorganic & Medicinal Chemistry Letters*, *19*(18), 5474-5477.

Al-Omary, F. A., Hassan, G. S., El-Messery, S. M., & El-Subbagh, H. I. (2012). Substituted thiazoles V. Synthesis and antitumor activity of novel thiazolo [2, 3-b] quinazoline and pyrido [4, 3-d] thiazolo [3, 2-a] pyrimidine analogues. *European Journal of Medicinal Chemistry*, *47*, 65-72.

Bhalla, M., Srivastava, V. K., Bhalla, T. N., & Shanker, K. (1993). Anti-inflammatory and analgesic activity of indolyl quinazolones and their congeners. *Arzneimittel-forschung*, *43*(5), 595-600.

Boyle, F. T., Matusiak, Z. S., Hughes, L. R., Slater, A. M., Stephens, T. C., Smith, M. N., ... & Jackman, A. L. (1993). Substituted-2-desamino-2-methyl-quinazolinones. A series of novel antitumour agents. In *Chemistry and Biology of Pteridines and Folates* (pp. 585-588). Springer.

Crews, P., Rodriquez, J., Jaspars, M., & Crews, R. J. (1998). *Organic structure analysis*. Oxford University press.

Decker, M., Kraus, B., & Heilmann, J. (2008). Design, synthesis and pharmacological evaluation of hybrid molecules out of quinazolinimines and lipoic acid lead to highly potent and selective butyrylcholinesterase inhibitors with antioxidant properties. *Bioorganic & Medicinal chemistry*, *16*(8), 4252-4261.

Anand, P. V., Kumar, K. S., Sivakumar, R., Solomon, W. S., & Jayaveera, K. N. (2009). Synthesis of quinazoline derivatives and their biological activities. *Asian Journal of Chemistry*, *21*(9), 6656-6660.

Vogels A.I.; (1994). *Text book of practical organic chemistry* (5th ed.). Longman Scientific & Technical.

El-Badry, Y. A., Anter, N. M., & El-Hashash, M. A. (2014). Synthesis and behaviour of 2-(furan-2-yl) vinyl-4H-3, 1-benzoxazin-4-one towards nitrogen and carbon nucleophiles. *Indian Journal of Chemistry*, *53* ,1574-1583.

Author Information

Hiba Amen AL-ALAAF University of Mosul, Department of Chemistry, Mosul/Iraq
Contact E-mail: hibaalaf80@gmail.com

Mohammed A. AL-IRAQI
College Al-Noor University
Bartella, Irak

To cite this article:

Al-Alaaf, H.A. & Al-Iraqi, M.A. (2021). Synthesis of some new hydrazones from quinazolinone moiety. *The Eurasia Proceedings of Science, Technology, Engineering & Mathematics (EPSTEM), 16*, 52-56.

The Eurasia Proceedings of Science, Technology, Engineering & Mathematics (EPSTEM)
ISSN: 2602-3199

The Eurasia Proceedings of Science, Technology, Engineering & Mathematics (EPSTEM), 2021

Volume 16, Pages 57-62

IConTES 2021: International Conference on Technology, Engineering and Science

Resistance Spot Weld Ability of Mild Steel Coated with Zn, Galfan and ZA12

Ibrahim CELIKYUREK
Eskişehir Osmangazi University

Adem TASDEMIR
Eskişehir Osmangazi University

Bedri BAKSAN
Eskişehir Osmangazi University

Abstract: In this study, the weldability of mild steel coated with different Zn-based materials to prevent corrosion with resistance spot welding process was investigated. For this purpose, the surfaces of mid steel were coated with pure Zn, Galfan (Zn5Al) and ZA12 (Zn11Al1Cu) alloys. Hot dipping technique was used for coating. Mild steels with dimension of 1.5X15X40 mm were immersed in the melted Zn and alloys, and the surfaces were coated by waiting for 2 minutes. Steel and coated steel pairs were joined by resistance spot welding process. The welding interface microstructures were examined under light optical microscopy (LOM). Weld interface strengths were measured by axial shear tests. The tests were performed at the room temperature and with a tensile speed of 5mmmin-1. Microstructure investigations showed a good bonding occurred between the coating and the steel and between the welded materials. Mechanical tests have shown that coating the steel reduces the weld strength and the decrease in strength continues with the increase of alloying elements in the coating.

Keywords: Mild steel, Coting, Welding, Strength

Introduction

Mild steels are widely used in various construction manufacturing in all areas of industry. Joining these materials, which can be in different forms, by welding techniques is a frequently used method, especially in the automotive sector. The temperature of the welding interface must be above or very close to the melting temperature for successful bonding. Although there are many different welding methods, we can collect them into two main groups as melting and solid-state welding methods. Resistance spot welding technique, which is a solid-state welding method, is used to join sheet-shaped materials.

Electric resistance spot welding is a method of welding with heat that occurs due to the resistance of the workpieces against the electric current passing through the workpieces held together under pressure between the electrodes. The contact surface of the parts to be welded is heated with low voltage and high current applied for a short time and transformed into a molten welding core. When the electric current is cut off, the molten metal quickly cools and solidifies. Meanwhile, the electrodes continue to hold the welded parts tightly and then retract and release the part. Welding process is usually completed in less than one second. (Yener, 1999; Baytemir, 2011).

The main resource variables affecting the welding quality are listed as follows; effect of the welding current, effect of the welding time, effect of electrode force, effect of electrode composition and shape on heating,

material of workpiece, effect of surfaces of parts to be welded, effect of distance between welded points, contact conditions of electrode and workpiece (Hayat, 2005). Resistance spot welding is an easily controllable process, inexpensive equipment and a serially repeatable method. The welding process widely used in joining metal sheets such as iron, steel, aluminum alloys, magnesium alloys, titanium alloys, super alloys, and joining of different metals (Kahraman, 2007; Qiu, et al.200; Han et al., 2010; Shirmohammadi et al., 2017; Bemani et al., 2020; Babua et al., 2012).

Corrosion and rust are an important problem that limits the use of metals and alloys. Corrosion and rust can result in large issues for safety equipment because of the potential weakening of the structure. In many cases, metals become unusable earlier than expected due to corrosion. Therefore, besides the mechanical and physical properties of metallic materials, their resistance to corrosion is of great importance. Many metals and alloys are affected by the environment in which they work. Different methods are used to increase the corrosion resistance of metallic materials. One of these is coating the surface of the metal with another corrosion-resistant metal or alloy.

Galvanizing is one of the most popular methods of coating and protecting the metal. Galvanization is done by applying a protective zinc coating to steel or iron. This coating is mainly done to prevent rust and corrosion, which provides a longer useful life and increased safety.

In this study, the joint ability of steel coated with different zinc alloys by spot resistance welding was investigated. The effects of the coating composition on the weld interface microstructure and strength were revealed.

Method

1.5mm thick mild steel is used for joining with resistance spot welding. The surfaces of the 1.5x15x40mm steels were ground before coating. Steel surfaces are coated with Zn, Galfan(Zn5Al), and ZA12 (Zn11Al1Cu) alloys by the hot-dipping method. The steels immersed in the melted metal or alloy were kept in the melt for 2 minutes. The samples removed from the melt were cooled in the open atmosphere.

The welding process was carried out in a 60KW resistance spot welding machine. The copper electrode diameter of the machine was 6 mm. Welding parameters applied to all samples during welding operations are determined as follows: Welding clamping force 500kgf, welding current 35A, welding time 40 periods, and cooling time 4sec.

After the welding process, a cross-section was taken from the middle of the welding interface. These cross-sections were prepared metallographically and the welding interface microstructures were examined under an optical light microscope.

Mechanical strengths were determined by applying axial shear to the welding interface. Shear tests were carried out on a universal testing device in the geometry shown in Figure 1. The tests were carried out at room temperature and a tensile speed of 5mmmin^{-1}.

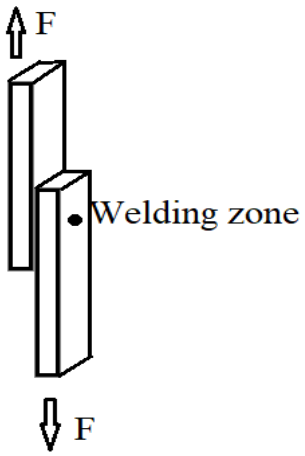

Figure 1. The shear test geometry

Results and Discussion

Optical microstructure photographs of the steel and surface coatings used in the welding process are given in Figure 2. From the microstructures, it is seen that the mild steel has a ferritic structure and the coatings on the surface adhere well to the steel. The surface of the steel could be coated with Zn, Galfan, and ZA12 without a gap or oxide layer between the steel and the coating. In addition, it can be seen from the microstructure pictures that all coatings are approximately the same thickness. The coating thickness is a reflection of the residence time in the melt.

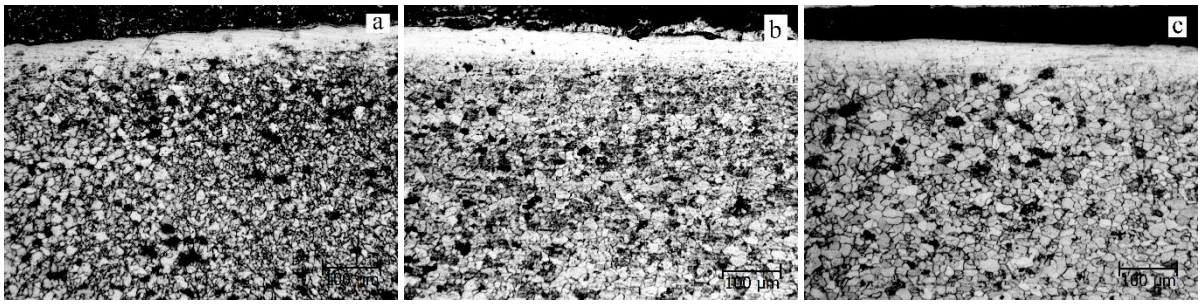

Figure 2. The cross-sections of coatings. a) coated with Zn, b) coated with Galgan, and c) coated with ZA12

Cross-sections of welding interfaces are seen in figure 3. These microstructure images were taken using the photo-merging method since the all-welding interface did not fit into the objective lens. From the figures, it can be seen that a nugget zone is formed at the welding interface. It was observed that the coatings were lost in the welding zone in all samples except the Zn coated sample. No significant nugget zone was formed in the Zn-coated sample. In the nugget zone at the heat-affected zone, columnar grains were formed, extending from the outside to the center. Grain coarsening of the steel was also observed at the boundary of the nugget zone. In general, no gap formation was found at the weld interface. Only in the sample coated with ZA 12, a large void was observed.

The shear test results at room temperature with a tensile speed of 5mmmin-1 are summarized in Figure 4. It was observed that the welding interface strength of the welded samples is decreased when the coating was applied. During the tests, it was determined that the fracture occurred in the form of tearing at the weld boundary in the uncoated mild steel, on the other hand, it was determined that the fracture occurred directly from the joint area in the coated samples. Tearing in uncoated samples is due to grain coarsening at the boundary of the nugget zone. Since the strength of the coarser grains is lower, the deformation took place in this region. In the coated samples, as the strength of the joint area is lower than that of mild steel, the fracture occurred in this area.

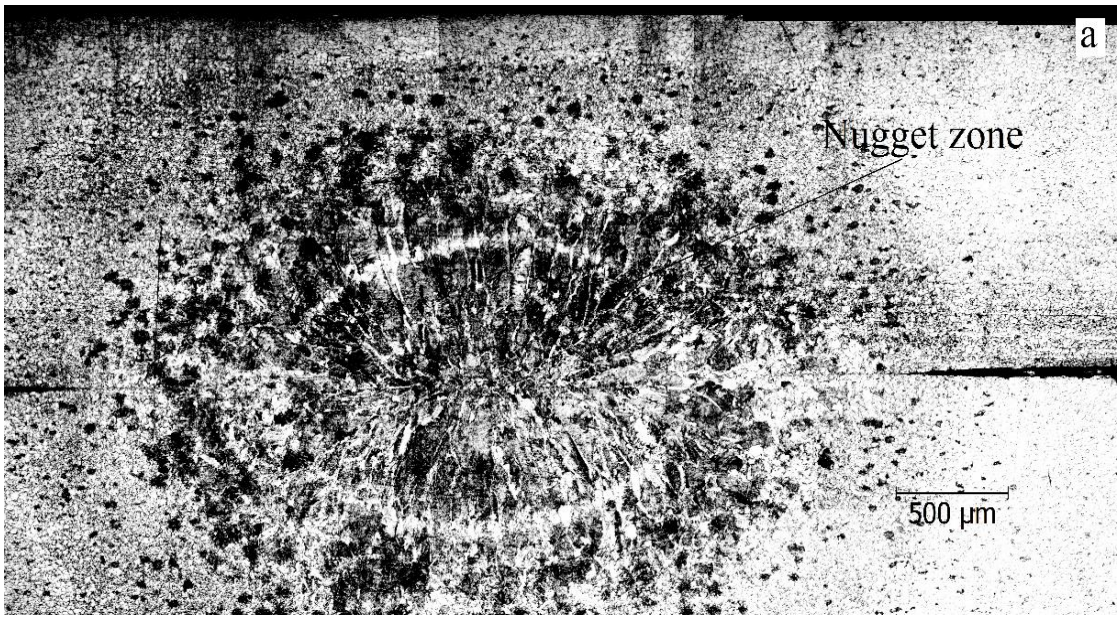

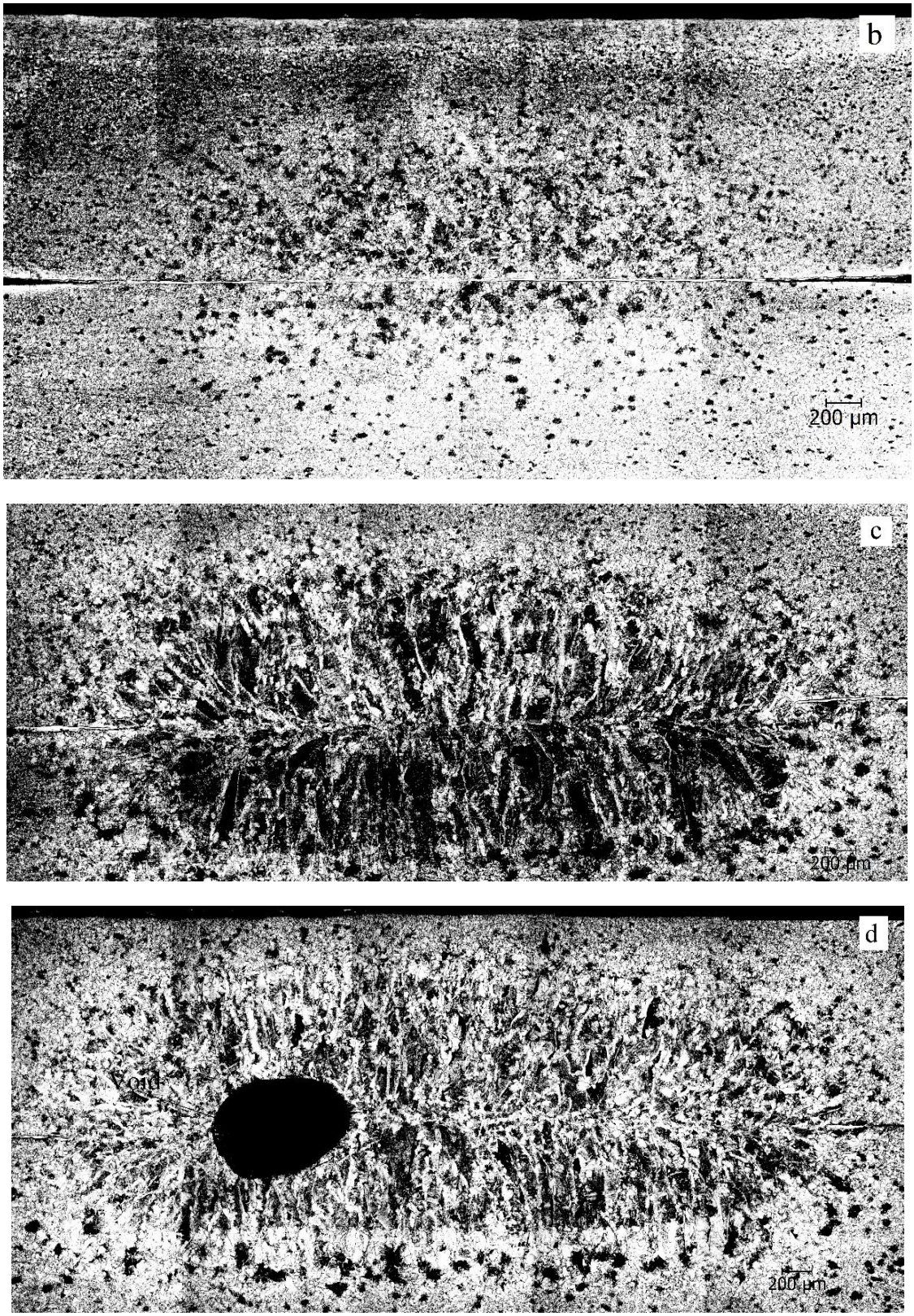

Figure 3. The cross-sections of welding interfaces. a) mild steel, b) Zn coating, c) Galfan coating, and d) ZA12 coating.

In addition, since none of the coatings were ductile, there was no plastic deformation during fracture. There was a slight decrease in the welding interface strength with only Zn coating, whereas there was a serious decrease in the welding interface strength of the Galfan and ZA12 coated samples. The Al content of the coating is considered to be effective in this result. It is known that Al is undesirable because it forms brittle intermetallic phases (Fe3Al, FeAl, etc.) in steels. These phases may be the cause of the decrease in strength.

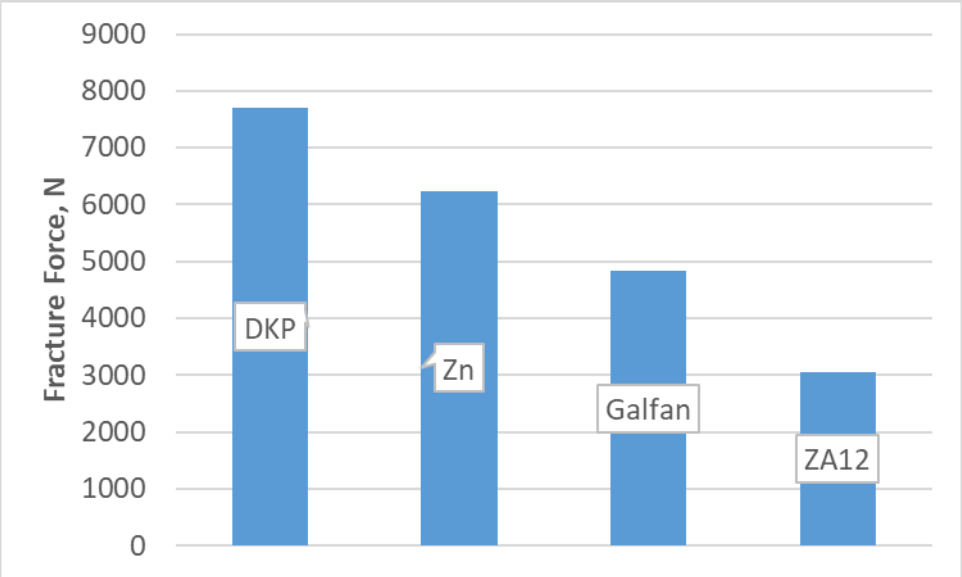

Figure 4. The strength of the welding interfaces.

Conclusion

At the end of this study, it has been proven that ZA12 alloy, which has higher corrosion resistance and does not change color over time, can be coated in addition to the traditionally hot-dipping galvanized (Zn coating) and partially widespread Galfan (Zn5Al) coating to increase the resistance of steels against rust and corrosion.

Since resistance spot welding is widely used for joining sheet-shaped materials, it is also important that steels coated with different materials can be joined in this way. In this study, it has been seen that steels coated with Zn-based materials can also be joined by resistance spot welding.

They do not form solid solutions with Fe both Zn and Al, which are the elements that make up the coating, on the contrary, they form intermetallic phases. Since the formed intermetallic phases are generally brittle, they determine the welding interface strength. Although the increase in Al content in the coating increases the corrosion resistance, the welding interface strength systematically decreased due to an increase in the amount of brittle intermetallic phases during the welding process.

Recommendations

1. The effects of coating thickness on the strength at the end of resistance spot welding should be investigated.
2. Since the welding parameters will affect the interface microstructure, the effects of welding parameters on the strength of the weld interface should be investigated by using different welding parameters.

Scientific Ethics Declaration

The authors declare that the scientific ethical and legal responsibility of this article published in EPSTEM journal belongs to the authors.

References

Babua N.K, Brauserb, S., Rethmeier M., & Cross C.E. (2012). Characterization of microstructure and deformation behaviour of resistance spot welded AZ31 magnesium alloy, *Materials Science and Engineering A, 549*, 149– 156.

Baytemir, M. (2011). Ostenitik *AISI 310-ferritik AISI 430 paslanmaz çeliklerin elektrik direnç nokta kaynağı ile birleştirilmesi ve mekanik özelliklerinin incelenmesi* [Yüksek Lisans Tezi, Sakarya Üniversitesi].

Bemani M., Pouranvari, M. (2020). Microstructure and mechanical properties of dissimilar nickel-based superalloys resistance spot welds, *Materials Science & Engineering A*, *773*, 138825

Han, L. Thornton, M. Shergold, M. (2010). A comparison of the mechanical behavior of self-piercing riveted and resistance spot welded aluminum sheets for the automotive industry. *Materials and Design*, *31*, 1457–1467.

Hayat, F. (2005). *Çift-fazlı çeliklerin nokta direnç kaynağında MHO ile kaynak süresinin mekanik özelliklere etkisi* [Yüksek Lisans Tezi, Zonguldak Karaelmas Üniversitesi].

Kahraman, N. (2007). The influence of welding parameters on the joint strength of resistance spot-welded titanium sheets. *Materils and Design*, *28*, 420–427.

Qiu, R. Iwamoto, C. Satonaka, S. (2009). Interfacial microstructure and strength of steel/ aluminum alloy joints welded by resistance spot welding with cover plate. *Journal of Materials Processing Technology*, *209* 4186–4193.

Shirmohammadi, D., Movahedi, M., Pouranvari, M. (2017). Resistance spot welding of martensitic stainless steel: Effect of initial basemetal microstructure on weld microstructure and mechanical performance, *Materials Science & Engineering A, 703*, 154–161

Yener, S. (1999). *Otomotiv sanayinde kullanılan direnç nokta kaynak elektrodu ömrünün deneysel analizi*. [Yüksek Lisans Tezi, İTÜ Fen Bilimleri Enstitüsü].

Author Information

Ibrahim CELIKYUREK
Eskişehir Osmangazi University
Eskişehir Osmangazi University, Fac. Of Eng and Arc.
Metallurgical and Materials Eng. Dept. Eskişehir, Turkey
Contact e-mail: cibrahim@ogu.edu.tr

Adem TASDEMIR
Eskişehir Osmangazi University
Eskişehir Osmangazi University, Fac. Of Eng and Arc.
Mining Eng. Dept. Eskişehir, Turkey

Bedri BAKSAN
Eskişehir Osmangazi University
Eskişehir Osmangazi University, Fac. Of Eng and Arc.
Metallurgical and Materials Eng. Dept. Eskişehir, Turkey

To cite this article:

Celikyurek, I, Tasdemir, A. & Baksan, B. (2021). Resistance spot weld ability of mild steel coated with Zn, galfan and ZA12. *The Eurasia Proceedings of Science, Technology, Engineering & Mathematics (EPSTEM), 16*, 57-62.

The Eurasia Proceedings of Science, Technology, Engineering & Mathematics (EPSTEM)
ISSN: 2602-3199

The Eurasia Proceedings of Science, Technology, Engineering & Mathematics (EPSTEM), 2021

Volume 16, Pages 63-68

IConTES 2021: International Conference on Technology, Engineering and Science

Effect of Secondary Aging of Copper-Chromium Alloys to Electrical Conductivity

Bedri BAKSAN
Eskisehir Osmangazi University

Ibrahim CELIKYUREK
Eskisehir Osmangazi University

Adem TASDEMIR
Eskisehir Osmangazi University

Abstract: Copper-chromium alloys are the most important spot-welding tips and disks; it is also used where high strength together with electrical conductivity is required. Electrical conductivity is also important for optimum energy consumption. It is obvious that if highly conductive materials are used, we need low electric current where today energy is a very precious thing. In our study due to the industrial requirement of highly durable and more consistent parts needs, secondary aging was used to obtain more efficient materials. Electrical conductivity is a must, therefore the copper chromium alloys were observed for their resistances for various processing conditions, like as cast, aged, and secondarily aged. The electrical resistance measurements for all conditions were done and compared. The aging heat treatment was done at 650 ^{o}C for 4 hours. Secondary aging heat treatment was done at 400 ^{o}C for 2, 4, and 6 hours. The lowest specific electrical resistivity was obtained from secondary aged at 400 ^{o}C for 2 hours as 0.0074 mΩ mm^2/mm. The resistance of as-cast copper-chromium alloy was measured as 0.078 mΩ mm^2/mm which is almost ten-fold resistive than secondarily aged sample therefore it can be said that the secondary aging heat treatment was found to have a favorable electrical conductance.

Keywords: Copper-Chromium Alloys, Aging, Microhardness, Electrical Conductivity

Introduction

Copper is an element that comes across in many areas, it is because of the properties that allow it to be used in many areas. Metals have been used in prehistoric times and at the beginning of the first uses of mankind. Copper was first used by people 10000 years ago. During the archaeological excavations, objects such as pendants, ornaments, containers were found. It is estimated that it was used around 8700 years ago. It is known that one of these substances is pure copper, which is obtained from ore. During the excavations carried out in Anatolia, the use of an alloy called a copper-tin alloy and the use of bronze this period, which began around the year B.C.7000, has been called the Bronze Age. In ancient times, there were findings obtained mainly in the direction of alloying techniques around Thailand. Bronze Age BC Technology transition and ended at 1200 iron experienced (C. A. D., 2010; Davis, 2001; Lipowsky, 2007; Schlesinger, 2011).

History uses copper as an element in terms of places from the past to the present, but it is one of them that has not transferred rare earth materials engineering. As copper can be used alone, different alloying elements can have very different properties with copper according to the purpose of use. Copper alloys, which are usually

used and named after the added alloying elements, are divided into nine groups. (Davis, 2001; Lipowsky, 2007). These alloys differ in their strength, corrosion resistance, etc. to increase it is used for supports.

The Cu-Cr alloys we are considering here are alloys where it is desirable to have high mechanical strength without compromising electrical conductivity as much as possible. Applications of these alloys in the industry; Impact resistant connection with the use of electrical conductivity as a high end in spot welding machines, especially with non-sparking tools in the petrochemical industry (C. A. D., 2010; Davis, 2001; Ellis et al., 1995; Gao et al., 2003; Kim et al., 1995; Raghavan et al., 2017; Sun et al., 2001; Wang et al., 2009) the measure of electrical conductivity is measured according to the conductivity, or electrical resistance of annealed pure copper for all materials. The internationally recognized conductivity unit is recognized as 100% IACS (International Annealed Copper Standard) for annealed pure copper (C. A. D., 2010; Davis, 2001). The electrical conductivity of the Cu - 1% Cr alloy discussed here was measured as 85% IACS.

Copper-Chromium Alloy

Copper alloys containing chromium, classified as a concentration of 0.6-1.2% Cr by weight. Cu-Cr alloys are preferred because of their high strength, corrosion resistance, and electrical conductivity. The tensile strength of Cu-Cr alloys is higher than that of pure copper (221-455 MPa), which can be applied to their strength by precipitation hardening, i.e. aging, and as a result of aging heat treatment can increase to fractions (234-593 MPa). (Davis, 2001). The mechanism of hardening of Cu-Cr alloys occurs by precipitation of chromium from a solid solution, and these high-strength alloys can maintain their strength even at high temperatures. The corrosion resistance of Cu-Cr alloys is better than that of pure copper since chromium forms a protective oxide that protects the alloy from corrosion. Cu-Cr alloy has good cold formability and hot workability, as well as high strength. (Davis, 2001; Durashevich et al., 2002; Krishna et al., 2015).

Resistance welding electrodes, seam welding discs, gears, switches, electrical, electrode holding the jaws, cable connectors, current-carrying arms and rods, circuit breaker parts, arc and bridge components, patterns in electron tubes used Cu-Cr alloys, spot welding tips, copper conductors that require more strength and the electrical and thermal ignition key is used. It is important to use Cu-Cr alloys; resistance welding electrodes, seam welding drives, key electric gears, electrode holding jaws, cable connectors, current-carrying arms and rods, circuit breaker components, electron tubes arc welding lugs and the bridge point of the model components, copper electrical conductors and heat resistance that require more than the ignition key is used.

The Aging Heat Treatment of the Copper-Chromium Alloy

In Cu-Cr alloys that can be hardened by precipitation, the temperature drop reduces the solid chromium solution in copper. The slow-cooled Cu-Cr structure is a two-phase mixture of chromium and a-copper. Superior mechanical properties can be achieved by rapidly cooling Cu-Cr alloys from the annealing temperature, so Cu is saturated with a solid solution of chromium. The microstructure of the rapidly quenched Cu-Cr alloy is similar to that of unalloyed copper. Rapid cooling prevents the accumulation of chromium during solid-state transformation, so the cast structure consists of a single a-copper phase. The first material that begins to solidify is pure copper, which is followed by a eutectic mixture of single a-copper and chromium. a-copper and chromium form a eutectic phase, the plate-like structure is formed in the interdendritic zones. a-copper consists of twin grains in a solid solution. In general, Chromium is quickly cooled so that it remains in the a-copper solid solution. Aging disperses chromium precipitates along with the matrix (Chakrabarti et al., 1984).
Aging heat treatment;

1. Solid solution
2. Quenching to obtain an over-saturated solution
3. Aging to form second phase particles to obtain the desired properties

Materials and Method

The copper and chromium elements were obtained from Alfa-Aeser of high purity 99.99 %. The melting and casting were done in the Leybold-Heraeus vacuum induction melting furnace under an argon atmosphere. The ingots were homogenized at 1000 °C for 72 hours. The samples were solutionized at 950 °C for 4 hours and quenched in water at room temperature. Aging heat treatment was done at 650 °C for 4 hours and quenched in

water. Secondary aging heat treatment was realized at 400 °C for 2, 4, and 6 hours. After completing the heat treatment procedure, the samples were polished and etched with 5 g $FeCI_3$ (ferric chloride), 50 ml HCI, and 100 ml H_20.

The microhardness testing was done by Futuretech make FV-800 instrument with 100 g load for 10 seconds. Electrical resistance measurements were realized by GW-Instek GOM-802 model D.C.Milli-Ohm Meter in auto mode.

Results and Discussion

The microhardness test results revealed that the secondary aging heat treatment improve the hardness. The hardness increases with aging time. The maximum value of hardness obtained in samples aged 650 °C for 4 hours and secondarily aged at 400 °C for 6 hours giving 75 H_v. This hardness value is 12% higher than the samples only aged at 650 °C for 4 hours. The trend in hardness differentiation was given in Figure 1.

Figure 1. Microhardness change versus aging heat treatment

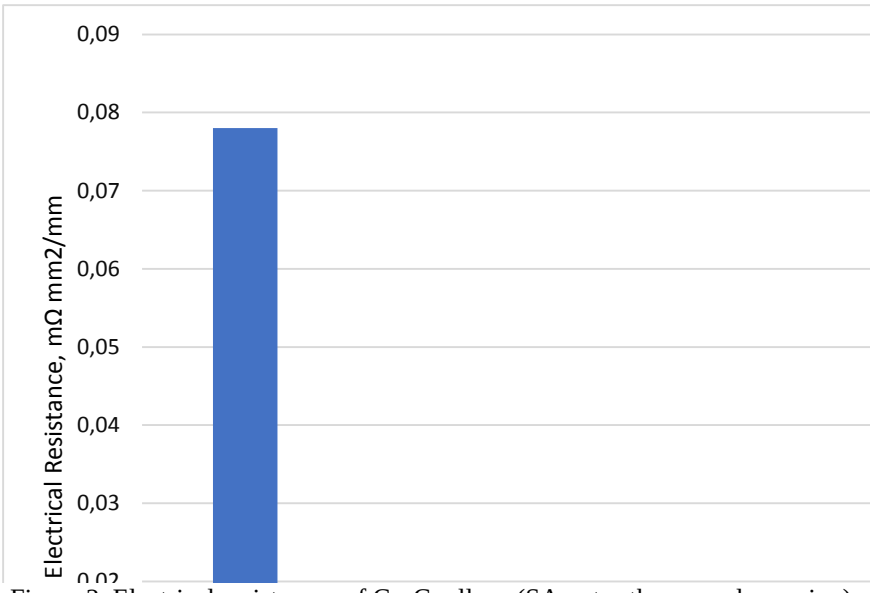

Figure 2. Electrical resistances of Cu-Cr alloys (SA notes the secondary aging)

The electrical resistance of as-cast, aged, and secondarily aged samples showed that electrical resistance was increasing with secondary aging time increase (Figure 2). The electrical resistance is low than the aged and very low than the as-cast condition. The resistance slightly increases with secondary aging time, only 6 hours is

higher than the aged sample, but this can be acceptable if the alloy strength and electrical resistance are taken into consideration together, 6 hours secondary aging time can be said preferrable with respect to aged one.

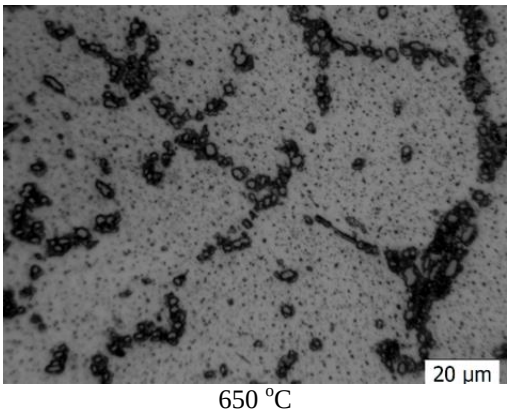

650 °C

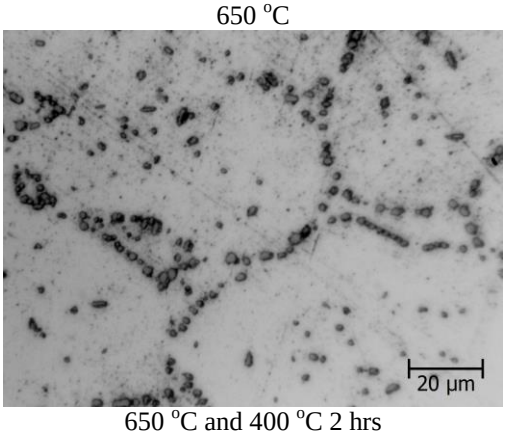

650 °C and 400 °C 2 hrs

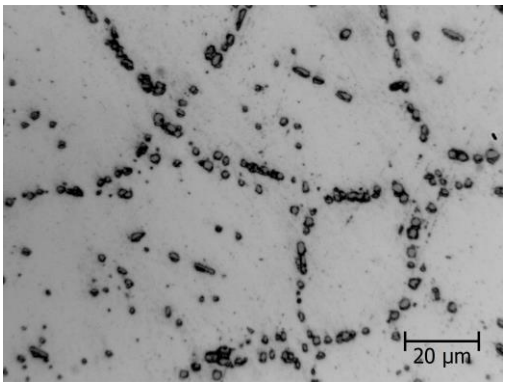

650-400- 4 hrs

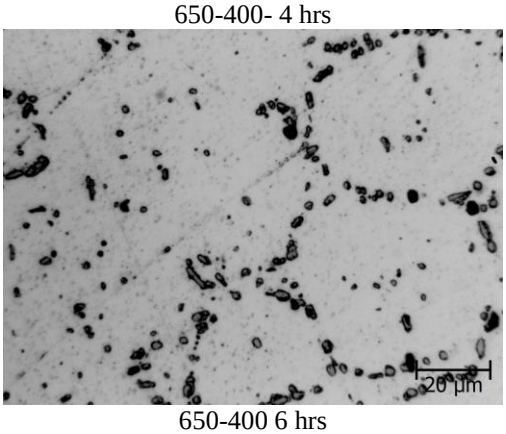

650-400 6 hrs

Figure 3. Microstructures of the aged and secondarily aged samples

The electrical resistance of the as-cast sample was found 0.078 mΩ mm^2/mm, in the aged samples the resistance drops to 0.011 mΩ mm^2/mm, by applying secondary aging for 2, 4, and 6 hours the results are 0.0074, 0.0094, and 0.012 mΩ mm^2/mm respectively. The electrical resistance drops dramatically with aging heat treatment. Additionally, a secondary aging heat treatment increases the conductance 10, 8, and 6.5 times more than the as-cast condition. If the mechanical strength and electrical conductivity are evaluated together secondary aging heat treatment is highly favorable when working in a welding workshop.

The microstructures of aged and secondarily aged samples were given in Figure 3. The microstructures revealed that the grains were coarsening by increasing time in secondarily aged samples. The factors causing the hardness increase are the second phase particles that have precipitated. During aging, with the effect of temperature, alloying elements first begin to gather under edge dislocations. The GP regions, which are clusters of atoms, cause a certain amount of distortion as they create internal stress in the lattice, and at the same time cause the structure to harden even a little. As the aging continues, these clusters begin to form β precipitates compatible with the α matrix phase. These precipitates play a role in increasing hardness. As the aging continues, the sediments grow further and reach a critical height, it is seen from the trend of the graph in Fig.1 that the time and temperature limit required for excessive aging is not reached in the study. Since the experiment was not continued any longer, it was not clear at this stage whether the highest hardness zone was reached. At higher magnifications, the grain coarsening and fine precipitates were seen. As the aging time increases the fine precipitates dispersed very fine all over the matrix. The precipitates in the grain borders were also getting smaller and dispersed through the matrix which confirms the increase of the hardness.

This situation may be useful for the production of materials with higher strengths in tool manufacturing. Especially, it may be a more suitable solution in the production of spot-welding tips, non-sparking tools such as keys and hammers used in petrochemical plants.

Conclusion

The secondary aging heat treatment would be an advantageous production method for increasing the strength of age hardenable alloys. This may also increase the service life of age-hardened parts. But the most important concern should be electrical conductivity. Due to increasing energy costs and production costs, energy saving is very important, with the secondary aging heat treatment it is possible to increase the electrical conductivity. The effect of the secondary aging heat treatment on the electrical conductivity is very good, considering the different heat treatment times, it is seen that the electrical conductivity can be increased from 650% to 1000%. Therefore, we can say that a minimum 50 % energy saving can be made according to aged Cu-Cr alloys.

Scientific Ethics Declaration

The authors declare that the scientific ethical and legal responsibility of this article published in EPSTEM journal belongs to the authors.

References

C. A. D. (2010, August). Copper's Bright Past and Brighter Future. Copper Devlopment Association. https://www.copper.org/publications/newsletters/discover/2010/August/

Chakrabarti, D., & Laughlin, D. (1984). The Cr-Cu (chromium-copper) system. *Bulletin of Alloy Phase Diagrams, 5*(1), 59-68.

Davis, J. R. (2001). *Copper and copper alloys.* ASM international.

Durashevich, G., Cvetkovski, V., & Jovanovich, V. (2002). Effect of thermomechanical treatment on mechanical properties and electrical conductivity of a CuCrZr alloy. *Bulletin of Materials Science, 25*(1), 59-62. doi:10.1007/bf02704596

Ellis, T. W., Kim, S. T., & Verhoeven, J. D. (1995). Deformation-Processed Copper-Chromium Alloys - Role of Age-Hardening. *Journal of Materials Engineering and Performance, 4*(5), 581-586. <Go to ISI>://WOS:A1995TF74800009

Gao, N., Huttunen-Saarivirta, E., Tiainen, T., & Hemmila, M. (2003). Influence of prior deformation on the age hardening of a phosphorus-containing Cu-0.61wt.%Cr alloy. *Materials Science and Engineering a-Structural Materials Properties Microstructure and Processing, 342*(1-2), 270-278. <Go to ISI>://WOS:000179568900031

Kim, S. T., Berge, P. M., & Verhoeven, J. D. (1995). Deformation-Processed Copper-Chromium Alloys - Optimizing Strength and Conductivity. *Journal of Materials Engineering and Performance*, *4*(5), 573-580. <Go to ISI>://WOS:A1995TF74800008

Krishna, S. C., Rao, G. S., Jha, A. K., Pant, B., & George, K. M. (2015). Analysis of Phases and Their Role in Strengthening of Cu-Cr-Zr-Ti Alloy. *Journal of Materials Engineering and Performance*, *24*(6), 2341-2345. <Go to ISI>://WOS:000354890800022

Lipowsky, H., Arpaci, E. . (2007). *Copper in the automotive industry*. Wiley-Vch Verlag GmbH & Co. KGaA.

Raghavan, R., Harzer, T. P., Djaziri, S., Hieke, S. W., Kirchlechner, C., & Dehm, G. (2017). Maintaining strength in supersaturated copper-chromium thin films annealed at 0.5 of the melting temperature of Cu. *Journal of Materials Science*, *52*(2), 913-920. <Go to ISI>://WOS:000387227300023

Schlesinger, Mark E., K. M. J., SoleKathryn C., Davenport William G.I. (2011). *Extractive Metallurgy of Copper* (5th Edition ed.). Elsevier.

Sun, S. J., Sakai, S., & Suzuki, H. G. (2001). Effect of alloying elements on the cold deformation behavior of Cr phase and the tensile strength of Cu-15Cr based in situ composites. *Materials Transactions*, *42*(6), 1007-1014. <Go to ISI>://WOS:000169993000015

Wang, Z. Q., Zhong, Y. B., Cao, G. H., Wang, C., Wang, J., Ren, W. L., . . . Ren, Z. M. (2009). Influence of dc electric current on the hardness of thermally aged Cu-Cr-Zr alloy. *Journal of Alloys and Compounds*, *479*(1-2), 303-306. <Go to ISI>://WOS:000267063300075

Author Information

Bedri BAKSAN
Eskisehir Osmangazi University
Metalurji ve Malzeme Muh.Bolumu, Eskisehir, Turkey
Contact e-mail: *baksan@ogu.edu.tr*

Ibrahim CELIKYUREK
Eskisehir Osmangazi University
Metalurji ve Malzeme Muh.Bolumu, Eskisehir, Turkey

Adem TASDEMIR
Eskisehir Osmangazi University
Maden Muh.Bolumu, Eskisehir, Turkey

To cite this article:

Baksan, B., Celikyurek, I. & Tasdemir, A. (2021). Effect of secondary aging of copper-chromium alloys to electrical conductivity. *The Eurasia Proceedings of Science, Technology, Engineering & Mathematics (EPSTEM), 16*, 63-68.

The Eurasia Proceedings of Science, Technology, Engineering & Mathematics (EPSTEM)
ISSN: 2602-3199

The Eurasia Proceedings of Science, Technology, Engineering & Mathematics (EPSTEM), 2021

Volume 16, Pages 69-76

IConTES 2021: International Conference on Technology, Engineering and Science

Transfer of Personal Driving Styles to Autonomous Vehicles

Silviu BUTNARIU
Transilvania University of Brasov

Florin GIRBACIA
Transilvania University of Brasov

Csaba ANTONYA
Transilvania University of Brasov

Abstract: This paper presents a learning model that can be implemented on autonomous vehicles, using a dedicated software platform, based on physics, which can also be used to track the behavior of components and subsystems of the vehicle. In order to prepare the data for entering the software platform, data (position, orientation, acceleration, instantaneous speed) were recorded from a vehicle driven by several drivers on a previously established route. By processing the data, a driving style was established based on the average values recorded, for each subject who participated in the experimental tests. A virtual environment was created to correspond to the real route in which an autonomous vehicle was modeled and the data on the previously established driving style (instantaneous speeds vs. positions) were transferred. Following the running in the virtual environment and the registration of the data about the behavior of the vehicle on the established route, the data obtained by the classical method and the virtual simulation were compared. Thus, corrections can be made on the speed profile implemented for the autonomous vehicle, in order to comply with the limits imposed by the use of this vehicle with passengers: speed limits, longitudinal and lateral acceleration limits, braking limits.

Keywords: Autonomous vehicle, Driving style, Driver behavior, Simulation.

Introduction

Lately, there have been very intense researches on the autonomous driving of vehicles, which led to an important change in the role of the driver, who goes from an active role to a passive one. These changes imply a new paradigm of the driver-vehicle interaction, the connection between these two elements being modified. On the other hand, the passengers of a car do not have to be additionally stressed if they use autonomous driving, they will have to feel comfortable while driving, as in the case of driving.

Therefore, a large part of the concerns in this field is directed towards the transfer of the driver's knowledge, style and abilities, optimized, if possible, to the autonomous driving system. Several elements have been identified that are measurable and that can define a driver's driving style: acceleration / braking and cornering / trajectory followed in curves. These parameters are measurable; they can be recorded while driving a classic car. Autonomous vehicles require an improved understanding of human driver behavior. This is necessary not only to ensure safe and adequate performance, but also to adapt to the needs of the drivers, enhance their acceptability and, ultimately, meet the preferences of drivers in a safe environment. Therefore, it is essential to recognize the driving style (DS) and deduce the driver's intention for the integration and development of these systems (Martinez, 2018).

State of the Art

In the literature, there have appeared, in the last years, a whole series of researches in the field of autonomous management. Some of this research focuses on a basic question: Is it possible to model an automated and customized driving style based on manual driving? In other words, a passenger will accept to use an autonomous vehicle only if he trusts the automated system and his experience will generate feelings of comfort for you (Sherer e al., 2015; Shi et al., 2015).

In recent years, studies have been conducted on algorithms characterization and recognition of driving styles, with a special focus on machine learning approaches by identifying measurable parameters that contribute to the perceived comfort of the passenger, their recording, processing, analysis and interpretation (Martinez et al., 2018).

Thus, in (Sherer et al., 2015), based on a driving simulation study, the acceleration and braking parameters were studied, as well as the longitudinal control, after which experimental tests were performed on a special track. One conclusion of this experiment was that the longitudinal control of the vehicle has a great impact on the comfort perceived by the subject.

In Van Li et al. (2013), studies were performed using the smartphone, more precisely the inertial sensors mounted on the phone, to record data on braking and turning, by segmenting and classifying driving events. In (Shi et al., 2015) a quantitative assessment of driving styles is proposed using personalized modeling of the driver, based on an algorithm with neural networks. It starts from the test data from the real environment of the vehicle and the road over which a standard driving cycle is tested in order to normalize the driving behavior and based on the analysis of the energy spectral density on the normalized behavior, an aggressiveness index is proposed to Quantitatively evaluate driving styles, which can be used to detect abnormal driving behavior.

In Shinar et al. (2011) a unified model for studying the driver's behavior is proposed, which combines aspects of his driving activity, respectively information about what he does but also the reason for performing a certain maneuver. The tests were performed on a single test driver and the vehicle and the environment have parameters with fixed values. The proposed model is used to evaluate new technologies taking into account the skills and style of a driver.

Other authors have studied particular aspects of activity management, for example, the transition on the railway level. They have tested 24 subjects who crossed a level crossing with passive protection and one with active light signal protection (Grippenkoven et al., 2016). Deficient behavior could be determined in the case of visual detection of a train approaching the level crossing. Several techniques for detecting drowsiness and distraction have been studied in recent years, and some of these techniques have been adopted and implemented by major car companies. In this study (Kaplan et al., 2015), the driver monitoring techniques were carefully examined and the pros and cons were presented, based on several classifiers: characteristics used, classification methods, accuracy rates, system parameters, and environmental details.

McDonald et al. (2019), proposes a review of articles studying automatic vehicle pickup and driver modeling to identify the factors that influence the driving style and their impact on automatic pickup performance. Relevant models for braking and steering operations were studied. Several factors have been identified that influence pick-up time and post-pickup control. It was found that drivers respond similarly between manual emergencies and automatic pick-ups, albeit with a delay.

Another level of research in the field is proposed in (Zhu et al., 2018), where the planning of autonomous leadership is done through the method of deep learning with reinforcement (deep RL - reinforcement learning). The aim is to obtain an optimal policy or a car tracking model, which can be continuously updated, which is intended to operate in a human-like manner, at least in aspects: speed, the relative speed between vehicles in a column, the distance between vehicles, and the acceleration of a vehicle.

In Martinez et al. (2018), an attempt was made to define the concept of "leadership style", taking into account the multitude of researchers studying this area. It was concluded that this is a complex concept, influenced by a very large number of factors that complicate its description, which led to the emergence of many terms, which usually do not have an agreed definition. The driving event is generally understood as maneuvers that occur during driving activity, such as acceleration, deceleration, turning and lane change, which can be used to identify the DS (Martinez et al., 2018).

About Driving Styles, Driver Behavior

Driver behavior can be modeled in one of two approaches (Shinar et al., 2011):

(i) "descriptive" models describing driving activity in terms of what the driver is doing
(ii) "functional" models that seek to explain why the driver behaves as he behaves and how drivers' performance is predicted in demanding and routine situations.

Demanding situations determine peak performance capabilities, and routine situations determine typical behavior (not necessarily the best). It seems that the optimal approach could be a hybrid of several types of models, extracting the most useful features of each (Shinar et al., 2011).

Development of Working Methodology

About Simcenter Prescan

PreScan is a simulation platform based on the laws of physics for the development of Advanced Driver Assistance Systems - ADAS and which can incorporate and use dedicated sensors: GPS, radar, LiDAR, video camera. At the same time, this software platform is used for the design / evaluation of vehicle-vehicle (V2V) and vehicle-infrastructure (V2I), controller (MIL) communication applications in real-time testing with software-in-the-loop (SIL) systems and hardware-in-the-loop (HIL). For calculations, PreScan uses the facilities of Matlab & Simulink (Mathworks, 2021).

In the process of validating the reliability of Advanced Driver Assistance Systems (ADAS), as well as the safety and automatic functionality of an autonomous vehicle, it is necessary to test a very large number of scenarios to cover many of the possible circumstances. Of course, this is very difficult to do with physical / real tests, so virtual simulation is a welcome solution. To perform this type of simulation, it is necessary to use a software platform based on the laws of physics (Siemens, 2021).

Thus, this platform can run various scenarios based on five steps:

(i) a real-world traffic scenario is created using elements from the software database (infrastructure elements, light sources, actors, roads, etc.);
(ii) various types of sensors are introduced;
(iii) the interaction between the vehicle and the environment is tested;
(iv) an interface is used for control systems, data processing, sensor fusion, decision, control;
(v) and various scenarios are run by modifying the input data (roads, sensors, algorithms, etc.).

This software can validate autonomous vehicle systems: emergency braking (AEBS), lane departure warning (LDW), traffic sign recognition (TSR), lane change assistance system (LCAS), etc. At the same time, HMI human-machine interface systems can be designed by using a loop driver and checking the hardware components of the ECU.

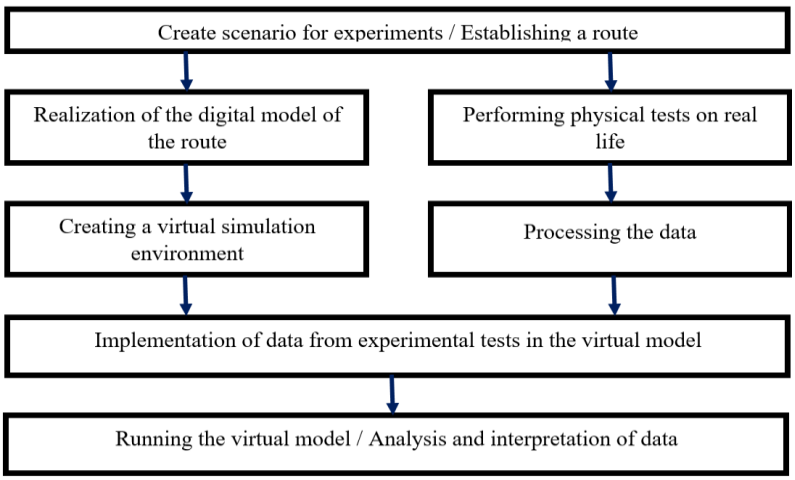

Figure 1. The scenario of experiments

Proposed Working Method

In order to achieve the objectives stated above, a method is proposed that includes the following main steps (Figure 1), including establishing a route, a circuit dedicated to motor vehicles on which practical tests can be performed, realization of the digital model of the route, at 1: 1 scale, proposing a physical testing scenario on the chosen route, performing physical tests and recording data on driving style, processing the data collected during the tests, creating a virtual simulation environment in the PreScan software, based on the proposed route, implementation of data from experimental tests in the virtual model, running the virtual model and recording the data, analysis and interpretation of data obtained from virtual simulation.

Digital Model of the Route

It was decided to use a route around the Research and Development Institute of the Transilvania University of Brasov, with a length of approximately 950 m, insignificant level difference, with a series of turns and speed alignments. In Figure 2, a is presented the area of the Institute, with the route around the buildings, from the *Google Maps* application (https://www.google.ro/maps/@45.6694209,25.5501715,447m/data=!3m1!1e3). In order to digitize the route, a free software application *OpenStreetMap* was used, available on the website https://www.openstreetmap.org/#map=18/45.66934/25.54988 (Figure 2,b). The procedure for obtaining a digitized route in file.osm file (Open Street Map) involves an automatic export of all streets in a selected window and then finishing the results, deleting streets that do not interest us and repairing incomplete ones. Thus, a path is obtained in an .osm file that can be further used in other software applications (Figure 2,c). The route was slightly modified, the lower right part not being accessible by car, creating a small connection segment (Figure 2, d).

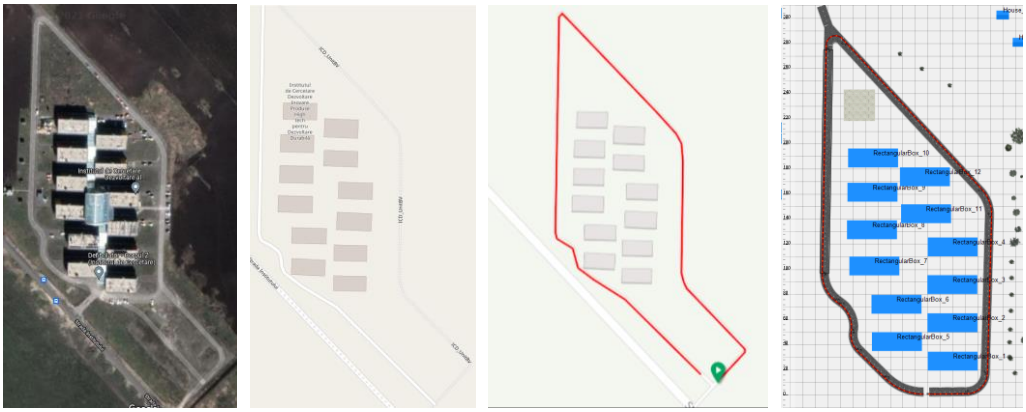

a. b. c. d.

Figure 2. Digital model of the route

Creating A Virtual Simulation Environment

Figure 3. The virtual environment

Based on the digital path obtained using the procedure explained above, a virtual environment is created for simulation in the Simcenter PreScan software program. Besides the digitized route, which is the most important

element, the environment can include other details: buildings, vegetation, traffic signs, other vehicles, pedestrians, etc (Figure 3).

Each element of the virtual environment can be customized, configured according to the needs of the experiment. Of course, an important actor is the vehicle on which the simulations will be made. For example, speed can be limited on a route segment. For a vehicle, the operating characteristics but also the number, type and characteristics of the sensors with which it is equipped can be configured.

Conducting Physical Tests

In order to record various characteristics of the personal driving style of the vehicles, experiments were performed using the track around the Research-Development Institute in Brasov, using two cars with different technical characteristics and two drivers (Mercedes GLC - 2018, Renault Laguna -2013). The data was recorded by the sensors of some mobile phones (Samsung Galaxy S20 and Xiaomi Redmi Note 10 Pro), mounted on the same plane support to simultaneously record the same data, using Matlab software (https://www.mathworks.com/). Two tests were performed for each driver and each car. The data recorded on the phone, in .csv files for each sensor, were taken on a personal computer where they were processed using the same program, Matlab. The recording settings sensors were: acceleration, magnetic field, orientation, angular velocity, position. Sensor recordings were made at different frequencies. If for accelerations, the reading frequency was 100 Hz, for position recording with the GPS sensor, the frequency was much lower, only 10 Hz.

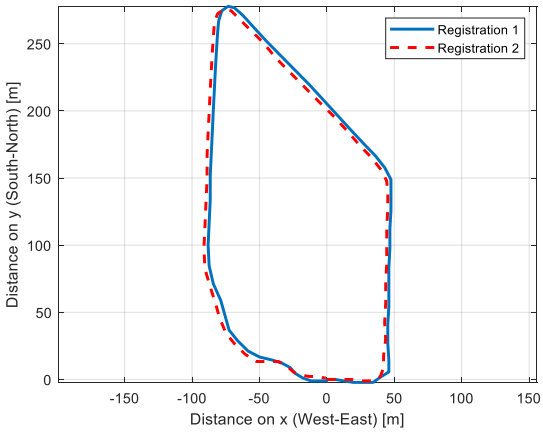

Figure 4. Car position registration

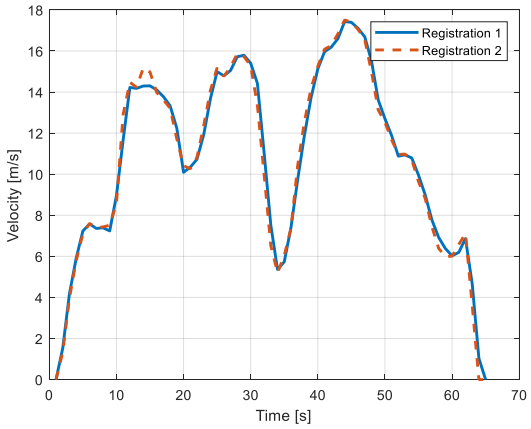

Figure 5. Speed variation

Because recordings of several sensors were made, the data fusion method was used in the data processing stage. The following figures show some of the results obtained: the variation of the position, in X and Y coordination, based on GPS measures (Figure 4) and the variation of the speed depending on the time during operation for the two cars (Figure 5).

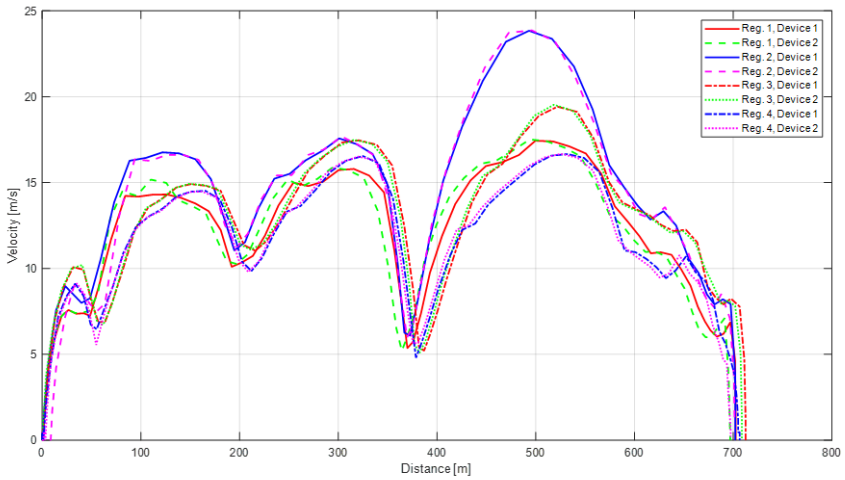

Figure 6. Instantaneous speed depending on the total distance traveled

Following the fusion of the data obtained by the sensors and the calculation of the instantaneous speed according to the position of the car, the graph below was made, where on the X-axis is found the total distance traveled by the car since the beginning of the experiment (Figure 6). In this graph, there are 8 curves performed in the experimental tests, which represent 4 runs on the chosen route registered with 2 devices. The curves marked with Reg.1 and Reg.4 belong to Subject no. 1, and those with Reg.2 and Reg.3 correspond to the actions of the Subject no. 2. There is some difference between the driving styles of the two drivers. One of them runs at a higher speed accelerating and decelerating in force, having a sportier style (Figure 6, Reg. 2). The other driver involved in the tests, runs at lower speeds, this requiring fewer spectacular accelerations and braking (Figure 6, Reg. 4).

Simulation of Driving in The Virtual Environment

First, the route in the virtual environment was compared with the route obtained from the physical tests, based on the measurements with GPS sensors and some small differences were repaired. Thus, following the measurements, a route of length between 697 ... 714 m was obtained. The route in the virtual environment, which corresponds in shape to the real route, has a total length of 704.39 m. The route was divided into several segments, each with different geometric characteristics (straight lines, curves of different radius sizes, in both directions). In order to simulate, the data regarding the speeds of the vehicles, recorded during the tests, on various segments of the route were used for the configuration of the autonomous vehicle introduced as an actor in the virtual environment (Figure 6, Reg.1, Device 1). For testing, a car from the software library was used (Citroen C3 Hatchback), capable of being configured within very wide limits (Figure 7). After configuring the system based on the scenario proposed at the beginning, the application is saved in PreScan and then transferred to be processed in Matlab / Simulink.

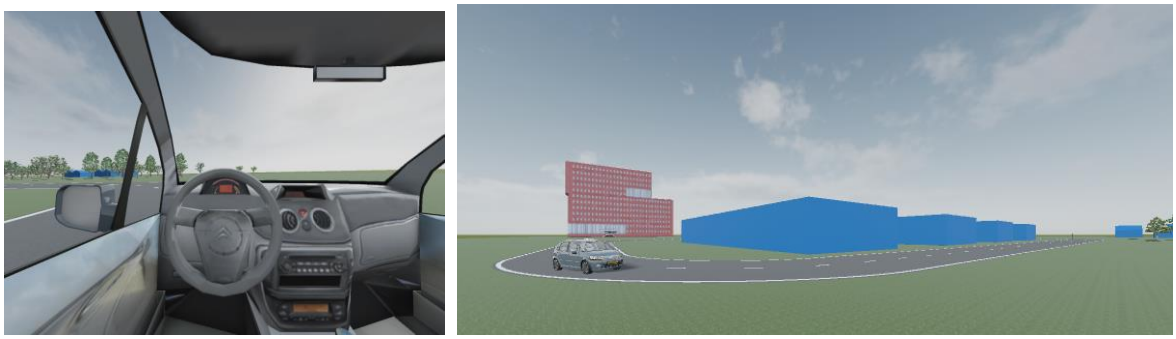

a. b.

Figure 7. Actors in Prescan: Citroen C3 Hatchback (a. cockpit view during simulation; b. view from a fixed point outside the route)

After running the Simulink model, various results can be obtained, depending on the input data and the test objectives: data on vehicle dynamics, data on the operation of certain subsystems (throttle pedal, brake, wheel direction, etc.).

Results and Conclusion

The present simulation aimed at the operation of an autonomous vehicle to which an individualized data set was transferred, which contains a series of speed recordings along an established route. After a first simulation, the behavior of the vehicle in operation can be observed, especially in the case of very small radius curve segments where it is possible not to follow the imposed trajectory due to high speeds. In this way, corrections can be made on the speed profile implemented for the autonomous vehicle, in order to respect some limits imposed by its use with passengers: speed limits, longitudinal and transversal acceleration limits, braking limits.

Figure 8 shows the variation of the speed of the autonomous vehicle as a function of time after running the scenario in the virtual environment. A comparison can be made with the input data, presented in Figure 5, Reg. 1, Device 1, continuous red line. There is a small difference between these two curves. These differences can come from various constants that can be set at the beginning of the simulation (environmental characteristics: air pressure, temperature; interaction between the vehicle and the road: friction coefficient; constructive characteristics of the vehicle).

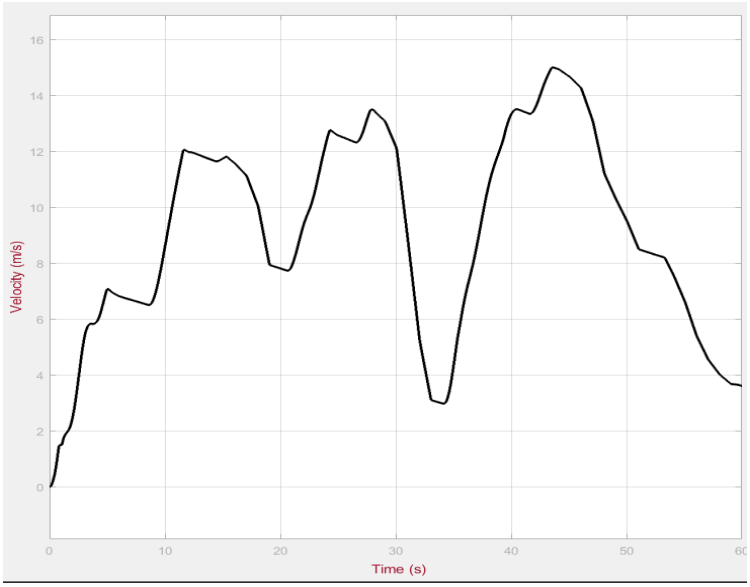

Figure 8. Results: vehicle speed variation

The proposed method can be used for programming and virtual testing of autonomous vehicles using driving styles recorded on various routes with classic vehicles. Passengers included in these field-tests can participate by answering various questionnaires that aim to identify the limit values of accelerations, decelerations, speeds, lateral accelerations. For example, in the case of bus public transport, they travel on urban roads, which are usually not designed to be used at high speeds. Therefore, although there are commonly accepted limit standards or values for speeds and accelerations, a real test is required for various route segments in order to establish adequate driving styles and accepted by passengers.

With the proposed virtual simulation, there will be no need for real tests, all changes can be made in the software program and the results obtained are accessed, verified, processed and discussed immediately. Thus, segments with a strong effect on passengers can be eliminated, passages between different speed values can be smoothed, and accelerations can be limited.

Acknowledgements

This work was supported by a grant of the Ministry of Research, Innovation and Digitization, CNCS/CCCDI – UEFISCDI, project number PN-III-P2-2.1-PED-2019-4366 within PNCDI III (431PED).

Scientific Ethics Declaration

The authors declare that the scientific ethical and legal responsibility of this article published in EPSTEM journal belongs to the authors.

References

Grippenkoven, J. and Dietsch, S. (2016). Gaze direction and driving behavior of drivers at level crossings. *Journal of Transportation Safety & Security*, *8*(1), 4-18. DOI: 10.1080/19439962.2015.1046620.

Kaplan, S., Guvensan, M. A., Yavuz, A. G., & Karalurt, Y. (2015). Driver behavior analysis for safe driving: A survey. *IEEE Transactions on Intelligent Transportation Systems*, *16*(6), 3017-3032. DOI: 10.1109/TITS.2015.2462084.

Martinez, C. M., Heucke, M., Wang, F. Y., Gao, B., & Cao, D. (2017). Driving style recognition for intelligent vehicle control and advanced driver assistance: A survey. *Transactions on Intelligent Transportation Systems*, *19*(3), 666-676. doi: 10.1109/TITS.2017.2706978.

Mathworks (2021, September 28) PreScan Simulation of ADAS and active safety. https://ch.mathworks.com/products/connections/product_detail/prescan.html.

McDonald, A. D., Alambeigi, H., Engström, J., Markkula, G., Vogelpohl, T., Dunne, J., & Yuma, N. (2019). Toward computational simulations of behavior during automated driving takeovers: a review of the empirical and modeling literatures. *Human Factors*, *61*(4), 642-688. doi: 10.1177/0018720819829572.

Scherer, S., Dettmann, A., Hartwich, F., Pech, T., Bullinger, A. C., & Wanielik, G. (2015, November). *How the driver wants to be driven-modelling driving styles in highly automated driving* [Conference presentation]. 7. Tagung Fahrerassistenzsysteme. Munich.

Shi, B., Xu, L., Hu, J., Tang, Y., Jiang, H., Meng, W., & Liu, H. (2015). Evaluating driving styles by normalizing driving behavior based on personalized driver modeling. *IEEE Transactions on Systems, Man, and Cybernetics: Systems*, *45*(12), 1502-1508. doi: 10.1109/TSMC.2015.2417837.

Shinar, D., & Oppenheim, I. (2011). Review of models of driver behaviour and development of a unified driver behaviour model for driving in safety critical situations. In *Human Modelling in Assisted Transportation* (pp. 215-223). Springer. https://doi.org/10.1007/978-88-470-1821-1_23.

Siemens (2021, September 2). S*imcenter Prescan - Develop more reliable and safer automated vehicle functionalities*. https://www.plm.automation.siemens.com/global/en/products/simcenter/prescan.html, acc sept.2, 2021.

Van Ly, M., Martin, S., & Trivedi, M. M. (2013, June). Driver classification and driving style recognition using inertial sensors. In *2013 IEEE Intelligent Vehicles Symposium (IV)* (pp. 1040-1045). IEEE. doi: 10.1109/IVS.2013.6629603.

Zhu, M., Wang, X., & Wang, Y. (2018). Human-like autonomous car-following model with deep reinforcement learning. *Transportation Research Part C: Emerging Technologies*, *97*, 348-368. https://doi.org/10.1016/j.trc.2018.10.024.

Author Information

Silviu BUTNARIU
Transilvania University of Brasov
29 Eroilor Blvd., RO-500036, Brasov, Romania

Florin GIRBACIA
Transilvania University of Brasov
29 Eroilor Blvd., RO-500036, Brasov, Romania

Csaba ANTONYA
Transilvania University of Brasov
29 Eroilor Blvd., RO-500036, Brasov, Romania
Contact e-mail: *antonya@unitbv.ro*

To cite this article:

Butnariu, S., Girbacia, F. & Antonya, C. (2021). Transfer of personal driving styles to autonomous vehicles. *The Eurasia Proceedings of Science, Technology, Engineering & Mathematics (EPSTEM), 16*, 69-76.

The Eurasia Proceedings of Science, Technology, Engineering & Mathematics (EPSTEM)
ISSN: 2602-3199

The Eurasia Proceedings of Science, Technology, Engineering & Mathematics (EPSTEM), 2021

Volume 16, Pages 77-81

IConTES 2021: International Conference on Technology, Engineering and Science

Study of the Lithium Diffusion Properties of (Mgconilizn)O High Entropy Oxide as an Anode in Lithium-Ion Battery

Ersu LOKCU
Eskisehir Osmangazi University

Mustafa ANIK
Eskisehir Osmangazi University

Resat Can OZDEN
Eskisehir Osmangazi University

Abstract: High-entropy oxide (HEO) based materials have recently significant attention as a conversion type anode material for lithium-ion batteries (LIBs) due to the high specific capacity, cycling stability and rate capability. However, the diffusion kinetics of HEO based anodes for conversion reactions, which occur during the charge and discharge processes have been not studied deeply in the literature. Therefore, the diffusion properties of lithium in the HEO electrodes need to be studied in detail. In this work, the (MgCoNiLiZn)O HEO anode was synthesized by conventional solid-state method. The obtained HEO sample was characterized structurally by X-ray diffraction (XRD) and scanning electron microscopy (SEM) techniques. The XRD analysis show that the HEO sample has been successfully synthesized with a single-phase rock-salt structure. The lithium diffusion properties of HEO sample were investigated by various electrochemical techniques including electrochemical impedance spectroscopy (EIS) and cyclic voltammetry (CV).

Keywords: High entropy oxide, Lithium diffusion coefficient

Introduction

Rechargeable Li-ion batteries, which have become the main power source for portable electronic devices since the day they were discovered. They are also the most promising systems in the short and medium term for applications where high capacities are required such as electric vehicles. Li-ion battery energy densities have reached around the 300 Wh/kg (18650 type battery configuration); however, studies are continuing rapidly and intensive efforts are being made to increase this value even more (Puthusseri et. al., 2018). In this context, most of the studies have focused on the synthesis of high-performance anode and cathode materials with a high energy density (Etacheri et. al., 2011; Lu et. al., 2018).

One of the main driving forces in materials science is the discovery of new materials with functional properties. The discovery of high entropy alloys in recent years is one of the best examples of this. The discovery of high-entropy alloys has also led to the emergence of many new high-entropy materials such as high-entropy carbide, nitride, boride, sulfur, and oxide (Rost et. al., 2015; Oses et. al., 2020)

Among these high entropy materials, it has been shown that the MgCoNiCuZnO material, which is included in the high entropy oxide class, has high-capacity cycling capability for Li-ion batteries and exhibits a behavior that is significantly different from the classical anode materials. It has been proven that this improvement in cycling ability is due to entropy stabilization (Sarkar et. al., 2018). Following this study, many high entropy

oxides were synthesized and investigated as anodes for Li-ion batteries. However, the diffusion kinetics of HEO based anodes for conversion reactions, which occur during the charge and discharge processes have been not studied deeply in the literature. In this work, we evaluated the lithium diffusion coefficients of rock-salt type (MgCoNiLiZn)O by using electrochemical impedance spectroscopy (EIS) and cyclic voltammetry (CV) techniques.

Materials and Methods

MgO, CoO, NiO, ZnO and Li_2O were mixed homogeneously in the equimolar ratios to get (MgCoNiLiZn)O high entropy oxide and they ball-milled at 300 rpm for 2 h by using the planetary ball mill (Fritsch Pulverisette 7 Premium Line). The obtained oxide mixture was then unaxially pressed into the pellet of 10 mm diameter at 300 MPa. Finally, the oxide pellet was sintered at 1000ºC for 12 h, and then it was air-quenched. The phase structures and morphologies of the as-synthesized (MgCoNiLiZn)O HEO were examined by XRD and SEM techniques, respectively.

The electrochemical tests of (MgCoNiLiZn)O electrode was performed in lithium half-cell configuration. The electrode was prepared by mixing 75 wt% ball-milled (MgCoNiLiZn)O, 15 wt% carbon black (Super P) and 10 wt% polyvinylidene fluoride (PVDF) in N-methyl pyrrolidinone (NMP) to form a homogeneous slurry. Then the slurry was coated onto Cu foil by brushing. CV tests were conducted in the voltage range of 0.01-3.0 V vs. Li/Li^+ under different scan rates. EIS measurements were performed with an amplitude of 5.0 mV in the frequency range from 100 kHz to 0.01 Hz.

Results and Discussion

Figure 1 shows the XRD pattern of as-synthesized (MgCoNiLiZn)O sample. The result shows that the sample has a single-phase rock-salt crystal structure. The XRD peaks are given with the MgO reference, which shift due to the presence of five different cations in the structure.

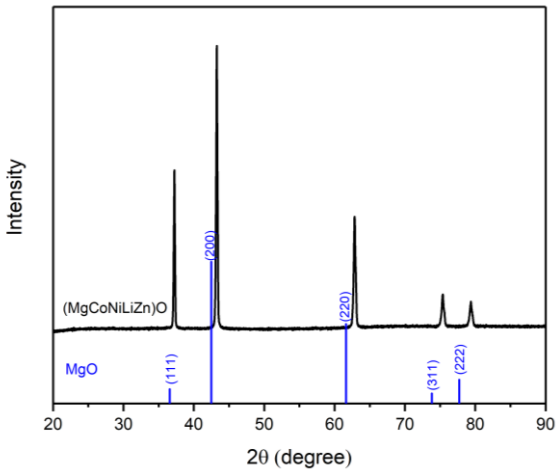

Figure 1. XRD pattern of the (MgCoNiLiZn)O sample

Figure 2 shows typical SEM micrographs of the as-synthesized (MgCoNiLiZn)O sample. The size of the particles ranges from about 0.5 μm to 40 μm. The variable morphological structure of the sample was attributed to the use of the conventional solid-state method in the synthesis process.

CV tests were performed under the different scan rates to investigate the lithium diffusion kinetics in the (MgCoNiLiZn)O electrode. As it is known, the peak current values in the CV curves for cathodic and anodic reactions changes according to the scan rate. This provides a way to understand the diffusion kinetics of lithium at the electrode/electrolyte interface. Figure 3 shows the CV curves with a different scan rate. The relationship and chemical lithium diffusion coefficient can be determined from the Randles-Sevcik equation: (Ding et. al., 2009)

$$i_p = (2{,}69 \times 10^5) n^{\frac{3}{2}} A D_{Li^+}^{\frac{1}{2}} C_{Li^+}^{*} v^{1/2}$$

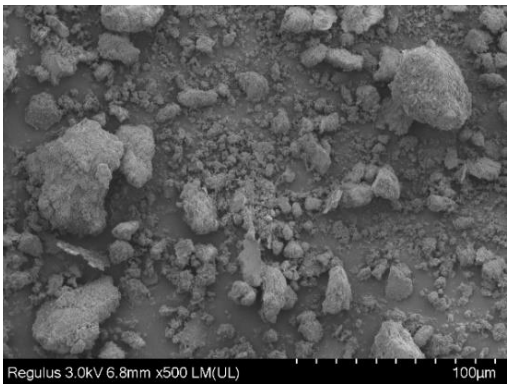

Figure 2. SEM image of the (MgCoNiLiZn)O sample

Where, i_p is the peak current, n is the charge transfer number in (MgCoNiLiZn)O, A is the contact area between electrode and electrolyte, C_{Li}^* is the bulk concentration of lithium in electrode, and ν is the scan rate. The peak current has a linear relationship with the square root of scan rate according to equation.

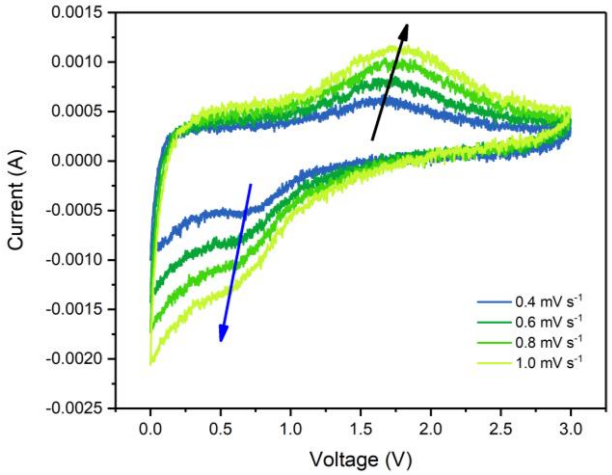

Figure 3. CV curves with a various scan rate of (MgCoNiLiZn)O electrode.

The D_{Li}^+ values calculated at different scan rates of the (MgCoNiLiZn)O electrode is given in Table 1. As seen from the table, The D_{Li}^+ values at different scan rates are in the range of 10^{-13} cm^2 s^{-1}. It has been observed that the diffusion coefficients of similar high entropy oxide-based electrodes changes in the order of 10^{-12} cm^2 s^{-1}-10^{-15} cm^2 s^{-1} in the literature. The high lithium diffusion coefficient in the electrode material indicates that the reaction requirement can be met and better rate performance can be achieved at high current densities.

Table 1. Calculated D_{Li}^+ values of (MgCoNiLiZn)O electrode.

(MgCoNiLiZn)O		Scan rate (mV s^{-1})			
		0.4	0.6	0.8	1.0
D_{Li}^+ (cm^2 s^{-1})	Anodic peak	$4.45x10^{-13}$	$5.11x10^{-13}$	$5.53x10^{-13}$	$5.69x10^{-13}$
	Cathodic peak	$3.52x10^{-13}$	$4.86x10^{-13}$	$6.35x10^{-13}$	$7.58x10^{-13}$

Figure 4 presents the Nyquist plot of (MgCoNiLiZn)O electrode. Based on the Warburg impedance, the diffusion coefficient of the lithium ion is calculated through the following equation (Qiu et. al., 2019)

$$D_{Li} = \frac{R^2T^2}{2A^2n^4F^4C^2\sigma^2}$$

Where, R is the gas constant, T is the absolute temperature, A is the surface area of the electrode, n is the charge transfer number in (MgCoNiLiZn)O, F is the Faraday constant, C is the molar concentration of Li^+ in the (MgCoNiLiZn)O and σ is the Warburg coefficient. The σ_w is calculated from the slope of Z' vs. $\omega^{-0.5}$ (ω is the angular frequency) in the Warburg region according to the following equation. The R_s and R_{ct} are solution and charge transfer resistance, respectively.

$$Z' = R_s + R_{ct} + \sigma\omega^{-1/2}$$

The D_{Li}^{+} value of (MgCoNiLiZn)O electrode at the charged state 3.0 V is calculated as 1.88 x10^{-13} cm^2 s^{-1} from EIS datas.

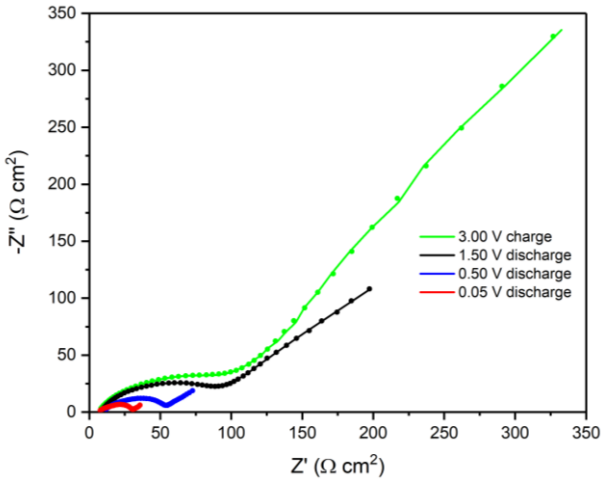

Figure 4. The Nyquist plots of (MgCoNiLiZn)O under different states.

Conclusion

As a conclusion, equimolar (MgCoNiLiZn)O HEO were synthesized with a single-phase rocksalt crystal structure by the conventional solid-state method. In addition, cyclic voltammetry and electrochemical impedance spectroscopy techniques were conducted to evaluate the lithium diffusion coefficient of (MgCoNiLiZn)O electrode. Lithium diffusion coefficients from CV and EIS were in the range of 10^{-13} cm^2 s^{-1}. These values are better than Lithium diffusion coefficients values of many conversions type single transition metal oxides.

Acknowledgement

This work was supported by The Scientific and Technological Research Council of Turkey under the contract number 219M269.

Scientific Ethics Declaration

The authors declare that the scientific ethical and legal responsibility of this article published in EPSTEM journal belongs to the authors.

References

Ding, N., Xu, J., Yao, Y.X, Wegner, G., Fang, X., Chen, C.H. & Lieberwirth, I. (2009). Determination of the diffusion coefficient of lithium ions in nano-Si. *Solid State Ionics*. *180*, 222–225.

Etacheri, V., Marom, R., Elazari, R., Salitra, G., & Aurbach, D. (2011). Challenges in the development of advanced Li-ion batteries: a review. *Energy & Environmental Science*, *4*(9), 3243.

Lu, J., Chen, Z., Pan, F., Cui, Y., & Amine, K. (2018). High-performance anode materials for rechargeable lithium-ion batteries. *Electrochemical Energy Reviews*, *1*, 35−53.

Oses, C., Toher, C., & Curtarolo, S. (2020). High-entropy ceramics. *Nature Reviews Materials*, *5*(4), 295-309. https://doi.org/10.1038/s41578-019-0170-8.

Puthusseri, D., Wahid, M., & Ogale, S. (2018). Conversion-type anode materials for alkali-ion batteries: State of the art and possible research directions. *ACS omega*, *3*(4), 4591-4601.

Qiu, N., Chen, H., Yang, Z., Sun, S., Wang, Y., & Cui, Y. (2019). A high entropy oxide (Mg0. 2Co0. 2Ni0. 2Cu0. 2Zn0. 2O) with superior lithium storage performance. *Journal of Alloys and Compounds*, *777*, 767-774.

Rost, C. M., Sachet, E., Borman, T., Moballegh, A., Dickey, E. C., Hou, D., ... & Maria, J. P. (2015). Entropy-stabilized oxides. *Nature communications*, *6*(1), 1-8.

Sarkar, A., Velasco, L., Wang, D. I., Wang, Q., Talasila, G., de Biasi, L., ... & Breitung, B. (2018). High entropy oxides for reversible energy storage. *Nature communications*, *9*(1), 1-9.

Author Information

Ersu LOKCU
Metallurgical and Materials Engineering
Eskisehir Osmangazi University
Contact e-mail: *elokcu@ogu.edu.tr*

Mustafa ANIK
Metallurgical and Materials Engineering
Eskisehir Osmangazi University

Resat Can OZDEN
Metallurgical and Materials Engineering
Eskisehir Osmangazi University

To cite this article:

Lokcu, E., Anik, M., & Ozden, R.C. (2021). Study of the lithium diffusion properties of (Mgconilizn)O high entropy oxide as an anode in lithium-ion battery. *The Eurasia Proceedings of Science, Technology, Engineering & Mathematics (EPSTEM), 16*, 77-81.

The Eurasia Proceedings of Science, Technology, Engineering & Mathematics (EPSTEM)
ISSN: 2602-3199

The Eurasia Proceedings of Science, Technology, Engineering & Mathematics (EPSTEM), 2021

Volume 16, Pages 82-86

IConTES 2021: International Conference on Technology, Engineering and Science

Evaluation of an Event Detection Algorithm for Russian and Kazakh Languages

Aigerim MUSSINA
Al-Farabi Kazakh National University

Sanzhar AUBAKIROV
Al-Farabi Kazakh National University

Paulo TRIGO
Universidade de Lisboa

Abstract: The Event Detection area is gaining increasing interest among researchers. The social media data growth induces the emergence of new algorithms along with the improvement of existing solutions. In this paper we propose to improve of existing algorithm for event detection, SEDTWik (Segment-based Event Detection from Tweets using Wikipedia). The authors define event as a set of similar segments of words within a given time window. A segment is defined as a word or phrase taken from the analyzed text data. The SEDTWik uses Wikipedia as a "supervisor" to identify the segments, to calculate the segments' bursty value and to calculate the segments' newsworthiness. We examined the SEDTWik algorithm using our data from Telegram online social network. The overall network message construction of Twitter is different from that of Telegram. Therefore, we transformed the Telegram meta-data to fit the SEDTWik requirements. Another much relevant difference in our experiment lies in the fact that our corpora contain messages in Russian and Kazakh languages. Our results show that the SEDTWik algorithm is strongly dependent on the broad and unfocused Wikipedia data. Such dependency was shown to have a loss effect on the event detection accuracy. This result founds our motivation to improve the SEDTWik algorithm using dynamically calculated segment probabilities from the analyzing data streams.

Keywords: Event detection, SEDTWik, Russian language, Kazakh language

Introduction

Social data analysis is gaining in importance due to the increasing use of social media by people. One of the social data analysis area is Event Detection. In this paper we present our initial and current steps in the field of Event Detection analysis. Our initial step was driven by the need to gather data from social media, so our previous work (Mussina, 2021) builds an architecture for data crawling from Online Social Networks (OSN). In our current step we are driven by the need to add an effective and accurate Event Detection module to our (already implemented) architecture.

We have chosen Telegram OSN as our first data source (Mussina, 2021) given that in January 2021 Telegram's world-wide monthly active users reached 500 million users. The Telegram is a popular social network among the countries from Commonwealth of Independent States (CIS). During our previous experiments we analyzed locally popular channels and groups that use the Russian and Kazakh languages. From those previous experiments we proceed to current work where we are focused on applying the Event Detection algorithm to the Russian and Kazakh language data.

During this research stage we examined several existing Event Detection algorithms. In the end we chose the work (Morabia, 2019) which presented the algorithm called SEDTWik (Segment-based Event Detection from Tweets using Wikipedia). In this algorithm the data stream divided by user-defined time window and goes as input data. SEDTWik starts with tweet text segmentation. After that the bursty value extracts from segment according to its expected probability and other meta-data. Segments with the highest value clustered to events. As a result, each event is characterized by time window, segments and newsworthiness. All details we describe in next section.

Related Works

During this research we explored the articles that provide publicly available code (Papers with code). Therefore, it was easy to us to reproduce the algorithms and understand whether it would be possible to apply each algorithm to our data. Several algorithms were tested on their test data.

The works (Hamborg, 2019; Du, 2020) are based on the idea of "answering questions". In Hamborg (2019) authors used 5W1H questions: What? Who? When? Where? Why and how? Another researcher (Du, 2020) used "almost natural questions". However, here we have many questions and small OSN messages could not give an answer to all of them. The work (Liu, 2018) suggests to extract multiple events from a single sentence. The data partition as a single sentence is similar to our OSN messages. However, the code was difficult to run and the explored dataset ACE 2005 is not free.

Finally, we examined the SEDTWik algorithm presented in a clearly written paper with, explaining formulas and illustrating examples. The code was easy to execute and test on small part of the Events2012 dataset (McMinn, 2013). The base idea of the algorithm is the usage of Wikipedia. Tweet is segmented by phrases and if segment is in the Wikipedia Titles Dataset (Wikimedia Downloads) then segment goes further. In the next step the bursty value is extracted using segment expected probability, user followers count, retweet count. The expected probability denotes the probability that a segment will appear in the text of a tweet. It is calculated on the dataset Events2012. Next segments with the highest bursty values clustered and generated event summary with newsworthiness. The newsworthiness calculated from Wikipedia Keyphraseness (Sun). Therefore, SEDTWik test on our data should include the substitution of Wikipedia English data to Russian and Kazakh data.

Method

In this section we present the adaptation of SEDTWik algorithm to fit the data from Telegram OSN. The main changes considered base programming model of OSN data and expected segment probability.

Table 1. Comparison of Twitter and Telegram

Twitter	Telegram
Users should be registered. Messages are small. Can use hashtags (#) and user mentioning (@).	
User can post tweet on his/her page	User should be a member of a group/channel to post a message in group's chat and in threads of channels
User can write a comment under another user's tweet	User can reply to all messages inside a group
User can retweet another user's tweet	User can forward another user's message
Users have own pages	Users can enter the groups, channels

Telegram Model

The Telegram and Twitter are different OSNs. The Telegram acts like messenger with extended opportunities. The Twitter is more like a place for self-expression and interaction with all users inside the network. We denoted common and different aspects of each network (Table 1). One of the main differences is that Telegram

has groups, super groups and channels. The member's capacity and administrators' opportunities are growing from groups to channels.

The SEDTWik data model includes tweet's text, creation date, user with its id and followers count, retweet count and entities. The entity is a hashtag and/or user mention inside tweet. Therefore, it doesn't have some functionalities presented in Twitter. For example, Telegram doesn't have retweets, user followers, and hashtags are available, but they are not usually used. We substituted some Twitter specific fields in a model to bring Telegram model (Figure 1). As depicted in the Figure 1, we substituted: a) followers count by count of chat/channel members, and b) retweet count by count of messages in thread.

Twitter	Telegram
{ "created_at": "2021-10-25 15:00:00", "text": "@Random, simple text #test", "user": { "id": 000000000, "followers_count": 118 }, "retweet_count": 100, "entities": { "hashtags": ["test"], "user_mentions": ["Random"] } }	{ "created_at": "2021-10-25 15:00:00", "text": "@Random, simple text #test", "user": { "id": 000000000, "chat_members_count": 118 }, "thread_message_count": 100, "entities": { "hashtags": ["test"], "user_mentions": ["Random"] } }

Figure 1. Twitter and Telegram JSON models

The authors of SEDTWik stated that tweets from users with millions of followers should have more weight than tweets from users with few followers. We transposed that idea to Telegram and propose that messages from chats/channels with thousands of members should have higher weight than those from chats/channels with few members.

The retweet transposition (from Twitter to Telegram) is a difficult task in terms of compliance. At first, we thought that message forwarding is similar to retweet process. Both the concepts of retweet and of forwarding a message are responsible for spreading information among members of groups or channels and retweets do the same. However, in Telegram it is difficult to know the amount of message forwarding. We only know that message was forwarded, but we don't know how many times. Another solution is to use Telegram threads that are a separate branch of conversation in channels and super chat groups. The number of messages in a thread may be used as a metric on the users' interest in a thread's discussion. Such a metric is similar to the retweet count metric, because retweet count also shows how many people are interested in a tweet.

English Wikipedia Substitution with Russian and Kazakh

Firstly, we need to substitute the Wikipedia Titles Dataset with publicly available Wikipedia dumps. We downloaded (Wikimedia Downloads) Wikipedia Titles Dataset for Russian and Kazakh languages. Secondly, we substituted the expected probabilities, we used our tokens frequency and calculated probability. Our tokens frequency calculated during text preprocessing. In our architecture, after a message is crawled it goes to the text preprocessing tokenization and token frequency calculation processes.

Thirdly, we need to substitute the Wikipedia Keyphraseness file, however it is hard to replace file quickly, because it was calculated separately and the Wikipedia articles dump creation date was January 30, 2010. So the data even for English data could be old. Since the Keyphraseness demonstrate the probability that segment could be anchor of Wikipedia article, we could replace it via our dictionary. The dictionary is a set of words with special thematicity value. Word is present in a dictionary if it is connected to the dictionary topic. For example, we took sport-topic dictionary. All words inside this dictionary describe the sport topic. The thematicity value denotes the degree of belonging to the dictionary. More details about dictionary extraction is given in our previous work (Mussina, 2017).

Results and Discussions

For the first tests, we subjectively chose the events that took place during the Olympic Games Tokyo 2020, from July 23 to August 8, 2021. The included events and the Event Detection results with Russian Wikipedia and our sport dictionary are presented below (Table 2). The event describing segments are translated to English from Russian and Kazakh for clarity in column 5. We created a sport dictionary based on two types of channels: sport and news. As a result, dictionary has actual information in period from 2021-07-01 to 2021-07-31.

Table 2. Sport event detection

	Event description	Date	Detected events	Detected events. Translation
1	Eldos Smetov won first medal for Kazakhstan in judo	2021-07-25	EVENT 1: игорь, сон, медаль, EVENT 2: нашим, состав, спорт,	EVENT 1: igor, son, medal, EVENT 2: our, composition, sport,
2	Igor Son won second medal for Kazakhstan in barbell			
3	Zulfia Chinshanlo third medal for Kazakhstan in barbell	2021-07-26	EVENT 1: бокс, алтын, олимпиада, EVENT 2: медаль, live, html, чиншанло,	EVENT 1: boxing, altyn, olympics, EVENT 2: medal, live, html, chinshanlo,
4	Vasiliy Levit losing in boxing	2021-07-27	EVENT 1: баландин, теннис, мугуруса,	EVENT 1: balandin, tennis, mugurus,
5	Strong tennis match Rybakina/Bencic in ½	2021-07-29	EVENT 1: рыбакина, бенчич, арна	EVENT 1: rybakina, benchich, arna,
6	Tennis match Rybakina/Svitolina in ½ for bronze	2021-07-31	EVENT 1: финале, победы, ошибки, EVENT 2: наши, медали, турция,	EVENT 1: finals, victories, mistakes, EVENT 2: our, medals, turkey,
7	Kamshybek Kunabayev losing in boxing	2021-08-04	EVENT 1: золото, равно, бокс, EVENT 2: завтра, мог, шанс,	EVENT 1: gold, equals, boxing, EVENT 2: tomorrow, might, chance

We can see that 3 out of the 7 events were detected (i.e., an accuracy of around 40%). Therefore, we consider these, lower than 50%, accuracy as foundational for the motivation to improve results. We propose that SEDTWik algorithm could be improved via Wikipedia substitution with topic dictionary. The implementation of topic dictionary could improve results and make them more focused. Nevertheless, topic dictionary could be dynamically constructed on the basis of interested data stream.

Conclusion

In this paper we briefly present the start of our research in the field of Event Detection. We examined the SEDTWik algorithm and exploited its applicability in our corpora. We substituted the English Wikipedia Titles Dataset with the Russian and Kazakh Wikipedia Titles Dataset, used our calculated token probability and used sport topic dictionary to cluster the events. Although the results on Event Detection are often subjective after our experiments, we can conclude that SEDTWik algorithm is applicable to our data. We also expect that changing the Wikipedia usage also could improve the results. In future work we will explore substituting the Wikipedia data with dynamically created topic dictionaries.

Scientific Ethics Declaration

The authors declare that the scientific ethical and legal responsibility of this article published in EPSTEM journal belongs to the authors.

References

Du, X., & Cardie, C. (2020). Event extraction by answering (almost) natural questions. *arXiv preprint arXiv:2004.13625*.

Hamborg, F., Breitinger, C., & Gipp, B. (2019). Giveme5w1h: A universal system for extracting main events from news articles. *arXiv preprint arXiv:1909.02766*.

Liu, X., Luo, Z., & Huang, H. (2018). Jointly multiple events extraction via attention-based graph information aggregation. *arXiv preprint arXiv:1809.09078*.

McMinn, A. J., Moshfeghi, Y., & Jose, J. M. (2013, October). Building a large-scale corpus for evaluating event detection on twitter. In *Proceedings of the 22nd ACM international conference on Information & Knowledge Management* (pp. 409-418).

Morabia, K., Murthy, N. L. B., Malapati, A., & Samant, S. (2019, June). SEDTWik: segmentation-based event detection from tweets using Wikipedia. In *Proceedings of the 2019 Conference of the North American Chapter of the Association for Computational Linguistics: Student Research Workshop* (pp. 77-85).

Mussina, A. B., Aubakirov, S. S., & Trigo, P. (2020, November). An Architecture for Real-Time Massive Data Extraction from Social Media. In *International Conference on Mathematical Modeling and Supercomputer Technologies* (pp. 138-145). Springer. https://doi.org/10.1007/978-3-030-78759-2_11

Mussina, A., & Aubakirov, S. (2018). Dictionary extraction based on statistical data. *Вестник КазНУ. Серия математика, механика, информатика*, *94*(2), 72-82.

Papers with code. (n.d.). *Event detection*. Papers with code. https://paperswithcode.com/task/event-detection

Sun Aixin. (n.d.). *Wikipedia Keyphraseness*. https://personal.ntu.edu.sg/axsun/datasets.html.

Wikimedia Downloads. (n.d.). Data downloads. https://dumps.wikimedia.org/

Author Information

Aigerim MUSSINA
al-Farabi KazakhNational University
71 al-Farabi Ave., Almaty, Republic of Kazakhstan, 050040
Contact e-mail: *mussina.aigerim95@gmail.com*

Sanzhar AUBAKIROV
al-Farabi KazakhNational University
71 al-Farabi Ave., Almaty, Republic of Kazakhstan, 050040

Paulo TRIGO
ISEL - Instituto Superior de Engenharia de Lisboa; GulAA; LASIGE, Faculdade de Ciências, Universidade de Lisboa, 1959-007, Lisbon, Portugal

To cite this article:

Mussina, A., Aubakirov, S. & Trigo, P. (2021). Evaluation of an event detection algorithm for Russian and Kazakh languages. *The Eurasia Proceedings of Science, Technology, Engineering & Mathematics (EPSTEM), 16*, 82-86.

The Eurasia Proceedings of Science, Technology, Engineering & Mathematics (EPSTEM)
ISSN: 2602-3199

The Eurasia Proceedings of Science, Technology, Engineering & Mathematics (EPSTEM), 2021

Volume 16, Pages 87-97

IConTES 2021: International Conference on Technology, Engineering and Science

Adaptable Fiber Laser Control Unit

Brindus COMANESCU
Optoelectronica 2001 S.A.

Paul SCHIOPU
University Politechnica of Bucharest

Marian VLADESCU
University Politechnica of Bucharest

Mihaiela ILIESCU
Institute of Solid Mechanics of the Romanian Academy

Abstract: Today fiber laser is widely used due to their performances and flexibility. They replace old types of lasers in the industrial machines. To develop a family of laser machines it is the need of having standard laser source that could efficiently be used and replaced in the equipment, independently of the laser source or types of lasers. This paper presents the concept and development of a new fiber laser control unit developed to be used for CW, QCW or pulsed regime. Control unit could be used in multiple laser source and satisfy complex requirements. The control unit of the fiber laser source is able to be used in a different type of fiber laser like: Yb doped fiber, Erbium fiber, thulium fiber. Control unit is designed to be used direct or with minimum modifications in different laser processing applications like: marking, engraving, cutting, drilling, welding, etc. Main parameters of control unit are: 3 working regime, frequency - 1 KHz (QCW), frequency in pulsed regime : 15KHZ - 500 KHz, control seed laser, control pre amplifier and amplifier. Control unit allows commands for machine control: start/stop, interlock, system ready/ fault.

Keywords: Fiber laser, Control unit, Fiber laser control, Laser processing

Introduction

LASER is an acronym for ***L***ight ***A***mplification by ***S***timulated ***E***mission of ***R***adiation. *Laser marking* is an application very used today in different industries like: machine production, automotive, aerospace, marketing etc. Main applications are related to mark a bar code, data matrix, serial number or on different types of components, parts, etc, Laser marking is used in marketing, commercial applications like: jewellery marking, logo, image, watch etc. Marked products are made from metals or non-metals like: wood, plastic. Laser marking has main advantage that is not easy to be removed from marked product but has also a big disadvantage from same reason. In case of a marking error, it needs to replace the part with a wrong marker and this is a problem especially for strictly controlled production. Laser marking is used as method to avoid counterfeit and for brand protection.

The main advantages of various types of laser marking are (Lazov, Narica, Deneva, 2015):

- durable process;
- non-contact technology;

- precise beam focusing;
- high speed machining;
- high contrast and quality of the treatment;
- high productivity and low operation cost;
- good accessibility, even if the surface is irregularly shaped;
- easy automation and integration in the manufacturing process;
- prompt localization of laser energy to the work piece;
- high accuracy;
- environmental technology.

Laser engraving is a particular case of laser marking, based on removal of material.

Laser Marking Methods

There are eight laser marking methods detailed below (Lasers, 2021; Marking Lasers, 2021; Optoelectronica 2001; Security Document Solutions, 2021; Laser Etching, Engraving & Annealing, 2021; Laser Marking, 2021; Cook, Cooper, & Tentzeris, 2013; Laser cutting makes antennas greener, 2013):

i) *Laser Engraving / Evaporation* - Engraving (Figure 1a, b) creates high heat during marking, which causes vaporization of the material. Material is removed during the process. Laser processing effect is concentrated just to surface avoid (Figure 1a, b).


a)


b)

Figure 1. Laser engraving - a) draft/outline principle, b) example

ii) *Laser etching* - Etching (Figure 2) occurs when laser beam heat and melt material of the surface. Melted material expands, causing a raised mark. Is named sometimes melting or foaming.


a)


b)

Figure 2. Laser etching - a) draft/outline principle, b) example

iii) *Laser Bonding* - Pigment (Figure 3) or other coating is applied to the surface of material. The heat generated by a laser beam bond coating to the surface.


a)


b)

Figure 3. Laser bonding - a) draft/outline principle, b) example

iv) *Laser coat* – This marking method is used when it is not possible to engrave directly the surface, because for example the surface is reflective. In that case surface of the material is coated with a paint or similar (Figure 4). When laser beam is directed to surface, laser beam remove coating and remains just surface. We have a contrast between surface non-coated and coating.


a)


b)

Figure 4. Laser coating - a) draft/outline principle, b) example

v) *Laser Coloration / Annealing* -
Coloration (Figure 5) is achieved by using low-power laser beam slowly across the material. This method uses pulsed laser regime and modify the pulse energy and repetition rate. Due to different surface heating, locally surface change the colour.

Figure 5. Laser coloration – example

It is also possible to coat the surface with a pigment (invisible), and under laser interaction the pigment become visible.

Annealing (Figure 6) is a particular case used especially in stainless steel medical tools marking. Tools suffer just a surface colour change because the surface is slow heated. There is no under surface engraving so for such case, there is no possible for bacteria or yields to remains.

 a)

b)

Figure 6. Annealing – - a) draft/outline principle, b) examples

vi*) Laser ablation* - Ablation (figure 7) is the process of coated surface engraving. This method creates excellent contrast without affecting the underlying material.

Figure 7. Laser ablation - draft/outline principle

vii) *Deep engraving* - is the process when laser removes the material under surface level of tens or hundreds of microns. It is used for example in jewellery engraving, or in industrial engraving (figure 8a). In some applications, material removed is fill in with another material to get a contrast like in figure 8b.

a)

b)

Figure 8. Deep engraving – examples

viii) *Laser application in RFID*
In figure 9a is presented an application of fiber laser etch used in making RFID. In figure 9b is another use of fiber laser engrave or cut used to obtain an RFID antenna. Antenna is printed on a substrate using metal ink and laser is used to engrave the exact profile of antenna or just to cut the antenna.

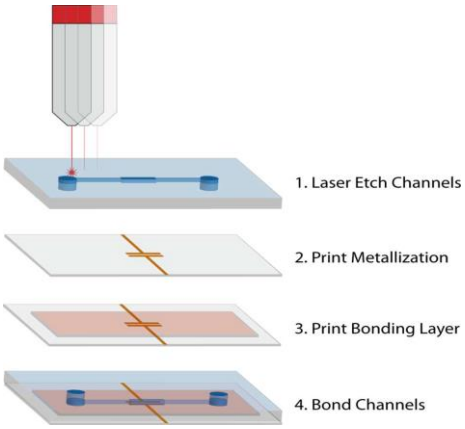

a)


b)

Figure 9. Laser application in RFID techniques – a) RFID laser etch, b) RFID laser engrave/cut

Laser Marking Machines

From point of view of marking machine there are 2 types of marking principles. Each type is used in appropriate application (Lazov, Narica & Deneva, 2015).

i) *Raster Marking* - is similar with principle of dot matrix printer. In this case there is a laser beam that interact with object instead of pins push by printing head to a ribbon and paper. The laser mark spot by spot on a line, after that the laser is moved to next line and mark a line of spots. Raster marking is used in applications were is necessary high speed, especially when are marked texts. Rarely this method is used to mark drawing images (photos/logos), i.e., where there is no need to have high quality and high volume of information (figure 10).

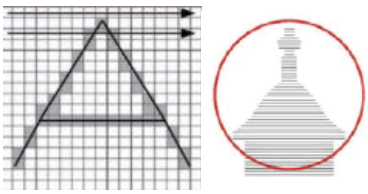

Figure 10. Raster marking

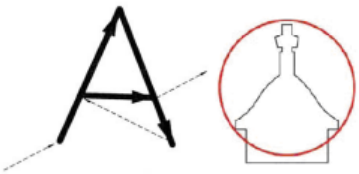

Figure 11. Vector marking

ii) *Vector marking* – This marking principle is used especially when it is need to have quality in marking numerical codes, bar codes, logos, etc (figure 11). Laser marking is like line drawings.

Both marking methods: vector and raster are implemented in fiber laser marking machines.
A fiber laser marking machine can be built in two construction types:
- with galvanometer head,
- with gantry or plotter type.

In this paper we consider galvanometer type fiber laser marking machine. Such type of machine is composed by: fiber laser source, galvanometer head, optical system, electronics. To develop a high quality fiber laser marking machine it is need to have: high quality fiber laser source, high quality optics. Laser source can work in CW in QCW or in pulsed regime. Below we will describe development of a adaptable fiber laser control unit used in laser source for fiber laser marking machine.

Method

Fiber Laser Control Unit Development

Below we will present the development of adaptable Control Unit (CU) for MOPA fiber laser (Optoelectronica 2001 S.A.). Control Unit is adaptable because with minimum of modification can be used for different types of

fiber laser: CW, QCW of pulsed fiber lasers. In figure 12 it is presented MOPA fiber laser control unit (Optoelectronica2001, 2015) the fiber laser block schema Fiber laser is composed by seed laser, pre amplifier, amplifier, cooling system, control unit and output system.

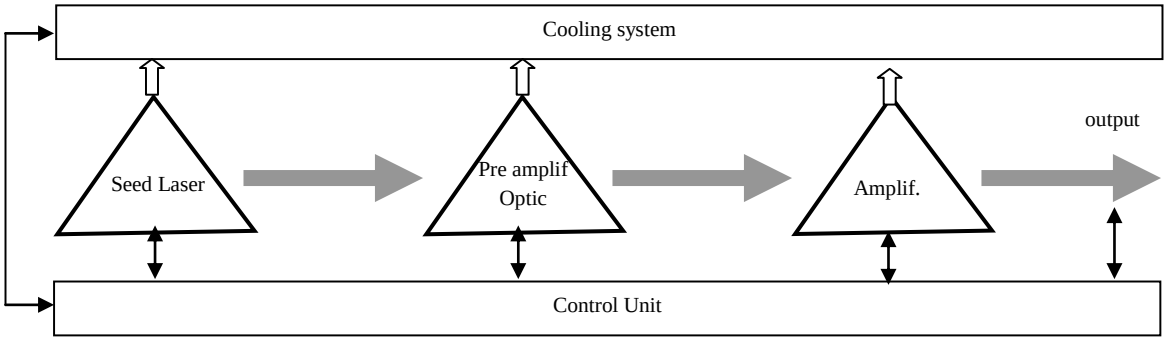

Figure 12. Fiber laser block schema

The CU is designed for MOPA fiber laser, and schema of such laser is shown in figure 13.

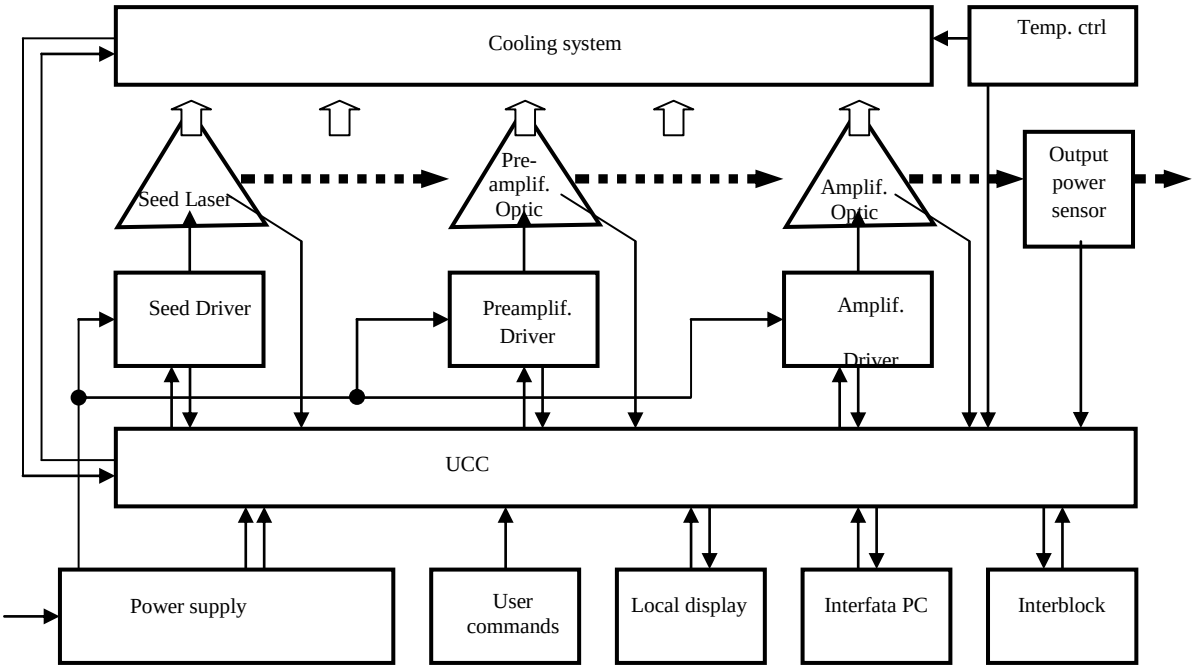

Figure 13. MOPA fiber laser

The MOPA fiber laser is composed by following assemblies:
Seed laser
Pre amplifier
Amplifier
Temperature measurement loop
Output power sensor loop
Cooling system
CU
Display
PC interface
Interblock
Power supply
MOPA fiber laser has 2 users: administrator (full access) user (limited access).
Commands that should be able to execute the CU are:

For LASER SEED:

- Command " Pulse Laser " - TTL output
- Read performing laser pulse - input TTL
- Read temperature fault driver - TTL input
- Read seed laser damage - TTL input

For Pre-Amplifier:

- " Pulse Laser " - TTL output
- ' current simmer ' - 0 -10V analogue output
- ' diode current " - 0 -10V analogue output
- Read diode current real - 0 -10V analogue input
- Read temperature fault driver - TTL input

Optical Amplifier:

- Pulse Laser - TTL output
- current simmer - 0 -10V analogue output
- diode current - 0 -10V analogue output
- Read diode current real - 0 -10V analogue input
- Read temperature fault driver - TTL input
- Laser Marker
- PWM output

Cooling System Command:

- Command cooling - serial RS232 / TT
- Command emergency cooling system - TTL input an optical floor to control the operation:
- Command diode temperature Pre-amplificator Optic - analogue input
- Command temperature diode optical amplifier - analogue input
- Command temperature fiber - analogue input
- Read laser power output - analogue input one for control commands and external interlock:
- Read switch " Interlock " - TTL input
- Read general emergency switch 'red button' - TTL input
- Read laser control switch type pedal - TTL input one for control commands from an external device:
- Read command " START Laser " - TTL input
- Read command " Fault" - TTL input
- Read command " External " - TTL input
- Command laser output power - 0 -10V analogue input
- Analog "external" - 0 -10V analogue input
- Order Laser Marker - TTL input
- Signalling ' System ready " - TTL output
- Signalling " Fault " - TTL output
- System for interfacing with a PC computing
- Serial Bus USB
- human operator for the local interface
- LCD with Touch Screen
- Generic interface: 4 digital lines

Administrator

CU developed has following working regimes (figure 14):

-*Continuous (CW)* – pumping diodes and seed diode are fed and laser radiation laser output power is controlled from the control current optical amplifier.
-*(QCW)* – pumping diodes and seed diode are fed, modulated (PWM) and laser radiation output power is controlled by the optical amplifier current command and the duty cycle of the PWM modulation - operating frequency 1Hz - 1kHz, 10% modulation - 90 %

-Pulsed (P) - seed diode is controlled by high frequency (15kHz - 500kHz) pulse duration is controlled in the ns regime. Current of the diodes in the pre amplifier and amplifier length is modulated (PWM) duty cycle also QCW mode is given by the number of laser pulses required functionality.
Thus, in this regime can control - Output frequency laser pulses, amplitude, duration and pulse train length.

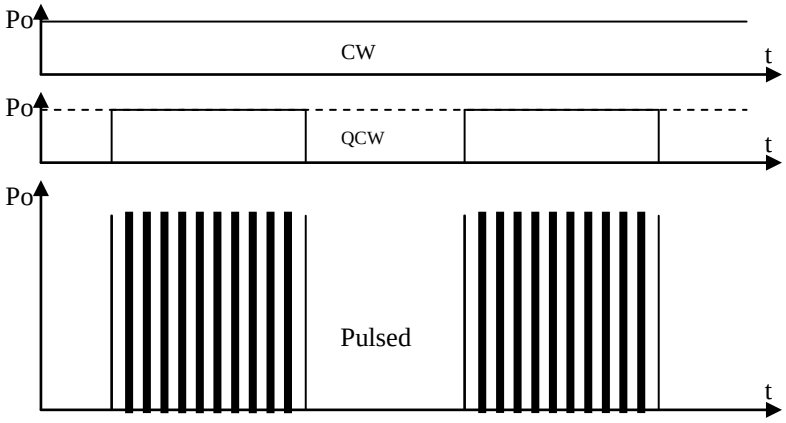

Figure 14. Working regime

Table 1. A CU developed as is described has following performances:

Parameter	Value
Working regime	CW, QCW, PULSE
Current command Pre amplifier driver	0 -10V- customized
Power supply command, Amplifier Driver	0 -10V- customized
Frequency command in QCW regime	1Hz .. 1KHz- customized
Frequency command in PULSE regime	15KHz…500KHz
Duty cycle QCW regime	1% … 100%
Pulse width	20ns ….500ns
Width pulse factor (multiple of)	10ns
External interface	UART, I2C
Outer command for machine tool	Output power
Outer command from machine tool	Start LASER
Outer command from machine tools	Start Laser Mark
Outer command from machine tool	System Ready, FAULT
Local commands	Interlock, Red push button
Local display	LCD, Color 65K, 480x272
Chiller control	UART
MTBF	100.000 hours
Cooling	Air/water
Power supply	5Vcc ± 5%
Maxim weight	300g
Size	180 x 120 x 25 mm
Temperature range	10 – 40^{o}C
Storage temperature.	0 + 50 ^{o}C
Humidity	5 - 85 %

Administrator MODE

Using an RS232 connection and connecting CU to a computer an administrator has access to the device using available commands (delete/insert CW/QCW/PULSE commands) as well as a quick sensors overview. Upon connection the admin is greeted with a message to provide authentication:

- log in: "***admin***"
- password: ***"ADMIN".***

User Mode

The user has access to 3 screens: command type selection, command selection (from the previously chosen type) and a screen to use the selected command.

Command Type Selection Screen

First the command class is chosen (by pressing on the "CW"/"QCW"/"PULS" icons). If there are no commands of that type in memory nothing will happen. To add commands, use a RS232 connection, log in with admin credentials and add commands

Command Selection Screen

All commands of that type will be displayed (left side of the screen), with a short description of the selected command in the right side of the display, to cycle trough the commands the buttons in the bottom left of the screen can be used.

In dynamic regime pulses for command optical pre amplifier and optical amplifier are in PWM regime with adjustable frequency in range 1 Hz - 1000 Hz and duty cycle between 10% and 90%. Pulses for seed laser has adjustable width in range 20 ns - 100 ns and frequency adjustable in range 15 KHz - 500 KHz. As conclusion we need a micro system able to control:

- 9 TTL output
- 14 TTL input from which 8 fault signals (critical)
- 3 UART serial line
- 1 serial line I2C
- 4 analog output from which one is critical (optical amplifier command)
- 8 analog inputs from which one is critical (Optical amplifier command)
- digital signal generator in rage 15KHz - 500KHz with controlled pulse in domain 15KHz- 500Khz with controlled pulse in the range 20 - 100ns.

Analog resolution are chosen for 0.1% error accordingly 1000 levels and accordingly 10 bits - 1024 levels.
Pulse generator clock should be Fck = 1/Tmin and correlated
Fck = 1/20ns.
Fck = 50Mhz
Resolution of pulse generator should be:
Nmax > Fck/ Fmin,
N> 50MHz / 15kHz, so N > 3333
We choose N = 4096 (12biti)
Rezolution of PWM generator is given by minimum and maximum frequency and control of duty cycle should be minimum in range 1-1000 -keeping error in limit 0.1%.
So, for maximum frequency of 1KHz timer clock should be
Fck = 1000 x Fmax,
Fck = 1000 x 1 kHz, Fck= 1MHz
Minimum frequency is Fmin = 1 Hz
Minimum resolution of timer PWM is: N = Fck / Fmin, N = 1.000.000. Because of pre-existence scale in micro systems: 1,8,64,256 and 1024, minimum resolutions attributes:
N1 = 125.000 according 17 bites and prescaler 8

N2 = 15.625 according 14 bites and prescaler 64
We chose needed resolution for PWM timer 16bits.
So, it is need to use a micro controller that fulfil followings criteria:

- Convertor Digital Analog (DAC) 10 bites;
- Convertor Analog Digital (ADC) 10 bites integrated;
- Interruption (INT0);
- Internal timer intern minim 50MHz (20ns pulse) with minim 12 bits;
- Timer with PWM with minim 16 bites;

We choose microprocessor Atmel AT90PWM3B.

Results and Discussion

The CU build according design consideration presented in paper is shown in figure 15.

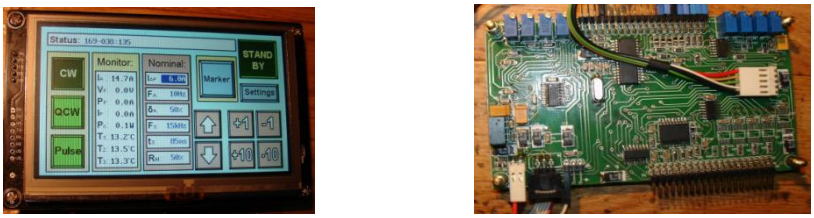

Figure 15. Fiber laser control unit – a) front face, b) back face

We assembly the fiber laser CU in a MOPA fiber laser. MOPA fiber laser is assembled in a laser engraving machine type galvanometer style.

In figure 16 there is presented the seed laser. Seed laser is composed by a seed diode emitting on 1064 nm +/- 5 nm. Diode is mounted on a laser driver. Driver allows CU control, connection with power supply from fiber laser.

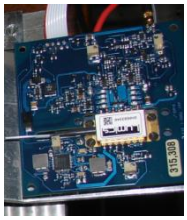

Figure 16. Seed laser

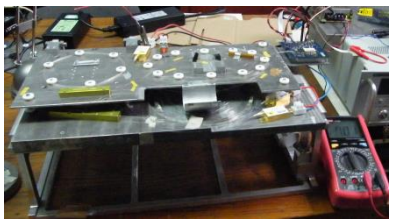

Figure 17. Fiber laser assembled

Figure 18. Laser output

In figure 17 is shown the fiber laser assembled. Right side is seed driver with diode mounted. In center is pre amplifier and amplifier.The CU is assembled on the front face of laser structure. Is not shown in the figure 17? In figure 18 is presented the laser emission of laser at output of MOPA fiber laser. Visually is demonstrated the quality of laser and practic were tested using dedicated device and result were M2< 1.5.

We make some tests in order to check the usage of CU for a MOPA fiber laser:

- output laser quality (see figure 18)
- laser power stability
- laser working regime
- output power
- engraving test

First test were demonstrate in figure 18. Laser power stability were check in following manner. The lasers were started and work 5 min without laser emission. Laser emission were started, CW regime were defined and power were increased until 3W were measured with laser power meter. Lasers were in function for 5 minute.

After that we start the laser stability test and we measure laser power with powermeter at each 5 minutes for 1 hour. The laser is stable and the graph is shown in figure 19.

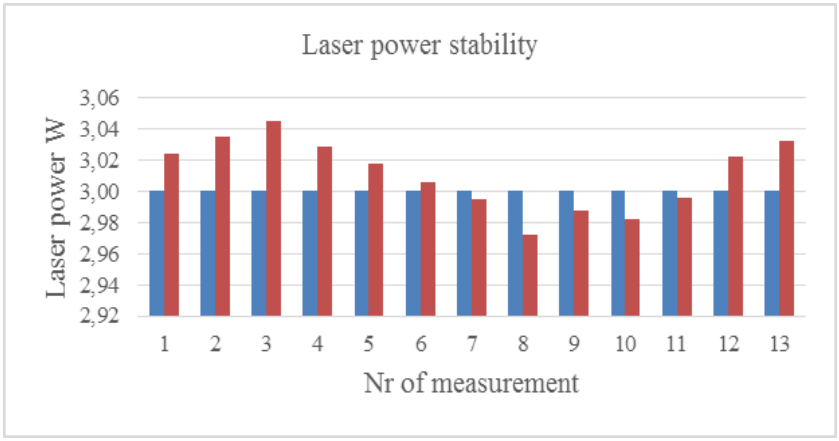

Figure 19. Laser stability measurement (legend blue – reference level, red – experimental values)

For working regime, we program the laser to work in CW regime and we are waiting 1 hour at 3 W and another 1 hour at 5 W. Laser works.
For laser QCW we program the laser to work and we are waiting 1 hour (figure 20 a,b,c). Laser works well.

a)

b)

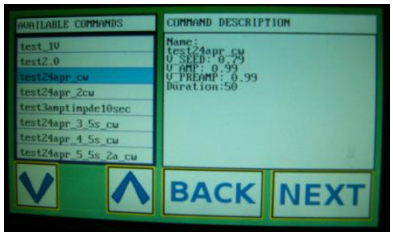

c)

Figure 20. Laser work programming - a) laser working regime selection, b) example of QCW program, c) laser working regime example

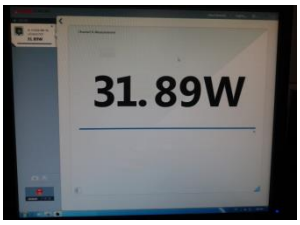

a)

b)

Figure 21. Laser power measurement – a) juno +F150A, b) laserstar +F150A

To test output power, we put laser to work in CW regime and we increase the power slowly up to maximum. We notice that maximum laser power is 100W. In figure 21a and figure 21b are examples of laser power measurements. Measurements were executed with Ophir instruments: Laser star with head F150A-BB-26 and Ophir Juno with same head. MOPA fiber laser equiped with CU works well.

Conclusion

We design execute and test a adaptable control unit for fiber laser MOPA style.
The CU is adaptable because can be used for different types of lasers with minimum modification.
The CU can be programmed to work in 1, 2 or all three-working regime with minimum modifications. Such type of CU allows develop a family of fiber lasers working in different regimes.
We demonstrate possibility of such CU to work.

Acknowledgements or Notes

The research results were obtained within the research project "Combined technologies for high security intelligent multilayer hologram development - TECOMHOLISIG "- 2020 - 2022under call **PN-III-P2-2.1-PTE-2019-0578.** The Laser unit was designed and realized in the" Production of a new type of fiber optic laser within the company S.C. FIBER LASER OPTICS S.R.L" – INOFLO research project (2013 – 2015)

Scientific Ethics Declaration

The authors declare that the scientific ethical and legal responsibility of this article published in EPSTEM journal belongs to the authors.

References

Cook, B.S., Cooper, J. R. & Tentzeris, M. (2013). An inkjet-printed microfluidic RFID-enabled platform for wireless lab-on-chip applications. *IEEE Transactions on Microwave Theory and Techniques, 61*(12), 4714-4723. doi:10.1109/TMTT.2013.2287478

Laser cutting makes antennas greener. (2013). Retrieved from https://www.elektormagazine.com.

Laser Etching, Engraving & Annealing. (2021). Retrieved from https://www.lasitlaser.com.

Laser Marking. (2021). Retrieved from https://www.laserax.com.

Lasers. (2021). Retrieved 2021, from https://www.pannier.com.

Lazov, L., Narica, P., Deneva, H. (2015). Laser Marking Methods. *10th International Scientific and Practical Conference - Environment. Technology. Resources ISSN 1691-5402. Volume I*, pp. , 108-115. Rezekne: Environment. Technology. Resources. doi:http://dx.doi.org/10.17770/etr2015vol1.221

Marking Lasers. (2021). Retrieved from https://www.trumpf.com.

Optoelectronica 2001 S.A., i. (n.d.).

Optoelectronica2001. (2015). *Technical Documentation for Ffiber Laser Optics Control Unit.*

Security Document Solutions. (2021). Retrieved from https://keit.bg.

Author Information

Brindus COMANESCU
Optoelectronica 2001 S.A.
Strada Lacului 35, Măgurele, 077125, |Romania
Contact e-mail: brindus_comanescu@yahoo.com

Paul SCHIOPU
Politehnica University of Bucharest
Splaiul Independenţei 313, Bucharest, 060042, Romania

Marian VLADESCU
Politehnica University of Bucharest
Splaiul Independenţei 313, Bucharest, 060042, Romania

Mihaiela ILIESCU
Institute of Solid Mechanics of the Romanian Academy
Strada Constantin Mille 15, Bucureşti 030167, Romania

To cite this article:

Comanescu, B., Schiopu, P., Vladescu, M. & Iliescu, M. (2021). Adaptable fiber laser control unit. *The Eurasia Proceedings of Science, Technology, Engineering & Mathematics (EPSTEM), 16*, 87-97.

The Eurasia Proceedings of Science, Technology, Engineering & Mathematics (EPSTEM)
ISSN: 2602-3199

The Eurasia Proceedings of Science, Technology, Engineering & Mathematics (EPSTEM), 2021

Volume 16, Pages 98-105

IConTES 2021: International Conference on Technology, Engineering and Science

Panalysis of the Efficiency of the VRS Algorithm in the Transmission of Weather Data

Bojan PRLINCEVIC
Kosovo and Metohija Academy of Applied Studies

Zoran MILIVOJEVIC
Academy of Technical and Educational Vocational Studies

Abstract: In the first part of this paper a Variable rate sampling, algorithm for prediction has been described. Variable rate sampling systems were used for reducing power demand, by reducing the number of sent samples. In the second part is performed an experiment where is tested algorithm for prediction of data for transmission and transmitted data. For the purpose of this analyze transmission and predictions are performed for temperatures, air pressure, wind speed, and visibility. Prediction on the side of the transmission is performed using three different extrapolations (*mam*, *mab*, and *ng*). At the receiving side reconstruction of the received signal is performed applying Linear, Cubic, Makima, and Spline extrapolations, built into Matlab. A simple reconstruction is also performed, using the last known value for prediction the next value (this prediction is in the paper named Step extrapolation). Objective quality measures SR (correlation coefficient of reducing the number of samples between a number of measured and transmitted samples), and MAE (mean absolute error between the measured and predicted values of temperatures, pressures and visibility values) were calculated. The results are presented in the table and graphically.

Keywords: VRS algorithm, Efficiency, Extrapolations, Low power system

Introduction

Wireless sensor networks (VSN) are very common in modern communications. During operation, they most often use chips of low power (Zhuo et al., 2020) and small dimensions. Chips most often use energy from battery power for their functioning. Due to limited power supply, it is necessary to ensure that the batteries have a long service life. The long life of a battery power source can be provided in two ways. The first way is to install high-power batteries, which limit is the size of the power source itself. Another way is to manage consumption. Consumption management can be achieved by applying a system with reduced consumption (Low-power consumption, LPC). LPC systems are applied in all spheres of society (consumer devices, military industry, medical devices, etc.). A characteristic example of the application of LPC system is measurement (pressure, temperature, river levels, etc.) where there is no constant and stable power source. In these systems, the connection of sensor to the central computer is usually through the radio connection. In order to save energy, i.e. reduce consumption, systems with dynamic consumption management (DPM) are used (Benini et al., 2000). DPM is used to control the power supply by voltage variation (Benini et al., 2000; Wu et al., 2014; Srivastava et al., 1996) or processor clock speed control (Zhuo et al., 2020; Benini et al., 2000; Rizvandi et al., 2017).

Error reduction is accomplished by applying algorithms with Variable-rate sample - VRS (Mark et al., 1981). The algorithm described in (Mark et al., 1981) changes the sampling time depending on the change rate of sampled signal parameters. The sampled signal parameters are compared with a threshold that is defined based

on the type of the signal. In (Irvine et al., 2003; Milivojević et. al., 2006; Prlinčević et. al., 2021), the VRS algorithm with prediction is presented.

In this paper, the VRS algorithm presented in (Irvine et al., 2003; Milivojević et. al., 2006; Prlinčević et. al., 2021) is analyzed. The algorithm was applied to the signal that was created for measured values, measured on measuring station "Sunčani vrhovi" at Kopaonik mountain, for the period from 01.09. to 30.09.2020. (W. 2 U. 2020).

The gain, that is, energy saving was determined by a coefficient that represents the ratio of the number of measured samples and the number of transmitted samples with the implemented VRS algorithm. The precision of prediction of used extrapolations methods was measured using MSE, which represents error between measured and predicted values for each extrapolation method.

The paper is organized as follow: Section 2 describes the problem description and methodology; section 3 describes the VRS algorithm. In section 4, an experiment was performed, and the results and analysis of the results were presented. The conclusion is given in section 5.

Problem Description

In digital processing systems, the sample rate of an analog signal is determined in relation to the maximum frequency of the analog signal. In most cases, the sampling rate is not variable over time, and therefore the application of the LPC system can reduce the sampling rate in order to reduce energy consumption. LPC systems can be also applied to VSN model if the intervention aimed at energy saving is conducted during the process of sending or receiving signal. This approach would ensure that there are no deviations in a quality of measured and transmitted information. The reduction of frequency of sending signal is realized in time intervals whereas small changes or constant amplitude can be observed on the analyzed signal. The selection the transmitting interval is very important because frequencies of sending samples directly affects the system performance and energy consumption. The sampling rate and sending samples rate can cause losses important information (Banerjee et al., 1970). Errors that occur can significantly affect the decisions made on such information.

Methodology

The application of the VRS algorithm was performed by sending a signal depending on the defined temperatures, pressures and visibility distances threshold. In addition, the VRS algorithm is set up in a way that after a certain time interval with no changes of parameters (temperature), it sends test signal to demonstrate that the system operates. Maximum sleeping time, where system do not send a signal, is defined as one of the parameters of the system.

On the transmitting side, for the purpose of detailed analysis, signal sampling with different sampling steps was performed. The signal transmission prediction was performed by extrapolations shown in (Irvine et al., 2003). The transmission signal is reconstructed on the received side. For the purpose of analysis, on the receiving side, signal reconstruction was performed using the functions for Linear, Cubic, Makima, and Spline extrapolations, built into Matlab. A simple reconstruction is also performed, that was used the last known value for the next value. This extrapolation for the purposes of this paper is called Step extrapolation.

Algorithms

In (Irvine et al., 2003; Milivojević et. al., 2006; Prlinčević et. al., 2021), a VRS algorithm was implemented in the systems for collection and transmission of data, which are battery powered. The connection between the VRS controller and the computer for data processing and archiving (base station) was realized by radio connection. The change of performance of a signal sent from the sensor is as such that the maximum change of the amplitude, the sampled signal of the temperatures, pressures and visibiliti distances, varied in the range from *min* (values) to *max*(values), and the change of sampling time was varied in the range from t_{min} to t_{max}.

Measured values $x(t)$ is converted, in sensor, into electrical signal $y(t)$. The sampling of the signal is conducted in the time interval t_n, where n=0,1,2, ..., and generates the signal y_n. After the sampled values y_n in the time t_n

prediction y_{n+1}^{p} was performed. At the time t_{n+1} the sampling of the signal y_{n+1} is performed, which presents the real value of the signal. Prediction error depends on sampling time h in $f(t,y)$. The prediction value can be defined as:

$$y_{n+1}^{p} = y_n + h \cdot f\left(t, y\right), \tag{1}$$

where $f(t,y)$ is predicted value between known values (t_n, y_n) and (t_{n+1}, y_{n+1}).
Different numerical methods for calculating $f(t,y)$ have been developed, which can be generally classified in two groups:

a) single step method (Euler method, Runge-Kutta method, ...); and
b) multistep method (Adams-Bashforth method, Adams-Moulton method, ...)

The prediction formula, based on the Adams-Bashforth formula of the fourth order (AB4), is (Rizvandi et al., 2017):

$$y_{n+1}^{ab} = y_n + h \cdot \left(\frac{55 f_n - 59 f_{n-1} + 37 f_{n-2} - 9 f_{n-3}}{24} \right). \tag{2}$$

The following three formulas are used for reconstructions of received signals. Adams-type formula, which contains only y values, is (Irvine et al., 2003):

$$y_{n+1}^{mam} = \frac{509 y_n - 534 y_{n-1} + 336 y_{n-2} - 146 y_{n-3} + 27 y_{n-4}}{192}\ , \tag{3}$$

where y_{n+1}^{mam} is a prediction using the modified combined Adams method?

The prediction formula based on the combined Adams-Bashforth-Moulton method is:

$$y_{n+1}^{mab} = \frac{79 y_n - 114 y_{n-1} + 96 y_{n-2} - 46 y_{n-3} + 9 y_{n-4}}{24}\ . \tag{4}$$

The prediction method, fourth-order N–G, backward differencing polynomial is (Irvine et al., 2003):

$$y_{n+1}^{ng} = 5 y_n - 10 y_{n-1} + 10 y_{n+2} - 5 y_{n-3} + y_{n-4}\ , \tag{5}$$

where y_{n+1}^{ng} is the result of extrapolating the N–G interpolation polynomial.

VRS Algorithm

The VRS algorithm (Irvine et al., 2003) implementation is based on that, we either halve or double the step size, depending on whether the most recent sample was outside or inside a given tolerance compared with the predictions described in (3), (4) and (5). That is, is doubled if the prediction is sufficiently accurate and halved if the prediction is inaccurate:

1) *Step Size Doubling*: The system requires that nine successive equispaced data values are stored in a first-in-first-out (fifo) structure. A calculation for y_{n+1}^{p} is performed using (3). At the next sample time, y_{n+1} becomes y_n and so on, and the previous value of y_{n-8} is discarded from the fifo. If the new value for y_n is within *tol/2* for the predicted value, the sample step h is doubled. Once the process of doubling h is complete, only four more samples must be taken before can be doubled again. However, can be halved on the next sample if required because only five readings are required.

2) *Step Size Halving*: To halve, the interpolated values of $y_{n-1/2}$, $y_{n-3/2}$, $y_{n-5/2}$, and $y_{n-7/2}$ must be calculated to refill the fifo with values at the new sample rate. Again, this can be achieved using the N–G fourth-order backward differencing polynomial in (5).

The VRS algorithm is implemented in the system as follows (Irvine et al., 2003):

/* *tol* tolerance */
/* h_{max} maximum sampling step */
/* h_{min} minimum sampling step */
Set *tol*
Set h_{max}
Set h_{min}
Set $h=h_{min}$
Read the first nine values $y_{n-8},\ldots,y_n$
Until data
Calculate y_{n+1}^{p}
Read y_{n+1}
Set $y_{n-8}=y_{n-7},\ldots,y_n=y_{n+1}$
If $\left|y_{n+1}^{p}-y_{n+1}\right|\geq tol$ **then**
If $h>h_{min}$ **then** halve h
else if $\left|y_{n+1}^{p}-y_{n+1}\right|<tol/2$ **then**
If $h<h_{min}$ **then**
If duplicating the last four values
then duplicating h
else do not change h
Loop

Experimental Results and Analyze

Experiment

In order to test the VRS algorithm application in the systems with reduced energy consumption, the base of single values of temperature, pressure, and visibility was created. The Base is created for September for the mountain Kopaonik where the values are taken from the measuring station "Sunčani vrhovi". The measured single values of temperatures, pressures, and visibility distances are for a time interval of 1h. Figure 1.a shows scale of all measured temperatures, figure 1.b shows scale of all measured pressures, and figure 1.c shows scale of all measured visibility for September 2020. For the requirements of the experiment, the signal was varied in a way where the change of temperature sampling was performed in the range from T_{min} = 0.01°C to T_{max} = 2°C, the change of pressure sampling was performed in the range from p_{min} = 0.01 mbar to p_{max} = 2 mbar, the change of visibility sampling was performed in the range from L_{min} = 5 m to L_{max} = 500 m, and the change of sampling time was varied in the range from t_{min} = 1h to t_{max} = 4h,

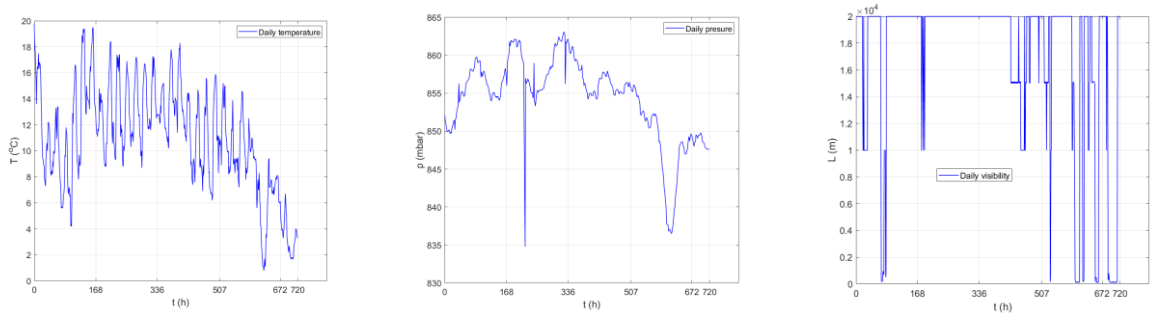

a) b) c)

Figure 1. Base of daily values (for September, hourly - 720 h): a) scale of temperatures, b) scale of temperatures, and c) scale of visibility

The minimum sampling time of temperature sending signal is t_{min} = 1 (h). This time is in line with intervals of temperature measurement at the sampling site. Maximum sampling time is limited at t_{max} = 4 (h) The measured temperatures had values rounded to one decimal place so that the tolerance values of sending samples were from 0.1 °C to 2 °C. The principle of operation of the VRS algorithm is shown in Figure 2.

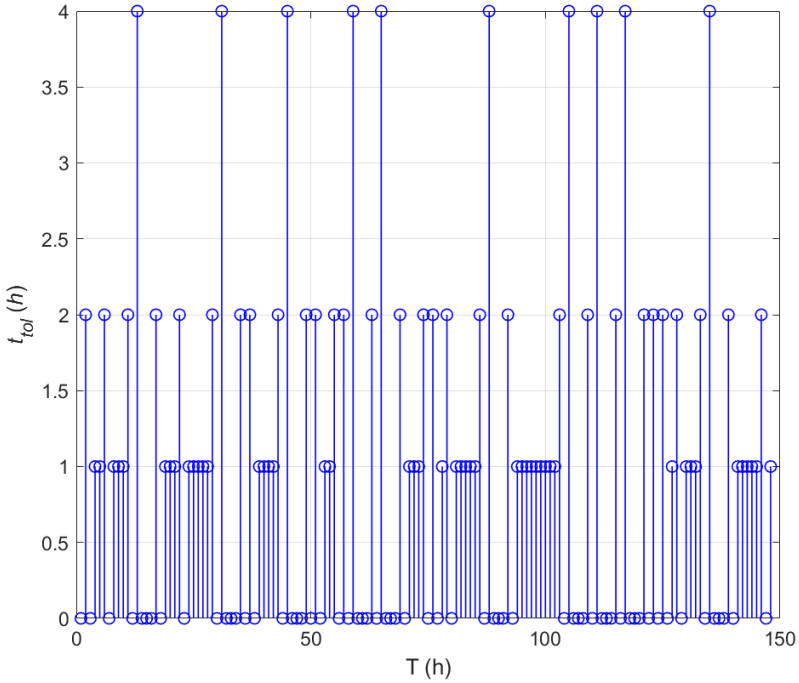

Figure 2. Principle of functioning the VRS algorithm, presented for temperatures in second week in September.

The effect of the VRS algorithm is observed on the reduced number of sent samples during the defined sending interval, and all in accordance to the parameters of the signal y(t). The Sample Ratio (SR) is introduced as a measure of reduced the number of data sent to the recipient:

$$SR = \frac{N_s - N_{s\_vrs}}{N_{s\_vrs}} \cdot 100\% \tag{6}$$

where N_s is number of samples at a constant sampling step, N_{s_vrs} number of samples at application the VRS algorithm.

As an objective quality measure between measured value of the signal (temperatures, pressures and visibility distances) and reconstructed value of the signal, the mean square error – MSE was used:

$$MSE = \frac{1}{N}\sum_{n=0}^{N-1}\left(y(n) - y_{rek}(n)\right)^2 \tag{7}$$

and Normalized correlation coefficient:

$$NC = \frac{\sum_{n=0}^{N-1}\left(y(n)\cdot y_{rek}(n)\right)}{\sqrt{\sum_{n=0}^{N-1}\left(y(n)\right)^2}\cdot\sqrt{\sum_{n=0}^{N-1}\left(y_{rek}(n)\right)^2}} \tag{8}$$

where N is the number of samples in the defined time interval.

Results

The result of the effect of applying the VRS algorithm for varying temperatures, pressures and visibility distances are presented in Figure 3. Tolerance of the temperature values was varied in the range from 0 to 2^{o}C with the step of 0.1^{o}C, fig 3.a. Tolerance of the pressure values was varied in the range from 0 to 1 mbar with

the step of 0.1 mbar, fig 3.b. Tolerance of the visibility distance values was varied in the range from 0 to 500 m with the step of 5 m, fig 3.c. Figure 4 shows a comparative diagram of MSE for all three prediction methods (*mam*, *mab* and *ng*). Figure 5 shows the values for objective measurement of quality NC for three applied predictive methods.

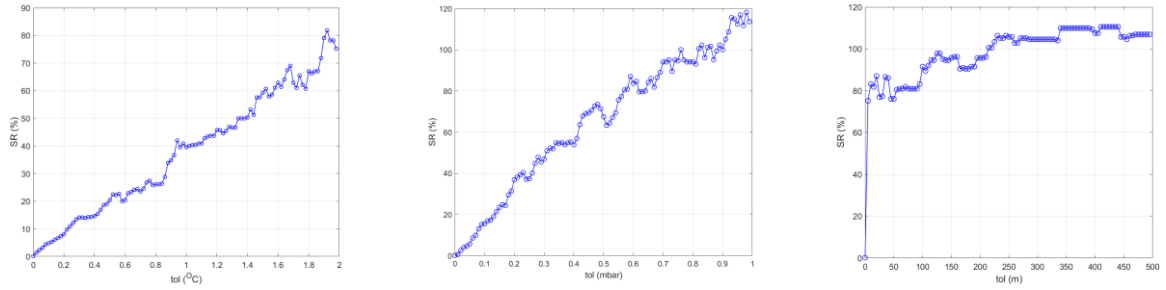

a) b) c)

Figure 3. Sample ratio for applied VRS algorithm for: a) temperatures, pressures, and visibility distances.

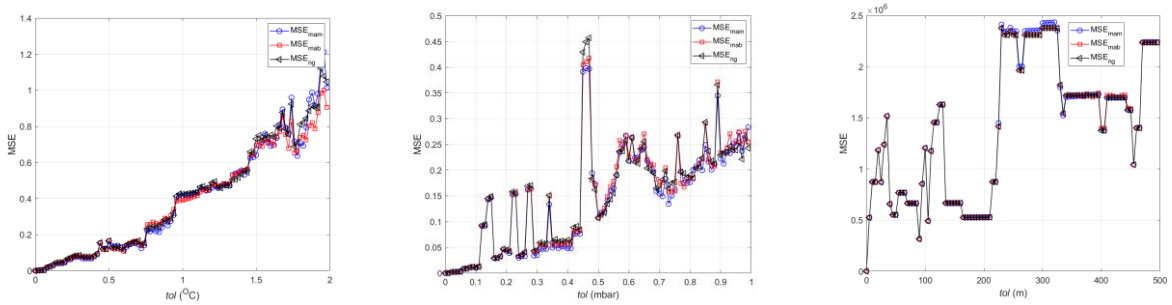

a) b) c)

Figure 4. MSE for applied prediction methods for: a) temperatures, pressures, and visibility distances.

.

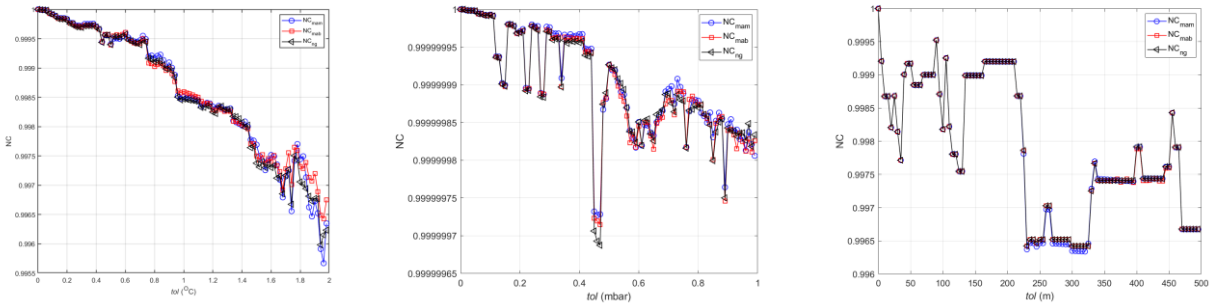

a) b) c)

Figure 5. NC for applied prediction methods for: a) temperatures, pressures, and visibility distances.

Analysis of Results

Based on the results shown in diagram presented on Figure 3.a, it can be concluded that with the increase of the sample rate temperature tolerance, the positive effect of the application of the VRS algorithm increases. Maximum SR is SR = 82 %. Based on the results shown in diagram presented on Figure 3.b, it can be concluded that with the increase of the sample rate pressure tolerance, the positive effect of the application of the VRS algorithm increases. Maximum SR is SR = 119 %. Based on the results shown in diagram presented on Figure 3.c, it can be concluded that with the increase of the sample rate visibility distance tolerance, the positive effect of the application of the VRS algorithm increases. Maximum SR is SR = 110 %. The higher value of SR indicates the lower energy consumption for signal transmission, that is, the smaller number of samples was sent.

Analyzing the values for MSE, presented on diagram shown in Figure 4, it can be concluded that as the tolerance of the sampled rate of measured values increases, the error that occurs with prediction also increases. The error that occurs is in small values, i.e., for maximum tolerance, MSE has a value of approximately

MSE = 1.2 (for temperatures), MSE = 0.45 (for pressures), MSE = $25x10^6$ (for visibility). Also, with results presented on Figure 4 it can be concluded that the three-prediction methods, *mam*, *mab* and *ng*, are with approximately the same errors.

Analyzing the values for NC, presented on diagram shown at Figure 5, it can be concluded that as the tolerance of sampled rate of measured values increases, the value for NC decreases, which implies that the error between the actual measured temperature and the predicted temperature increases. The correlation between the measured and predicted values for maximum used tolerance is approximately NC = 0.9955 (for temperatures), NC = 0.9999997 (for pressures), NC = 0.9965 (for visibility), which is an extremely good correlation.

Conclusion

Using the experiment, the paper analyzes efficiency of VRS algorithm for transmission of values for temperatures, pressures and visibility from measurement station "Sunčani Vrhovi" on the mountain Kopaonik for September. Using the experiment, the results of objective quality measures of VRS algorithm (SR, MSE and NC) are obtained. Based on the values of objective measures, it can be concluded that application of the VRS algorithm for the reduction of energy consumption through the reduction of the number of sending samples, gives positive result. For parameters that have a small range of value changes, higher SR is obtained, a smaller number of samples are sent, the saving in energy consumption is greater. For example, for sampling tolerance of the temperature of 2^oC, the gain in reduction of sent samples in amount of approximately 80% was observed. For sampling tolerance of the pressure of 1 mbar, the gain in reduction of sent samples in amount of approximately 120% was observed. For sampling tolerance of the visibility distance of 500 m, the gain in reduction of sent samples in amount of approximately 110% was observed. For smaller sampling values the MSE is smaller, signal isrekonstructed with higher precision. Based on presented results, it can be concluded that VRS algorithm, in which the reconstruction of the signal on the receiving side is based on the *mam*, *mab* and *ng* prediction method, can be used for application in real - time operation systems

Scientific Ethics Declaration

The authors declare that the scientific ethical and legal responsibility of this article published in EPSTEM journal belongs to the authors.

References

Banerjee, A., Dhar, A. S., & Banerjee, S. (2001). FPGA realization of a CORDIC based FFT processor for biomedical signal processing. *Microprocessors and Microsystems*, *25*(3), 131-142. https://www.infona.pl/resource/bwmeta1.element.elsevier-13f94baa-1d66-3bb8-b16f-fadc9b20042e.

Benini, L., Bogliolo, A., & De Micheli, G. (2000). A survey of design techniques for system-level dynamic power management. *IEEE transactions on very large scale integration (VLSI) systems*, *8*(3), 299-316. https://ieeexplore.ieee.org/document/845896.

Irvine, G. B., Wang, L., Dickman, P., & Cumming, D. R. (2003). Variable-rate data sampling for low-power microsystems using modified Adams methods. *IEEE transactions on signal processing*, *51*(12), 3182-3190. https://ieeexplore.ieee.org/document/1246524.

Mark, J., & Todd, T. (1981). A nonuniform sampling approach to data compression. *IEEE Transactions on communications*, *29*(1), 24-32. https://ieeexplore.ieee.org/document/1094872.

Milivojević, Z. N., & Prlinčević, B. P. (2006). *Analysis of the VRS prediction algorith at a low-power system*.

Prlinčević, B. P., & Milivojević, Z. N. (2021, October). *Section - information technology and mechanical engineering*. http://vpts.edu.rs/sed/fajlovi/inf.pdf.

Rizvandi, N. B., Zomaya, A. Y., Lee, Y. C., Boloori, A. J., & Taheri, J. (2012). Multiple frequency selection in DVFS-enabled processors to minimize energy consumption. *arXiv preprint arXiv:1203.5160*.. https://researchers.mq.edu.au/en/publications/multiple-frequency-selection-in-dvfs-enabled-processors-to-minimi.

Srivastava, M. B., Chandrakasan, A. P., & Brodersen, R. W. (1996). Predictive system shutdown and other architectural techniques for energy efficient programmable computation. *IEEE Transactions on Very Large Scale Integration (VLSI) Systems*, *4*(1), 42-55. https://ieeexplore.ieee.org/document/486080.

W. 2 U. (2020, September). *Istorijski Meteorološki podaci beograd – synop*. Weather2Umbrella ltd. https://www.weather2umbrella.com/istorijski-podaci-beograd-srbija-sr.

Wu, P. C., Kuo, Y. P., Wu, C. S., Chuang, C. T., Chu, Y. H., & Hwang, W. (2014, September). PVT-aware digital controlled voltage regulator design for ultra-low-power (ULP) DVFS systems. In *2014 27th IEEE International System-on-Chip Conference (SOCC)* (pp. 136-139). IEEE. https://ieeexplore.ieee.org/document/6948914/.

Zhuo, C., Luo, S., Gan, H., Hu, J., & Shi, Z. (2019). Noise-aware DVFS for efficient transitions on battery-powered IoT devices. *IEEE Transactions on Computer-Aided Design of Integrated Circuits and Systems*, *39*(7), 1498-1510. https://ieeexplore.ieee.org/document/8718252.

Author Information

Bojan Prlinčević
Kosovo and Metohija Academy of Applied Studies
st. Dositeja Obradovića bb, Leposavić, Serbia
Contact e-mail: *bojan.prlincevic@akademijakm.edu.rs*

Zoran Milivojević
Academy of Technical and Educational Vocational Studies
st. Beogradska 18, Niš, Serbia

To cite this article:

Prlincevic , B. & Milivojevic, Z. (2021). Panalysis of the efficiency of the VRS algorithm in the transmission of weather data. *The Eurasia Proceedings of Science, Technology, Engineering & Mathematics (EPSTEM)*, *16*, 98-105.

The Eurasia Proceedings of Science, Technology, Engineering & Mathematics (EPSTEM)
ISSN: 2602-3199

The Eurasia Proceedings of Science, Technology, Engineering & Mathematics (EPSTEM), 2021

Volume 16, Pages 106-116

IConTES 2021: International Conference on Technology, Engineering and Science

An Approach to Mobile Augmented Reality in Microcontroller Learning

Yusuf UZUN
Necmettin Erbakan University

Resul BUTUNER
Beypazarı Fatih Vocational and Technical Anatolian High School

Yasin ER
Turkish State Meteorological Service

Abstract: Augmented Reality is a virtual display of information created using a computer on a real environment. Arduino is an open source microcontroller platform. It was aimed to increase the education and learning quality of the students by integrating mobile augmented reality technology into the materials of the microcontroller course. In this study, a mobile augmented reality application was developed in order to see the output of an electronic circuit created using Arduino in the microcontroller course and to get information about the circuit elements. Experimental studies were carried out with a group of 30 students to determine the productivity and quality of this study and a questionnaire about the study was applied to the students after the experiment. It was observed that the experimental applications in which the augmented reality technology was used were performed more efficiently than the experimental applications in the classical methods. In addition, augmented reality technology has introduced an independent learning strategy from the teacher. According to the results of the survey, the mobile augmented reality application was showed to have contributed significantly to the learning process without the need of any expert. In addition, the social presence and motivation of the students were examined with a number of tests and positive results were obtained.

Keywords: Augmented reality, Virtual reality, Microcontroller

Introduction

Augmented Reality (AR) is a display technology developed by adding virtually produced information on the real world environment in real time (Wikipedia, 2018). AR technology is different from Virtual Reality (VR). VR is expeted to live in the world that is prepared virtually in a computer environment. AR is a technology created by placing graphical objects, videos and texts designed on the real world. In other words, AR technology is a technology that constantly connects real and virtual life (Chang et al, 2010). Mobile Augmented Reality is an AR technology that we can carry with us everywhere. Mobile learning facilitates the social learning model with the transformation possibilities provided by digital devices (Cook et al, 2016). The history of AR technology goes back to the 1960s and the first developed system infrastructure was used for both AR and VR. The idea of how two-dimensional objects can be represented in three dimensions has been tested using computers that can perform a limited number of operations (Sutherland, 1968). Emerging technologies such as Mobile AR and VR will gain new knowledge through learning theories based on pedagogical strategies (Aguayo et al, 2017).

The role of mobile technology in education is to actively facilitate the learning process of learners in a number of culturally sensitive and meaningful ways. This process can be designed not only by learning with new learning technologies such as mobile augmented reality, but also by developing socially relevant learning modes

(Aguayo et al, 2017). AR has become an important area of study for mobile learners, with the widespread use of mobile AR browsers allowing 1 users to create and share content (Cochrane et al, 2016), AR technology is widely used in many fields such as medicine, industry, automotive, education, manufacturing and its importance is increasing day by day. According to the New Media Consortium reports, AR is one of the most up-to-date technologies in the education and training process (NMC, 2012). The traditional method of education involves the execution of the information and learning process by a teacher (De Freitas et al, 2009). Learning methods depend on classical paper-based methods and materials (Huang et al, 2012). In addition to current learning methods, more and more useful methods are being explored to improve education and training. Technology evolves began to acquire more space in our lives. As a result, it has begun to be considered that we need to make some changes in our education and teaching methods (Nincarean et al, 2011).

Many factors to improve quality and diversity in the education and training process should be addressed in this process. Taking into consideration the preparation of curriculum contents, teaching strategies, laboratory, libraries, evaluation process and feedback from students, raising qualifications in the education and training process should be considered as the main objective. Therefore, all current and technological applications should be used. Learning can be examined under two conditions: location and time. Depending on these conditions, a number of problems have been raised. Some problems arise such as the inadequacy of physical materials, limited working hours, inability to get help from specialists and difficulty in reaching the laboratory environment. Such difficulties encountered constitute an obstacle in the education and training process. These problems can be solved by providing alternative teaching resources that are used by mobile learning tools (Holzinger et al,2005).

Mobile learning is a big part of our lives. Achieving information quickly and easily increases the importance of mobile applications day by day. When we look at classical learning methods, for example, in textbooks, there are many deficiencies in visual terms. Particularly in micro-controller course textbooks it is seen that there are visual deficiencies in the stages of recognition of circuit and electronic circuit elements. Therefore, learning with mobile application increases the mobility of learners in the learning process and provides a exible working environment (Norman et al, 2011) When mobile learning is viewed as a term, it is the use of portable devices such as mobile phones and tablets as learning tools (Jamali et al,2015). The development of technology provides a great opportunity to capture the change in education and learning process and to provide an engaging environment (Kirkley et al., 2002). According to research, many factors inuence the quality of learning. Among these factors, we can say that the student should develop motivation and learning skills for self-learning (Markwell, 2016). The possibilities provided by AR in teaching and learning have been accepted by educational researchers (Wu et al, 2013). Depending on technological developments, smart devices such as smartphones and tablets have begun to be used intensively in the field of education. Devices such as tablets, smartphones and computers are needed to be able to use the AR applications. With the increase in AR applications, the number of applications developed for mobile devices has increased day by day.

Microprocessor and microcontroller concepts are often confused. The microprocessor consists only of processing and memory units. The microcontroller consists of peripherals such as memory, analogue digital converter and timer. Today, microprocessors are generally used in personal computers. Microcontrollers can often be described as specialized microprocessors designed to perform industrial control and automation tasks. Microcontrollers can often be described as specialized microprocessors designed to perform industrial control and automation tasks. It is difficult to understand the lessons that circuit elements such as microcontrollers are complex. In this study, experimental study, circuit elements, object and purpose of the circuit will attempt to improve the learning ability of students presenting with mobile augmented reality. The Arduino Microcontroller card is used in the electronic experimental applications. The Arduino card only controls and responds to electrical communication. This card interacts with a number of custom components in the real environment. In the questionnaire survey, students will be asked and answered a series of questions such as knowledge acquisition,43 effective learning skills and competence to use AR technology in microcontroller course.

Method

Experimental materials of microcontroller course are divided into 3 parts as Arduino circuits, electronic circuit elements and android mobile devices. Mobile AR application was developed for android devices. In Mobile AR application, an interactive interface was designed by preparing models and objects related to experimental subjects of microcontroller course. The developed application was created on two different platforms as marker and object recognition. The platform structure of the developed mobile AR application is shown in Figure 1.

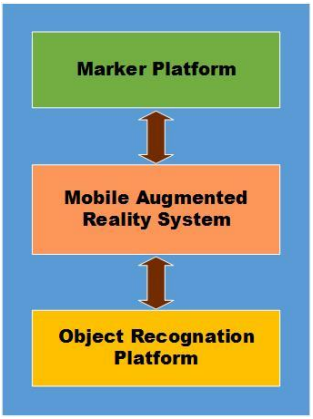

Figure 1. The structure of the mobile AR application.

In both developed platforms, technical information about the circuit components was presented to the students through a menu. The general framework of the designed application is shown in Figure 2.

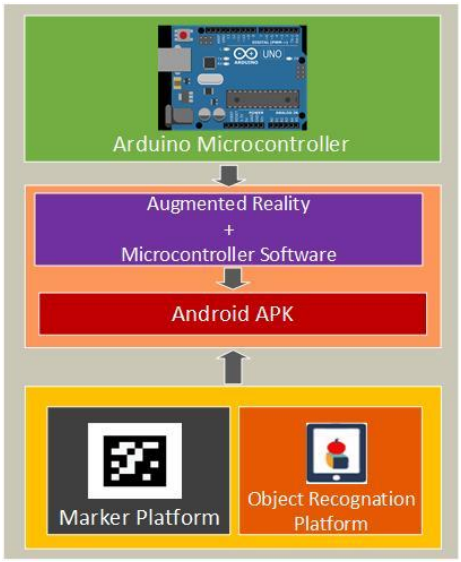

Figure 2. The general framework of the mobile AR application.

In the course of microcontroller, a few experimental applications were prepared using Arduino and electronic circuit elements for the experimental work of the students. The microcontroller software needed to provide control of the designed electronic circuitry was coded in the Arduino editor and the code was transferred to the microprocessor on the Arduino board. In order to reach the data generated by the sensors on the Arduino card, the mobile AR application was developed. The data produced by the sensors was transferred to the AR application via a Bluetooth device. An Android APK application was developed to be able to empower the mobile part of the developed AR application and seamlessly implement the Bluetooth transfer to the AR application. The mobile AR application developed for the experimental study was designed to support both the marker platform and the object recognition platform at the same time. To test the validity of the study, the students were asked a number of questions by means of the prepared survey and the results of the survey were subjected to a number of tests.

Marker Platform

A marker-based platform is obtained by physically adding markers to the object to which the AR operation is to be applied. Markers must have a suitable design according to the situation of the area to be used. Markers placed on real objects must have already been introduced on the system. In order for the markers to be detected quickly and easily, the positions on the real objects must be previously determined in the AR system. A successful marker should be easily and reliably detectable under all circumstances. Markers that have a proper placement angle are easily recognizable by the camera. In this way, the success of the marker-based tracking process

depends on the visibility of the marker used. In some cases, the availability of a marker-based tracking platform is not possible. There are many objects (machines, devices, etc.) that affect the trackability of the marker in the industrial environment. This causes the tracking problem in the AR system (Palmarini et al,2013). In order for AR technology to accurately present information on the real physical environment, the AR system needs information about the user's location and the point of view. Usually, the user uses a camera-enabled mobile devices to access the AR information. The AR system can show the virtual objects in the right place by determining the location and direction of the camera. In this platform, students' ability to recognize Arduino-based electronic circuits and learn about circuit elements has been tried to be developed using a marker-based learning method. First, an environment in which the experimental work is done is already prepared. In the next step, the electronic circuit and marker designed using Arduino are placed on the working environment. The process of using the application by the student consists of two steps. In the first step, the selection process is carried out using the menu in the mobile AR application. In the second step, the camera of the mobile device is brought close to an angle where the marker can be detected. Information about the purpose and design of the electronic circuit used is displayed on the mobile screen.

Object Recognition Platform

In the process of object detection and recognition, the steps are as follows: 1) capture a scene with a camera on a mobile device, 2) scan the captured image from the library to detect a match, 3) identify and recognize objects in the scene, and finally 4) passing the obtained result information to the user. In this method, circuitrecognition is performed in 2 steps. First, a selection operation is performed with the help of the menu for the circuit to be studied from the mobile AR application screen. In the second step, the camera of the mobile device is brought close to an angle where the marker can be detected. Object recognition is performed by this method. Information about the purpose and design of the electronic circuit used is displayed on the mobile screen. Instead of classical marker-based learning, this method focuses on the learning process by object recognition method.
The designed 3D model 1 is shown on the mobile device's screen using Eq. (1) (Zhang, 2002).

$$S = \begin{pmatrix} u \\ v \\ l \end{pmatrix} = \begin{pmatrix} f & 0 & c_x \\ 0 & f & c_y \\ 0 & 0 & 1 \end{pmatrix} (R_{3x3}\ T_{3x1}\ ) \begin{pmatrix} X \\ Y \\ Z \\ 1 \end{pmatrix} \qquad (1)$$

In the equation, s is the value of the expansion or reduction factor, and u and v are the position of the object in the screen coordinates. The variable f is the focal length, and cx and cy are the coordinates of the center of the image. These values are the internal parameter values of the camera. The external parameter values of the camera are R, 3x3 dimensional rotation matrix and T is the 3x1 dimensional camera translation matrix. The X, Y, and Z values indicate the position of the object in the real world coordinates. The internal parameters are used to calculate the camera's calibration. The external parameters represent the position and position data of a camera and have special values according to the point of view of each photograph. When the AR system is used, external parameters must be calculated.

Finding

SPSS 17.0 was used to analyze and test the data collected from the students during the study. A survey consisting of 20 questions was applied to the students to measure and evaluate the availability of the mobile AR application. In the answer section of the survey, a 5-point Likert scale (1 = strongly disagree to 5 = strongly agree) was used. In the experimental study, the t-test and the Wilcoxon test were used to calculate the social presence and motivation values of the students.

The mobile AR application developed in this study was tested in the computer application laboratory of Necmettin Erbakan University, Seydisehir Ahmet Cengiz Faculty of Engineering. The experiment group consisted of 30 students, 7 female and 23 male students, who took microcontroller course at Necmettin Erbakan University. The students who participated in the study had no previous experience of AR. The lecturer has shown how the mobile AR application is used and the process of operation is applied to the students before the experimental work begins. The students who participated in the experimental study were asked to run the mobile AR application and to learn the electronic circuit elements without help from the course supervisor. In order to benefit from the Bluetooth support in the developed Mobile AR application, a separate Android encoding was written. The values from the temperature, humidity and light sensors on the Arduino circuit were

transferred via the Bluetooth device to the mobile AR application. Appropriate image models were created for 2these values and real time sensor values were displayed on the models.

A single marker was used for all experimental studies to avoid marker complexity in the study. In this study, image marker type was used. In this marker system, unlike barcode type markers, natural images are used as markers. Figure 3 shows an example of the use as a marker of the image used in an experimental study. We have carried out a number of process steps for marker detection respectively. In the image acquisition step, an image was provided for the marker detection process. Before to detection of the marker, a grayscale image of the system was obtained. An RGB image captured by the camera was converted to a grayscale intensity image using a conversion technique. In the designed system, the marker detection system works with a grayscale image.

In AR application, the image to be used as marker has been converted to gray scale format. After the conversion process, the graph of the histogram equalization of the image was examined. It was considered that the horizontal histogram value of the image was distributed over a wide range. Also, the image with the least vertical uctuations in the histogram was preferred. Thus, the markers placed on the picture spread over a wider area and the mobile 1 camera perceived the markers more precisely in every respect. After the experiments, the students were asked their opinions about the lessons that were done using the mobile AR application and without using it. During the use of the developed marker-based AR application, students' learning behaviors and abilities were observed. The use of the marker-based AR application in the microcontroller course is shown in Figure 3.

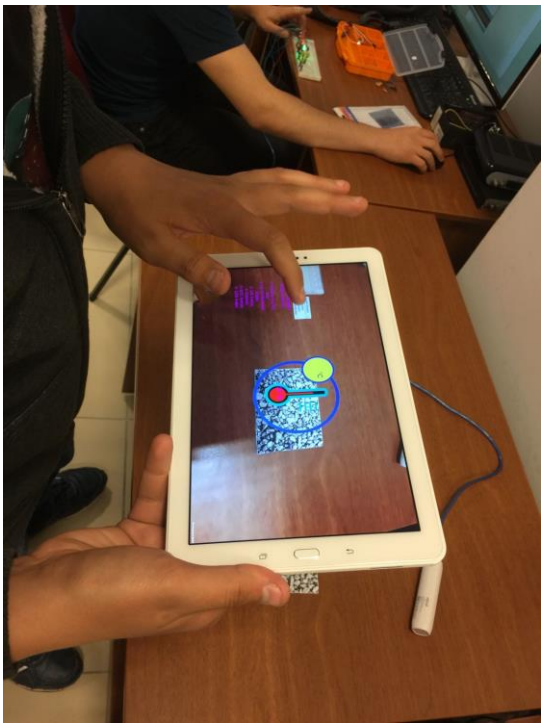

Figure 3. Marker-based mobile AR application.

In the marker-based mobile AR application, the data of the Arduino circuit can be obtained from many places in the access area of the Bluetooth device. In this process, it was considered one of the most important advantages of this platform. The students were informed about the application before using object-based mobile AR application. The learning behaviors and abilities of students were observed during the use of object recognition based mobile AR application. In this platform, students' ability to recognize Arduino-based electronic circuits and learn about circuit elements has been tried to be improved using object recognition-based learning method. In the designed system, Arduino based electronic circuits and elements are scanned using the 3D Mesh method with the help of the camera. An object database is created from the scanned objects. The use of the object recognition based AR application in the microcontroller course is shown in Figure 4.

The mobile AR application, which is based on the object recognition platform, could not be run independently of the experimental environment. The application absolutely has to detect the object. This has shown that the object recognition platform does not have the advantage of exible usability.

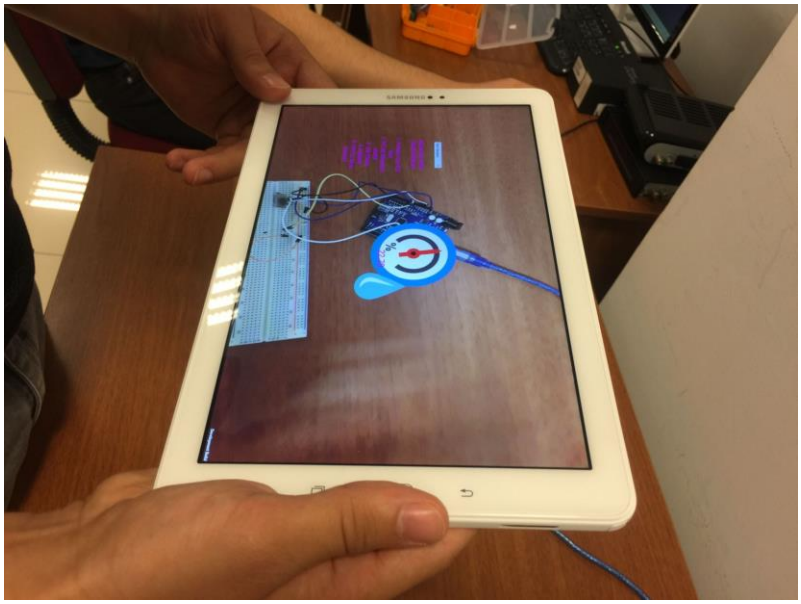

Figure 4. Object recognition based AR application.

In Figure 5, the statistical and graphical results of the responses given to the survey about the importance and perception of the microcontroller course were shown. The students who did not give an opinion to the questions were not taken into consideration in the evaluation of the statistical data. It was seen that 90% of the students who participated in the experimental study showed interest in Arduino applications. It was determined that 90% of students who learned the microcontroller course developed their projects using Arduino. It was seen that 80% of the students learn basic knowledge about electronic circuit elements in microcontroller course. It has been observed that 80% of the students give importance to microcontroller course as much as other vocational courses. It was observed that 83.4% of the participants in the experimental study had the opinion that the Arduino application could be easily understood and improved.

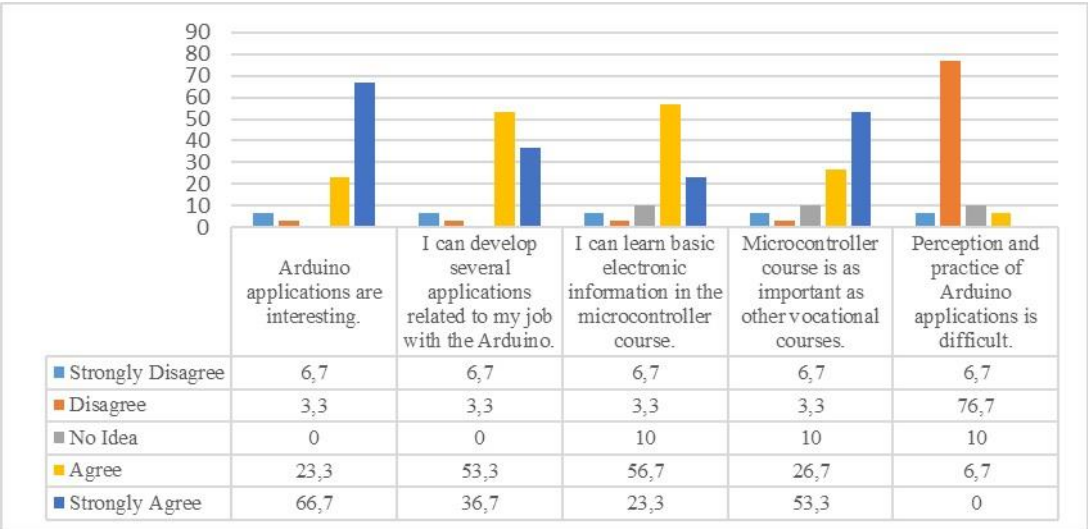

	Arduino applications are interesting.	I can develop several applications related to my job with the Arduino.	I can learn basic electronic information in the microcontroller course.	Microcontroller course is as important as other vocational courses.	Perception and practice of Arduino applications is difficult.
Strongly Disagree	6,7	6,7	6,7	6,7	6,7
Disagree	3,3	3,3	3,3	3,3	76,7
No Idea	0	0	10	10	10
Agree	23,3	53,3	56,7	26,7	6,7
Strongly Agree	66,7	36,7	23,3	53,3	0

Figure 5. The important and learning of microcontroller course.

In Figure 6, the statistical and graphical results of the responses given to the survey about the cost and difficulty of the microcontroller course were shown. The students who did not give an opinion to the questions were not taken into consideration in the evaluation of the statistical data. It was observed that 50% of the students who participated in the experimental study thought that the course materials were not costly. It was found that 63.4% of the students had the opinion that the microcontroller course was difficult to learn without needing expert help. It was determined that 80% of the students thought it was difficult to find a mobile application for the microcontroller course.

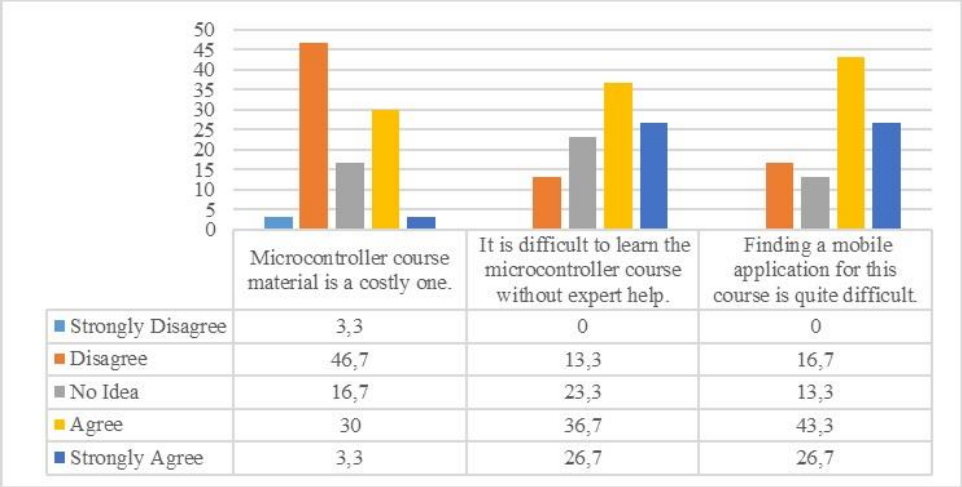

	Microcontroller course material is a costly one.	It is difficult to learn the microcontroller course without expert help.	Finding a mobile application for this course is quite difficult.
Strongly Disagree	3,3	0	0
Disagree	46,7	13,3	16,7
No Idea	16,7	23,3	13,3
Agree	30	36,7	43,3
Strongly Agree	3,3	26,7	26,7

Figure 6. Cost and difficulty of the course.

In Figure 7, 1 the statistical values and graphs of the answers to the questions related to the importance and use of the AR method were shown. The students who did not give an opinion to the questions were not taken into consideration in the evaluation of the statistical data. It was determined that 53.2% of the students who participated in the experimental study had sufficient knowledge about the AR method. It was observed that 90% of the students who participated in the experimental study could use to AR method in their studies. It was seen that 73.3% of the students who participated in the experimental study thought that the AR method reduced the costs in many areas. It was determined that 70% of the students who participated in the experimental study had the idea that the use of AR was not difficult. It was observed that all of the students who participated in the experimental study thought that the education quality increased significantly by using the AR method in the course material.

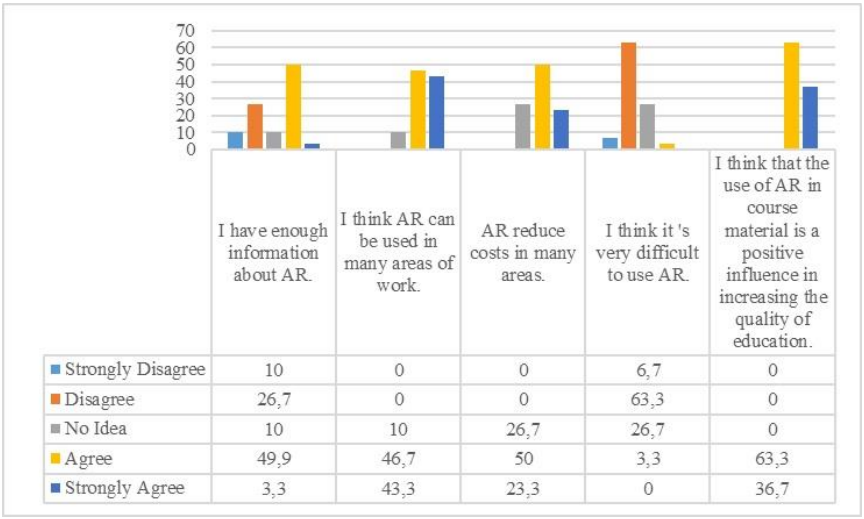

	I have enough information about AR.	I think AR can be used in many areas of work.	AR reduce costs in many areas.	I think it 's very difficult to use AR.	I think that the use of AR in course material is a positive influence in increasing the quality of education.
Strongly Disagree	10	0	0	6,7	0
Disagree	26,7	0	0	63,3	0
No Idea	10	10	26,7	26,7	0
Agree	49,9	46,7	50	3,3	63,3
Strongly Agree	3,3	43,3	23,3	0	36,7

Figure 7. Use and importance of the AR method.

In Figure 8, the statistical values and graphs of the answers to the questions related to the educational contribution of the AR application were shown. The students who did not give an opinion to the questions were not taken into consideration in the evaluation of the statistical data. It was observed that 96.6% of the students who participated in the experimental study thought had created a more entertaining and instructive environment by using AR technology in Arduino applications. It was seen that 76.6% of the students who participated in the experimental study could learn information about electronic circuit elements without needing any expert help with AR application. It was determined that 73.3% of the students who participated in the experimental study could learn courses with mobile AR at cheaper cost. It was detected that 73.3% of the students who participated in the experimental study could learn courses with mobile AR at cheaper cost. In Figure 9, the statistical values and graphs of the answers to the questions related to the educational contribution of the mobile AR application were shown. The students who did not give an opinion to the questions were not taken into consideration in the evaluation of the statistical data. It was determined that 96.7% of the students who participated in the

experimental study thought that AR method was more effective and useful than classical learning methods in education. It was observed that 76.7% of the students who participated in the experimental study could see the experimental results of the microcontroller course with mobile AR application without the need of computers and peripherals. Analysis of the study in terms of social assets; Since the normality assumption of the dependent t-test for 30 students was violated (t - test = 0:147; p > 0:05), a Wilcoxon test was applied to examine the importance of the study in terms of social existence. The results of Wilcoxon test showed a significant difference in terms of social presence (Z = -3:621; p < 0:05). Analysis of the study in terms of motivation; Since the normality assumption of the dependent t-test for 30 students was not violated (t - test = 0:108; p < 0:05), the study showed a significant difference in terms of motivation.

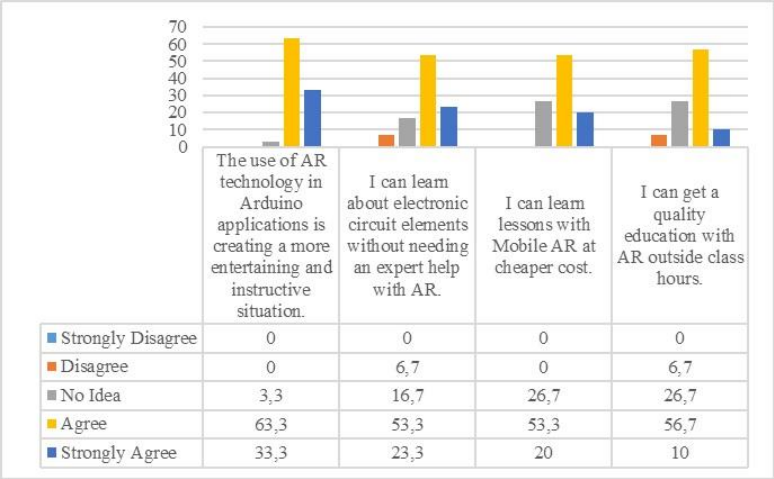

	The use of AR technology in Arduino applications is creating a more entertaining and instructive situation.	I can learn about electronic circuit elements without needing an expert help with AR.	I can learn lessons with Mobile AR at cheaper cost.	I can get a quality education with AR outside class hours.
Strongly Disagree	0	0	0	0
Disagree	0	6,7	0	6,7
No Idea	3,3	16,7	26,7	26,7
Agree	63,3	53,3	53,3	56,7
Strongly Agree	33,3	23,3	20	10

Figure 8. Educational contribution of AR application.

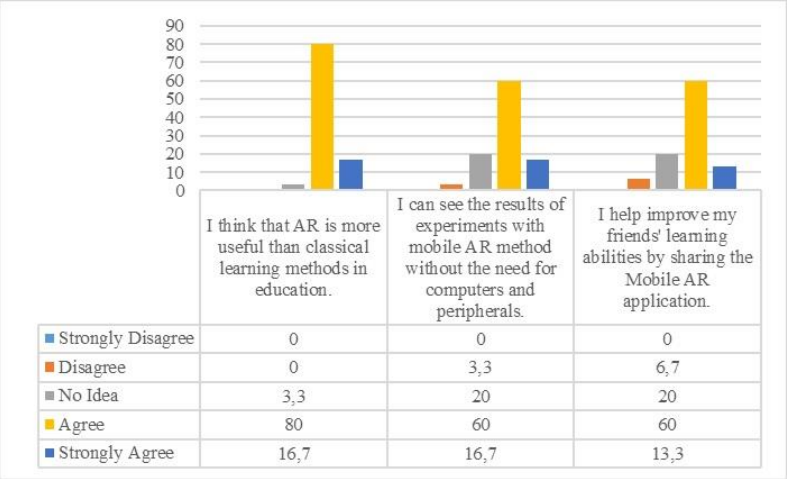

	I think that AR is more useful than classical learning methods in education.	I can see the results of experiments with mobile AR method without the need for computers and peripherals.	I help improve my friends' learning abilities by sharing the Mobile AR application.
Strongly Disagree	0	0	0
Disagree	0	3,3	6,7
No Idea	3,3	20	20
Agree	80	60	60
Strongly Agree	16,7	16,7	13,3

Figure 9. Educational contribution of mobile AR application.

Discussion

This study investigated how to improve the interactivity and availability of mobile AR application for Arduino based microcontroller courses. In the literature review, we did not encounter a Bluetooth supported AR microcontroller training on Android system. While the course contents were prepared, a more effective and interactive working environment $_{1}$ was provided by using the AR method. The improved mobile AR application allowed multiple learners to work simultaneously on a single experimental study. Students were able to get the necessary information about the experimental work quickly, without the need for expert assistance, with the help of AR mobile application. It has been seen that AR mobile application is a useful platform for dynamic content preparation and transfer of current information to end users. The developed mobile AR application was designed to be able to use both marker and object recognition platforms at the same time. One of the most important advantages of the designed application is that the user can define both markers and objects through a single mobile application. The most important feature of the marker-based recognition process in the designed mobile AR application is that the Arduino circuits used in the experimental study can be seen through a single $_{marker}$. In

the object recognition process, the Arduino circuit which will be used in the experimental work was scanned with the camera of the mobile application using the 3D mesh method. As a result of face-to-face interviews and experimental studies with students, object recognition was observed to be more useful than the marker method. It has been observed that the vast majority of students are interested in microcontroller course and Arduino applications. It has been understood that the microcontroller course can't be learned without expert help and this problem has been removed with the developed mobile AR application. The use of mobile AR application as course material provided a low cost and high efficiency training environment. In addition, an experimental study independent of the laboratory environment by use mobile AR application was performed. This study has also made an important contribution to the students' easy perception of Arduino circuits in terms of their knowledge of the material and the information about the experiment on the AR screen. The students reached the information they wanted about the experiment with the help of the designed menus very easily. As a result of this study, AR mobile application has increased its interactive learning ability in education. AR was observed that mobile learning is one of the arguments used effectively in education. As a result of the knowledge and experience gained without this study, it was concluded that similar studies should be carried out in other educational institutions as well. In this study, we have determined that the use of AR-aided learning is often beneficial to the spatial experience, practical capability and conceptual understanding of the learner, butthat more research on learning experience and learning features is needed. This study also examined the social presence and motivation of students in the microcontroller course through the use of the AR learning environment. According to the questionnaires and experimental studies, the participation of students in the course of social existence increased significantly. In a study conducted, it is stated that social presence is a fundamental characteristic of virtual practice environments(Steuer, 1992) . Jin's study showed that using the e-learning experience in the framework of students' social entities provides a significant interaction with their motivations (Jin, 2011).

Conclusion

This study has explored whether augmented reality applications are beneficial for developing perceptual and learning skills in microcontroller education and learning. Our study demonstrates that it can benefit students by offering an interactive, interesting and original educational experience. This study provides to the current literature an experimental support for the inuence of the characteristics of interactive learning environments on the social participation and motivation of students. Experimental study results show that mobile AR application is a potential solution tool especially for non-laboratory working environments. In summary, mobile AR can improve quality and effeciency in the education sector. Using mobile AR application, students have improved their knowledge more effectively by gaining their own unique and independent learning experiences. In addition, they gain a number ı of experiences to improve communication and collaboration skills, technology use skills and social skills. In our surveys, we have identified a number of positive developments and evidence that mobile AR application developers have had the opportunity to identify their own ideas, identify new research skills, and implement them. In higher education, we have concluded that a general study on the integration and adoption of mobile AR applications is very important. We aim to expand the scope of our research on the benefits of students and best practice delivery options. For this reason, we plan to develop more interactive and effective mobile AR applications considering future technological approaches. For researchers, we suggest that there is a lot of work to be done on AR Technologies and that there is an open space for development. For researchers, research studies including problem-based and project-oriented different teaching approaches are proposed. This study does not provide a detailed explanation of the study results as no qualitative data were used. Qualitative data can be collected via face-to-face interviewsor open-ended surveys to gather more student feedback. In the future, we plan to make more interactive and realistic studies considering disabled people. We aim to move the existing AR study to mixed reality technology. We plan to increase the motivation of the participants to practice by preparing more realistic and interactive models in future work. The limitations of this work are related to the mobile AR studies limited to the field of Arduino-based Microcontroller applications. Although the work is not complicated, future research will benefit from a Bluetooth-enabled mobile AR approach that includes different curriculum frameworks. There are some restrictions in the AR system. For example, the AR system can display the enhanced image only from the viewpoints where the actual view is. For example, a user can see a virtual model from ground level by looking at the screen of the mobile device, but the scene does not look bird's eye view. To provide such visualizations, applications often complete the AR with virtual reality mode. Other limitations result from the limited capacity of the mobile devices to which the AR application is to be run. The battery consumption is very high, the memory capacities of the devices are very low and the resolution of the cameras is very low. If the level of these constraints is reduced in the future, more realistic and faster AR applications will be developed.

Scientific Ethics Declaration

The authors declare that the scientific ethical and legal responsibility of this article published in EPSTEM journal belongs to the authors.

References

Aguayo, C., Cochrane, T., & Narayan, V. (2017). Key themes in mobile learning: Prospects for learner-generated learning through AR and VR. *Australasian Journal of Educational Technology*, *33*(6), 27-40

Aguayo, C., & Eames, C. (2017). Community partnerships in sustainability education research. In *Realising innovative partnerships in educational research* (pp. 235-244). Brill Sense.

Wikipedia (2018, August 20). Augmented Reality. https://en.wikipedia.org/wiki/Augmented_ reality

Chang, G., Morreale, P., & Medicherla, P. (2010, March). Applications of augmented reality systems in education. In *Society for Information Technology & Teacher Education International Conference* (pp. 1380-1385). Association for the Advancement of Computing in Education (AACE).

Cook, J., & Santos, P. (2016). Three phases of mobile learning state of the art and case of mobile help seeking tool for the health care sector. In *Mobile learning design* (pp. 315-333). Springer.

Cochrane, T., Narayan, V., & Antonczak, L. (2016). A framework for designing collaborative learning environments using mobile AR. *Journal of Interactive Learning Research*, *27*(4), 293-316.

De Freitas, S., Rebolledo- Mendez, G., Liarokapis, F., Magoulas, G., & Poulovassilis, A. (2010). Learning as immersive experiences: Using the four- dimensional framework for designing and evaluating immersive learning experiences in a virtual world. *British Journal of Educational Technology*, *41*(1), 69-85.

Huang, H. W., Wu, C. W., & Chen, N. S. (2012). The effectiveness of using procedural scaffoldings in a paper-plus-smartphone collaborative learning context. *Computers & Education*, *59*(2), 250-259.

Holzinger, A., Nischelwitzer, A., & Meisenberger, M. (2005). Lifelong-learning support by m-learning: example scenarios. *Elearn*, *2005*(11), 2-15.

Jamali, S. S., Shiratuddin, M. F., Wong, K. W., & Oskam, C. L. (2015). Utilising mobile-augmented reality for learning human anatomy. *Procedia-Social and Behavioral Sciences*, *197*, 659-668.

Jin, S. A. A. (2011). Leveraging avatars in 3D virtual environments (Second Life) for interactive learning: The moderating role of the behavioral activation system vs. behavioral inhibition system and the mediating role of enjoyment. *Interactive Learning Environments*, *19*(5), 467-486.

Kirkley, S. E., & Kirkley, J. R. (2005). Creating next generation blended learning environments using mixed reality, video games and simulations. *TechTrends*, *49*(3), 42-53.

Markwell, D. (2003). Improving teaching and learning at universities. *B HERT News*, *18*, 1-40.

New Media Consortium (N. M. C.) (2012). *The 2012 horizontal report*. Educause. http://www.nmc.org/publications/ horizon-report-2012-higher-ed-edition

Nincarean, D., Alia, M. B., Halim, N. D. A., & Rahman, M. H. A. (2013). Mobile Augmented Reality: the potential for education. *Procedia-Social and Behavioral Sciences*, *103*, 657-664.

Norman, H., Din, R., & Nordin, N. (2011). A preliminary study of an authentic ubiquitous learning environment for higher education. *Learning*, *3*(4), 89-94.

Palmarini, R., Erkoyuncu, J. A., Roy, R., & Torabmostaedi, H. (2018). A systematic review of augmented reality applications in maintenance. *Robotics and Computer-Integrated Manufacturing*, *49*, 215-228.

Steuer, J. (1992). Defining virtual reality: Dimensions determining telepresence. *Journal of Communication*, *42*(4), 73-93.

Sutherland, I. E. (1968, December 9-11). A head-mounted three dimensional display. *Fall Joint Computer Conference, Part I* (pp. 757-764).

Wu, H. K., Lee, S. W. Y., Chang, H. Y., & Liang, J. C. (2013). Current status, opportunities and challenges of augmented reality in education. *Computers & Education*, *62*, 41-49.

Zhang, Z. (2000). A flexible new technique for camera calibration. *IEEE Transactions On Pattern Analysis and Machine İntelligence*, *22*(11), 1330-1334.

Author Information

Yusuf UZUN
Necmettin Erbakan University
Seydişehir Engineering Faculty Seydişehir / Konya, Turkey
Contact e-mail: *yuzun76tr@gmail.com*

Resul BUTUNER
Beypazarı Fatih Vocational and Technical Anatolian High School Ayvaşık Neighborhood Saraybosnian Street Beypazarı/Ankara, Turkey

Yasin ER
Turkish State Meteorological service
Kutukcu Ali Bey st N:4 Kalaba Kecioren Ankara, Turkey

To cite this article:

Uzun, Y., Butuner, R. & Er, Y. (2021). An approach to mobile augmented reality in microcontroller learning. *The Eurasia Proceedings of Science, Technology, Engineering & Mathematics (EPSTEM), 16*, 106-116.

The Eurasia Proceedings of Science, Technology, Engineering & Mathematics (EPSTEM)
ISSN: 2602-3199

The Eurasia Proceedings of Science, Technology, Engineering & Mathematics (EPSTEM), 2021

Volume 16, Pages 117-131

IConTES 2021: International Conference on Technology, Engineering and Science

Analysis and Prediction of Students' Academic Performance and Employability Using Data Mining Techniques: A Research Travelogue

Maria Elisa Linda Taeza CRUZ
University of Nizwa

Riah Elcullada ENCARNACION
Oman Tourism College

Abstract: Higher education institutions (HEIs) handle tons of data to analyze and generate the most relevant information. Data mining is considered a useful tool to extract knowledge to predict future educational trends in this process. Hence, such a method is significant to HEIs to understand and predict students' employability and other critical academic elements. A comprehensive and systematic literature review was conducted to identify data mining techniques, algorithms, and the various data sets that will lead to the smart prediction and accuracy of student employability. The same method was used to determine the relationship between academic achievement and the employability of students. According to the research findings, the most frequently used data mining techniques for determining students' academic achievement and employability are Classification techniques, specifically the J48(C4.5) algorithm, the Naïve Bayes algorithm, and the CHAID Decision Tree algorithm. The most frequently used data sets or attributes for predicting students' academic performance and employability are their cumulative grade point average (CGPA), gender, technical, communication, problem-solving, analytical, critical thinking, and decision-making skills, extracurricular activities, and age, as well as psychomotor factors such as behavior and attendance and training/internship placement. Academic performance is the primary determinant of employability. The application of data mining techniques in academia has demonstrated its value in enhancing the performance of higher education institutions (HEIs). As a result, more research is urgently needed to ascertain the efficacy of the approaches, algorithms, and data sets identified as predictors of students' employability. Moreover, automated approaches should be utilized to ascertain their accuracy.

Keywords: Student employability, Data mining techniques, Datasets, Prediction, Student academic performance

Introduction

Graduates' employability is considered one of the key performance indicators for educational achievement and a measurement of the success of every higher education institution. A higher employment rate also signifies that HEIs have provided quality education and their graduates possess the necessary knowledge, skills, and values needed by industries. Much research has proven that academic qualifications and employability skills are vital in the employment process (Brown, 2002; Tholen, 2014). With this, many HEIs have put a considerable amount of effort into providing students with proper knowledge and employability skills to fulfill employment demands (Santiago et al., 2008).

However, regardless of the large number of graduates produced each year and the best pedagogies followed by HEIs, they still face the problems of high drop-out rates, low academic performance, and high unemployment among their students. According to Andrews et al. (2008), several concerns including the gap between the

- Selection and peer-review under responsibility of the Organizing Committee of the Conference

needed graduate attributes and the industry requirements. The primary concern of industries has been that higher education institutions globally are failing to produce graduates with the necessary professional and life-long learning capabilities to prosper in the workplace (Mwita, 2018). Many studies have found that graduates must possess employability skills before immersing themselves in the workplace (Atkins, 1999; Billing, 2003; Crebert, et al., 2004a). This has strongly put pressure on HEIs to enhance graduates' employability and ensure that the knowledge, skills, and competencies they have gained will satisfy the labor market (Pitan, 2017).

Understanding and analyzing students' academic performance factors and predicting their employability using powerful tools such as data mining techniques can provide HEIs with valuable input for making policies and derive an appropriate solution. Information systems and educational databases serve as the backbone of HEIs' daily operations. The use of data mining has proven its worth in marketing, finance and banking, advertising, and recently in the academic setting. The enormous amount of students' data collected by HEIs can be a great source of relevant knowledge and the use of data mining techniques can reveal hidden patterns. Thus, these precious discoveries can help HEIs meet the industry requirements and provide them with high-quality graduates.

This paper conducted a thorough literature review of research and various sources on data mining techniques used to analyze and predict students' academic performance and employability. This research sought to answer the following questions:

1. What data mining techniques are frequently used to assess students' academic performance and employability?
2. Which data mining methods are most appropriate for predicting academic performance and employability of students?
3. Which data sets are most frequently utilized to predict academic performance and employability of students?
4. What is the relationship between the academic performance and employability of students?

Method

The purpose of this paper is to undertake a comprehensive review of relevant data mining methodologies and algorithms for predicting students' employability and academic performance based on earlier research. Furthermore, it sought to identify data sets that may be used to predict students' academic and employabilty. Finally, it reviewed research studies on the relationship between academic performance and employability of students. Thus, Table 1 illustrates how researchers previously used a variety of data mining techniques to predict students' academic performance and employability.

Table 1. Summary of the reviewed related studies on data sets, data mining techniques and algorithms used and the authors' findings

No.	Author/s	Datasets	Data Mining Techniques and Algorithms Used	Findings
1	Girase et al. (2018)	Academic Performance, Extra Curricular Activities, Personality Development, Technical, Training, Placement	Classification Techniques	• By utilizing the classification techniques, the number of students who would likely pass the examination will be successfully predicted. • The study demonstrated that the Decision Tree method outperformed the other data mining techniques tested.

No.	Author/s	Datasets	Data Mining Techniques and Algorithms Used	Findings
2	Mishra et al. (2016)	Socio-economic conditions, academic performances and a few more emotional skill factors (assertion, leadership skill empathy, decision making, drive strength, time management, self-esteem, stress management).	Bayesian methods, Multilayer Perceptrons and Sequential Minimal Optimization (SMO), Ensemble Methods and Decision Trees	For predicting employability, J48 is the most effective.
3	Thakar et al. (2017)	Personal Information, Demographic Information, Academic Records, Family Information, Social Parameters, Marketing, Cognitive Aptitude, Leadership Capabilities, Core Technical Skills Personality/Psychometric Aptitude, Finance Aptitude, English Aptitude, Quantitative Aptitude, Logical Aptitude, Mathematical Aptitude	• Clustering and classification techniques • Using chi-square analysis, clustering on two levels (k-means kernel); combination of four classifiers: k-star, random tree, simple cart, and random forest	High accuracy rates were seen with all classifier types.
4	Piad (2018)	Student's biographical information and their cumulative grade point average (CGPA) in their major and general subjects	• Logistic Regression • Chaid Algorithm (Different Classification algorithms were used to general models)	The most accurate algorithm was logistic regression, followed by the CHAID algorithm.
5	Piad et al. (2016)	Sudent's biographic information and Cumulative Grade Point Average (CGPA)	Classification techniques were employed to construct data models.	The Chaid Decision Tree has the highest accuracy, followed by Naïve Bayes and J48.
6	Othman et al. (2018)	Age, faculty, subject of study, co-curricular activities, marital status, industrial internship, and English proficiency were all taken into account. Age, industrial internship, and faculty all contain significant amounts of data and influence the final class, i.e., employability status.	• J48 • Multilayer • Perceptron (MLP) • Self-Organizing Maps (SOM)	J48 outperformed the other approaches.
7	Denila, P., et al. (2020)	Grades and First Employment	• C4.5 • Naïve Bayes	C4.5 classification is the most suitable algorithm
8	Tan et al. (2019)	Age, CGPA, Employability	• Logistic Regression • Decision Tree • Naïve Bayes • kNearest Neighbor • Support Vector Machine • Neural Network	Neural Network achieved the highest accuracy, followed by Support Vector Machine and Decision Tree

No.	Author/s	Datasets	Data Mining Techniques and Algorithms Used	Findings
9	Sapaat et al. (2011)	Graduate's gender, age, university/institution of current qualification, level of study for current qualification, field of study, CGPA, current employment status, levels of IT skills, Malay and English language proficiency, general knowledge, interpersonal communication, creative and critical thinking, analytical skills, problem solving, instillation of positive values, and teamwork acquired through the study program.	• J48 • Naïve Bayes • Information Gain	J48 performed with the highest accuracy compared to Bayes algorithms
10	Jantawan et al. (2013)	Prefix, Gender, Province, Degree, Educational Background, Faculty, Program, GPA, WorkProvince, Status, Talent, Position, Satisfaction, PeriodTimeFindWork, WorkDirectGraduate, ApplyKnowledgeWithWork, ReasonNotWork, ProblemofWork, RequirementsofStudy, LevelofStudyRequired, InstitutionNeed	• BFTree • NBTree • REPTree (J4.8 in WEKA) • Naïve Bayes classifier with five variants, including Averaged One-Dependence Estimators (AODE), BayesNet, HNB, and NaiveBayes, as well as Weightily Averaged One-Dependence Estimators (WAODE)	The method with the highest accuracy was the WAODE algorithm, a variant of the Bayes algorithm.
11	Sunday, et al. (2020)	Class Test Score, Completed Assignments, Class Laboratory Work, and Class Attendance	• ID3 • J48	J48 has a higher classification accuracy than the ID3 algorithm.
12	Al Lluhaybi, et al. (2018)	Admission, Course Related Data and Level 1 Final Grades	• C4.5 Decsion Tree • Naïve Bayes	• Naïve Bayes is better than C4.5 decision tree algorithm in predicting the students at high risk of failing. • Final grades influenced the results of the students in Level 2.
13	Funmilayo, O. and Ibukun, A. (2019)	Graduation CGPA, Biodata, Pre-admission requirements/results and performance in the university.	• Multiple linear Regression • C4.5	Multiple Linear Regression for a more effective prediction.

No.	Author/s	Datasets	Data Mining Techniques and Algorithms Used	Findings
14	Anuradha, C. and Velmurugan, T. (2016)	Student Gender, Students Branch, Students' Grade in High School, Students' Grade in High School, Medium of Instruction, Students' Residence Location whether a Student lives in a hostel or Not, Students' Family Size, Family Type, Family Annual Income, Fathers' and Mothers' Qualifications, Previous Semester Grade, Class Test Grade, Seminar Performance Assignment, Assignment, General Proficiency, Attendance, Lab Work and End Semester Marks	• Fast Boost Decision Tree algorithm	Datasets should be tried out on a set of qualifiers and the best one should be used.
15	Baradwaj et al., (2011)	Attendance, Class Test, Seminar and Assignment Marks	• Decision Tree	A decision tree was utilized to identify students who require additional attention and assistance in the upcoming semester exams.
16	Osmanbegovic et al. (2012)	Attained high school results, entrance exam scores, attitude toward learning and grades.	• Naïve Bayes • Decision Tree • Neural Network Methods	Naïve Bayes outperformed in prediction decision tree and neural network methods.
17	Shahiri et al. (2015)	Internal Assessment, CGPA, Extracurricular Activities, Student Demographics, High School Background, Scholarship, Interaction with Social Networks, Internal Assessment, Assessment, External Assessment	• Decision Tree • Artificial Neural Networks • Naïve Bayes • K-Nearest Neighbor • Support Vector Machine	Classification technique is most popular in predicting students' performance.
18	Kavyashree et al. (2016)	Gender, Education of the Father, Education of the Mother, Father's Occupation, Mother's Occupation Income, Loan, and Annual Family Income, Early Life, Instructional Medium, Performance in 10th Grade, 12th Grade, First Semester, and Second Semester, Academic Hours, Type of Graduation Degree, Gap Year Assertion, Empathy, Leadership, Drive and Management of Stress	• Modelling • Classification	Classification techniques can be used to identify weak students and take necessary action when developing a decision support system.
19	Sayana, (2015)	CGPA, Graduation Percentage, Attendance, Assignment Work and Unit Test Performance	• Decision Trees • Clustering using K-Means • Association	K- means clustering is preferred than other types.

No.	Author/s	Datasets	Data Mining Techniques and Algorithms Used	Findings
			Rule	
20	Ashraf, A., Anwer, S. & Khan, MG. (2018)	**Student Demographics** Age, Gender, Region, Place of Residence, and Information on the Guardian **Previously Obtained Results** Certificates, Scholarships and Results **Grades** Assessment Results, Quizzes, Final Exam, Cumulative Grade Point Average (CGPA) and Attendance **Social Network Details** Interaction with Social Media Websites **Extra-Curricular Activities** Games Partitions, Sports, Hobbies **Psychometric Factors** Behavior, Absence and Remarks	Decision Tree algorithms: ADTree, JRip, Ridor, logistic regression and neural network approach	The Decision Tree algorithms: JRip, Ridor ADTree, logistic regression and neural network approaches all produce accurate results when predicting and helping the educational system.
21	Thakar et al. (2015)	**Primary Attributes** Age, Secondary Percentage, Senior Secondary Percentage, Stream in Senior Secondary, Graduation Degree, Graduation %, Type (Regular/Distance), Graduating University, Post Graduate Sem 1%, Post Graduate Sem 2%, No. of Supplementaries in 1st Year, Gap in years between Graduation and PG **Secondary Attributes** Gender, Permanent Address, State, English, Quantitative Ability, Logical Ability, Attention to Detail, Computer Programming, Computer Science, Psychometric	Naïve Bayes from Bayes Category, RBF Network and Multilayer Perceptron from Functions Category, IB1 and IBk from Lazy Category, PART and DTNB from Rules Category, J48, Random Tree and Random Forest from Trees Category.	The secondary attributes played an essential role predicting accuracy of students' employability.
22	Limbu et al. (2019)	Gender, Age, Previous Year's Academic Performance (Academic), Family's Highest Level of Education, and Psychometric Factors (Have you ever achieved the highest grade in your class?, I study because I am interested in learning., I am willing to devote time to studying., My academic performance is contingent upon my efforts. Generally, my state of mind is positive and I feel good., I understand the purpose of the	Hybrid Algorithm (i.e., combination of K-means Algorithm and Support Vector Machine Algorithm)	By using an unsupervised machine learning algorithm (such as the K-means Clustering Technique) results in a high level of output accuracy, using a hybrid model results in an even higher level of output accuracy than using any other single machine learning technique.

No.	Author/s	Datasets	Data Mining Techniques and Algorithms Used	Findings
		course contents., I establish a conducive environment for effective study., I select acceptable classmates for teamwork., What makes me comfortable when I study.)		
23	Yusuf et al. (2018)	Socio-Economic, Psychometric Factors, University Entrance Examination, Senior, Secondary Graduation Examinations Performance, CGPA	Decision Tree, Artificial Neural Networks, Naïve Bayes, K-Nearest Neighbor and Support Vector Machine	The CGPA was employed by most studies and internal assessments to predict students' academic success. Classification is a frequently used method. Researchers generally employ the Decision Tree method to predict students' academic performance.
24	Shade et al. (2013)	Family Background Factors, Previous Academic Achievement, Cumulative Grade Point Age (CGPA)	10 Classification Models (Random Forest, Random Tree, J48 Decision Stump and REPTree and five rule induction algorithms – Jrip, OneR, ZeroR, PART and Decision Table)	The performance of Random Trees has been proved to be superior to that of other algorithms. The findings of the study back up Quadri and Kalyankar's (2010) and Yadav et al. (2012) findings that Decision Trees are the best algorithms for predicting student performance.
25	Kumar et al. (2016)	Students Branch, Gender, High School Grade, Senior Grade, Secondary Grade, Student's Family Size, Students Family Status, Fathers Qualification, Mother's Qualification, Father's Occupation, Mother's Occupation, Result in BTech First Year	J48, Random Forest, REPTree and LADTree	The J48 classification method is the most accurate of the many decision trees.
26	Estrera et al. (2017)	GPA, student demographics (gender), psychometric variables (study habits, interest in studies, and time spent studying), extracurricular activities, and student demographics	Classification model was used (Decision Tree, Artificial Neural Networks, Naïve Bayes, K-Nearest Neighbor and Support Vector Machine)	The Decision Tree Method is the most effective algorithm for predicting student achievement.
27	Yadav et al. (2012)	Students Branch, Students Sex, Students Category, Students Grade in High School, Students Grade in Senior Secondary, Admission Type, Medium of Teaching, Living Location of Student, Student Live in Hostel or Not, Student's Family Size, Students Family Status, Family Annual Income,	Classification Techniques (ID3, C4.5, CART)	The decision tree predicted how many students would pass, fail, or be promoted to the next year. When the results were compared, it became clear which students required further assistance to improve their performance.

No.	Author/s	Datasets	Data Mining Techniques and Algorithms Used	Findings
		Father's Qualification, Mother's Qualification, Father's Occupation, Mother's Occupation, Result in BTech First Year		
28	Kumar et al. (2019)	**Student Attributes** (Possible Values Used in all Research Papers while Implementing DM Algorithm)**, Academic Attributes** (Internal and External Assessment, Lab Marks, Sessional Marks, Attendance, CGPA, semester marks, grade, seminar performance, assignment, attendance, school marks, etc.), **Personal Attributes** (Age, Gender, height, weight, student interest, level of motivation, sports person, hobbies, etc.), **Family Attributes** (Qualification, Occupation, Income, Status, Support, Siblings, Responsibilities, etc.), **Social Attributes** (number of friends, social networking, girls/boys friends, movies, trip outings, and friend parties, etc.) (Teaching Medium, Accommodation, Infrastructure, Water & Toilet facilities, Transportation system, Class Size, School Reputation, School Status, Class Size, School Type, Teaching Methodology, etc.)	Classification Algorithms (Decision Tree, Naïve Bayes, Neural Network, K-Nearest Neighbor Algorithm, Support Vector Machine Algorithm)	Predictions are made using the CGPA, as well as internal and external assessment marks. Classification is the most commonly used technique for performance prediction.
29	Jayaprakash et al. (2018)	**Student Pre-enrollment Data** (Junior and Higher Secondary Grades, Entrance Exam Scores, Medium of Study), **Continuous Assessment** (Attendance, Team Scores, Lab Performance, Course and Lecturer Assessment, Forum Participation, Effective Use of Resources), **Psychological Data** (Personality, Social Activities), **Socio Economic Status** (Parents Education Qualification, Parents Occupation, Place of Stay/Distance Travelled, Family Size)	Naïve Bayes Algorithm, Rule-Based Classifier, SPPN (Students Performance Prediction System), Ensemble Learning	Sudents' pre-enrollment data, ongoing assessment data, and psychological data all contribute significantly to the prediction of academic performance. The Naïve Bayes Algorithm and Rule-Based Classifier can be used to perform predictive analysis.
30	Aziz et al. (2013)	Race, Gender, Hometown, Family Income, University Entry Mode and Grade Point	Naïve Bayes Classifier	The Naïve Bayes Classifier predicts with a precision of 57.5 percent.

No.	Author/s	Datasets	Data Mining Techniques and Algorithms Used	Findings
		Average		The study discovered that the income of students' families, their gender, and their locality all have an effect on their academic achievement. Additional data should be collected to improve the accuracy of the prediction model.

Scope and Limitations

This investigation focused on the application of data mining techniques to the education sectors of education. It emphasizes on the analysis and prediction of students' performance and employability. Due to the COVID19 pandemic, the study adopted the online research approach. It analyzed primary research and secondary data published from 2010 to 2020 only to ensure their timeliness and relevance to the present scenario. The complete literature review, analyzing journal articles, blogs, case studies, and primary studies, lasted for three months. It was not aimed at achieving a concluding resolution to the pressing problem but to unveil information that could enhance awareness among educational stakeholders on the usefulness of data mining techniques.

The Input-Process-Output (IPO) diagram below shows three significant boxes with their series of activities and requirements. The flow of control is shown by the arrows depicting the first stage to the third stage. The researchers were able to develop a conceptual framework suitable to the study by substituting generic model variables.

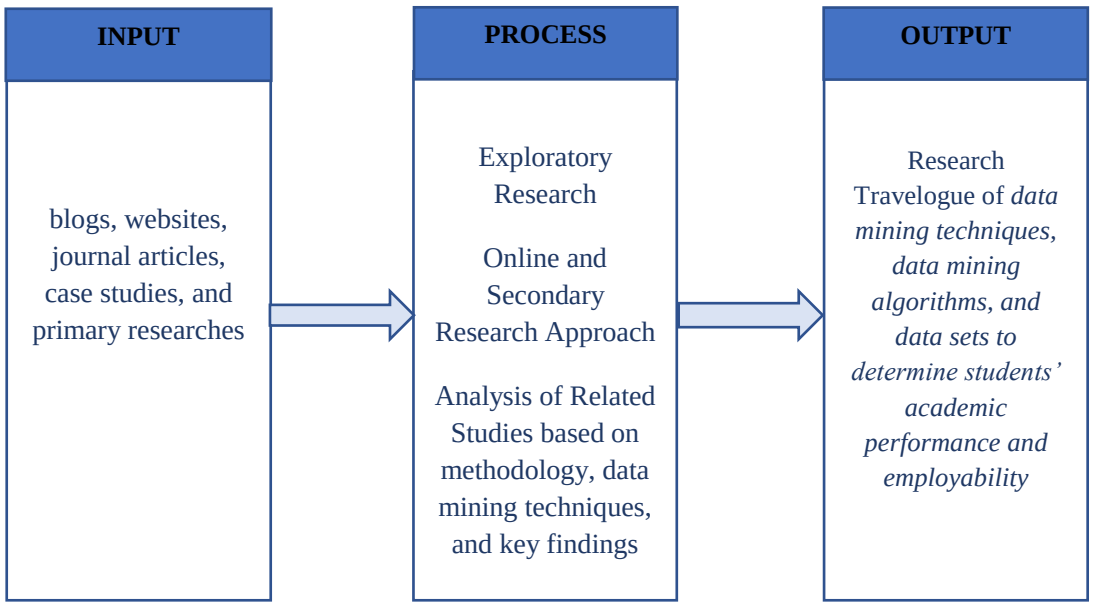

Figure 1: The Conceptual Framework of the Study

As depicted in Figure 1.0, the Input stage is the initial phase that identified the study's requirements taken from blogs, websites, journal articles, case studies, and primary researches. The Process is the second stage in the model where the inputs were analyzed, processed, and evaluated using an online research approach. Finally, the Output summarizes important discoveries such as the data mining techniques, algorithms, and data sets /variables essential to determine students' employability and students' academic performance.

Research Design

This present study was classified as exploratory research. It is considered a novel effort to comprehensively review various significant investigations in educational data mining techniques in a single study. According to Bhat (2020), exploratory research results aim to provide a hypothetical or theoretical idea for further investigation.

Data Collection and Analysis

The online research approach was used to gather the desired amount of data from the internet. The study only covers those pieces of literature that are undisputable and reliable. The secondary research approach was employed to summarize, collate, and synthesize existing primary research sources and generate the necessary information. A total of thirty (30) related studies were analyzed and synthesized. The results were then categorized according to data mining techniques/algorithms used, the variables or dimensions used and the research findings.

Results and Discussion

The results and findings of the study are found below:

The Most Common Data Mining Methods to Determine Students' Academic Performance and Employability

Generally, it was found out that among the different studies conducted to predict graduates' employability and students' academic performance, Classification techniques were the most common. A complete description was presented by the various authors, specifying the methods, the results and discussion of the results.

The application of Classification techniques in education was very useful for determining students' employability. These include predicting students' successful examinations (Girase et al., 2018), developing of emotional skills (Mishra et al., 2016), promising job offers & employment (Mishra et al., 2016; Piad, 2018; Piad et al., 2016; Denila et al., 2020; Jantawan et al., 2013), constructing a unified employability prediction model (Thakar et al., 2017; Sapaat et al., 2011), and identifying critical factors affecting employment probability (Othman et al., 2018; Tan et al., 2019).

Meanwhile, there are also many benefits of utilizing Classification techniques for analyzing students' academic performance (Sunday et al., 2020; Kumar et al., 2016; Kumar et al., 2019; Aziz et al., 2013), predicting the high risks for failure (Al Lluhaybi et al., 2018; Baradwi, 2011; ; Oladapo et al., 2019), identifying weak students (Kavyashree et al., 2016), developing a predictive system of academic performance (Funmilay et.al., 2019; Anuradha, et.al., 2016), predicting successful academic performance (Baradwi, 2011; Osmanbegovic et al., 2012; Shahiri et al., 2015; Sayana, 2015; Estrera et al., 2017), and enhancing the educational system (Ashraf et.al., 2018)

The Most Suitable Data Mining Algorithms to Predict Students' Academic Performance and Employability

The literature review revealed that J48 (C4.5), Naïve Bayes algorithms, and CHAID Decision Tree algorithms are the most appropriate data mining algorithms for predicting students' employability and determining students' academic performance.

The J48 algorithm is one of the most effective machine learning algorithms for constructing a decision tree that categorizes and constantly classifies input. It outperformed the other procedures and produced the highest accuracy result Othman et al., 2018; Denila et al., 2020; Sapaat et al., 2011; Sunday et al., 2020; Kumar et al., 2016). The J48 algorithm is a simple classifier of C4.5 algorithms in an open-source Java platform of Weka Data mining tool and developed by Ross Quinlan (Girase et al., 2018). A decision model tree is built for the classification process using this method. After the tree has been constructed, it is applied to each tuple in the database and classified accordingly.

Denila et al. (2020), Tan et al., (2019), Jantawan et al. (2013), Sapaat et al. (2011), and Aziz et al. (2013) all agreed that the Naïve Bayes agorithm is the most common algorithm for classification tasks, notably in assessing and predicting students' employability. The Naïve Bayes method is a probabilistic machine learning algorithm based on Rev. Thomas Bayes' Bayes Theorem (Al Lluhaybi, et al., 2018; Tan et al., 2019). The algorithm uses binary and multi-class classification categories to build a model (Sapaat et al., 2011) for predicting high student academic success (Osmanbegovic et al., 2012; Shahiri et al., 2015) as well as, on the other hand, for predicting high student failure rates (Al Lluhaybi, et al., 2018).

The Chi-square Automatic Interaction Detector (CHAID) Decision Tree algorithm was used to build a predictive model and identify the relationships between variables (Piad et al., 2016; Piad, 2018). It was designed by Gordon V. Kass in 1980 (Piad, 2018); the process involved continuous splitting the predictors (nominal, ordinal, and continuous data) into categories and cross tabulating each categorical predictor to derive the best result. In this technique, a classification tree is generated, showing the relationships between the split categories and the related factors within the tree.

The Most Commonly Used Data Sets or Variables for Predicting Students' Academic Performance and Employability

Twenty-seven (27) out of thirty (30) papers identified Cumulative Grade Point Average (CGPA) as the most significant data set used in predicting students' performance and employability. The reason why most of the researchers used CGPA and grades as a measure was because of its tangible value that can predict student employability and career performance (Shahiri et al., 2015; Piad, 2018; Tan et al., 2019; Durga et al., 2019) as well as for determining high academic performance (Funmilayo et al., 2019; Shahiri et al., 2015; Sayana, 2015; Ashraf et al., 2018; Estrera et al., 2017).

Other datasets that were found significant include gender (Ashraf et al., 2018; Thakar et al., 2017; Kavyashree et al., 2016; Anuradha et.al., 2016; Jantawan et al., 2013; Sapaat et al., 2011; Limbu et al., 2019; Estrera et al., 2017; Aziz et al., 2013), technical, communication, critical thinking, problem solving, analytical and decision-making skills (Mishra et al., 2016; Thakar et al., 2017; Sapaat et al., 2011; Kavyashree et al., 2016), extra-curricular activities (Girase et al., 2018; Shahiri et al., 2015; Ashraf et.al., 2018; Oathman, Z., et al., 2018; Estrera et al., 2017), age (Tan et al., 2019; Sapaat et al., 2011; Oathman, Z., et al., 2018; Ashraf et.al., 2018; Limbu et al., 2019), psychomotor factors such as behavior and attendance (Ashraf et.al., 2018; Sayana, 2015; Anuradha et.al., 2016; Kavyashree et al., 2016; Limbu et al., 2019; Jayaprakash et al., 2018) and training/internship placement (Girase et al., 2018; Oathman, Z., et al., 2018; Gault et al., 2010; Weible et al., 2011).

The Relationship Between Students' Academic Performance and Employability

The review of various studies signified that students' academic performance dramatically influences employability. Thus, the main predictor of students' employability is academic performance (Gokuladas, 2011; Hassanbeigi et al., 2011; Imose et al., 2015; Johansen, 2014; Kuncel et al., 2010; Funmilayo et al., 2019; Shahiri et al., 2015; Sayana, 2015; Ashraf et.al., 2018; Tentama et al., 2019; Pan et al., 2011; Edinyang et al., 2015; Moya Clemente et al., 2020; Kumar et al., 2019). This was also supported by other authors that revealed that it is the main predictor of employability (Funmilayo et al., 2019; Shahiri et al., 2015; Sayana, 2015; Ashraf et al., 2018; Yusuf et al., 2018; Vasan et al., 2018.

Multiple linear regression analysis was utilized by Tentama et al. (2019) to find a significant relationship between academic achievement and employability. On the other hand, Pan et al., (2011) looked into the relationship and discovered that academic performance is closely linked to employability skills such foreign language proficiency, computer literacy, application and theory to work, and stability and pressure resistance. As a result, their data revealed that employability is linked not just to the employment process but also to academic performance.

Academic achievement is a key influence in graduate employability in a specific discipline, according to studies by Edinyang et al. (2015) and Vasan et al. (2018). Furthermore, academic factors may influence a student's ability to find work in a given field. As a result, the authors advise that industry sectors collaborate with policymakers and academic curriculum developers to meet the demands of the global labor market. Moya

Clemente et al., (2020) discovered that participation in international exchanges and internships, in addition to academic performance, predict future employability.

Conclusion

In general, this in-depth study proved that data mining is an interesting field of data science and has been widely used in the educational setting for years. Moreover, various studies have shown remarkable outcomes in predicting students' employability and identifying academic performance. The Classification Techniques were predominantly used for prediction and analysis tasks, specifically the use of J48 (C4.5), Naïve Bayes algorithms, and CHAID Decision Tree algorithms, because of their high accuracy results.

The analysis yielded some common variables that were used for classification, such as CGPA, gender, technical, communication, analytical and decision-making skills, problem-solving, critical thinking, extra-curricular activities, age, psychomotor factors such as behavior and attendance and training/internship placement. In addition, the systematic review of related literature and studies manifested that academic performance greatly influences students' employability.

Recommendations

From the present study's findings, it can be deduced that data mining techniques are significantly relevant in uplifting the performance of every HEI around the world. The discovery of precious knowledge is essential for facilitate the planning of services and guide actions for improvement. Therefore, a follow-up developmental research is deemed necessary to apply the identified data mining algorithms in Omani Higher Education and the identified attributes/datasets and reveal their importance for students' employability and academic performance. Moreover, automated methods will be used to determine the efficacy of the attributes/datasets and the accuracy of the identified data mining algorithms. It is also recommended that HEIs utilize the findings of the study. The industry should also strongly collaborate with the academe to identify and set the needed skills to meet the labor market requirements.

The findings of this investigation could generate a better understanding and social awareness of the usefulness of data mining techniques from the academic perspective. Moreover, it highlighted their implications on students' academic performance and employability. Thus, academic stakeholders particularly the students, industry partners, and educational providers, are the greatest benefactors of this study. Future researchers could also use the results of this exploration as additional literature for review and further investigative study.

Scientific Ethics Declaration

The authors declare that the scientific ethical and legal responsibility of this article published in EPSTEM journal belongs to the authors.

References

Al Lluhaybi, M., Tucker, A. & Yousef, L. (2018). The prediction of student failure using classification methods: a case study. *Computer Science and Information Technology, 79-90.* DOI: 10.5121/csit.2018.80506.

Andrews, J., & Higson, H. (2008). Graduate employability,'soft skills' versus 'hard'business knowledge: A European study. *Higher education in Europe, 33*(4), 411-422.

Anuradha, C. & Velmurugan, T. (2016). fast boost decision tree algorithm: a novel classifier for the assessment of student performance in educational data. *Printed in Portugal*, *31*(11), 139-155.

Ashraf, A., Anwer, S., & Khan, M. G. (2018). A Comparative study of predicting student's performance by use of data mining techniques. *American Scientific Research Journal for Engineering, Technology, and Sciences (ASRJETS)*, *44*(1), 122-136.

Atkins, M. J. (1999). Oven- ready and self- basting: taking stock of employability skills. *Teaching in higher education*, *4*(2), 267-280.

Aziz, A. A., Ismail, N. H., Ahmad, F., & Hassan, H. (2015). A framework for students's academic performance analysis using naive bayes classifier. *Jurnal Teknologi*, *75*(3), 13-19. DOI: 10.11113/jt.v75.5037.

Baradwaj, B. & Pal, S. (2011). Mining Educational Data to Analyze Students' Performance. International *Journal of Advanced Computer Science and Applications*, *2*(6), 63-69.

Bhat, A. (2020, January 24). *Exploratory research, definition, methods, types and examples.* https://www.questionpro.com/blog/exploratory-research/#Secondary_research_methods.

Billing, D. (2003). Generic cognitive abilities in higher education: An international analysis of skills sought by stakeholders. *Compare: A Journal of Comparative and International Education*, *33*(3), 335-350.

Brown, BL. (2002). *Generic skills in career and technical education: myths and realities.* Educational Resources Information Centre.

Moya Clemente, I., Ribes Giner, G., & Sanahuja Vélez, G. (2020). Towards sustainability in university education. ımproving university graduates chances of employability by participation in a high achievement academic program. *Sustainability*, *12*(2), 1-17. doi: 10.3390/su12020680.

Crebert, G., Bates, M., Bell, B., Patrick, C. J., & Cragnolini, V. (2004). Ivory tower to concrete jungle revisited. *Journal of education and work*, *17*(1), 47-70.

Denila, P. G., Delima, A. J. P., & Vilchez, R. N. (2020). Analysis of IT graduates employment alignment using C4. 5 and Naïve Bayes algorithm. *Int J Adv Trends ComputSciEng*, *9*(1), 745-752.

Durga, V. S., & Thangakumar, J. (2019). A complete survey on predicting performance of engineering students. *Int. J. Civ. Eng. Technol*, *10*(2), 48-56.

Edinyang, S.D., Odey, C., & Joseph, G. (2015). academic factors and graduate employability in Nigeria. *Global Journal of Human Resource Management*, *3*(5), 9-17.

Estrera, P.J., Natan, P., Rivera, B.F. & Colarte, Faith, B. (2017). *International Journal of Engineering and Techniques*, 2(5), 147-154.

Funmilayo, O. & Ibukun, A. (2019). Student's performance prediction using multiple linear regression and decision tree. *International Journal of Advanced Research in Computer Engineering & Technology (IJARCET)*, *8*(7), 256-268.

Gault, J., Leach, E., Duey, M. (2010). Effects of business internships on job marketability: the employers' perspective. *Journal of Education and Training*, *52*, 76-88.

Girase, M., Lad, S., & Pachpande, P. (2018). Student's employability prediction using data mining. International *Journal of Scientific & Engineering Research*, *9*(4), 27-29.

Gokuladas, V. K. (2011). Predictors of employability of engineering graduates in campus recruitment drives of Indian software services companies. *International Journal of Selection and Assessment*, *19*(3), 313-319. https://doi.org/10.1111/j.1468-2389.2011.00560.x,

Hassanbeigi, A., Askari, J., Nakhjavani, M., Shirkhoda, S., Barzegar, K., Mozayyan, M. R., & Fallahzadeh, H. (2011). The relationship between study skills and academic performance of university students. *Procedia-Social and Behavioral Sciences*, *30*, 1416-1424.

Imose, R., & Barber, L. K. (2015). Using undergraduate grade point average as a selection tool: A synthesis of the literature. *The Psychologist-Manager Journal*, *18*(1), 1-11.

Jantawan, B. & Tsai, C. (2013). The application of data mining to build classification model for predicting graduate employment. *(IJCSIS) International Journal of Computer Science and Information Security*, *11*(10), 1-7.

Jayaprakash, S., & Jaiganesh, V. (2018). A Survey on Academic Progression of Students in Tertiary Education using Classification Algorithms. *International Journal of Engineering Technology Science and Research IJETSR*, *5*(2), 136-142.

Johansen, V. (2014). Entrepreneurship education and academic performance. *Scandinavian Journal of Educational Research*, *58*(3), 300-314.

Kavyashree, K. R., & Laksmi, D. (2016). A review on mining students' data for performance prediction. *International Journal of Advanced Research in Computer and Communication Engineering*, *5*(4), 1104-1106.

Kumar, M., & Salal, Y. K. (2019). Systematic review of predicting student's performance in academics. *Int. J. of Engineering and Advanced Technology*, *8*(3), 54-61..

Kumar, M. & Singh, A.J. (2016). Predicting students' performance using classification techniques in data mining. *International Journal of Technology and Computing (IJTC)*, 2(10), 489-494.

Kuncel, N. R., Ones, D. S., & Sackett, P. R. (2010). Individual differences as predictors of work, educational, and broad life outcomes. *Personality And İndividual Differences*, *49*(4), 331-336.

Limbu, J. & Sah, S. (2019). Prediction on Student Academic Performance Using Hybrid Clustering. *LEBF Research Journal of Science, Technology and Management*, *1*(1), 1-22.

Mishra, T., Kumar, D., & Gupta, S. (2016). Students' employability prediction model through data mining. *International Journal of Applied Engineering Research*, *11*(4), 2275-2282.

Mwita, K. M. (2018). Tanzania graduate employability: Perception of human resource management practitioners. *International Journal of Human Resource Studies*, *8*(2), 263-272.

Oladapo, K.A. & Adedokun, A. (2019). Data mining technique for early detection of at-risk students. *2nd International Conference on Information Technology in Education and Development*, Lagos, Nigeria.

Osmanbegovic, E., & Suljic, M. (2012). Data mining approach for predicting student performance. *Economic Review: Journal of Economics and Business*, *10*(1), 3-12.

Othman, Z., Shan, S. W., Yusoff, I., & Kee, C. P. (2018). Classification techniques for predicting graduate employability. *International Journal on Advanced Science, Engineering and Information Technology*, *8*(4-2), 1712-1720.

Pan, Y. J., & Lee, L. S. (2011). Academic performance and perceived employability of graduate students in business and management–an analysis of nationwide graduate destination survey. *Procedia-Social and Behavioral Sciences*, *25*, 91-103.

Pıad, K. C. (2018). Determining the dominant attributes of information technology graduates employability prediction using data mining classification techniques. *Journal of Theoretical & Applied Information Technology*, *96*(12). 3780-3790.

Piad, K. C., Dumlao, M., Ballera, M. A., & Ambat, S. C. (2016, July). Predicting IT employability using data mining techniques. In *2016 Third International Conference on Digital Information Processing, Data Mining, and Wireless Communications (DIPDMWC)* (pp. 26-30). IEEE.

Pitan, O. S. (2016). Towards enhancing university graduate employability in Nigeria. *Journal of Sociology and Social Anthropology*, *7*(1), 1-11. https://doi.org/10/1080/09766634.2016.11885696.

Santiago, P., Tremblay, K., Basri, E., & Arnal, E. (2008). *Tertiary education for the knowledge society* (Vol. 1). OECD. https://doi.org/10.1787/978926406351-hu/.

Sapaat, M. A., Mustapha, A., Ahmad, J., Chamili, K., & Muhamad, R. (2011, July). A classification-based graduates employability model for tracer study by MOHE. In *International Conference on Digital Information Processing and Communications* (pp. 277-287). Springer, Berlin, Heidelberg.

Sayana, TS. (2015). Prediction of students academic performance using data mining: analysis. *International Journal of Engineering Research & Technology*, *3*(20), 1-4.

Shade, K., Goga, N., Awodele, & Okolie, S. (2013). Optimal algorithm for predicting students' academic performance. *Internal Journal of Computers & Technology*, *4*(1), 63-75.

Shahiri, A. M., & Husain, W. (2015). A review on predicting student's performance using data mining techniques. *Procedia Computer Science*, *72*, 414-422. doi:10.1016/j.procs.2015.12.157, pp. 414-422.

Sunday, K., Ocheja, P., Hussain, S., Oyelere, S., Samson, B., & Agbo, F. (2020). Analyzing student performance in programming education using classification techniques. *International Journal of Emerging Technologies in Learning (iJET)*, *15*(2), 127-144.

Tan, K., Abdul Rahman, NA., Lim, C. (2019). A comparative of predictive model of employability. *International Journal of Innovative Technology and Exploring Engineering (IJITEE)*, *8*(8), 375-378.

Tentama, F., & Abdillah, M. H. (2019). Student Employability Examined from Academic Achievement and Self-Concept. *International Journal of Evaluation and Research in Education*, *8*(2), 243-248.

Thakar, P., Mehta, A. & Manisha, D. (2015). Role of secondary attributes to boost the prediction accuracy of students' employability via data mining. *International Journal of Advanced Computer Science and Application. 6*(11), 84-90.

Thakar, P., & Mehta, A. (2017). A unified model of clustering and classification to improve students' employability prediction. *International Journal of Intelligent Systems and Applications*, *9*(9), 10. DOI: 10.5815/ijisa.2017.09.02.

Tholen, G. (2014). Graduate employability and educational context: a comparison between Great Britain and the Netherlands. *British Educational Research Journal*, *40*(1), 1-17. DOI: 10.1002/berj.3023.

Vasan, T. M., Sharma, K. J., & Chauhan, N. C. (2018). A comparative study of student's employability prediction model using data mining technique. *International Journal of Creative Research Thoughts (IJCRT)*, *6*(1), 264-270.

Weible, R. & McClure, R. (2011). An exploration of the benefits of student internships to marketing departments. *Marketing Education Review*, *21*(3), 229-240.

Yadav, S. K. & Pal. S. (2012). Data Mining: A prediction for performance improvement of engineering students using classification. *World of Computer Science and Information Technology Journal (WCSIT)*, *2*(2), 51-56.

Yusuf, A. & Lawan, A. (2018). Prediction of students' academic performance using educational data mining technique: Literature review. https://www.academia.edu/34009565/prediction_of_students_academic_performance_using_educational_datamining_technique_literature_review.

Author Information

Maria Elisa Linda Taeza CRUZ
University of Nizwa
Birkat Al Mouz, Nizwa, Oman
Contact e-mail: *mariacruz@unizwa.edu.om*

Riah Elcullada ENCARNACION
Oman Tourism College
P.O. Box 2008, C.P.O, Postal Code 111, Muscat, Oman

To cite this article:

Cruz, M.E.L.T. & Encarnacion, R.E. (2021). Analysis and prediction of students' academic performance and employability using data mining techniques: A research travelogue. *The Eurasia Proceedings of Science, Technology, Engineering & Mathematics (EPSTEM), 16*, 117-131.

The Eurasia Proceedings of Science, Technology, Engineering & Mathematics (EPSTEM)
ISSN: 2602-3199

The Eurasia Proceedings of Science, Technology, Engineering & Mathematics (EPSTEM), 2021

Volume 16, Pages 132-139

IConTES 2021: International Conference on Technology, Engineering and Science

Knowledge Acquisition Base Learning: An Interactive Learning Approach

Mohammad MALKAWI
Jordan University of Science and Technology

Abstract: The Corona Covid-19 Pandemic revealed a deep deficiency in the current e-learning system. Many of the current e-Learning schemas have pursued their goals in conventional ways, albeit transferring the lecture hall to an online medium presentation. In essence, there had been little innovation above traditional classroom lecturing. In this paper, we propose a novel approach aimed at optimizing the learning outcomes of learning per student. Namely, we propose Iterative and Interactive e-Learning Platform, where the main focus is shifted towards the learner, i.e., the student. The role of the instructor is directed more towards the construction and presentation of interactive education material in a manner to enable the learner to acquire the minimum required knowledge and to achieve the intended outcomes in the most effective manner. Therefore, the proposed model is a knowledge-acquisition based learning management system (KA-LMS). Unlike the traditional ways of classroom or online lecturing, a student using KA-LMS is expected to achieve a quality of learning, never before achieved via standard offline or online pedagogical methodologies. The Iterative and Interactive KA-LMS is sought to enable various academic institutions to achieve quality standards in both online and on premise setup, thus avoiding the calamities of pandemics, such as the one imposed by the Corona Covid-19. The proposed KA-LMS will enable graduates to achieve the required skills and knowledge, which allow them to compete in a more vigorous and competitive marketplace at the local and global levels. The proposed KA-LMS has the inherent capability to monitor and control the progress of the learner entity based on the quantity and quality of the knowledge acquired by the learner. The proposed model will be tested in school and college environments, with real education subjects.

Keywords: Online learning, Iterative learning, Interactive learning, Knowledge acquisition, Covid-19

Introduction

This paper aims at solving several dilemmas faced by learnings in the current conventional and/or electronic learning systems. These dilemmas include:

Dilemma 1

Selection and presentation of education material to meet learning outcomes: This is attributed to wide diversity and availability of teaching materials including textbooks, power-point, audio-visual material, and augmented virtual reality. This dilemma is further complicated by the cost associated with education material, which increases the education divide between developed and under developed countries.

To address this dilemma, the paper provides a methodology to create tools and templates to allow an instructor to structure and present the material in a manner to allow simple learning, and to enable iterative interactive learning process. (Cho et al., 2009).

Dilemma 2

Variation of learning capabilities among student's population, may restrict the rapid progress of the gifted students, while depriving the least gifted ones. Pace adjustment of learning is not readily possible in classical classrooms or in current e-Learning systems, which merely transferred the education from the classroom to remote video presentations. The classical structure of semester based education limits the progress of the gifted and impede the progress of the less gifted.

This paper discusses the means of enabling students to learn at self-pace, in a manner to allow a student to progress in an incremental manner based on his/her capabilities (Meng et al., 2017). Thus providing an environment, where students can choose and select their pace at which they can achieve their learning objectives (Tullis et al., 2011).

Dilemma 3

The delivery process of education material lacks the ability to provoke dynamic engagement and interaction with each and with every learner. Thus it is bound to leave behind dis-involved students, who will eventually lag behind. Current methods of online e-learning methods suffer from serious lack of interactivity between instructor and learners Meng et al. (2017).

In this paper, the author addresses novel methods of delivering the education material in a manner to enforce engagement and interaction, which allows controllability and observability of the learning process Minka et al. (1997) and Barker (1994).

Dilemma 4

The current assessment and evaluation processes rely on assessing the final knowledge acquired by a student, which may not be a true assessment. Furthermore, current systems allow students to fail a subject, to pass with a low threshold, or below an acceptable line. The overwhelming fact is that a graduate with low grades or insufficient knowledge will suffer great deal while looking for a good work; in the end many of such graduates end up changing their careers, accepting low paying jobs, or remain unemployed for a long time. As such the economy of the individual as well as of the state at large suffers great deal, Andrabi et al. (2018).

In this paper, we provide an incremental, iterative, and adaptive evaluation and assessment process in a manner to guarantee the required level of knowledge acquisition. This objective is meant to steer the learning process based on a preset education quality level. For example, it would be possible for an academic department to set a minimum level of achievement for each and every student in a particular discipline, Malkawi et al (2006; 2006; 2007; 2008)

Significance of the Research

The presented research is sought to provide several significant outcomes and results in the field of online e-Learning. Covid-19 pandemic had exposed many of the shortcomings of current system. As a result, many students (both school and higher education students) suffered great deal. The presented research provides a model which aims at restructuring the learning material in a manner, which allows a student to increase the knowledge acquisition through incremental learning and accumulative evaluation and assessment. The progress of learning should be based on both quantity and quality of knowledge acquired by the learner rather than based on time spent studying a certain material and the result of the final and midterm exams results. The new learning model provides a mechanism to enable a given department or instructor to adjust and adapt the learning system to each student individually based on smart adaptive algorithms. In the course of providing the material, it is possible to set and define a standard of knowledge acquisition per student, per department, or per institute. While doing so, each student should be able to learn at own pace, thus allowing to take care of natural differences in students' capabilities. In an education world moving rapidly towards interdisciplinary education, the proposed model provides a well-structured integration of knowledge acquisition within a given discipline as well as across multiple disciplines. The most important part of the proposed novel approach for learning is that it enables both online or offline learning to achieve maximum student interaction with the subject material.

The proposed model is expected to have an impact on the overall quality of education within any given organization. This includes the reduction in the overall cost of the education system, by shifting the center of the learning process to the learning student, and transferring the role of the instructor to preparing, modifying, and perfecting the interactive electronic material.

The model will have a direct impact on the overall education systems in developing countries. It is sought to reduce the education divide between developed and developing countries by allowing students to benefit from state of the art education material without the need of expensive class room setting. The model guarantees the acquisition of minimum level of accepted knowledge in the field of study, thus allowing graduates of different countries irrespective of their economic status to compete in the local, regional, and international market scopes.

The new model will have a direct impact on the advancement of knowledge based economy by producing graduates with proven skills rather than graduates with diplomas and low score transcripts. With this model, it is possible to provide directed education material to enable the creation of required skills in each area (country, region, global world). The presented model will have a direct impact of the education system in several segments including primary education schools, higher education institutions, training centers, continuous training and education.

Related Work

Several e-learning platform systems have been developed over the past few years. Among the most commonly used platforms are:

1- Moodle (https://moodle.org/). Moodle is developed with free source code, thus making it most favorable for education organizations. The major strength of Moodle is the ability to host material in several formats and shapes including word, pdf, excel, images, audio, and video. It also provides tools for examination systems, quiz and assignment assessment. The main deficiency of Moodle in lieu of the proposed project is the lack of the ability to monitor and control the progress of the learner with the acquired knowledge. Also, Moodle does not provide a presentation platform of the material. Recently it has been augmented with video based presentation platforms such as ZOOM.
2- Blackboard (www.blackboard.com). This tool is very much similar to Moodle with the exception that is not free source platform. Similar to Moodle, Blackboard does not provide a tool to monitor and control the advancement of a student in the course with the acquired knowledge.
3- Udemy (https://elearningindustry.com). This platform provides a pool of more than 20000 Subject Matter Experts. Udemy eLearning platform has many content creation tools such as PDF documents, PowerPoint, etc. text and video content. They can be utilized to create and publish courses. It is very much based on video based education. The instructor must provide a high quality video and upload it to the platform. In essence, it is more like a youtube video repository, which provides no added value to the listener or learner. Its services are mostly paid services.
4- Teachable (https://elearningindustry.com/directory/elearning-software/teachable). This is another platform, which allows instructors to upload material in various formats for each course. It hosts more than 20000 courses created by 7500 instructors. It is a paid service
5- Other e- learning systems include: Ruzuku, Educadium, LearnWorlds, Thinkific, Academy Of Mine, CourseCraft, Skillshare, Coursera and many others.

The existing e-learning platforms provide a rich set of features. However, they all suffer several deficiencies such as:
1- The inability to monitor the exam integrity and/or to minimize the cheating and plagiarism.
2- The inability to tightly couple the student's progress with ongoing assessment
3- Do not distinguish between the assessment and the rate of knowledge acquisition,

Method

The proposed adaptive e-learning system is implemented according to the following well defined methodology. The main infrastructure of the model is constructed as an electronic portal system.

1. The portal system provides a portal for the students, teachers, and organization.

2. The proposed system will develop and provide the organization with tools and templates which enable the organization to define and set:
a. Standards of learning including: rate and level of knowledge acquisition
b. Method of calculating and computing the knowledge acquired by a learner student
c. Method for calculating the final grade score of a student. This method includes besides the knowledge, the time it took to acquire the knowledge and the number of repeated attempts to achieve the required knowledge.
d. The hierarchical structure of each discipline, which includes the subjects (courses), the modules per course, units per module and sub units.
3. The proposed system will develop and provide tools and templates for the teacher/instructor to perform the functions:
a. Brake the subject into modules
b. Break each module into units and/or sub units
c. For each unit/sub unit identify the immediate learning outcome and the related module outcome and the subject learning outcome
d. The system will provide a flow mechanism, by which an instructor can set a well-defined flow for the material, while observing parallel paths, dependent paths, and independent paths.
e. The instructor will be able to use the tool to upload trough the portal the unit/sub unit material to the course.
f. The tools and templates will enable the instructor to create questions for each unit/sub unit, and to organize a question bank.
g. The tools will enable the instructor to classify the questions in a given question bank with various indexes such as difficulty index, skill index, proficiency index, etc.
h. The instructor will be able to set the expected time spent on each unit
4. The tools and templates will provide exam, quiz, and pop-up questions delivery mechanism.
5. Ability to advance the learning progress based on achievements and student's own pace.
6. Ability to provide extra learning material to improve learner's performance
7. Method to compute final achievement score based on several criteria including achieved score, time to achieve score, number of attempts to achieve the required score.
8. The system will provide exam monitoring tools using biometrics, photo IDs, real-time photo identification and verification. This is necessary to control the exam taking environment.
9. The system will provide a final certification for the course with full authentication and verification.
10. The system portal can be configured to work online, cloud based, or offline self-learning

Expected Outcomes

The proposed project is sought to provide several significant outcomes and results, such as restructuring the learning material in a manner, which allows a student to increase the knowledge acquisition. It will also provide a tool for incremental learning and accumulative evaluation and assessment, where the learning progress is based on quantity and rate of knowledge acquisition. The system will provide tools to adjust and adapt the learning system to each student based individually based on smart adaptive algorithms, and to set and define a standard of knowledge acquisition per student, per department, or per institute. The system tools will enable students to learn at own pace, and provides a well-structured integration of knowledge acquisition within a given discipline as well as across multiple disciplines. The portal will be able to operate online or offline with maximum interaction with the subject material.

Impacts

The presented model will have an impact on

1. The overall quality of education within the organization
2. Reduce the cost of the overall education system
3. Shift the center of the learning process to the learning student

Impact on the Overall Education Systems in Developing Countries

1. Reduce the education divide between developed and developing countries by allowing students to benefit from state of the art education material without the need of expensive class room setting
2. Guarantee the acquisition of minimum level of accepted knowledge in the field of study, thus allowing graduates to compete in the local, regional, and international market scopes.

Impact on Knowledge Based Economy

1. Producing graduates with proven skills
2. Providing directed education material to enable the creation of requied skills in each area (country, region, global world)

Results and Discussion

A pilot model was created for the proposed knowledge acquisition based learning system. The pilot model was created using different platforms, which were integrated to provide a comprehensive tool. The main components were used from Moodle system, H5P system, SCORM and other.

The platform provides a course building templates as shown in Figure 1.

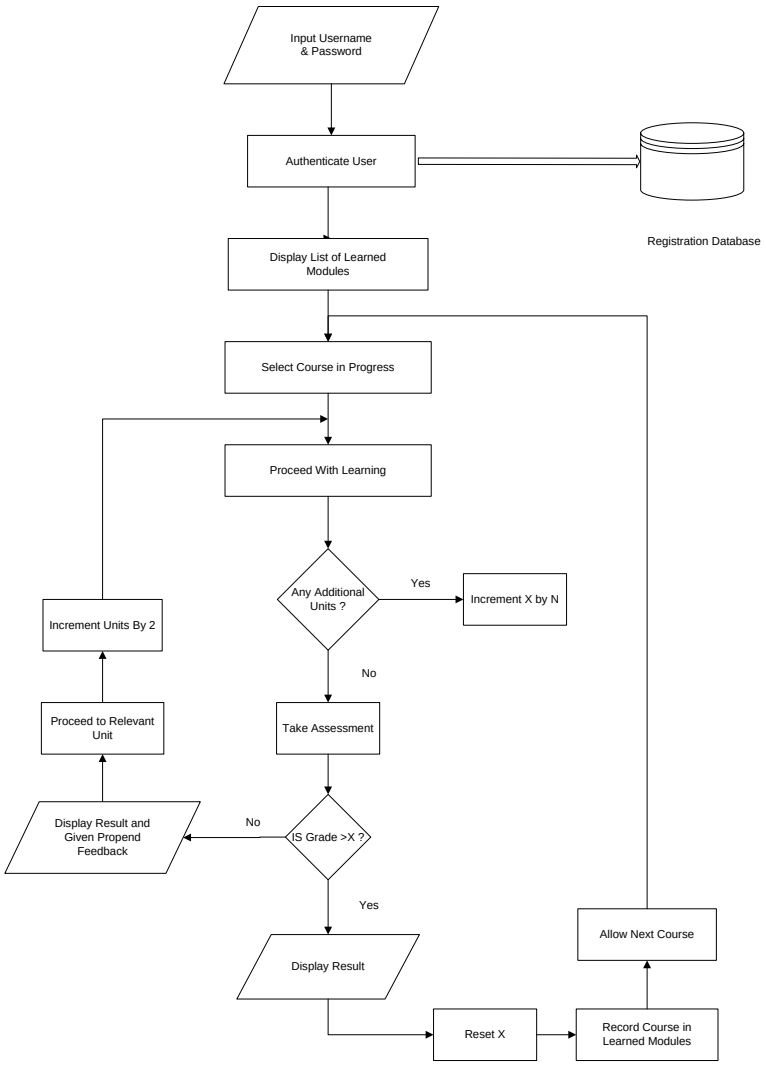

Fig.1 Flowchart Representing the Process of Iterative E-learning

Figure 1. Shows an example of iterative and interactive video, which is part of a course taught by the instructor, and developed by the proposed platform.

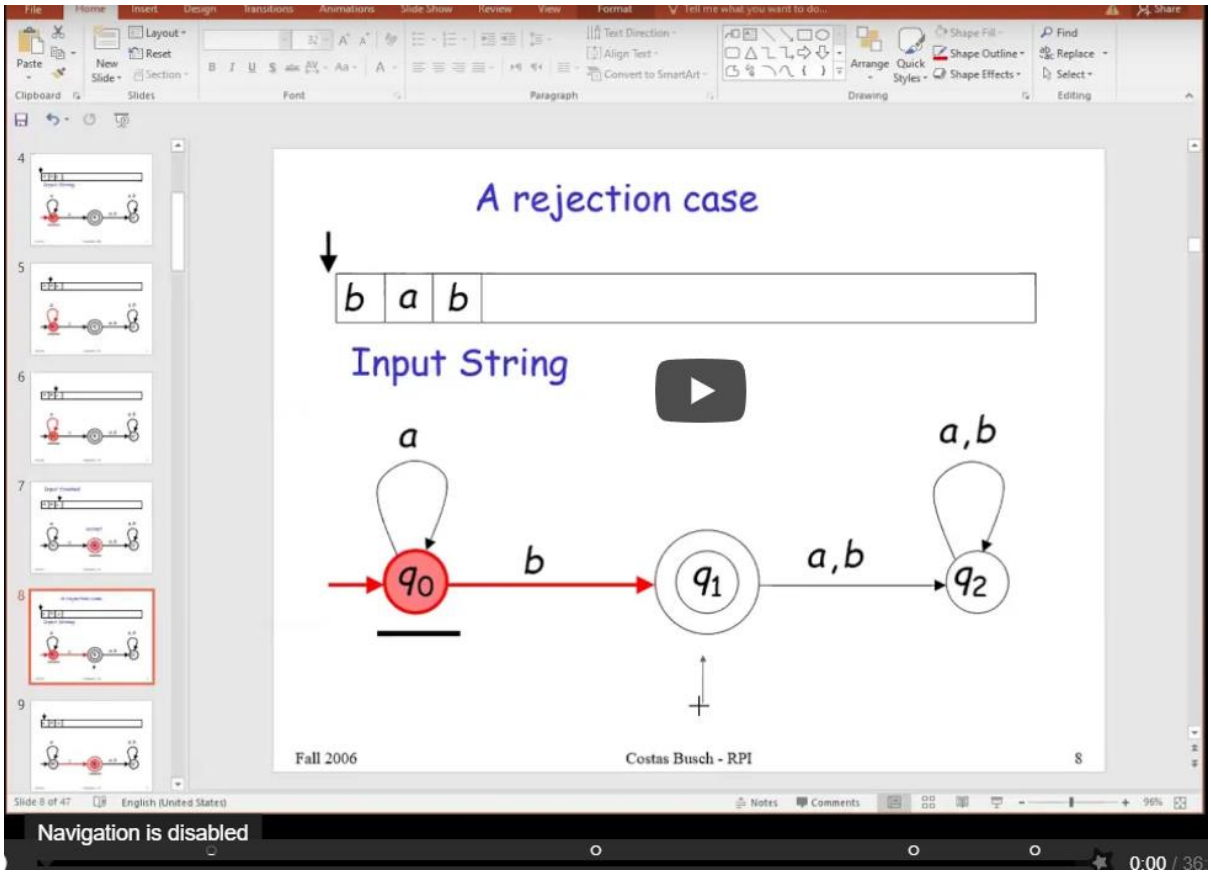

Figure 2. Iterative and interactive video

The interactive video is part of a software engineering course. The course is completely interactive and iterative. A student can watch the video in Figure 2 only if all the preceding material, upon which this video material depends, is completed by a student, and the required score is achieved. The video itself has pop-up questions indicated by the small circles on the lower bar of the video. When the video hits an interactive point, pop-up questions appear and the student must answer the questions correctly (or with a given score). If the student fails to answer or achieve the required score, then he/she is forced to go back to a predetermined time in the vieo. The student can advance past a given circle only if he/she achieves the required score. If the student fails to answer the questions given at one point, he might be directed to another location to study and learn more before he can continue trying to solve the given problems. As indicated at the right bottom of the video, a student cannot fast navigate the video, thus being forced to watch and listen to the material and then to answer questions. The instructor can design the pop-up questions locations, frequency and method of responding to students' answers.

This course was built with 34 interactive videos, with an average of one hour per video; a total of 34 interactive videos. An average of 5 pop-up interactive question breaks, and 3 questions per pop-up. Thus a total of 510 questions are provided for the entire course in an interactive form.

With a class of 40 students, each student spent on the average 30% more time than the video actual time in order to finish the video with the required score. For all the videos, the required score was set at 80% of the total grade. The student's grade for a given video is calculated as a function of the achieved score (which must be $\geq$ 80%) and the percentage of extra time spent watching the video and solving the problems. For example, a student achieved a score of 90% and spent 20% more time on the video. His final grade is calculated as (G = 90-0.2*90) = 78.00. The instructor can build his own grading scale.

Another test was made for this system by comparing the achievement of the students who completed the course using the interactive approach with the students who completed the course with physical face-to-face approach. The average grade for the interactive class was 80.5%, while the average for the classical approach was 71%,

The final observation made for the pilot test is that 2 of the students in the class were able to finish all the class requirements 3 weeks before the rest of the class. Both completed the course with full 100% grade. This

indicates that highly motivated and/or intelligent students can have completed the course at a faster rate than the rest of the students.

Conclusion

This paper presented a new and novel method for enhancing and harvesting the online education platforms, with emphasis on knowledge acquired by the students. The proposed method allows students to learn at their own pace, while making sure that they achieve a minimum level of learning. A pilot project was created and tested in a real education environment, at Jordan University of Science and Technology. The obtained results show that the proposed method achieves good performance for a controlled environment, where 40 students in a class achieved more than 80% of the grade in a given class. More testing and results are required before final conclusions can be made for this method of online learning. The platform is being configured to test primary and high school students using the new methodology.

Acknowledgements or Notes

The author would like to acknowledge Shoman Research Foundation, Jordan and the faculty of scientific research at JUST for funding this project.

Scientific Ethics Declaration

The author declares that the scientific ethical and legal responsibility of this article published in EPSTEM journal belongs to the author.

References

Andrabi, A. & Jabeen, N. (2018). Relationship between socio-economic status and academic achievement. *Strength for Today and Bright Hope for Tomorrow, 11*(6), 690-695. https://doi.org/10.13140/RG.2.2.32707.91683

Barker, P. (1994). Designing interactive learning. In *Design and production of multimedia and simulation-based learning material* (pp. 1-30). Springer. https://doi.org/10.1007/978-94-011-0942-0_1

Cho, V., Cheng, T. E., & Lai, W. J. (2009). The role of perceived user-interface design in continued usage intention of self-paced e-learning tools. *Computers & Education*, *53*(2), 216-227. https://doi.org/10.1016/j.compedu.2009.01.014.

Malkawi, M. & Talib, A. (2008, October 6-7). Building arab software industry: an expansion to the indian model [Conference Presentation]. *International Conference on Ubiquitous ICT for Sustainable Education and Cultural Exchange*, Hämeenlinna, Finland.

Malkawi, M. (2006, April 25-27). Optimizing engineering education in arab universities: toward industry-oriented outcomes [Conference Presentation]. *International Forum on Engineering Education - Integrating Teaching and Research with Community Service*, University of Sharjah Sharjah, United Arab Emirates

Malkawi, M. (2006, April 25-27). Technology education using a novel approach in e-learning—towards optimizing the quality of learning outcomes [Conference Presentation]. *International Forum on Engineering Education - Integrating Teaching and Research with Community Service*, University of Sharjah Sharjah, United Arab Emirates

Malkawi, M. (2007, March 20-22). Emerging trends in biomedical informatics: designing a curriculum to address the current job market [Conference Presentation]. *The International Medical Informatics And Biomedical Engineering Symposium*, Jordan.

Meng, D., Zhao, Q., & Jiang, L. (2017). A theoretical understanding of self-paced learning. *Information Sciences*, *414*, 319-328. https://doi.org/10.1016/j.ins.2017.05.043.

Minka, R. W. (1997). Picard, Interactive learning with a "society of models". *Pattern Recognit*, *30*, 565-581. https://doi.org/10.1016/S0031-3203(96)00113-6.

Tullis, J. G., & Benjamin, A. S. (2011). On the effectiveness of self-paced learning. *Journal of memory and language*, *64*(2), 109-118. https://doi.org/10.1016/j.jml.2010.11.002.

Author Information

Mohammad MALKAWI
Jordan University of Science and Technology
Irbid, Jordan
Contact e-mail: *mimalkawi@just.edu.jo*

To cite this article:

Malkawi, M. (2021). Knowledge acquisition base learning: An interactive learning approach. *The Eurasia Proceedings of Science, Technology, Engineering & Mathematics (EPSTEM), 16*, 132-139.

The Eurasia Proceedings of Science, Technology, Engineering & Mathematics (EPSTEM)
ISSN: 2602-3199

The Eurasia Proceedings of Science, Technology, Engineering & Mathematics (EPSTEM), 2021

Volume 16, Pages 140-144

IConTES 2021: International Conference on Technology, Engineering and Science

Synthesis and Electrochemical Performance of Spinel Crystal Structured $((FeNiCrMn)_{1-x}Co_x)_3O_4$ (x=0.1, 0.2, 0.3) High Entropy Oxides

Meltem CAYIRLI
Eskisehir Osmangazi University

Esra ERDOGAN-ESEN
Eskisehir Osmangazi University

Ersu LOKCU
Eskisehir Osmangazi University

Mustafa ANIK
Eskisehir Osmangazi University

Abstract: High entropy oxides are a new class of materials with a single-phase structure consisting of five or more components. Due to their high structural stability and electrochemical performance, they have attracted a lot of attention in recent years. In this study, high entropy oxides with the composition $((FeNiCrMn)_{1-x}Co_x)_3O_4$ (x=0.1, 0.2, 0.3) were synthesized using the solid state method and their electrochemical performances as anode material for lithium-ion battery were investigated. Spinel crystal structured of high entropy oxides were characterized by X-ray diffraction (XRD) technique. The electrochemical performance of anodes were evaluated by assembling CR2016 type coin cell. As a result of galvanostatic charge/discharge experiments the initial discharge capacities of $((FeNiCrMn)_{1-x}Co_x)_3O_4$ (x=0.1, 0.2, 0.3) anodes at a current density of 50 mA g^{-1} were calculated as 1993 mA h g^{-1}, 1651 mA h g^{-1} and 1706 mA h g^{-1}, respectively. Among the synthesized high entropy oxide anodes, the $((FeNiCrMn)_{0.9}Co_{0.1})_3O_4$ anode shows high initial discharge capacity, while their capacity retention rates at the end of 10^{th} cycle were calculated as 53.9%, 55.1%, 59.7%. This study clearly indicates that the electrochemical performances of high entropy oxide anodes are affected by the Co content.

Keywords: High entropy oxide, Spinel crystal structure, Li-Ion batteries

Introduction

Due to the increasing energy demand and environmental issues, many studies have been focused on the development of efficient and renewable energy sources (Shen et. al., 2018). Rechargeable batteries are mainly power sources for electric vehicles. On the other hand, they can be used as energy storage devices. Therefore, they are considered as sustainable energy storage systems (Etacheri et. al., 2011; Lu et. al., 2013). Today, Li-ion batteries are the most widely used rechargeable batteries. The most important advantages of these batteries are their high energy storage capacity and long cycle life (Velàzquez-Martinez et. al., 2019; Kim et. al., 2019).

Graphite is the most commonly used anode material in Li-ion batteries. It has high electronic conductivity and low cost. However, its theoretical capacity is low (372 mA h g^{-1}) (Nitta et. al., 2015; Long et. al. 2017). Another group of anode material is conversion type anodes. Conversion type transition metal oxides show high theoretical capacity but generally suffer from significant volume change and poor electrical conductivity (Zou

et. al., 2011). In recent years, high entropy oxide based anodes have extensively studied as an alternative to transition metal oxide based anodes.

In 2015, the concept of high entropy oxide was used for the first time. High entropy oxides are a single phase structure consisting of five or more major elements (Rost et. al., 2015). In addition, for the first time in 2018, rock-salt crystal structure ($Co_{0.2}Cu_{0.2}Mg_{0.2}Ni_{0.2}Zn_{0.2}$)O was used as the anode material in Li-ion batteries, and this oxide compound showed excellent electrochemical performance even at 500 cycles (Sarkar et. al., 2018). In other study $(MgCoNiZn)_{1-x}Li_xO$ (x=0.5-0.35) high entropy oxides were synthesized with different Li^+ concentrations. The increase in Li^+ concentration caused an increase in the oxygen vacancy in Li-ion batteries. This has resulted in an increase in the discharge capacity (Lökçü et al., 2020). In another study spinel $(Mg_{0.2}Ti_{0.2}Zn_{0.2}Cu_{0.2}Fe_{0.2})_3O_4$ anode exhibited a reversible capacity of 504 mA h g^{-1} after 300 cycles at a current density of 100 mA g^{-1} (Chen et. al., 2020).

In this study, $((FeNiCrMn)_xCo_{1-x})_3O_4$ (x=0.1, 0.2, 0.3) high entropy oxide anode materials were synthesized and their electrochemical performances were investigated in Li-ion batteries.

Materials & Methods

Fe_3O_4, NiO, Cr_2O_3, MnO and CoO oxides were mixed in the specified molar ratios with determined stoichiometry and were ground at 300 rpm for 2 hours using a ball mill (Fritsch Pulverisette 7 Premium Line). Then the obtained oxide mixtures were pressed into pellets with a diameter of 10 mm under a pressure of 300 MPa. Finally, the oxide pellets obtained were sintered at 1100 ° C for 12 hours. X-ray Diffraction (XRD) was used to characterize the synthesized $((FeNiCrMn)_xCo_{1-x})_3O_4$ (x=0.1, 0.2, 0.3).

$((FeNiCrMn)_xCo_{1-x})_3O_4$ (x=0.1, 0.2, 0.3) electrodes were prepared by mixing in a ball mill at NMP using Super P carbon black and PVDF (75:15:10 by weight). The prepared mixture was coated on Cu foil and dried in a vacuum atmosphere at 80 °C for 12 h. Anode materials are electrochemically tested in a CR2016 type coin cells. The coin cells were assembled in an argon-filled glove box with H_2O and O_2 levels less than 0.1 ppm. Lithium metal was used as the counter and reference electrode, while the glass microfiber filter was used as a separator. As the electrolyte, 1 M Lithium hexafluorophosphate ($LiPF_6$) was used in EC: DMC in a ratio of 1:1 by volume. Charge-discharge tests were performed galvanostatically in the potential range of 0.01 and 3.00 V (vs. Li^+/Li) at a current density of 50 mA g^{-1} by using Gamry Reference 3000 Potentiostat/Galvanostat/ZRA.

Results and Discussion

Figure 1 shows the XRD pattern of a synthesized $((FeNiCrMn)_xCo_{1-x})_3O_4$ (x=0.1, 0.2, 0.3). The patterns show that the samples are crystalline and spinel crystal structure. These characteristic peaks of the spinel structure, (111), (220), (311), (222), (400), (422), (511), (440), (531), (620), (533), (622), (444), (711) and (642) planes. A heat treatment temperature of 1100 °C seems sufficient for the synthesis of $((FeNiCrMn)_xCo_{1-x})_3O_4$ (x=0.1, 0.2, 0.3) samples.

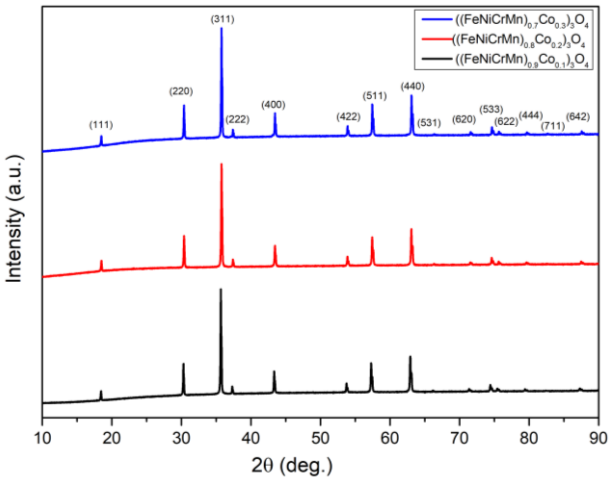

Figure 1. XRD patterns of the as-synthesized $((FeNiCrMn)_xCo_{1-x})_3O_4$ (x=0.1, 0.2, 0.3) samples.

The first charge-discharge curves of the anodes are given in Figure 2. When the initial discharge curves are examined, a discharge plateau is observed at approximately 0.5 V. This plateau represents the reduction of metal oxides and the formation of the SEI layer. The initial discharge capacities of $((FeNiCrMn)_{0.9}Co_{0.1})_3O_4$, $((FeNiCrMn)_{0.8}Co_{0.2})_3O_4$ and $((FeNiCrMn)_{0.7}Co_{0.3})_3O_4$ anodes are 1993 mA h g^{-1}, 1651 mA h g^{-1} and 1706 mA h g^{-1}, respectively. The initial charge capacities of $((FeNiCrMn)_{0.9}Co_{0.1})_3O_4$, $((FeNiCrMn)_{0.8}Co_{0.2})_3O_4$ and $((FeNiCrMn)_{0.7}Co_{0.3})_3O_4$ anodes are 1381 mA h g^{-1}, 1191 mA h g^{-1} and 1203 mA h g^{-1}, respectively. In addition, the initial coulombic efficiencies are 70.5%, 72.1% and 69.3%, respectively. The low initial coulombic efficiencies are due to the reaction caused by the SEI film.

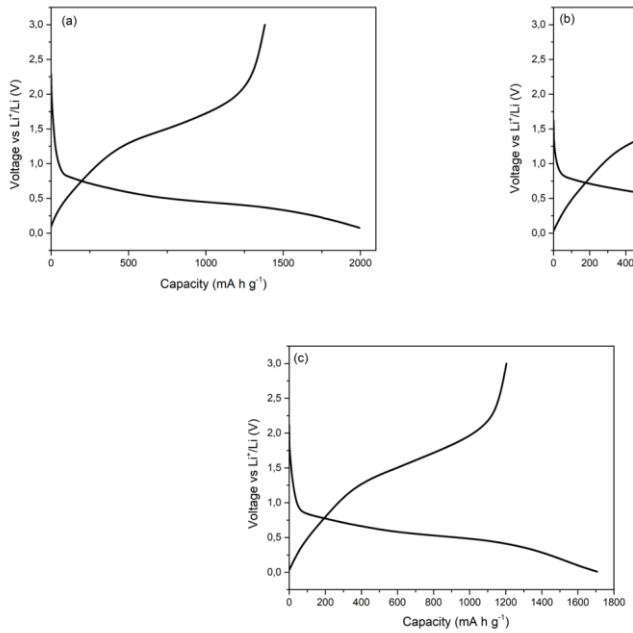

Figure 2. Discharge-charge curves of (a) $((FeNiCrMn)_{0.9}Co_{0.1})_3O_4$, (b) $((FeNiCrMn)_{0.8}Co_{0.2})_3O_4$ and (c) $((FeNiCrMn)_{0.7}Co_{0.3})_3O_4$ anodes for the first cycle in the voltage range of 0.01 - 3.00 V at a current density of 50 mA g^{-1}.

Cycling performance of the $((FeNiCrMn)_xCo_{1-x})_3O_4$ (x=0.1, 0.2, 0.3) anodes under 50 mA h g^{-1} current density is shown in Figure 3. The $((FeNiCrMn)_{0.9}Co_{0.1})_3O_4$, $((FeNiCrMn)_{0.8}Co_{0.2})_3O_4$ and $((FeNiCrMn)_{0.7}Co_{0.3})_3O_4$ anodes deliver capacities of 1075 mA h g^{-1}, 909 mA h g^{-1} and 1018 mA h g^{-1} at 50 mA g^{-1} current densities and at the end of the 10th cycle, respectively. At the end of the 10th cycle, the coulombic efficiencies of the anodes are 95.7%, 96.5% and 97.2%, respectively. Between the 1st and 10th cycles, the capacity retention of $((FeNiCrMn)_{0.9}Co_{0.1})_3O_4$, $((FeNiCrMn)_{0.8}Co_{0.2})_3O_4$ and $((FeNiCrMn)_{0.7}Co_{0.3})_3O_4$ anodes are 53.9%, 55.1% and 59.7%, respectively. These results show that the electrochemical performances of high entropy oxide anodes are affected by the Co content.

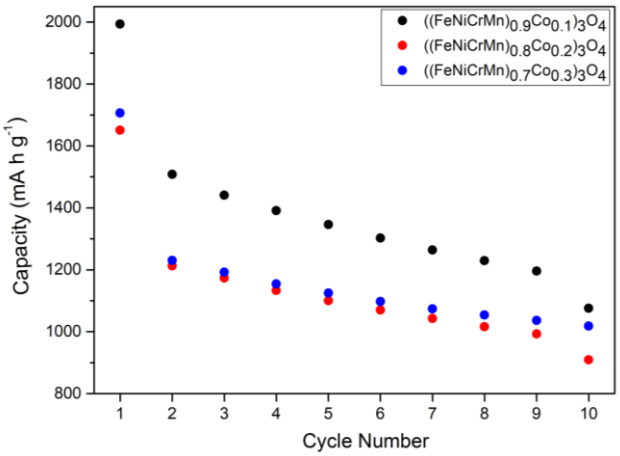

Figure 3. Cycling performance of $((FeNiCrMn)_xCo_{1-x})_3O_4$ (x=0.1, 0.2, 0.3) anodes under current density at 50 mA g^{-1}.

Conclusion

In this work, $((FeNiCrMn)_xCo_{1-x})_3O_4$ (x=0.1, 0.2, 0.3) anodes were synthesized with a spinel crystal structure by the conventional solid-state method and their electrochemical performances were observed in the Li-ion batteries. Charge-discharge measurements showed that the $((FeNiCrMn)_{0.9}Co_{0.1})_3O_4$ anode delivers a high initial discharge capacity of 1993 mA h g^{-1} and reversible capacity of 1075 mA h g^{-1} at the end of 10^{th} cycle. It was observed that the capacity retention rate of the cell increased depending on the increase in the amount of Co. These capacity values are quite promising as alternative anode material for Li-ion batteries.

Scientific Ethics Declaration

The authors declare that the scientific ethical and legal responsibility of this article published in EPSTEM journal belongs to the authors.

References

Chen, H., Qiu, N., Wu, B., Yang, Z., Sun, S., & Wang, Y. (2020). A new spinel high-entropy oxide $(Mg_{0.2}Ti_{0.2}Zn_{0.2}Cu_{0.2}Fe_{0.2})_3O_4$ with fast reaction kinetics and excellent stability as an anode material for lithium ion batteries. *RSC Advances, 10(16)*, 9736–9744.

Etacheri, V., Marom, R., Elazari, R., Salitra, G., & Aurbach, D. (2011). Challenges in the development of advanced Li-ion batteries: a review. *Energy & Environmental Science, 4(9)*, 3243.

Kim, T., Song, W., Son, D.Y., Ono, L. K., & Qi, Y. (2019). Lithium-ion batteries: outlook on present, future, and hybridized technologies. *Journal of Materials Chemistry A, 7*, 2942-2964.

Lökçü, E., Toparli, Ç., & Anik, M. (2020). Electrochemical performance of (MgCoNiZn)1-xLixO high-entropy oxides in lithium-ion batteries. *ACS Applied Materials & Interfaces, 12*, 23860-23866.

Long, W., Fang, B., Ignaszak, A., Wu, Z., Wang, Y.J., & Wilkinson, D. (2017). Biomass-derived nanostructured carbons and their composites as anode materials for lithium ion batteries. *Chemical Society Reviews, 46(23)*, 7176–7190.

Lu, L., Han, X., Li, J., Hua, J., & Ouyang, M. (2013). A review on the key issues for lithium-ion battery management in electric vehicles. *Journal of Power Sources, 226*, 272–288.

Nitta, N., Wu, F., Lee, J. T., & Yushin, G. (2015). Li-ion battery materials: present and future. *Materials Today, 18(5)*, 252–264.

Rost, C. M., Sachet, E., Borman, T., Moballegh, A., Dickey, E. C., Hou, D., Jones, J. L., Curtarolo, S., & Maria, J. P. (2015). Entropy-stabilized oxides. *Nature Communications, 6*, 1−8.

Sarkar, A., Velasco, L., Wang, D., Wang, Q., Talasila, G., de Biasi, L., Kübel, C., Brezesinski, T., Bhattacharya, S. S., Hahn, H., & Breitung, B. (2018). High entropy oxides for reversible energy storage. *Nature Communications, 9(3400)*, 1-9.

Shen, X., Liu, H., Cheng, X.B., Yan, C., & Huang, J.-Q. (2018). Beyond lithium ion batteries: Higher energy density battery systems based on lithium metal anodes. *Energy Storage Materials, 12*, 161–175.

Velàzquez-Martinez, O., Volio, J., Santasalo-Aarnio, A., Reuter, M., & Serna-Guerrero, R. (2019). A critical review of lithium-ion battery recycling processes from a circular economy perspective. *Batteries, 5(68)*, 1-33.

Zou, Y., & Wang, Y. (2011). Microwave-assisted synthesis of porous nickel oxide nanostructures as anode materials for lithium-ion batteries. *Rare Metals, 30*, 59–62.

Author Information

Meltem CAYIRLI
Metallurgical and Materials Engineering
Eskisehir Osmangazi University
Contact e-mail: *meltem.cayirli@ogu.edu.tr*

Esra ERDOGAN-ESEN
Nanoscience and Nanotechnology
Eskisehir Osmangazi University

Ersu LOKCU
Metallurgical and Materials Engineering
Eskisehir Osmangazi University

Mustafa ANIK
Metallurgical and Materials Engineering
Eskisehir Osmangazi University

To cite this article:

Cayirli, M., Erdogan-Esen, E., Lokcu, E., & Anik, M. (2021). Synthesis and electrochemical performance of spinel crystal structured ((FeNiCrMn)1-xCox)3O4 (x=0.1, 0.2, 0.3) high entropy oxides. *The Eurasia Proceedings of Science, Technology, Engineering & Mathematics (EPSTEM), 16*, 140-144.

The Eurasia Proceedings of Science, Technology, Engineering & Mathematics (EPSTEM)
ISSN: 2602-3199

The Eurasia Proceedings of Science, Technology, Engineering & Mathematics (EPSTEM), 2021

Volume 16, Pages 145-152

IConTES 2021: International Conference on Technology, Engineering and Science

Investigation of the Effect of Some Factors on Resistance Spot Welding of DKP Steel Using Response Surface Method

Adem TASDEMIR
Eskişehir Osmangazi University

Bedri BAKSAN
Eskişehir Osmangazi University

Ibrahim CELIKYUREK
Eskişehir Osmangazi University

Abstract: Due to many advantages of Resistance Spot Welding (RSW) such as inexpensive, easy to automate, and high-quality joints capability, it is preferred and used mostly in automative industry. In the RSW process, metals are joined based on the contact resistance between the electrodes and metals. During the process, the cause of the welding nugget on the surface is the increase in temperature because of the electrical resistance of the materials and the melting formed. Many factors affect the success of the RSW process. In this research, we investigated the possibility of mild steel (DKP) sheets welding using the RSW method. There important factors, i.e., time, pressure, and current were tested. The results were evaluated by measuring the shear strength of DKP sheets having 1 mm thickness. To reduce the number of experiments, the experiments are designed and carried out according to the Box-Behnken experimental design. It is one of the most useful response surface methods (RSM). It was aimed to find the effects of investigated parameters and their possible interactions on tensile strength of DKP sheets joined by RSW process. Another important purpose was to generate a mathematical model which can be used to estimate tensile strength as a function of tested parameters. As a result, a second-order model which was important statistically was developed and it was capable of to estimate the dependent variable in very high accuracy.

Keywords: Resistance spot welding, DKP steel, Tensile strength, Response surface method, Box-behnken design

Introduction

Mild steels are widely used in various construction manufacturing in all areas of industry. Joining these materials, which can be in different forms, by welding techniques is a frequently used method, especially in the automotive sector. The temperature of the welding interface must be above or very close to the melting temperature for successful bonding. Although there are many different welding methods, we can collect them into two main groups as melting and solid-state welding methods. Resistance spot welding technique, which is a solid-state welding method, is used to join sheet-shaped materials.

Electric resistance spot welding is a method of welding with heat that occurs due to the resistance of the work pieces against the electric current passing through the work pieces held together under pressure between the electrodes. The contact surface of the parts to be welded is heated with low voltage and high current applied for a short time and transformed into a molten welding core. When the electric current is cut off, the molten metal quickly cools and solidifies. Meanwhile, the electrodes continue to hold the welded parts tightly and then retract

and release the part. Welding process is usually completed in less than one second. (Yener, 1999; Baytemir, 2011).

The main resource variables affecting the welding quality are listed as follows; effect of the welding current, effect of the welding time, effect of electrode force, effect of electrode composition and shape on heating, material of workpiece, effect of surfaces of parts to be welded, effect of distance between welded points, contact conditions of electrode and workpiece (Hayat, 2005). Resistance spot welding is an easily controllable process, inexpensive equipment and a serially repeatable method. The welding process widely used in joining metal sheets such as iron, steel, aluminium alloys, magnesium alloys, titanium alloys, super alloys, and joining of different metals (Kahraman, 2007; Qiu et al., 2009; Han et al., 2010; Shirmohammadi et al., 2017; Bemani et al., 2020; Babua et al. 2012).

For the resistance spot welding, welding pressure, duration and current affect the welding quality depending on the sheet thickness. In this study, the effects of these three parameters on shear strength of resistance spot welded mild steels were determined using Box-Behnken experimental design.

Material and Method

In this study, we used sheets 1,0 mm in thickness and 20 mm x 40 mm in sizes (Figure 1). The diameter of spot size was 6 mm.

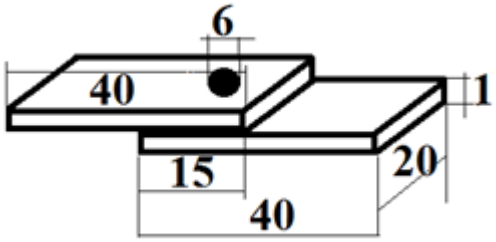

Figure 1. Dimensions in mm of the mild steels and welding diameter

The welding conditions were designed by Box-Behnken experimental method. The welding parameters used and their application values are:

Welding pressures: 500, 1000 and 1500 N
Welding currents: 2, 4 and 6 kA
Welding time: 20, 30 and 40 period

After welding, the strengths of the welds were determined using a universal tensile testing machine. An axial load was applied on room temperature with a chunk speed of 10 mm/min (Figure 2). The ultimate shear forces were reported as strength.

Figure 2. Determination of shear forces by universal tensile testing machine

Box-Behnken Design (BBD) of Experiments

In this research, Box-Behnken Design (BBD) which is one most important nonlinear model of Response Surface Methodology (RSM) was applied to reduce the number of experiments and to determine the main effects, interaction effects of the tested parameters (pressure, time and current) on the shear strength of resistance spot welded mild steels. The BBD also enables a quadratic model to estimate dependent variable(s) as a function of independent variables and optimize the desired input and output process parameters (Myers, et al., 2016).

In this study, we applied a BBD with 3 parameters and 3 levels to optimize 3 process parameters (pressure, time and current) in determining shear strength of resistance spot welded mild steel. Table 1 shows the coded and real levels of independent parameters. In this design, required number of experiments is 15 when repeated experiments at the middle levels of variables are 3 (Myers et al., 2016). Trial version of Design Expert 7.0 software was used for the Box-Behnken design of experiments and analyzing the results of experiments.

Table 1. Parameters tested and their levels

Independent parameters	Symbol	Code levels		
		-1	0	1
Pressure (N)	A	500	1000	1500
Time(period)	B	20	30	40
Current (kA)	C	2	4	6

Table 2 gives the 15 randomized experiments' levels of BBD in coded unites. Here, the codes -1, 0 and 1 are high, medium and low levels of the parameters respectively.

Table 2. The BBD of experiments and their coded levels

Experiment no	(A) Pressure (N)	(B) Time(Period)	(C) Current (kA)
1	-1	-1	0
2	1	-1	0
3	-1	1	0
4	1	1	0
5	-1	0	-1
6	1	0	-1
7	-1	0	1
8	1	0	1
9	0	-1	-1
10	0	1	-1
11	0	-1	1
12	0	1	1
13	0	0	0
14	0	0	0
15	0	0	0

While analysing the 3 parameters and 3 levels BBD, a quadratic mathematical model which involves main, interaction and second order terms are obtained. General form of quadratic model for 3 parameters design to estimate the response is as following:

$$Y = b_0 + b_1A + b_2B + b_3C + b_{12}AB + b_{13}AC + b_{23}BC + b_{11}A^2 + b_{22}B^2 + b_{33}C^2 \quad \text{.....(1)}$$

Results and Discussion

Analysis of Box-Behnken Design of Experiments

The shear force values obtained from the experiments that was designed according to the 3 parameters 3 levels BBD are given in Table 3. Using the trial version of Design Expert 7.0 software, these results were analysed. After evaluating the BBD, a second order mathematical model (Equation 2) where the shear force is estimated as a function of pressure, time and current variables was obtained. Equation in terms of coded factors is as following:

Shear force (N) = 5338.33+86.37A+359.37B+1990.25C+71.25AB+24.50AC+148.50BC+553.71A^2-683.29B^2 -1181.04C^2

The determination coefficient (R^2) of Equation 2 is 0.9703. This means that 97,03% of the total variation in estimating the shear force of resistant spot welded mild steels by using tested 3 variables can be explained by Equation 2, the remaining variance can be explained by the experimental errors.

Signaficance importance of the model terms of Equation 2 and adequacy of model was evalutaed by ANOVA (Analysis of Variance) and the results are given in Table 4. The model has a F value of 18.14 and p value of 0,0026, i.e., the model suggested is staticically significant at % 95 significance level (p<0,05). Therefore, this model is statistically adequate for estimating shear force of resistance welded mild steels. Lack of fit of the model is insignificant (p=0,0549>0,05) which is desired for a good model. The statistically important terms at 95% significance level are current and time. The linear (C) and second order effects of current (C^2) abd time (B^2) variables have more important effect on shear pressure than the other variables. Linear term of time (B) and second order term of pressure (A^2) are statistically important term at 90% significance level. The order of importance is C>C^2>B^2>A^2>B. Interaction terms (AB, AC and BC) are all insignificant.

Table 3. The BBD result of shear strength for resistance welded mild steels

Runs	(A) Pressure (N)	(B) Time(Period)	(C) Current (kA)	Shear force (N)
1	500	20	4	5000
2	1500	20	4	5050
3	500	40	4	5225
4	1500	40	4	5560
5	500	30	2	3016
6	1500	30	2	3120
7	500	30	6	6253
8	1500	30	6	6455
9	1000	20	2	750
10	1000	40	2	1523
11	1000	20	6	5128
12	1000	40	6	6495
13	1000	30	4	5492
14	1000	30	4	5336
15	1000	30	4	5187

Table 4. Analysis of Variance (ANOVA) table of response surface quadratic model (Eq. 2)

Source	Sum of Squares	df	Mean Square	F Value	p-value Prob > F	Significance
Model	$4.111x10^7$	9	$4.568x10^6$	18.14	0.0026	significant
A-Pressure (N)	59685.12	1	59685.12	0.24	0.6469	insignificant
B-Time(Period)	$1.033x10^6$	1	$1.033x10^6$	4.10	0.0986	*
C-Current (kA)	$3.169x10^7$	1	$3.169x10^7$	125.88	< 0.0001	**
AB	20306.25	1	20306.25	0.081	0.7878	insignificant
AC	2401.00	1	2401.00	9.538E-003	0.9260	insignificant
BC	88209.00	1	88209.00	0.35	0.5796	insignificant
A^2	$1.132x10^6$	1	$1.132x10^6$	4.50	0.0874	*
B^2	$1.724x10^6$	1	$1.724x10^6$	6.85	0.0473	**
C^2	$5.150x10^6$	1	$5.150x10^6$	20.46	0.0063	**
Residual	$1.259x10^6$	5	$2.517x10^5$			
Lack of Fit	$1.212x10^6$	3	$4.041x10^5$	17.37	0.0549	insignificant
Pure Error	46520.67	2	23260.33			
Cor Total	$4.237x10^7$	14				

*: Significant at 90% confidence level, **: Significant at 95% confidence level

Figure 3 shows that disribution of the residuals (difference between the actual and predicted shear force) fits very well to normal distribution (left handside plot). Right handside plot in Figure 3 depicts the actıal versus predicted shear force by the model. As seen clearly, there is an excellent accordance and the points are very near to 1:1 line. Figure 3 confims the adequacy of the second order model which formulated in Equation 2.

Main Effects of Parameters

Figure 4, gives the main effects of tested parameters of pressure, time and current on shear force of resistance welded mild steels. In each plot, other varibles kept at their middle levels. While keeping the pressure and current at middle values, shear force increaese with increasing time uptu 30 period, then decreases slightly. It is evidence that time has a quadratic effect. The shear force of resistance welded mild steels almost remains unchanged with increasing pressure. It decreases very slightly up to 1000 N, then increases very slowly. The shear force is most affected from the increase of current parameter. Keeping the time and pressure in middle values of 30 period and 1000 N respectively, shear force increases very quickly and reach the maximum at 6 kA current value.

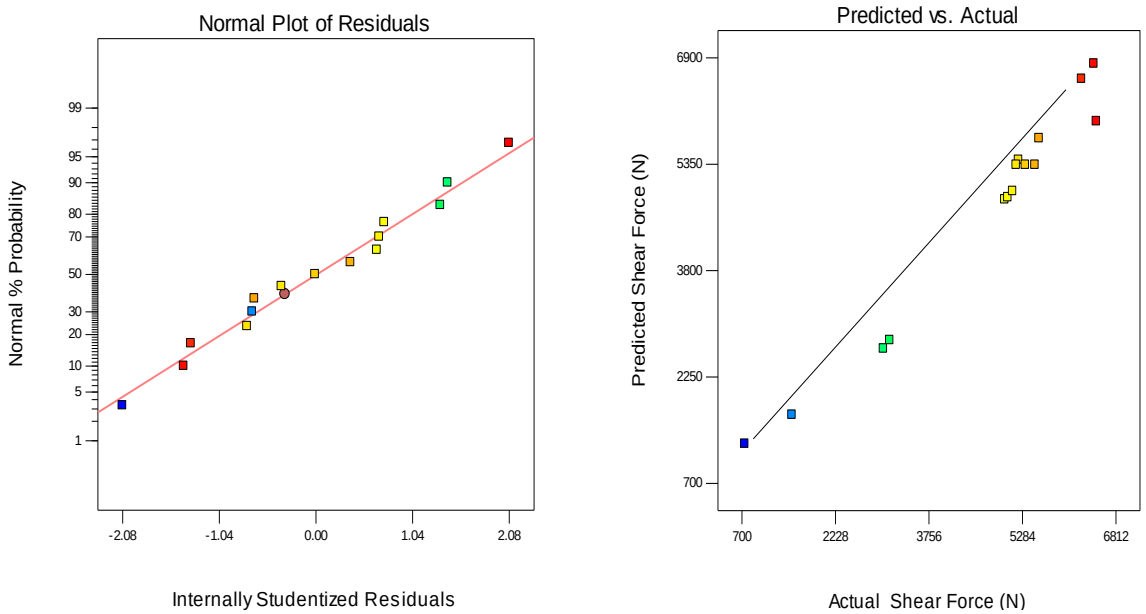

Figure 3. Normal distribution plot of model residuals and actual versus predicted shear force plot

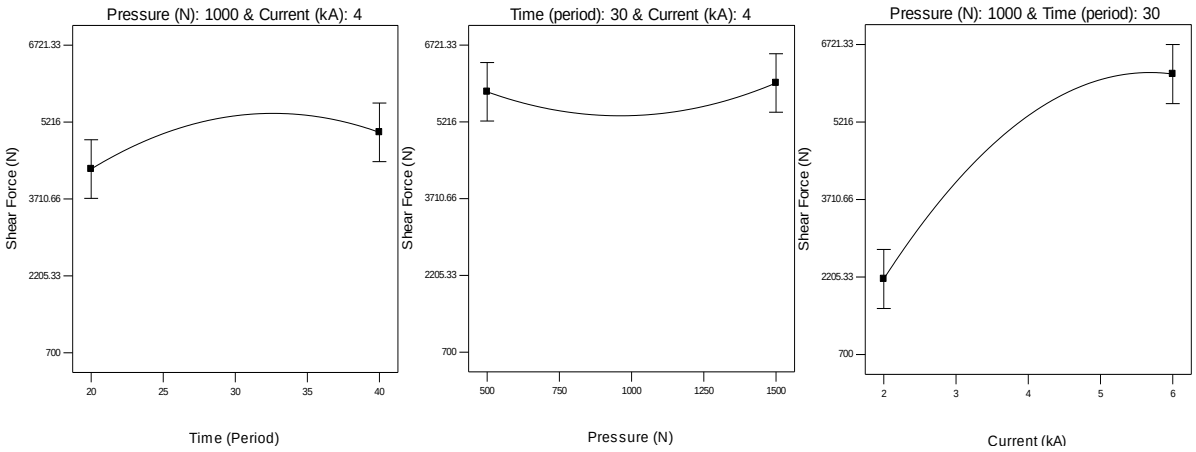

Figure 4. Main effects of tested parameters on the sheer force of resistance welded mild steels (all the other parameters is kept at their middle values)

Interaction Effects of Parameters On Resistance Welded Mild Steel

Figure 5, 6 and 7 shows the relationships between shear force and 3 parameters tested. In these plots, two parameters are within their studied ranges while the third parameter at its middle level.

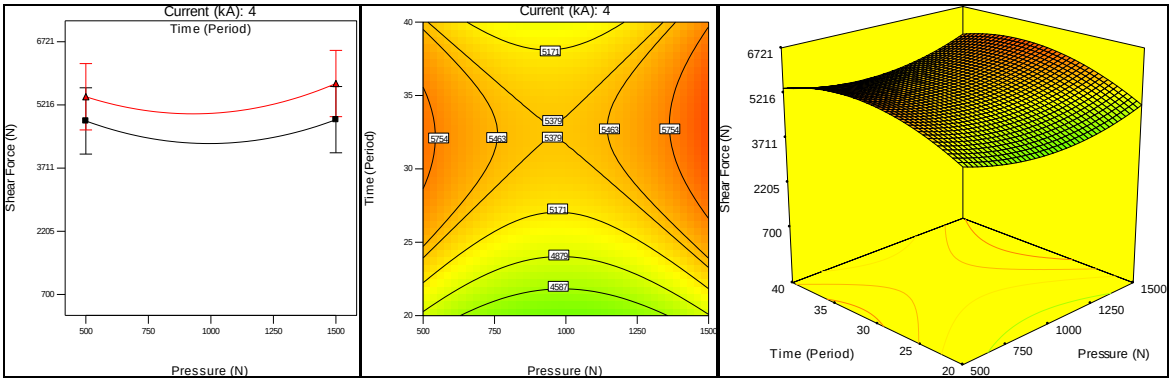

Figure 5. Effect of time and pressure on tensile strength: Interaction plot (left), contour plot (middle) and 3D surface plot (right).(Current: 4 kA; ■: 20 period; ▲: 40 period)

Figure 5 depicts interaction, contour and 3D response surface plots between time and pressure at the middle level of current (4 kA). The is no intersection between plots in interaction plot (left plot). There is intersection between the curves in intersection plot (left), since they are parallel and near to each other. This character confirms there is interaction between time and pressure as in determined in ANOVA results in Table 4. When the time increases from 20 to 40 period at current 4 kA, shear force increases slightly and it remains almost constant with increasing pressure.

The plots in Figure 6 indicates that current has an important factor on shear force and there is no any interaction between current and pressure factors. Shear force increases with increasing current and increasing pressure at tle lower and higher level of current has almost no effect on the shear force of resistance welded mild steels.

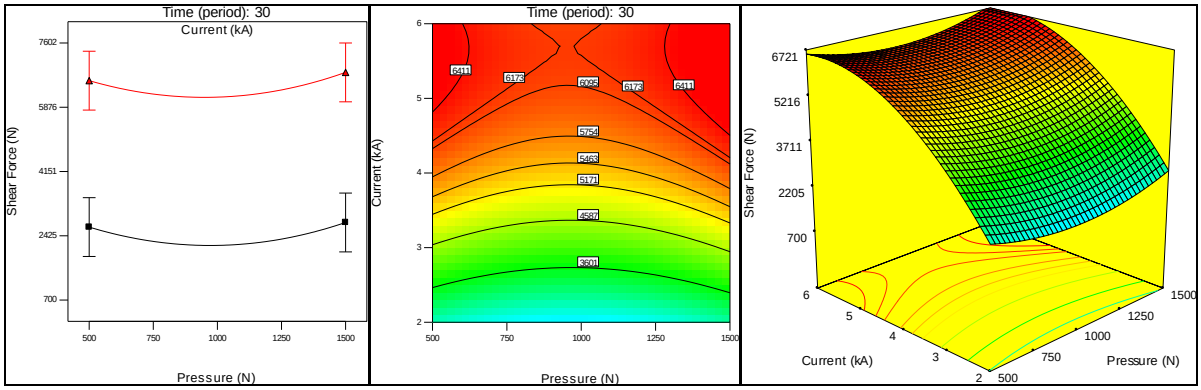

Figure 6. Effect of current and pressure on tensile strength: Interaction plot (left), contour plot (middle) and 3D surface plot (right). (Time: 30 period; ■: 2 kA; ▲: 6 kA)

Figure 7 shows that higher shear force can be obtained at higher current values and higher time. Even the interaction between time and current was found statistically unimportant, theier relationship is more effective than the other factor interactions.

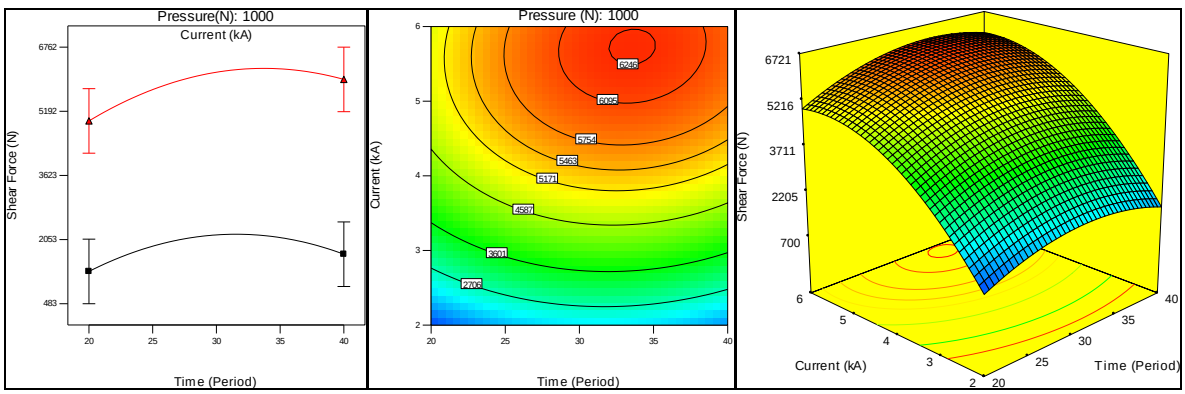

Figure 7. Effect of current and time on tensile strength: Interaction plot (left), contour plot (middle) and 3D surface plot (right). (Pressure: 1000 N; ■: 2 kA; ▲: 6 kA)

Conclusion

The Box-Behnken Design (BBD) was applied successfully in order to determine the effects of pressure, current and welding time on the shear force of resistance welded mild steels. According to BBD results, the welding pressure seems to have a negligible effect on shear force. However, its quadratic effect was found significant at 90% confidence level and the quadratic effects the other parameters were significant at 5% significance level. The current parameter was the most important parameter on shear force and it has both linear and quadratic effect at %5 significance level. All interaction effects between parameters were determined insignificant, i.e., their individual effects were more dominant.

A second order mathematical model, which is statistically important and has R^2 of 97,03 determination coefficient, was developed to predict the shear for of resistance spot welded mild steel as a function time, current and pressure. This model is valid within the limits of parameters tested and can be used conveniently to detect shear force in untested parameter conditions.

Scientific Ethics Declaration

The authors declare that the scientific ethical and legal responsibility of this article published in EPSTEM journal belongs to the authors.

References

Babua, N. K., Brauserb, S., Rethmeierb, M. & Cross, C. E. (2012). Characterization of microstructure and deformation behaviour of resistance spot welded AZ31 magnesium alloy. *Materials Science and Engineering A 549*, 149– 156.

Baytemir, M. (2011). *Ostenitik AISI 310-ferritik AISI 430 Paslanmaz Çeliklerin Elektrik Direnç Nokta Kaynağı ile Birleştirilmesi ve Mekanik özelliklerinin incelenmesi* [Unpublished Master Thesis Sakarya Üniversitesi].

Bemani, M. & Pouranvari, M. (2020). Microstructure and mechanical properties of dissimilar nickel-based superalloys resistance spot welds. *Materials Science & Engineering A, 773*, 138825.

Han, L., Thornton, M. & Shergold, M. (2010). A comparison of the mechanical behavior of self-piercing riveted and resistance spot welded aluminum sheets for the automotive industry. *Mater Des. 31*, 1457–1467.

Hayat, F. (2005). *Çift-fazlı çeliklerin nokta direnç kaynağında MHO ile kaynak süresinin mekanik özelliklere etkisi* [Unpublished Master Thesis Zonguldak Karaelmas Üniversitesi].

Qiu, R., Iwamoto, C., & Satonaka, S. (2009). Interfacial microstructure and strength of steel/aluminum alloy joints welded by resistance spot welding with cover plate. *Journal of Materials processing technology*, *209*(8), 4186-4193.

Kahraman, N. (2007). The influence of welding parameters on the joint strength of resistance spot-welded titanium sheets. *Mater Des. (28)*, 420–427.

Myers, R. H., Montgomery, D. C. & Anderson-Cook, C. M. (Eds.) (2016). *Response surface methodology: Process and product optimization using designed experiments* (4th ed.). John Wiley & Sons.

Shirmohammadi, D., Movahedi, M. & Pouranvari, M. (2017). Resistance spot welding of martensitic stainless steel: Effect of initial basemetal microstructure on weld microstructure and mechanical performance, *Materials Science & Engineering A, 703,* 154–161.

Yener, S. (1999). *Otomotiv sanayinde kullanılan direnç nokta kaynak elektrodu ömrünün deneysel analizi*. [Unpublished Master Thesis İstanbul Teknik Üniversitesi].

Author Information

Adem TASDEMIR
Eskişehir Osmangazi University
Mining Engineering Department 26480, Batı Meşelik, Eskişehir, Turkey
Contact e-mail: *atasdem@ogu.edu.tr*

Bedri BAKSAN
Eskişehir Osmangazi University
Metallurgy and Materials Engineering Department 26480, Batı Meşelik, Eskişehir, Turkey

Ibrahim CELIKYUREK
Eskişehir Osmangazi University
Metallurgy and Materials Engineering Department 26480, Batı Meşelik, Eskişehir, Turkey

To cite this article:

Tasdemir, A., Baksan, B. & Celikyurek, I. (2021). Investigation of the effect of some factors on resistance spot welding of DKP steel using response surface method. *The Eurasia Proceedings of Science, Technology, Engineering & Mathematics (EPSTEM), 16*, 145-152.

The Eurasia Proceedings of Science, Technology, Engineering & Mathematics (EPSTEM)
ISSN: 2602-3199

The Eurasia Proceedings of Science, Technology, Engineering & Mathematics (EPSTEM), 2021

Volume 16, Pages 153-161

IConTES 2021: International Conference on Technology, Engineering and Science

Optimization Parameter of the 1P Keys Interpolation Kernel Implemented in the Correlation Algorithm for Estimating the Fundamental Frequency of the Speech Signal

Zoran MILIVOJEVIC
Academy of Applied Technical and Preschool Studies

Bojan PRLINCEVIC
Kosovo and Metohija Academy of Applied Studies

Natasa SAVIC
Academy of Applied Technical and Preschool Studies

Abstract: The first part of this paper describes an algorithm for estimating the fundamental frequency F_0 of a speech signal, using an autocorrelation algorithm. After that, it was shown that, due to the discrete structure of the autocorrelation function, the accuracy of the fundamental frequency estimate largely depends on the sampling period T_S. Then, in order to increase the accuracy of the estimation, an interpolation of the correlation function is performed. Interpolation is performed using a one parameter (1P) Keys interpolation kernel. The second part of the paper presents an experiment in which the optimization of the 1P Keys kernel parameter was performed. The experiment was performed on test Sine and Speech signals, in the conditions of ambient disturbances (N8 Babble noise, SNR = 5 to -10 dB). MSE was used as a measure of the accuracy of the fundamental frequency estimate. Kernel parameter optimization was performed on the basis of the MSE minimum. The results are presented graphically and tabularly. Finally, a comparative analysis of the results was performed. Based on the comparative analysis, the window function, in which the smallest estimation error was achieved for all ambient noise conditions, was chosen.

Keywords: Fundamental frequency, Parametric convolution, Convolution kernel, Speech signal.

Introduction

For several decades, digital speech signal processing has been actual in multimedia systems. Algorithms have been developed for: a) speaker recognition, b) semantic speech recognition, c) speaker health analysis, d) language recognition, e) speech extraction from the background noise, f) dereverberations, d) echo suppression, h) speech signal quality corrections, etc. (Qiu et al., 2000). Increasing intelligibility requires increasing the quality of the speech signal (Rao et al., 2000). One way to increase speech intelligibility is by applying an algorithm to reduce dissonant frequencies (Milivojevic et al., 2009). Many speech signal processing algorithms require an estimate of the fundamental frequency of the speech, as well as the dominant harmonics. Algorithms for estimating the fundamental frequency are based on the processing of the speech signal in: a) the time domain, b) the spectral domain and c) the cepstrum domain (Kacha et al., 2004).

Estimation of the fundamental frequency in the spectral domain is based on the application of the DFT and peak peaks in the spectrum (Pang et al., 2000). The spectrum, calculated using DFT, is discrete. The accuracy of the fundamental frequency estimate is directly dependent on the length of the DFT. However, in reality the

- Selection and peer-review under responsibility of the Organizing Committee of the Conference

fundamental frequency can be located between the spectral components (Milivojevic et al., 2013). In this case, the estimation is performed using interpolations. Interpolation with convolutional kernel is often applied (Keys, 1981). Third-order interpolation kernel, due to their numerically low complexity, allow high estimation speeds (Meijering, 2003).

The time domain estimation algorithms are based on the analysis of time waveforms. If the waveform of the signal is periodic, then the period can be observed and F_0 can be estimated on its basis. The TD algorithms intensively uses autocorrelation functions (Rabiner et al., 1978) to detect the pitch period. In (De Cheveigné et al., 2002), an algorithm, called the YIN algorithm, where the estimation is performed using the autocorrelation function (ACF), was proposed.

The ACF of a discrete periodic signal is a discrete and a periodic function (Milivojevic et al., 2017). The ACF components have a time interval witch equal to the sampling time periods, T_S, of the signal. Determining the period of the discrete signal implies locating the first, dominant peak, at the ACF. Then the fundamental frequency is equal to the reciprocal of the time shift of the peaks in relation to the beginning of the ACF. Here, the problem of estimating of the fundamental frequency arises when the actual dominant peak of ACF is not located on an integer product of T_S, but somewhere between two adjacent components with the highest energy. In this case, estimation of the position is performed by selecting the position of the peak and, thus, a significant estimation error F_0 occurs. The estimation error reduction can be done by applying an interpolation algorithm (Milivojevic et al., 2021).

This paper presents an algorithm for estimating the fundamental frequency in the time domain. The algorithm is based on the application of autocorrelation function and interpolation using the interpolation 1P Keys kernel (Milivojevic et al., 2017). After that, an experiment, in which the effect of window functions on the accuracy of the fundamental frequency estimate was analyzed, is described. First, the Sine test signal and the Speech test signal are processed using window functions. Then, effect of changing of the kernel parameter, α, on the estimation error, was analyzed. Mean square error, MSE, is used as the estimation error. By minimizing the estimate error MSE, the optimal value of the kernel parameter, α_{opt}, is calculated. Analyzes were performed for Test signals with superimposed acoustic interference (N8 Babble noise). The Test signals with SNR = -5 to 5 dB was formed. The results are presented in tables and graphs. Finally, a comparative analysis was performed. Based on the results of the comparative analysis, a window function suitable for implementation for real-time operation was selected.

Estimation F_0 Using Autocorrelation Function

Correlation is a measure of the similarity of two signals. It is defined as the similarity of one signal at time k and another at time $k + m$. In this case, the correlation function is cross correlation. The autocorrelation function is a measure of the similarity of the same signal at time k and at time $k + m$. For a discrete signal $x(n)$, whose length is N, an autocorrelation function is defined by (Milivojevic et al., 2021):

$$r_{corr}(m) = \frac{1}{N}\sum_{n=0}^{N-1} x(n)\cdot x(n+m), \ \mathrm{m} = 0,1,2,\ldots \tag{1}$$

On Figure 1.a the Speech test signal $x(n)$ is shown. Its spectrum is shown in Figure 1.b and autocorrelation function r_{corr} is shown on Figure 1.c. The waveform of x can be complex and unsuitable for determining periods. The autocorrelation function r_{corr} is more suitable for calculating the signals period. On Figure 1.b the position of fundamental frequency is denoted by F_0. On Figure 1.c the position of the maximum of the autocorrelation function is denoted by N_{max}. The signal period is $T_0 = N_{max} * T_S$, where T_S is the sampling frequency of the time continuous signal $x(t)$. The fundamental frequency of the signal $x(n)$ is $F_0 = 1 / T_0 = 1 / (N_{max} * T_S)$. Determining the position of the maximum component of the autocorrelation function is realized by the Peak-Picking algorithm.

After determining the autocorrelation function and locating the peak, it is possible to accurately estimate the fundamental frequency only for signals whose fundamental frequency is $F_0 = 1 / (k * T_S)$ for $k = 1, 2, 3, \ldots$ For signals, whose fundamental frequency F_0 is in the interval $(k + 1) * T_S) < F_0 < 1 / (k * T_S)$, the estimation is performed by rounding and, thus, causes an estimation error. The calculation of F_0 is realized using the Nearest Neighbor method.

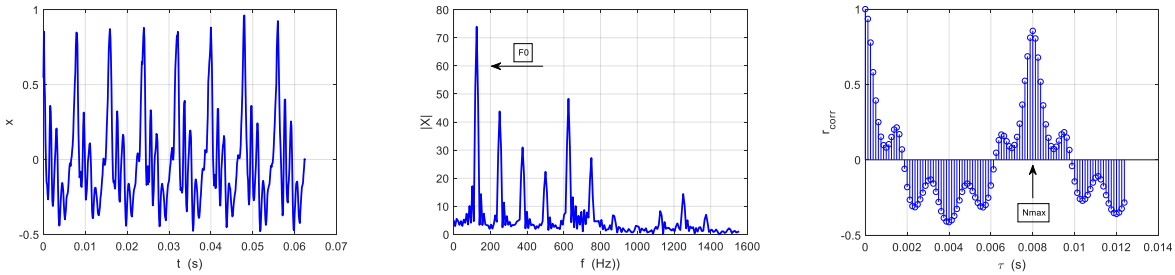

a) b) c)

Figure 1. Speech test signal: a) time form, b) amplitude characteristic, c) autocorrelation function.

On Figure 2.a shows the actual F_0 of the signal x sampled with F_S = 8 kHz in the range (125 - 140.625) Hz, which corresponds to the components k = 57 - 64 of the autocorrelation function (symbol '-'). Using the Peak-Picking algorithm, the values of F_0 for node k = 57 - 64 (symbol 'o') were calculated. The estimated values of the fundamental frequency, F_{0NN}, determined by applying the Nearest Neighbor method in the interval k = 57 - 64 are shown by the symbol '--'. The estimation error, $e(f)$, is shown on Figure 2.b.

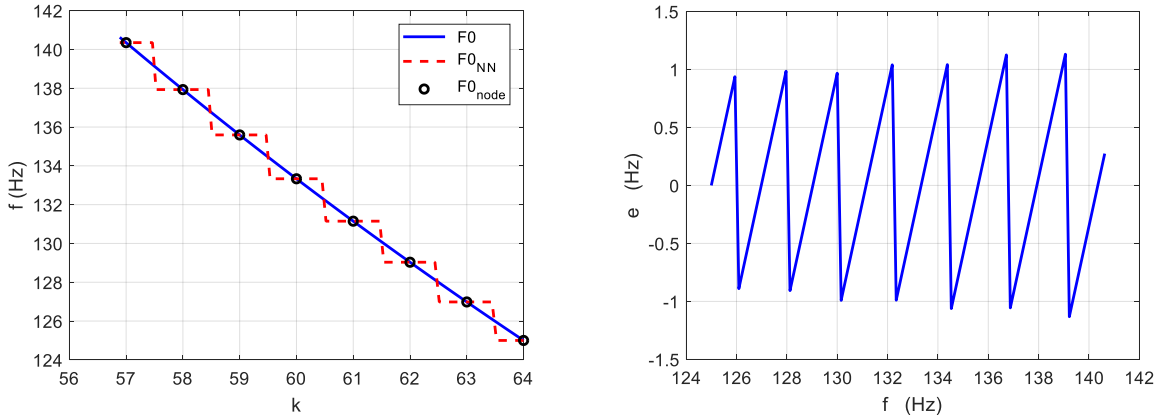

a) b)

Figure 2. a) Fundamental frequency F_0 trajectory between (57-64) autocorrelation components, value F_{0NN} estimated by rounding and value F_{0node} in nodes k, and b) estimation error e caused by Nearest Neighbor method.

Reducing the fundamental frequency estimation error, $e(f)$, can be done by applying interpolation. By interpolation, based on the position of the maximum value of the autocorrelation function, N_{max}, a series of m = $\{N_{\max}$ -1, $N_{\max}$, $N_{\max}$ + 1, $N_{\max}$ + 2$\}$ is formed and the position of the maximum is interpolated and, based on it, the fundamental frequency is calculated.

Algorithm for Fundamental Frequency Estimation

The algorithm for estimation of the fundamental frequency (*Estimation_algorithm*) is applied over the i-th block $\mathbf{x}_I$ of the signal $\mathbf{x}$, and consists of the following steps (Milivojevic et al., 2021):

Input: $\mathbf{x}_I$ - frame of discrete signal $\mathbf{x}$. N - frame length. F_0 -real fundamental frequency. T_S - sampling period.
Output: F_e - estimated fundamental frequency. MSE - estimation error.

Step 1: The $\mathbf{x}_I$ signal is modified by the window function w:

$$\mathbf{x}_{IW} = \mathbf{x}_I * \mathbf{w}\,, \tag{2}$$

Step 2: Determine the autocorrelation function r_X
Step 3: Using the Peak-Picking algorithm, the position of the maximum of the autocorrelation function, N_{max}, is calculated.

Step 4: By applying parametric interpolation with the interpolation kernel r_{PCC}, the continuous function R_X is determined.
Step 5: By differentiating the function R_X and equalizing with zero, the position of the maximum between the two n_{max} samples is determined. The real position of the maximum is $N_M = N_{max} + n_{max}$.
Step 6: The estimated fundamental frequency is:

$$F_e = 1/\left(\left(N_{\max} + n_{\max}\right)\cdot T_S\right), \tag{3}$$

Step 7: The mean square error of the fundamental frequency estimate is:

$$MSE = \overline{(F_0 - F_e)^2}\ . \tag{4}$$

In the continuation of this paper, an experiment is described in the framework of which the efficiency of the fundamental frequency estimation algorithm at Sine and Speech signal was tested.

Experimental Results and Comparative Analysis

Experiment

An experiment with the aim of determining the efficiency of the fundamental frequency estimation by a correlation algorithm, was performed. Increasing the accuracy of the assessment was achieved by applying window functions for processing the Test signal in the time domain. After that, a further increase in accuracy was achieved with the application of the interpolation algorithms. MSE was used as a measure to analyze the accuracy of the assessment. Using the Test Algorithm, which is explained later in this section, the trajectories of the MSE estimation error were calculated. By minimizing the estimate error, the optimal parameters of the parametric cubic interpolation kernel are determined. Kernel parameters are specified for some standard, time-symmetric, window functions. All analyzes were performed in the presence of background acoustic interference.

Test signals were created with F_S = 8 kHz and with windows with length N = 256, which assures the analysis of frame that last 32 ms. The results presented further in this paper relate to F_0 = 125-140.625 Hz (frequencies between the eighth and ninth DFT components). Number of frequencies in the specified range for which the estimation is done is M = 100. The Sine test signal is with K=10 harmonics. All further analyzes will relate to a) Hamming, b) Hanning, c) Blackman, d) Rectangular, e) Kaiser and f) Triangular window. N8 Babble noise (SNR = {5, 2.5, 0, -2.5, -5, -7.5, -10} dB) was used as acoustic interference (Figure 3.b). The 1P Keys interpolation kernel (Keys, 1981) was used, which was defined as

$$r(f) = \begin{cases} (\alpha+2)|f|^3 - (\alpha+3)|f|^2 + 1, & |f| \le 1, \\ \alpha|f|^3 - 5\alpha|f|^2 + 8\alpha|f| - 4\alpha, & 1 < |f| \le 2, \\ 0, & \text{otherwise} \end{cases} \tag{5}$$

where α is the kernel parameter. The time form of the 1P Keys kernel, for some values of the parameter α, is shown in Figure 3.a.

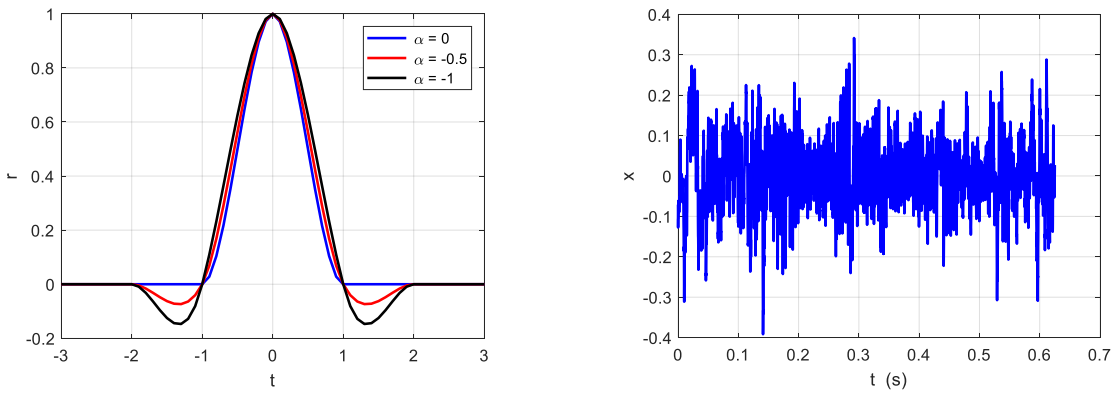

a) b)

Figure 3. a) 1P Keys window, b) Babble noise N8.

Test Algorithm

The Test algorithm was implemented in the following steps:

Input: x_I - frame of discrete signal *x*. *N* - frame length. F_{0_real} - real fundamental frequency. T_S - sampling period. ($\alpha_{\min}$, $\alpha_{\max}$) parameter limits, Δα - step, *w* - window function,
Output: $\mathrm{MSE}_{\min}$. α_{opt}.

FOR $\alpha = \alpha_{\min}: \Delta\alpha: \alpha_{\max}$
FOR $\mathrm{SNR} = \mathrm{SNR}_{\min}$: Step: $\mathrm{SNR}_{\max}$
Step 1: Create a Test Signal with SNR:

$$x_{Ib} = x_I + k \cdot x_b \,, \tag{6}$$

Step 3: Estimation of the fundamental frequency (algorithm described earlier in the previous section)
$[F_e, \mathrm{MSE}_s]$ = *Estimation_algorithm* (x_{Ib}, α, *N*, *w*, T_s)
END

$$MSE(\alpha) = \overline{MSE_s} \,, \tag{7}$$

END
Step 4: Determining minimum of the estimate error:

$$MSE_{\min} = \min(MSE). \tag{8}$$

Step 5: Determining the optimal kernel parameter:

$$\alpha_{opt} = \arg\min_{\alpha}(MSE), \tag{9}$$

Test Signal

PCC algorithm for the fundamental frequency estimation will be applied to: a) Sine test signal, and b) Speech test signal. Simulation Sine signal for testing of PCC algorithm is defined in (Pang et al., 2000):

$$s(t) = \sum_{i=1}^{K}\sum_{g=0}^{M} a_i \sin\left(2\pi i\left(F_o + g\frac{F_s}{NM}\right)t + \theta_i\right), \tag{10}$$

where F_0 is fundamental frequency, θ_i and a_i are phase and amplitude of the *i*-th harmonic, respectively, *K* is the number of harmonics, and *M* is the number of points between the two samples in spectrum. The Sine test signal is shown on Figure 4.: a) time form, b) amplitude characteristic and c) autocorrelation function. The real Speech test signal is obtained by recording of a speaker in the real acoustic ambient. The Speech test signal is shown on Figure 1.: a) time form, b) amplitude characteristic and c) autocorrelation function.

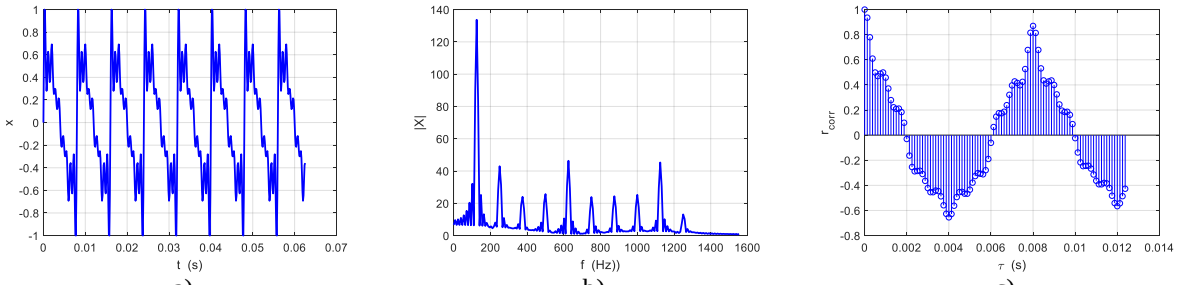

a) b) c)

Figure 4. Sine test signal: a) time form, b) amplitude characteristic, c) autocorrelation function.

Results

Using the Test algorithm, described in the previous section, MSE trajectories for all tested window functions were calculated. The MSE trajectories for the rectangular window are shown on: a) Figure 5.a (Sine test signal) and b) Figure 5.b (Speech test signal). The minimum values of MSE and the optimal kernel parameters, for the Sine test signal and the Speech test signal, are shown in Table 1. The trajectories of the minimum MSE for SNR

= -5 to 5 dB are shown on: a) Figure 6.a (Hamming), a) Figure 6.b (Hann), a) Figure 6.c (Blackman), a) Figure 6.d (Rectangular), a) Figure 6.e (Kaiser) and a) Figure 6.f (Triangular).

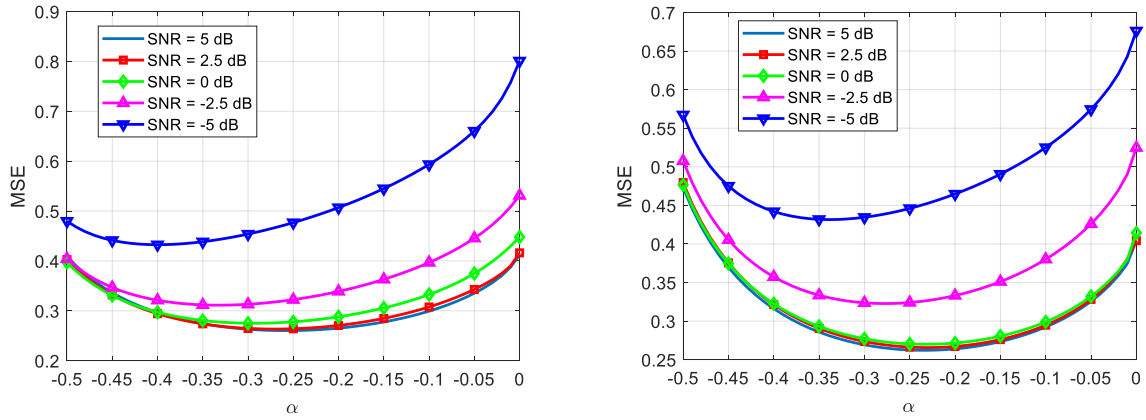

a) b)

Figure 5. MSE for Rectangular window: a) Sine test signal, b) Speech test signal.

Table 1. Optimal parameters and estimates error for testing windows

Window	SNR (dB)	Sine test signal α_{opt}	MSE	MSE_{NN}	Speech test signal α_{opt}	MSE	MSE_{NN}
Hamming	5	-0.1250	0.2864	4.4057	-0.1250	0.3133	4.9651
	2.5	-0.1250	0.2908	4.2141	-0.1250	0.3056	4.6656
	0	-0.1250	0.3222	3.8738	-0.1250	0.3355	4.2339
	-2.5	-0.1250	0.4444	3.4930	-0.1250	0.4677	3.6422
	-5	-1.3400	0.5433	2.6137	-1.3400	0.8381	2.8477
	-7.5	-0.5300	11.1040	13.7504	-10.250	7.6133	7.0663
	-10	-10.250	77.2945	69.7670	-0.5300	44.6659	56.9970
			$\overline{MSE_{sine}}$ = 12.8979	$\overline{MSE_{sin\_NN}}$ = 14.5882		$\overline{MSE_{speech}}$ = 7.7913	$\overline{MSE_{sp\_NN}}$ = 12.0597
Hann	5	-0.1250	0.2907	4.4057	-0.1250	0.3226	4.9627
	2.5	-0.1250	0.2961	4.2141	-0.1250	0.3196	4.6747
	0	-0.1250	0.3322	3.8738	-0.1250	0.3662	4.3238
	-2.5	-0.1250	0.4557	3.4182	-0.1250	0.5101	3.6668
	-5	-1.3400	0.6204	2.5644	-1.3400	1.7657	3.5394
	-7.5	-0.5300	12.6568	15.4588	-10.250	7.8694	7.2064
	-10	-0.5300	51.3111	70.2882	-0.5300	44.8402	59.4322
			$\overline{MSE_{sine}}$ = 9.4233	$\overline{MSE_{sin\_NN}}$ = 14.8890		$\overline{MSE_{speech}}$ = 7.9991	$\overline{MSE_{sp\_NN}}$ = 12.5437
Blackman	5	-0.1250	0.2883	4.3133	-0.1250	0.3206	4.8683
	2.5	-0.1250	0.2932	4.0458	-0.1250	0.3380	4.5908
	0	-0.1250	0.3688	3.9673	-0.1250	0.3935	4.1463
	-2.5	-0.5300	0.5326	3.3815	-0.1250	0.5787	3.6113
	-5	-1.3400	0.6519	3.8943	-0.9350	3.1323	3.9570
	-7.5	-0.5300	16.1659	19.8547	-10.250	16.3176	14.9718
	-10	-0.5300	48.0547	71.8709	-0.5300	37.3017	58.8938
			$\overline{MSE_{sine}}$ = 9.4793	$\overline{MSE_{sin\_NN}}$ = 15.9040		$\overline{MSE_{speech}}$ = 8.3403	$\overline{MSE_{sp\_NN}}$ = 13.5770
Rectangular	5	-0.1250	0.2871	4.5004	-0.1250	0.2815	4.5866
	2.5	-0.1250	0.2950	4.4080	-0.1250	0.2840	4.5866
	0	-0.1250	0.3177	4.2426	-0.1250	0.2883	4.5090
	-2.5	-0.1250	0.3784	3.9317	-0.1250	0.3640	4.3959
	-5	-0.5300	0.5379	3.3755	-0.1250	0.5064	3.9829
	-7.5	-1.3400	0.8136	2.8734	-1.3400	3.8830	5.4915
	-10	-1.3400	1.9469	2.8648	-0.5300	6.4847	7.3310

			$\overline{MSE_{\text{sine}}}$ =	$\overline{MSE_{\text{sin\_NN}}}$ =		$\overline{MSE_{\text{speech}}}$ =	$\overline{MSE_{\text{sp\_NN}}}$ =
			0.6538	3.7423		1.7274	4.9834
	5	-0.1250	0.2912	4.4997	-0.1250	0.3203	5.0716
	2.5	-0.1250	0.2936	4.3133	-0.1250	0.3210	4.8728
	0	-0.1250	0.3294	4.1271	-0.1250	0.3167	4.3127
Kaiser	-2.5	-0.1250	0.4128	3.5589	-0.1250	0.4489	3.8147
	-5	-1.3400	0.5505	2.8017	-1.3400	0.7412	2.9532
	-7.5	-0.5300	7.9480	10.5746	-0.5300	3.2700	6.2004
	-10	-0.5300	61.2133	68.1588	-0.5300	45.0961	52.9036
			$\overline{MSE_{\text{sine}}}$ =	$\overline{MSE_{\text{sin\_NN}}}$ =		$\overline{MSE_{\text{speech}}}$ =	$\overline{MSE_{\text{sp\_NN}}}$ =
			10.1484	14.0049		7.2163	11.4470
	5	-0.1250	0.2926	4.4997	-0.1250	0.3069	4.9651
	2.5	-0.1250	0.2945	4.3133	-0.1250	0.3397	4.9627
	0	-0.1250	0.3206	4.0458	-0.1250	0.3369	4.4027
Triangular	-2.5	-0.1250	0.4157	3.4930	-0.1250	0.4516	3.8106
	-5	-1.3400	0.5510	2.7381	-1.3400	0.7809	3.0417
	-7.5	-0.5300	8.8860	11.3704	-10.250	6.7040	6.4624
	-10	-0.5300	64.5430	68.4134	-0.5300	41.9750	53.4811
			$\overline{MSE_{\text{sine}}}$ =	$\overline{MSE_{\text{sin\_NN}}}$ =		$\overline{MSE_{\text{speech}}}$ =	$\overline{MSE_{\text{sp\_NN}}}$ =
			10.7576	14.1248		7.2707	11.5895

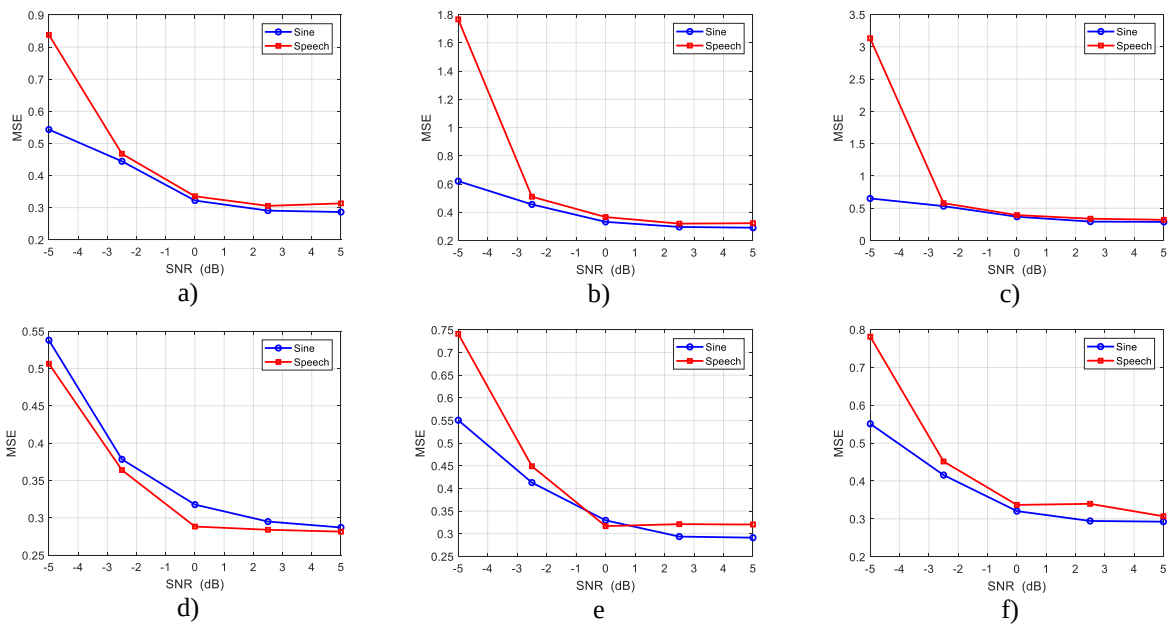

Figure 6. MSE estimation errors, for superimposed noise N8 Babble, for: a) Hamming, b) Hann, c) Blackman, e) Rectangular, e) Kaiser and f) Triangular window.

Analysis of Results

Based on the results shown in Table 1 and graphically on Figure 5-6, it is concluded that:

a) Sine test signal: $\overline{MSE_{\text{sine}}}$ is the lowest when applying the rectangular window ($\overline{MSE_{\text{sine}}}$ = 0.6538). Compared to the application of other window functions the accuracy is higher: $\overline{MSE_{\text{sine}}}$ / $\overline{MSE_{rect}}$ = 12.8979 / 0.6538 = 19.7276 (Hamming), 9.4233 / 0.6538 = 14.4131 (Hann), 9.4793 / 0.6538 = 14.4988 (Blackman), 10.1484 / 0.6538 = 15.5222 (Kaiser) and 10.7576 / 0.6538 = 16.4540 (Triangular) times. Compared to the estimation of the fundamental frequency without interpolation, when applying interpolation, the accuracy is higher $\overline{MSE_{\text{sin\_NN}}}$ / $\overline{MSE_{\text{sine}}}$ = 3.7423 / 0.6538 = 5.7239 times.

b) Speech test signal: $\overline{MSE_{\text{speech}}}$ is the lowest when applying the rectangular window ($\overline{MSE_{\text{speech}}}$ = 1.7274). Compared to the application of other window functions the accuracy is higher: $\overline{MSE_{\text{speech}}}$ / $\overline{MSE_{rect}}$ = 7.7913 / 1.7274 = 4.5104 (Hamming), 7.9991 / 1.7274 = 4.6307 (Hann), 8.3403 / 1.7274 = 4.8282 (Blackman), 7.2163 / 1.7274 = 4.1776 (Kaiser) and 7.2707 / 1.7274 = 4.2090 (Triangular) times. Compared to the estimation of the fundamental frequency without interpolation, when applying interpolation, the accuracy is higher $\overline{MSE_{\text{sp\_NN}}}$ / $\overline{MSE_{\text{speech}}}$ = 4.9834 / 1.7274 = 2.8849 times.

c) The accuracy of estimate of the fundamental frequency with the Speech test signal compared to the estimates fwith the Sine test signal, using the rectangular window, is $\overline{MSE_{speech}}$ / $\overline{MSE_{\text{sine}}}$ = 1.7274 / 0.6538 = 2.6421 times lower.

d) The optimal value of the kernel parameter with 1P Keys kernel is $\alpha_{\text{opt}} = \overline{\alpha_{opt\_\text{Sine}} + \alpha_{opt\_Speech}}$ = -0.4432.

With the fact that the numerical complexity of the 1P Keys kernel is small, and as such, it is suitable for real-time operation. The optimal choice is the implementation of the rectangular window and the kernel parameter $\alpha = \alpha_{\text{opt}}$ = -0.4432.

Conclusion

This paper describes an algorithm for estimating the fundamental frequency of a Speech signal in the time domain. The estimation algorithm is based on autocorrelation. The increase in precision was achieved by applying parametric interpolation with a 1P Keys interpolation core. Through experimentation, it has been shown that an additional increase in estimation accuracy can be achieved by processing Speech signals with window functions. MSE was used as a measure of precision. A detailed analysis of the experimental results showed that the rectangular window function was optimal. The error of estimating the fundamental frequency by autocorrelation is higher in relation to the error of estimating by interpolation: a) $\overline{MSE_{\text{sin\_NN}}}$ / $\overline{MSE_{\text{sine}}}$ = 3.7423 / 0.6538 = 5.7239 (Sine test signal) and b) / $\overline{MSE_{\text{sin\_NN}}}$ / $\overline{MSE_{\text{sine}}}$ = 4.9834 / 1.7274 = 2.8849 times. For the Rectangular window, the optimal value of the kernel parameter is α_{opt} = -0.4432. These results recommend the application of the correlation algorithm and interpolation with the 1P Keys core in real-time systems.

Scientific Ethics Declaration

The authors declare that the scientific ethical and legal responsibility of this article published in EPSTEM journal belongs to the authors.

References

De Cheveigné, A., & Kawahara, H. (2002). YIN, a fundamental frequency estimator for speech and music. *The Journal of the Acoustical Society of America*, *111*(4), 1917-1930.

Kacha, A., Grenez, F., & Benmahammed, K. (2005). Time–frequency analysis and instantaneous frequency estimation using two-sided linear prediction. *Signal Processing*, *85*(3), 491-503.

Keys, R. (1981). Cubic convolution interpolation for digital image processing. *IEEE transactions on acoustics, speech, and signal processing*, *29*(6), 1153-1160.

Meijering, E., & Unser, M. (2003). A note on cubic convolution interpolation. *IEEE Transactions on Image processing*, *12*(4), 477-479.

Milivojević, Z. N., & Balanesković, D. Z. (2009). Enhancement of the perceptive quality of the noisy speech signal by using of DFF-FBC algorithm. *Facta universitatis-series: Electronics and Energetics*, *22*(3), 391-404.

Milivojević, Z. N., & Brodić, D. (2013). Estimation of the fundamental frequency of the speech signal compressed by mp3 algorithm. *Archives of Acoustics*, 363-373.

Milivojevic, Z., & Prlincevic, B. (2021). *Estimation of the fundamental frequency of the speech signal using autocorrelation algorithm*. Unitech.

Milivojevic, Z. N., Brodic, D. T., & Stojanovic, V. (2017). Estimation of fundamental frequency with autocorrelation algorithm. http://vtsnis.edu.rs/wp-

Pang, H. S., Baek, S., & Sung, K. M. (2000). Improved fundamental frequency estimation using parametric cubic convolution. *IEICE TRANSACTIONS on Fundamentals of Electronics, Communications and Computer Sciences*, *83*(12), 2747-2750.

Qiu, L., Yang, H., & Koh, S.-N. (1995). Fundamental frequency determination based on instantaneous frequency estimation. *Signal Processing*, *44*(2), 233-241.

Rabiner, L.R. and Schafer, R.W. (1978) *Digital processing of speech signals*. Prentice Hall.

Rao, P., & Barman, A. D. (2000). Speech formant frequency estimation: evaluating a nonstationary analysis method. *Signal Processing*, *80*(8), 1655-1667.

Author Information

Zoran MILIVOJEVIC
Academy of Applied Technical and Preschool Studies
A. Medvedeva 20, 18000 Niš, Serbia
e-mail: *zoran.milivojevic@akademijanis.edu.rs*

Bojan PRLINCEVIC
Kosovo and Metohija Academy of Applied Studies
Dositejeva bb, 38218 Leposavic, Serbia

Natasa SAVIC
Academy of Applied Technical and Preschool Studies
A. Medvedeva 20, 18000 Niš, Serbia

To cite this article:

Milivojevic, Z., Prlincevic, B., & Savic, N. (2021). Optimization parameter of the 1P keys interpolation kernel implemented in the correlation algorithm for estimating the fundamental frequency of the speech signal. *The Eurasia Proceedings of Science, Technology, Engineering & Mathematics (EPSTEM), 16*, 153-161.

The Eurasia Proceedings of Science, Technology, Engineering & Mathematics (EPSTEM)
ISSN: 2602-3199

The Eurasia Proceedings of Science, Technology, Engineering & Mathematics (EPSTEM), 2021

Volume 16, Pages 162-166

IConTES 2021: International Conference on Technology, Engineering and Science

Synthesis of Graphene/g-C_3N_4 Composite Photo-Electrodes for Li – Ion – Oxygen Battery

Nilay KACAR
Eskisehir Osmangazi University

Ersu LOKCU
Eskisehir Osmangazi University

R. Can OZDEN
Eskisehir Osmangazi University

Mustafa ANIK
Eskisehir Osmangazi University

Abstract: Graphene was synthesized by the chemical vapor deposition (CVD). Initially ratios of Ar, H_2 and CH_4 gases were optimized to get a single layer graphene by CVD. Raman characterizations showed that the optimized synthesis conditions provided I_{2D}/I_G ratio as 3 that this ratio indicated the formation of the single layer graphene. The synthesized single layer graphene was mixed with melamine at the certain ratios to obtain the graphene/graphitic-C_3N_4 (g-C_3N_4) semiconductor composites. All the synthesized composites were prepared as the photo-electrode to be used in the photo-assisted charging of the lithium-ion oxygen battery. The photo-current levels produced by the photo-electrodes were determined by the linear sweep voltammetry technique.

Keywords: Graphene, Lithium oxygen battery, Chemical vapor deposition, g-C_3N_4

Introduction

The extraordinary properties (conductivity, transmittance, flexibility, strength) of graphene enable its use in critical applications such as electronics, composites, membranes and renewable energy technologies. There are numerous studies on the synthesis of graphene that mechanical exfoliation, liquid-phase exfoliation and chemical vapor deposition (CVD) can be counted as the main synthesis techniques. Among these techniques CVD is relatively inexpensive and the most promising method to get the monolayer graphene on the large areas (Li et al., 2016).

Graphitic carbon nitride (g-C_3N_4) can be simply synthesized from a convenient precursor via series of poly-condensation reactions and it can be used as effective photo-electrode semiconductor or electro-catalyst for the Li ion oxygen battery cathodes since it catalyzes both the oxygen reduction and oxygen evolution reactions (Niu et al., 2012). In this work the CVD graphene was chemically mixed with g-C_3N_4 to get the efficient composite photo-electrode. g-C_3N_4 has approximately 2.7 eV band gap and this value makes it attractive visible light photocatalyst (Wang et al., 2008). The chemically mixed CVD graphene is expected to increase the conductivity and decrease the band gap of g-C_3N_4 to make g-C_3N_4 excellent sunlight harvesting semiconductor.

Method

Graphene was synthesized with a prescription provided in Figure 1 on 2x2 cm Cu substrates. After synthesis, Cu substrates were dissolved in 0.5 M $FeCl_3$ + %50 HCl solution and then cleaned with distilled water (Figure 2). The synthesized graphene was kept in methanol until starting to the synthesis process. If graphene was needed for the characterization, then the Cu substrate was coated with PMMA solution on the spin coater and then they dried at 140°C for 30 min. The graphene/PMMA film was cleaned with distilled water after the Cu substrates were dissolved and dried at 60°C for 30 minutes. For the characterizations the cleaned graphene/PMMA film was transferred either onto wafer (for Raman) or onto TEM grit (for SEM). The transferred graphene/PMMA film was cleaned with acetone and isopropanol to remove PMMA.

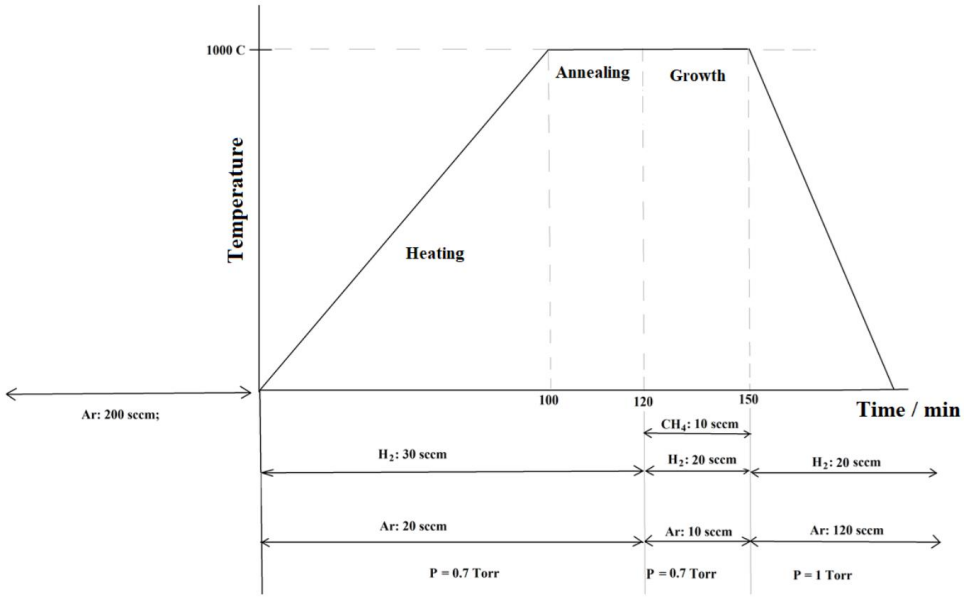

Figure 1. CVD graphene synthesis.

Figure 2. Cleaning and transfer processes of graphene after synthesis by CVD.

For the photo-electrode synthesis, melamine ($C_3H_6N_6$) and graphene were mixed in methanol in an alumina crucible at 50°C for several h until all methanol volatilized. After drying completely, the mixture heated at a rate of 3°C/min up to 550°C and it kept at this temperature for 3 h under continuous Ar flow in a fully sealed crucible. Then it left to cool down to RT inside the furnace to get g-C_3N_4 - graphene composite.

The composite photo-catalyst was coated on the conductive surface of ITO (8 mm x 6 cm) with 0.1 mg cm^{-2} loading by spin coater for the photo-current experiments and then the ITO specimens were dried at 100°C for overnight in a vacuum oven. The photo-currents were measured by lineer sweep voltammetry technique by using Gamry Reference 3000 potentiostat in 0.1 M KCl / 0.1 M H_2PO_4 (pH 7) solution in a spectral cuvette as in Figure 3. During the experiments light was sent by solar simulator (A-type 150 W, 1-3 SUN, Xenon lamb, 1.5 AM Filter: 400 nm - 700 nm visible light).

X-ray diffraction (XRD) analyses were performed on a PANalytical Empyrean diffractometer with Cu K-alpha radiation at a scanning rate of 2° min^{-1}. The morphologies of the electrodes were examined with a ZEISS Ultraplus scanning electron microscope (SEM). Raman spectra was obtained using a RENISHAW RAMAN inVia Microscope with 532 nm wavelength laser.

Figure 3. The photo-current measurements of CVD graphene - g-C_3N_4 composites.

Results and Discussion

Characterization

Raman spectra of synthesized graphene according to the prescription provided in Figure 2 is shown in Figure 4. In general, there are three main peaks of graphene in Raman spectra that they are labeled as G (~1580 cm^{-1}), D (~1360 cm^{-1}) and 2D (~2700 cm^{-1}) bands. The intensities (I) and the relative intensity ratios of these peaks provide the information about the quality and the layer numbers of graphene. As the layer number of graphene increases, the intensity of G band increases and that of 2D band decreases. D band represents the disorder and if this band disappears completely then the synthesized graphene is accepted as flawless. In Figure 4, there is no D band peak and the ratio of the 2D band intensity to G band intensity (I_{2D}/I_G) is approximately 3. This ratio indicates that the synthesized graphene according to the prescription provided in Figure 2 is single layer graphene.

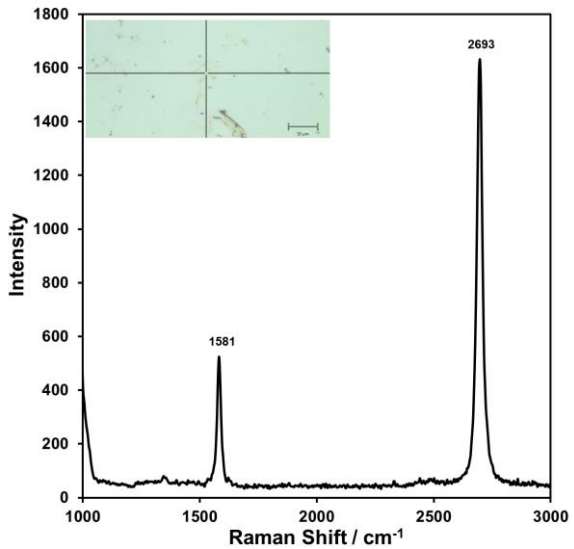

Figure 4. 532 nm Raman spectra of synthesized graphene.

Photo-Current Measurement

CVD graphene - g-C_3N_4 composite photo-electrodes were synthesized based on the graphene area ratio (cm^2) to g-C_3N_4 weight (mg). The obtained chopped photo-currents (on-off) depending on the potential is depicted in Figure 5. Obviously as the CVD graphene ratio increases in the composite, the photo-catalytic efficiency of the of the composite electrode increases. Graphene shows the dual action that firstly it increases conductivity and thus decelerates the rate of the hole – electron re-combinations in g-C_3N_4 semiconductor. Secondly graphene

decreases band gap of g-C_3N_4 since it is defined as zero band gab semiconductor. Both actions of graphene increase the sunlight harvesting capacity of g-C_3N_4.

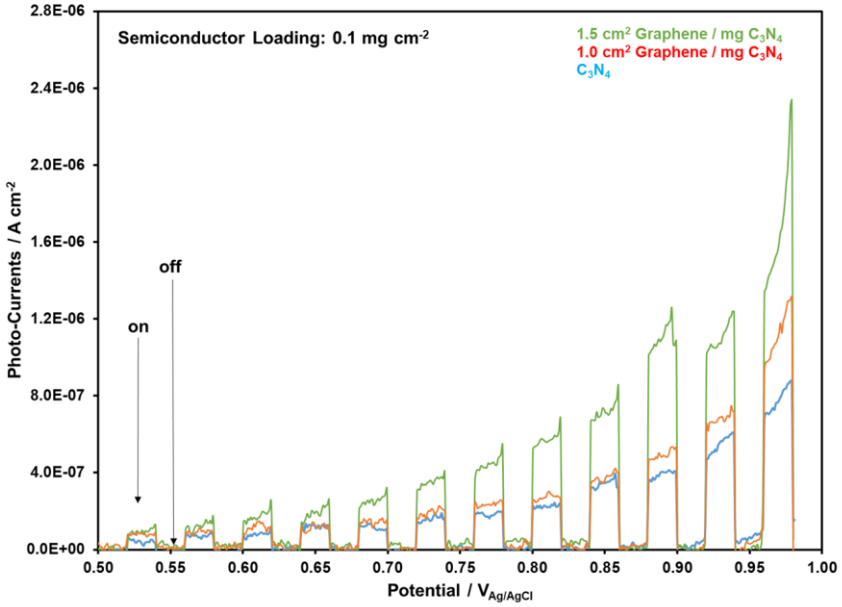

Figure 5. Photo-currents of CVD graphene - g-C_3N_4 composites.

Conclusion

Initially single layer graphene was synthesized by chemical vapor deposition (CVD) and then CVD graphene - g-C_3N_4 composite photo-electrodes were synthesized. Photo-current measurements showed that graphene improved the photo-catalyst efficiency of g-C_3N_4 significantly.

Acknowledgements

This work was supported by The Scientific and Technological Research Council of Turkey under the contract number 219M269.

Scientific Ethics Declaration

The authors declare that the scientific ethical and legal responsibility of this article published in EPSTEM journal belongs to the authors.

References

Li, X., Colombo, L., & Ruoff, R. S. (2016). Synthesis of graphene films on copper foils by chemical vapor deposition. *Advanced Materials*, *28*(29), 6247-6252.

Niu, P., Zhang, L., Liu, G., & Cheng, H. M. (2012). Graphene- like carbon nitride nanosheets for improved photocatalytic activities. *Advanced Functional Materials*, *22*(22), 4763-4770.

Wang, X., Maeda, K., Thomas, A., Takanabe, K., Xin, G., Carlsson, J. M., ... & Antonietti, M. (2009). A metal-free polymeric photocatalyst for hydrogen production from water under visible light. *Nature materials*, *8*(1), 76-80.

Author Information

Nilay KACAR
Metallurgical and Materials Engineering
Eskisehir Osmangazi University
Contact e-mail: *nilaykacar032@gmail.com*

Ersu LOKCU
Metallurgical and Materials Engineering
Eskisehir Osmangazi University

R. Can OZDEN
Metallurgical and Materials Engineering
Eskisehir Osmangazi University

Mustafa ANIK
Metallurgical and Materials Engineering
Eskisehir Osmangazi University

To cite this article:

Kacar, N., Lokcu, E., Ozden, R.C., & Anik, M. (2021). Synthesis of graphene/g-C3N4 composite photo-electrodes for Li – ion – oxygen battery. *The Eurasia Proceedings of Science, Technology, Engineering & Mathematics (EPSTEM), 16*, 162-166.

The Eurasia Proceedings of Science, Technology, Engineering & Mathematics (EPSTEM)
ISSN: 2602-3199

The Eurasia Proceedings of Science, Technology, Engineering & Mathematics (EPSTEM), 2021

Volume 16, Pages 167-181

IConTES 2021: International Conference on Technology, Engineering and Science

Time Governed Multi-Objective Optimization

Moses Oyaro OKELLO
Jiangsu University of Science and Technology

Abstract: Multi-objective optimization (MOO) is an optimization involving minimization or maximization of several objective functions more than the conventional one objective optimization, which is useful in many fields. Many of the current methodologies addresses challenges and solutions that attempt to solve simultaneously several Objectives with multiple constraints subjoined to each. Often MOO are generally subjected to linear inequality, equality and or bounded constraint that prevent all objectives from being optimized at once. This paper reviews some recent articles in area of MOO and presents deep analysis of Random and Uniform Entry-Exit time of objectives. It further breaks down process into sub-process and then provide some new concepts for solving problems in MOO, which comes due to periodical objectives that do not stay for the entire duration of process lifetime, unlike permanent objectives which are optimized once for the entire process duration. A methodology based on partial optimization that optimizes each objective iteratively and weight convergence method that optimizes sub-group of objectives are given. Furthermore, another method is introduced which involve objective classification, ranking, estimation and prediction where objectives are classified based on their properties, and ranked using a given criteria and in addition estimated for an optimal weight point (pareto optimal point) if it certifies a coveted optimal weight point. Then finally predicted to find how far it deviates from the estimated optimal weight point. A Sample Mathematical Tri-Objectives and Real-world Optimization was analyzed using partial method, ranking and classification method, the result showed that an objective can be added or removed without affecting previous or existing optimal solutions. Therefore, suitable for handling time governed MOO. Although this paper presents concepts work only, it's practical application are beyond the scope of this paper, however base on analysis and examples presented, the concept is worthy of igniting further research and application.

Keywords: Optimization, Multi-objective optimization, Decision-making, Time

Introduction

To introduce Multi-Objective Optimization, individual terms are first defined. So, what is Optimization? Optimization is defined as finding or making the best effective use of situation or resources available. An Objective is simply defined as a goal or aims. Then, Constraint is simply limitation or restriction. Therefore, Overall Multi-Objective Optimization can be defined as an approach for seeking best resources to attain desire goals whether in the present of constraint(s) or not.

Optimization of process is of paramount eminence in many fields such as Science, Engineering, Technology and many more. Its application ranges from biological process Optimal Control, Chemical industrial control to physical process control, Data Science and many more. Optimization succor in abridging cost and wastage of resources and minimizes time for process execution within given constraints to meet desire objectives as illustrated in many articles presented by Vinter et el (2010), (Lewis et el (2012), Khalil et el (1996) and Kwakernaak et el (1972). Take for example a case in a flight or marine vessel, which is required to maximize the amount of load (goods) it carries meanwhile minimizing it weight and size. Some common approach is to minimize the amount of fuel it uses, as reduction in fuel use is directly proportional to decrease in overall weight of a vessel and ultimately the size of the fuel tank. Nevertheless, how does one reduce fuel without affecting the

distance to be cover by the vessel? Some engineers would use the shortest path/rout possible for navigation; others might use the approach of redesigning an energy efficient engine to ensure minimum consumption and minimum wastage of fuel as presented by Kumar et el (2012) and Xiao et el (2018) during navigation. All these are targeting at minimizing cost and wastage of resources such as fuel.

Another example, in chemical industrial setting, where the objective is to maximize the product of reaction. Some engineers would device a methodology by maximizing rate of reaction but some reactions are endothermic which requires too much input energy to run the reaction process fully and efficiently. So how does one minimize energy inputs required to run such endothermic reaction meanwhile maximizing product of the reaction? All these are some of the notable situations that require good optimization strategy.

A simple System often consists of a single objective and perhaps a single constraint and they are linear normally. However, a system start getting complicated when it's non-linear and in addition, when there are more than one or many constraints and many or multiple objectives to be solve simultaneously. Such systems are quite not straightforward to optimize due to their Complexity.

In MOO, Objectives can have influence over other Objective, this makes it difficult to solve such problem. I.e., the influence can be either negative or positive. A negative influence is when solving Objective results in degrading the optimal solution of at least one or more of the other remaining Objectives in MOO. Therefore, this means, to obtain the best optimal solution of such objective, the remaining objective may have poor optimal solution or even worst solution or vice versa.

This is often referrers to as non-dominated, non-inferior, Pareto efficient, or Pareto optimal if not any of the objective values can be upgraded without devaluing some of the other objective values. Most challenges in multi-objective optimization often referred to as multi-criteria programming are generally subjected to linear inequality, equality and or bounded constraint(s) that prevent all objectives from being simultaneously solve for instance a case where number of objectives are more than that of controllable variable or, perturbation that generates uncertainties. Many scholars have put several approaches and model for finding optimal weight point of multi-objective optimization in place. The methods address several challenges in multi-objective optimization and their application in many fields such as science, finance, engineering and many more. For instance, in field of electricity in electrical power balance where trade-off between voltage and electrical grid requirement Wang et el (2013) and where demand of electricity and electricity generation needs to be balance by considering constraints bonded to it.

The challenges involve in multi-objective optimization is finding an optimal weight point solution thought there may exist multiple solution for a given multi-objective optimization problem, however the problem is finding such solution which is not simple such as that of a single objective optimization. The following functions are use throughout the entire text to give the general problem definition see (1) extracted from article by Blank et el (2020).

$$\begin{aligned} &\min f_k(X) && k = 1, \dots, K \\ s.t\ \ &g_j(X) \le 0, && j = 1, \dots, J \\ &h_m(X) = 0, && m = 1, \dots, M \\ &x_i^L \le x_i \le x_i^U, && i = 1, \dots, N \end{aligned} \tag{1}$$

Where the following are defined in MOO with total variable N, and total Objectives as K. In addition, total constraints are defined a as J for inequality, M for equality. In addition, lower L and upper boundaries U for each variable x_i^L, x_i^U are define too.

Optimization can be express as minimization of an objective function or maximization of Objective function. However, in most cases such as in (1), it is often express as minimization as many objectives are model in term of cost or time. Therefore, minimizing cost and or time mean an optimal performance, which is less costly, or time wasting. For some model of Objective function, may require maximization of Objective function such as maximizing products, maximizing profit etc.

Literature Review

Here are some of the notable multi-objective optimization methods and their application in many fields such as Science, Engineering, Economics, Data Science and many more. In addition, to currently and often use standard

approach by setting a fix optimal weight point among multiple objectives. This paper is a polished and extended version of an article which initially appeared in preprint Okello (2020), which presented some of review in Multi-Objective Optimization field. MOO approaches are categories into four major categories as describe by Sayin et el (1999) and Miettinen (2008) as below i.e. No preferences, Priori method (lexicographical programming, Goal programming, Utility programming), Posteriori Method and Interactive Method.

In the literature review here, in addition to theoretical manuscripts, discussion about some selected application of Multi-Objective Optimization such as in Data Science, Engineering, and Economics etc. A paper by Stefan et el (2020), introduces an approach based on transformation of multi-stage optimal control model (OCM) with random switching time. They separated the problem into two sub-domains i.e., optimal control with random time horizon and Multi-Stage Optimal Control Model (OCM).

In their model and reformulation as deterministic (OCM), they assume that switching time divides the time horizon that is define as stage 1 and stage 2 or even more by random variable τ out of sample space $\Omega = [0, \infty]$. They further applied reformulation problem introduced in by Boukas et el (1990) about deterministic Optimal Control Model with infinite time horizon and they got the results (2) and (3) and there is probability at some point that the switch has not occurred as they pointed out.

$$\begin{aligned} &\max_{u(t)} \int_{t_0}^{\infty} e^{-\rho t} z1(t)\,[g1(x(t),u(t),t) + \eta(x(t),u(t),t)V^*(x(t),t)]dt \\ &s.t \qquad \dot{x} = f_1(x(t),u(t),t), \qquad x(t_0) = t_0 \\ &\qquad\quad z1(t) = -\eta(\dot{x}(t),u(t),t), \qquad z1(t_0) \end{aligned} \tag{2}$$

with

$$\begin{aligned} V^*\big((t),t\big) &= \max_{u(t)} \int_t^{\infty} e^{-\rho(s-t)} g2(x(s),u(s),s,x(t),t)ds \\ s.t\ \dot{x}(s) &= f_2(x(s),u(s),s,x(t),t) \qquad x(t)\lim_{t' \nearrow t} \varphi\big((t')\big) \end{aligned} \tag{3}$$

A case study by Białaszewski et el (2016) showed their method base on genetic gender approach for solving multi-objective optimization challenges of detection observers. In their method, the previous knowledge about a single gender of all included solutions is use for making difference among groups of objectives. The knowledge is from fitness of a single person and used during current parental crossover in evolutionary multi-objective optimization process.

An approach by Fazlollah et el (2015) on multi-objective optimization model for sizing and operation optimization district heating system with heat storage tanks. The model includes process design and energy integration method for optimizing the temperature interval, the volume and the operation strategy of thermal storage tanks.

The application of multi-objective optimization in water distribution system by Shokoohi et el (2017), they use Ant-Colony-Optimization for the optimization algorithm which concern with water quality base objectives in Water Distribution System design alongside other common objectives.

A multi-objectives decision support system developed for rehabilitation planning of public infrastructure by Farran et el (2015). Their method provides decision makers a collection of optimal rehabilitation tradeoff over a preferred analysis period. They handled two main objective's function cost and performance at once, together with the collection of attached constraints. The mechanism is based on a fitness-oriented method where challenges information is taken into account. To further analyze, cost and performance all together, a normalization method of all objectives is attained through time-value concept for both cost and condition states. Their proposed methodology is based on life-cycle costing approach using a dynamic markov chain to constitute the degeneration methodology and optimal rehabilitation profile is found using algorithm.

A study by Paul et el (2018) on Multi-Objective Bayesian Optimization (MOBO) problem presented a framework for taking user choices in (MOBO). They called the improvement approach as Expected Weighted Hypervolume Improvement (EWHI). They defined the hyper-volume of the dominated region based on continuous unlike Lebesgue. Sampling approximation method was also used for EWHI computation as the EWHI take a form of integral in which no close form expression exists in general case.

They demonstrated this on a Bi-Objective Optimization problem (4) where there is preference over one Objective and in addition, there is preference over a certain region.

$$\begin{cases} f_1(x_1, x_2) = \frac{1}{15} e^{-\frac{x_1}{15}} . \frac{1_{[0,150]}(x_1)}{150} . \frac{1_{[0,60]}(x_2)}{60} \\ f_2(x_1, x_2) = \frac{1}{2}\left(\varphi(x, \mu_1,) + \varphi(x, \mu_2, C)\right) \end{cases} \quad (4)$$

Where $\varphi(x, \mu_1,)$ denotes Gaussian probability density function, for means and covariant matrix are denoted as μ and C respectively evaluated at x. According to them, $f_1(x)$ is entirely based on user preference.

Blank (2020) presented some work in Multi-Objective Optimization in Python, which solve challenges that most framework in Python programming Language does not address such issue. They developed *pymoo*, a multi-Objective Optimization framework in Python. They implemented their framework that can be modified by user by inputting custom operators. Furthermore, sample test Challenges are presented too where gradients can be retrieved by automatic differentiation out of the box.

Here are some of the common methods often use in solving Multi-Objective Optimization problems,

$\varepsilon - Constraint\ Method$: In the constraint method, one of the Objective is optimized but the remaining of the objectives are set as the constraints within the user preference see (5) extension from (1)

$$\begin{aligned} min\ f_q(X) \leq \varepsilon_\mu, \quad & k = 1, \dots, K, \quad k \neq q \\ s.t\ \ g_j(X) \leq 0, \quad & j = 1, \dots, J \\ h_m(X) = 0, \quad & m = 1, \dots, M \\ x_i^L \leq x_i \leq x_i^U, \quad & i = 1, \dots, N \end{aligned} \quad (5)$$

The method can be used in either convex or non-convex MOO problems. However, there is need to take care while choosing $\varepsilon - vector$ to ensure that it is within the range of minimum and maximum values of the individual objective function.

Weighted Sum Methods: in this method, all the objectives in the MOO, or set of Objectives are first scalarize into a single objective by summing each objective pre-multiplied by user defines or supplied weight. See (6)

$$\begin{aligned} minmize\ \ F(x) = & \sum_{k=1}^{K} w_k f_k(x) \\ s.t\ \ g_j(X) \leq 0, \quad & j = 1, \dots, J \\ h_m(X) = 0, \quad & m = 1, \dots, M \\ x_i^L \leq x_i \leq x_i^U, \quad & i = 1, \dots, N \end{aligned} \quad (6)$$

Weighted Metric Method: This is another method just like weighted sum method, this one adds up all the multiple Objective based on weighted distance metric of any solution from the ideal solution z^* see (7) for the expression of such condition.

$$\begin{aligned} l_p(x) = & \left(\sum_{k=1}^{K} w_k |f_k(x) - z_k^*|^p \right)^{\frac{1}{p}} \\ s.t\ \ g_j(X) \leq 0, \quad & j = 1, \dots, J \\ h_m(X) = 0, \quad & m = 1, \dots, M \\ x_i^L \leq x_i \leq x_i^U, \quad & i = 1, \dots, N \end{aligned} \quad (7)$$

Several applications of multi-objective optimization problem have been extensively using in many fields for example in large scale clustering presented in article by Zhang et al (2016) and Wang et el (2018) and in some of the field like the one presented on the paper by Taboada et el (2012).

In conclusion, many scholars propose several methods; however, some method might be feasible for one or more situations while in another situation it might not be perfectly feasible.

Multi-Objective Optimization Proposed Concepts

This portion discusses, analyzes and presents some of the challenges and solution involve in multi-objective optimization, which do not appear in single objectives optimization, and then it gives ways forward in solving those problems.

First is to classify objectives base on how long they take in a process lifetime during process execution. It is classified into two categories as describe here below.

Permanent/Long-Term Objectives

Permanent or long-term objective is defined as the one that stay or is needed from the starts of a process execution up to the end of process execution that does not result in redesigning the optimal weight point since the optimal weight point remains the same. For instance, if a given process starts at time (t_0) and ends at time (t_n) , permanent objectives also start at time (t_0) and ends at time (t_n) as the process.

Periodical/Short-Term Objectives

Unlike in Permanent or Long-term objective in multi-objective optimization, a temporal objective is the one that is needed only for a particular period or for a short while, less than the time for process execution and not throughout the entire process. Periodical objectives can pop in or out at any moment during process execution time, these could be due to perturbation or any other factor which may cause it, for example consider the objectives function given below (8) in MOO

$$\min\big(f_1(x), f_2(x) \dots f_k(x)\big) \tag{8}$$

Where integers, $k \geq 2$ are the number of objectives. Out of total objective $f_k(x)$, one or more might be very crucial from the start of the process or in the middle or even towards the end of process execution but not throughout the entire process execution and somewhere somehow, the periodical objective will be no longer relevant once it is not needed.

This periodical objective which switches on and off, may results in the entire multi-objectives optimization solution being solve again and again, with and without the periodical objective, when in and out of the process execution as the optimal weight point of multi-objectives varies and are not the same when one includes or remove a given objective from many objectives.

For example, the optimal weight feasible range x^* of $W_1 \neq W_2$ of the equation in multi-objective (9) and (10) are not the same because of the absent of the objective, in other word, W_1 is not an optimal weight point of equation (10) whose optimal weight point is W_2 and $w \coloneqq [f(x^*), x^*]$

$$W_1 \coloneqq \min\big(f_1(x), f_2(x), f_3(x), f_4(x), f_5(x)\big) \tag{9}$$

The MOO (9) contains five objectives functions that need to be minimize.

$$W_2 \coloneqq \min\big(f_1(x), f_2(x), f_3(x), f_4(x), f_5(x), f_6(x)\big) \tag{10}$$

In addition, the MOO (10) contains six objectives' functions not the same as equation (9) however all the five objectives are the same with additional objective.

These gives challenge of redesigning another new optimal weight point, which is optimal for the remaining objectives, which are only relevant during execution excluding the objective that is no longer needed, or including the additional objectives as in equation (10).

Random Entry-Exit Time

Here Objectives are Indexed and ranked base on time in multi-objective optimization when dealing with short-term/periodical objectives and long-term objectives/permanent objectives mixed altogether within a process lifetime. It is very crucial to index objectives based on time they either enter (t_i) or exit $(t_i{}')$ a process for all the objectives involve for easy ranking, classification, and solving using partial optimization technique

presented here. Given time series for entry time $T = \{t_0, t_1, t_2, t_3, \dots, t_n\}$ and exit time as $T' = \{t_0', t_1', t_2', \dots, t_n'\}$.

Random Entry Time

In this case, all objectives are assumed to ends at the same time a process terminates however, their entry time into the process varies randomly. Given example of objectives function from (10) are index based on time objectives enter in a process but first their time of entry is estimated.

Supposed the following estimated time for objectives in (10) are recorded, such that $f_1(x)$ enter at t_0 , $f_2(x)$ enter at t_6, $f_3(x)$ enter at t_3, $f_4(x)$ enter at the same time as $f_2(x)$, and $f_5(x)$ enter at (t_7)

Indexing the five objectives as below:

$$(f_1(x))_{t_0}, (f_2(x))_{t_6}, (f_3(x))_{t_3}, (f_4(x))_{t_6}, (f_5(x))_{t_7} \tag{11}$$

Rearranging (11) in ascending order of entry time such that objective that enter first is rank first and given high priority, and those that enter last are given last priority or ranked last. However, for two or more objectives with same time of entry are ranks using any other criteria such as dependency on other conditions to give them high priority. If no such or any other condition exist, those objective with same entry time can be put at any order see condition (12) after rearranging.

$$(f_1(x))_{t_0}, (f_3(x))_{t_3}, (f_4(x))_{t_6}, (f_2(x))_{t_6}, (f_5(x))_{t_7} \tag{12}$$

In (12), $f_4(x)$ enter at the same time as $f_2(x)$, however it is rank first than $f_2(x)$ as it is assumed that $f_2(x)$ is dependent on $f_4(x)$. Incase such condition do not exist, and then their order of ranking won't be an issue.

Random Exit Time

Here, all objectives are assumed to enter at the same time when process execution begins however, their exit time out of the process varies. Given example of objectives function from (12) are indexed base on time objectives exit a process but first their time of exit out of the process is estimated.

Supposed the following estimated exit time for objectives in (12) are noted, such that $f_1(x)$ exit at t'_2 , $f_2(x)$ exit at t_6', $f_3(x)$ exit at t'_3, $f_4(x)$ exit at the same time as $f_2(x)$, and $f_5(x)$ exit at t'_7

Indexing the five objectives as below:

$$(f_1(x))_{t'_2}, (f_2(x))_{t'_6}, (f_3(x))_{t'_3}, (f_4(x))_{t'_6}, (f_5(x))_{t'_7} \tag{13}$$

Rearranging (13) in descending order of exit time such that objective that exit first is rank last and given low priority, and those which exit last are given high priority or ranked first. However, for two or more objective with same time of exit are ranked using any other criteria such as dependency on other conditions, to give them high priority. If no such or any other condition exist, those objectives with same exit time can be put at any order see condition (14) after rearranging.

$$(f_7(x))_{t'_2}, (f_4(x))_{t'_6}, (f_2(x))_{t'_6}, (f_3(x))_{t'_3}, (f_1(x))_{t'_2} \tag{14}$$

In (14), $f_4(x)$ exit at the same time as $f_2(x)$ however, it is ranked first than $f_2(x)$ as it is assumed that $f_2(x)$ is dependent of $f_4(x)$. Incase such condition do not exist, then their order of ranking won't matter.

Mixed Random Entry-Exit Time

In this scenario, it is based on the idea that in multi-objective optimization some objectives have random entry and exit time in that an objective can enter at any time and exit at any time before the process terminate and for

all objectives in a process, their entry and exit times are scatter randomly within the process. Also considering this process also contains permanent objectives. It is like a combination of objective with varying entry-exit time.

Take for instance the case below:

$$\begin{cases} f_1(x) \Longrightarrow \text{enter}(t_0) \rightarrow \text{exit}(t'_2) \\ f_2(x) \Longrightarrow \text{enter}(t_4) \rightarrow \text{exit}(t'_6) \\ f_3(x) \Longrightarrow \text{enter}(t_3) \rightarrow \text{exit}(t'_3) \\ f_4(x) \Longrightarrow \text{enter}(t_6) \rightarrow \text{exit}(t'_6) \\ f_5(x) \Longrightarrow \text{enter}(t_7) \rightarrow \text{exit}(t'_7) \end{cases}$$

For case above with different entry-exit time, there are two scenarios prior to ranking using time of entry or exit.

We consider Exit time(T') and Entry time(T) so we rank them by taking which is more important, Entry time or Exit time. If we priorities Entry time (T), then we can rank them base on entry time only and ignore exit time(T'), See (11) where it is ranked base on entry time so exit time is of less or no priority.

However, for the case when exit time is of high priority, entry time is ignored. See (14). Many approaches can be use more efficiently for this special case.

Uniform Exit-Entry Time

In this case, all objectives, exit at (t_i') and another enter at (t_i) in a process at the same time; one or more time in a process $P(Y)$ noting that $t_i' = t_i$. The question is how to handle this scenario. One of the way presented here is to split the process into multi-Process referred to as sub-process $p(y)$ within a process. Given that $\{p_1(y), p_2(y), p_3(y), \dots, p_n(y)\} \in P(y),\ y \in Y$ and parameter (y) of the process represents the objectives to be executed within a process $y = \{f_1(x), f_2(x), f_3(x) f_4(x), f_5(x) \dots . f_k(x)\}$. Where the objective ends, a new one starts. In addition, each sub-process is solved separately by using the presented methods just normally like a full objective within a process.

However, splitting a process into a sub-process does not means terminating the entire process. The previous sub-process terminates and the new sub-process continuous instantaneously as the previous sub-process exits. For example, of two sub-processes $p_1(y)$, $p_2(y)$ see (15) where objectives $f_1(x), f_2(x), f_3(x)$ all terminates at time t_6' and objectives $f_4(x), f_5(x)$ begins at time t_6 but as you know $t_6 = t_6'$

$$P(y) = \left\{ p_1(y) \begin{cases} f_1(x) \Longrightarrow enter(t_0) \rightarrow exit(t'_6) \\ f_2(x) \Longrightarrow enter(t_4) \rightarrow exit(t'_6) \\ f_3(x) \Longrightarrow enter(t_3) \rightarrow exit(t'_6) \end{cases} \middle| p_2(y) \begin{cases} f_4(x) \Longrightarrow enter(t_6) \rightarrow exit(t'_8) \\ f_5(x) \Longrightarrow enter(t_6) \rightarrow exit(t'_{10}) \end{cases} \right\} \tag{15}$$

Given that $t_i = t_{i+1}$

Now for the first sub-process can be group, index using random Entry-Exit time method for ranking and solve by either partial optimization or Objective Classification, ranking, Estimation and Predictive measurement presented here below.

The second sub-process also follows the procedure for the first one and it continues for all the sub-process up to the last one.

Partial Optimization Concept in Multi-Objective Optimization

In response to the challenges due to the presents of periodical objective in multi-objective optimization, I present some concepts that is about partial optimization of many objectives in multi-objective optimization; two initial ideas related are presented.

Iterative Multi-Level Approach

The approach is iterative in that, it involves taking two or more solvable set from multiple objectives set and their optimal weight W_q for the sub-set solve. This solution becomes or is set as constraints of the next solvable set or objectives from the multiple set. It is done iteratively until all objectives are finished and the final optimal weight point is assumed the most optimal weight among multi-objectives, which favor the objective with the highest priorities.

Consider objective function (16) or recall the equation from (1).

$$min\big(f_1(x), f_2(x), f_3(x), \dots, f_k(x)\big) \quad \text{Where} \quad x \in X \tag{16}$$

In addition, integers $k \geq 2$ are the number of objectives set X are input variables of objective function. However, element $x^* \in X$ is further defined as feasible solution or feasible decision of an objectives vector.

$$W \coloneqq [f(x^*), x^*] \in \mathbb{R}^k \tag{17}$$

Initially, first take the second objective function $f_2(x)$ and set the previous (first) objective function $f_1(x)$ as a constraint. Find the optimal weight W_0 as their optimal weight between the two objectives just like the one presented in a paper by Yang (2012) which attempt to solve two or more objective by setting one objective as a constraint and another objective to be minimize. However, the difference in their method is that when solving many objectives, one of the objectives is optimized meanwhile the rest of the remaining objectives are set as constraints. For this partial optimization, an objective is optimized and their optimal weight feasible range is set as a constraint of the next objective to be optimized in the MOO. This is done iteratively until all objectives are finished.

Please note (18) shows the condition is also subjected to constraints either inequality, equality and or bounded constraint as explained in (1).

$$\begin{gathered} W_0 \coloneqq \min\big(f_2(x)\big) \\ s.t \;\; f_1(x) \leq \varepsilon_q \,, \;\; g_j(X) \leq 0, \qquad j = 1, \dots, J \\ h_m(X) = 0, \qquad m = 1, \dots, M \\ x_i^L \leq x_i \leq x_i^U, \quad i = 1, \dots, N \\ W_l \leq \varepsilon_1, \;\; l = 1, \dots, L \end{gathered} \tag{18}$$

Next iteration is to take objective function $f_3(x)$ and set the previous optimal weigh W_0 for objectives function $f_1(x),\ f_2(x)$ as a constraint to find optimal weight W_1. See (19).

We set W_0 as constraints of the currently being optimized function simply to ensure that the currently being optimized function should not interfere with already optimized function (weight).

$$\begin{gathered} W_1 \coloneqq \min\big(f_3(x)\big) \\ s.t \;\; W_0 \leq \varepsilon_1 \end{gathered} \tag{19}$$

The process continues until all the functions in multi-objectives $f_k(x)$are finished and the final weight W_μ is assumed the optimal weight for all objectives. An overall formulation is as below (20):

$$\begin{gathered} W_q \coloneqq min\big(f_{q+2}(x)\big) \\ s.t \;\; W_{q-1} \leq \varepsilon_q \end{gathered} \tag{20}$$

However, alternatively instead of using the method presented in (18) for solving bi-objective optimization, the first objective is optimized as single objective optimization problem as below (21):

$$\begin{gathered} W_0 \coloneqq min\big(f_1(x)\big) \\ s.t \;\; g_j(X) \leq 0, \\ h_m(X) = 0, \end{gathered} \tag{21}$$

So followed by second optimization while setting first optimal weight as constraint to second optimization see (22)

$$W_1 \coloneqq \min\left(f_2(x)\right) \quad s.t \;\; W_1 \leq \varepsilon_0 \tag{22}$$

The process continues until all the functions in multi-objectives $f_k(x)$are finished and the final weight W_μ is assumed the optimal weight for all objectives. An overall formulation is as below (23):

$$W_q \coloneqq \min\left(f_{q+1}(x)\right) \quad s.t \;\; W_q \leq \varepsilon_{q-1} \tag{23}$$

Weight Convergence Optimization

The second approach is by dividing a given set of objectives into several small sub-sets of objectives, which is easily solvable without much burden, and each sub-set, solve separately see (24). Let $W_{q,i}$ where μ, and i are integers of weight level and set of weight respectively. Weight Level zero $W_{0,i}$

$$min\begin{pmatrix} W_{0,0}\left(f_1(x), f_2(x), f_3(x), \dots, f_{k1}(x)\right), W_{0,1}\left(f_{k1+1}(x), f_{k1+2}(x), f_{k1+3}(x), \dots, f_{k2}(x)\right), \dots \\ \dots, W_{0,i}\left(f_{kn+1}(x), f_{kn+2}(x), f_{kn+3}(x), \dots\dots, f_k(x)\right) \end{pmatrix} \quad s.t \;\; W_{0,i} \leq \varepsilon_0 \quad k1 < k2 < kn < k; n \in \mathbb{N} \tag{24}$$

The process continues up to a set of weight with a single element (weight point) $W_{q,0}$ and that is assume to be an optimal weight point for multi-objective optimization see (25). Weight Level μ for $W_{q,0}$

$$min\left(W_{q,0}(\dots\dots), W_{q,1}(\dots\dots.), W_{q,2}(\dots\dots.), \dots., W_{q,i}(\dots\dots)\right) \quad s.t\, W_{q-1,i} \leq \varepsilon_q \tag{25}$$

Objectives Classification, Ranking, Estimation, Prediction

The second approach, which is based on the followings, objective classification, Ranking, Estimation, and Predictive measurement to find how far a system will deviate from a preferred optimal weight. This is in the present of a decision maker (DM), where there could be preference.

The following steps are how the process can be executed in order to find an optimal weight point.

Step 1: Objectives Classification

Several criteria can be used to classify objectives. For instance, each objective can be categories as independence and dependence objective. Independence is an objective which does not rely on other objectives as oppose to dependence objective, which depend on other objectives in other word solving one objective, affect the other which is dependent on it also known as Pareto Optimal solution which means a solution that cannot be improve without degradation of at least some of the solutions. Another way of classifying objectives is by categorizing them into either temporary or permanent objective as discussed above. This is mainly to priorities and takes care of objectives such that when dynamically choosing weight, such objectives are taken care of.

Step 2; Objective Ranking

In this step 2 of objective ranking, in a set of multi-objectives, objectives are first rank in order of preference or merit base. Second, each individual participating objective their minimum or maximum optimal weight point is determined such that when finding weight such points are taken care of. Furthermore, objective can be rank in order with which they exit process execution, starting with the one that exit earliest being the last to be optimize and the one that exit last being the first to be optimize in partial optimization. The same applies to the order with which Objectives enter into a process, i.e., those that enter first are rank first up to the one that enter last into the process.

For instance, x_i^L and x_i^U are defined as lower and upper bound limits or constraints see (1) for both minimum and or maximum optimal weight point for a given single objective see condition (26) or from condition (1).

$$x_i^L \leq x^* \leq x_i^U \tag{26}$$

Step 3: Objective Estimation

In estimation stage, this requires prior knowledge of objectives ranking and classification, then an optimal weight point is first estimated that certifies the ranking and classification in step 1 and 2.

Step 4: Objective Prediction.

This step is based on the principle of predictive measurement in that control variable can be predicted base on prior and current state, and hence a control strategy is using such that a controller parameter is adjusted accordingly to meet the estimated weight point of multi-objective optimization base on step 1 and 2.

Suppose δd is deviation between estimated desired optimal weight W_e and predicted optimal weight W_p and in addition W_e and W_p if are quantifiable i.e., can be express numerically as express in (27):

$$\delta d = |W_e - W_p| \tag{27}$$

As $\delta d \to 0$, the better as the condition can be express as $0 \leq \delta d \leq \Delta$ where Δ is deviation limits within which δd is unacceptable and an appropriate strategy needs to be put in place to drive the system towards zero i.e., $\delta d \leq \Delta$.

The best predicted optimal weight occurs when $\delta d = 0$ or when $|W_e - W_p| = 0$. Although theoretically it is convincing and achievable, in practice it could be very difficult to reach $\delta d = 0$, however $\delta d \leq \Delta$ is fine.

Objective Alignment in Partial Optimization.

In the above method presented under partial optimization, Objectives has to first be aligned in order to make it easily possible to remove an objective or many objectives without needs to redesign the entire solution. This is purposely to give temporary objective less priority and permanent objective very high priority.

a. Classification.
First before beginning to optimize the entire multi-objective using method of either iterative or weight convergence, it is first classified into either periodical or permanent objectives. This is to give temporary objective less priority and permanent objective very high priority

b. Ranking
After classifying the objective, it is further ranked base on the time the objectives take to exit the process before the process execution ends, then optimization is done in a way that objective which are classified as permanent are optimized first without any preference. In addition, the one that are classified as temporary or periodical objective are then optimized later by ranking them in the order with which they enter or exit the process and the one that exit earliest or enter last will be optimized last such that removing will not affect or need to redesign the entire equation. See equation below (28) and (29) where $f_5(x)$ is removed and the previous weight W_2 automatical become the weight of the current equation without the present of the objective function $f_5(x)$.

$$W_3 \coloneqq \min\big(f_1(x), f_2(x), f_3(x), f_4(x), f_5(x)\big) \tag{28}$$

The MOO (28) contains five objectives function, which need to be minimized.

$$W_2 \coloneqq \min\big(f_1(x), f_2(x), f_3(x), f_4(x)\big) \tag{29}$$

The same applies to weight convergence method where permanent objectives are classified and optimized separately and the one, which are temporary or periodical, are optimize separately. Then later they are finally

optimized such that removing portion of the periodical objectives does not affect the entire solution weight (optimal weight point) and resulting in reo.

Sample Problem

Here two sample examples are disused from different point of view such as graphical, analytical and the second example is about real-world example which involve time governed Multi-Objective Optimization problem with bounded constraints.

Mathematical Optimization Sample Problem

Example 1: Consider an example of time governed Tri-Objectives Optimization problems (30) where there are three objectives with bounded unconstraint,

$$\begin{gathered} f_1(x) = 0.5x^2 + sin(x^2) \quad ; \quad t_0 \rightarrow t_6' \\ f_2(x) = x^2 - 1.4x - 1.5 \quad ; \; t_3 \rightarrow t_6' \\ f_3(x) = x^2 - 1.1e^{-x^2} - 1 \quad ; \; t_0 \rightarrow t_4' \\ \text{Search domain} \quad -3 \leq x \leq 3 \end{gathered} \tag{30}$$

From the above, to optimize the three objectives, we first optimize single objective under bounded constraint given above. So, since objective $f_1(x)$ is the only objective that starts from beginning up to the end of the process. it is given highest priority followed by objective $f_3(x)$ which starts from beginning but stop somewhere in the middle of the process, and last is objective $f_2(x)$ which enter into the process not from the beginning but in the middle and stops at the end of the process.

First Step:

$$\begin{gathered} w_0 = \min f_1(x) \\ \text{s.t} \; -3 \leq x \leq 3 \end{gathered}$$

Therefore, $w_0 := [f_1(x^*), x^*]$ so, $[f_1(x^*), x^*] = [2.9e^{-31}, 4.44e^{-16}]$

Which is approximately in the range of $0 < x < 0.1$ for the feasible solution of the first objective.

This feasible solution range is therefore use to set bounded constraints for the next objective to solve to ensure that the feasibility range of the first optimized objective is protected.

Second Step:

$$\begin{gathered} w_1 = \min f_3(x) \\ \text{s.t} \quad 0 < x < 0.1 \end{gathered}$$

So, since $f_3(x)$ is next to be optimized, $w_1 := [f_3(x^*), x^*]$ so, $[f_3(x^*), x^*] = [-2.1, 3.998e^{-5}]$

Which is approximately in the range of $0 < x < 0.1$ for the feasible solution of the first objective.

These feasible solution range is therefore use to set bounded constraints for the next objective to be solve to ensure that the feasible range of the second optimized objective is protected. However, if we are to keep the bound rang of the first Objective, $-3 \leq x \leq 3$ one finds that $[f_3(x^*), x^*] = [-2.1, -3.3307e^{-16}]$ which is still within the range. We take the range of $0 < x < 0.1$

Third Step:

$$\begin{gathered} w_2 = \min f_2(x) \\ \text{s.t} \quad 0 < x < 0.1 \end{gathered}$$

Finally, $f_2(x)$ the last to be optimize, $w_2 := [f_2(x^*), x^*]$ so, $[f_2(x^*), x^*] = [-1.63\ , 0.1]$.

However, if we are to keep the bound range for the first one $-3 \leq x \leq 3$, one finds that $[f_2(x^*), x^*] = [-1.99\ , 0.7]$ which makes the feasible solution range of $0 < x < 0.7$ when the first and the second objectives are not priorities or given higher rank. If given higher rank, so the range has to be in $0 < x < 0.1$. To ensure that optimal weight point is given respect, favors objectives with higher priority, and not deviated when finding the least objective in the rank. Therefore, any solution in the range of $0 < x \leq 0.7$ would be an optimal solution for the three objectives.

Please note an Objective in MOO may be short live (periodical) but still have the highest priority, likewise, an objective may too be long live (permanent) but still have lowest priority.

See below figure 1 shows graph of the three objectives plotted on a graph.

See figure 1.

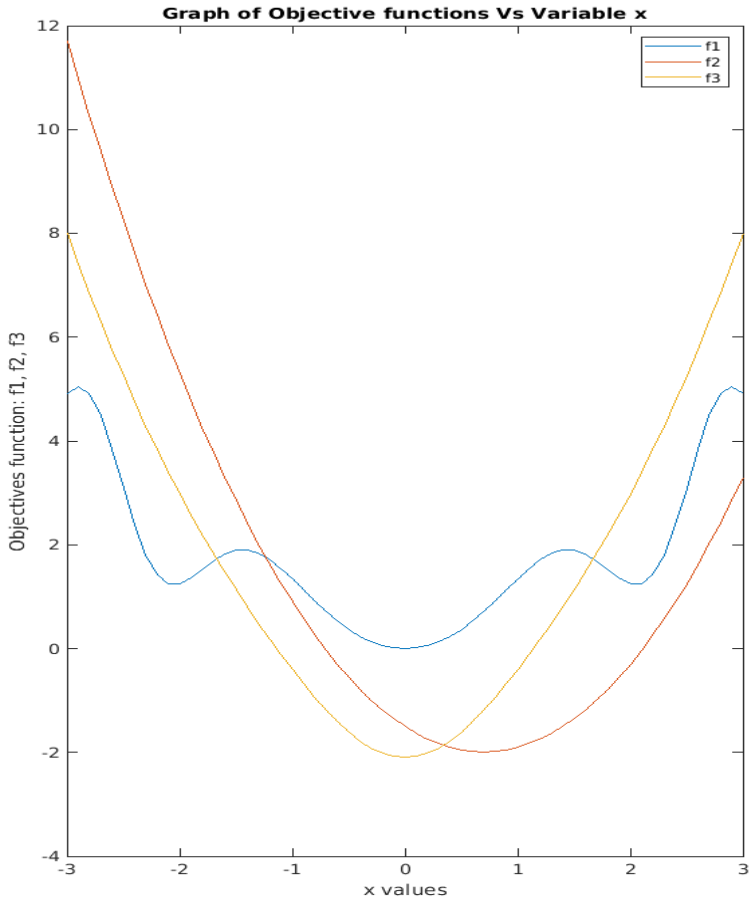

Figure 1. Shows graph of Objectives function (f1, f2, f3) against x variable

Example 2:

Another example here in (31) shows MOO with two input variables i.e., x_1, x_2
It is extended from example (30), so reader can try to solve.

$$\begin{aligned} f_1(x_1, x_2) &= 0.5(x_1^2 + x_2^2) + sin(x_1^2 + x_2^2) \quad ; \quad t_0 \rightarrow t_4' \\ f_2(x_1, x_2) &= (x_1^2 + x_2^2) - 1.4(x_1 + x_2) - 1.5 \quad ; \quad t_3 \rightarrow t_6' \\ f_3(x_1, x_2) &= (x_1^2 + x_2^2) - 1.1e^{-(x_1^2 + x_2^2)} - 1 \quad ; \quad t_0 \rightarrow t_6' \end{aligned} \tag{31}$$

Search domain $-3 \leq x_1, x_2 \leq 3$

Solutions:

This sample problem is left for reader.

Real World Optimization Sample Problem

Here is another example 3, a Bi-Objective Optimization Problem where first Objective is to minimize time for cargo loading and Offloading on Cargo Ship and the second Objective is to minimize Space in the Cargo Ship by proper arrangement. This is based on Sipping industry where Cargo (Container) ship need to be optimized for transportation. This example is an extract from published article by (Ajay Menon, Marine Insight, 2021) webpage, and modified in order to fit this scenario.

Please note: This example 3 may not be a perfect example to depict the situation in Time Governed MOO, but it is an illustration of such scenario, author's attempt to show.

Example 3:

A Cargo (Container) Ship is set to sail from Port A to port C via Port B. The Ship is supposed to load a total of $'n'$ Containers from Port A of which half of it i.e $0.5n$ will be unloaded at Port B and from Port B, another 3 container will be loaded onto the ship for final destination to port C $(0.5n + 3)$.

1-Design loading arrangement plan of the Containers on the Cargo Ship such that time for transporting is minimized in a way that unloading and loading container at port mid-way to final destination does not result into unloading the entire containers to access those at the bottom, hence causing delays of time and wastage of energy.

2-Minimize space of the Cargo Ship too with the arrangement plan.

a. Unconstraint

In this part, no condition or constraint is attached.

Solution:

The solution for this is quite straight forward as there is no constraint attached to the container arrangement plan.

Answer: Containers to be transported from Port A to final destination Port C should be loaded first at the bottom on the Container Ship.

The remaining Containers to be unloaded at mid-way Port B should be loaded on top such that at Port B, unloading them won't affect those at the bottom and won't result into unloading the entire container to access those at the bottom hence minimizing time for unloading and loading.

Please note different arrangement plan can be design for these.

b. Constraint

The constraints in this case is that the heaviest Containers should be loaded first at the bottom followed by heavier one, up to the lightest containers loaded on top. This is to avoid damaging lighter container when loaded at the bottom and distorting Cargo Ship stability. I.e. To avoid shifting center of gravity of the Cargo Ship. This implies that heavier containers should be at the bottom and Containers should be equally distributed or spread across the Ship's bed so that it does not concentrate on only one side.

If out of the $0.5n$ containers to be unloaded at port B, about 0.75 of those are containers carrying heavy materials and all the containers to be unloaded at final destination are light containers. In addition, the three Containers to be loaded from port B are very heavy Containers.
Design loading plan for such a Scenario to minimized time for transportation, and empty spaces on the Cargo ship.

Solution

Solution is left for reader.

Analysis of the Concepts

The following analysis attempt to shows some drawback of existing methods and advantages of this propose methodology compared to the currently existing methods

Disadvantage of Existing methods Compared to Presented Concepts

In most of the current methodologies presented by many scholars tries to solve all multi-objective problem simultaneously which when periodical/short-term objectives is added or remove may result in destabilizing the optimal weight point hence need to redesign the entire solution again. This is not that much problem, however during runtime, it could be tiresome and the hardship to resolve the same thing repeatedly. for example, in equation given in (9) and (10) where objective is removed and the entire weight are not the same as (28) and (29).

Advantage of Presented Concepts

The advantage of this solution presented here is that unlike other existing solutions, partial objective optimization an objective can be remove safely without need to redesign the entire equation as the previous solution become the current solution without need to solve again. In addition, addition of an objective does affect much, all is needed is to optimize that objective together with existing solution as explained above. However, objective classification and ranking should be carefully done to ensure alignment before optimization.

Conclusion

Due to ultimatum in seeking the best optimal solution in multi-objective optimization, this paper discusses some notable published paper by scholars, which presents the novel technique in tackling problems in multi-criteria optimization such as evolutionary algorithm methods, flower pollination algorithm and many more. However, the author further notices some dare in the area of multi-objective optimization where there is situation when one or more objectives are needed either in the beginning or towards the ends or even in the middle of the process execution. The author called this as periodical or temporary objectives or short-term Objective unlike usual objectives that are needed from the start up to the end of process execution. This is called permanent or long-term objectives. The problem with this is that every time we add or remove an objective from a running process with multiple objectives may results in destabilization of existing optimal weight point as shown in example (9) and (10). In respond to the challenges, the author presented a theoretical concept, which uses partial optimization iteratively including some methods which use objective classification, ranking, estimation and predictive measurement. These concepts are very convincing theoretically, however their feasibility is far beyond the scope of this paper. Further in-depth studies will still be conducted to check the practical application and its feasibility in real world scenario including a numerical simulation or any analytical solution when conducted.

Future research direction: Although this paper presents concepts about partial optimization, and Objective Classification, Ranking, Estimation and Prediction, Further examination or testing of concepts about Estimation and Prediction need to done, as the paper only cover concepts on partial optimization, Classification and, Ranking. Therefore, Estimation and Prediction remains concepts proposed but their feasibility is still beyond the scope of this paper.

Scientific Ethics Declaration

The author declares that the scientific ethical and legal responsibility of this article published in EPSTEM journal belongs to the author.

References

Białaszewski, T., & Kowalczuk, Z. (2016). Solving highly-dimensional multi-objective optimization problems by means of genetic gender. In *Advanced and Intelligent Computations in Diagnosis and Control*. (pp. 317-329). Springer.

Blank, J., & Deb, K. (2020). Pymoo: Multi-objective optimization in python. *IEEE Access*, *8*, 89497-89509.

Boukas, E. K., Haurie, A., & Michel, P. (1990). An optimal control problem with a random stopping time. *Journal of Optimization Theory and Applications*, *64*(3), 471-480.

Farran, M., & Zayed, T. (2015). Fitness-oriented multi-objective optimisation for infrastructures rehabilitations. *Structure and Infrastructure Engineering*, *11*(6), 761-775.

Fazlollahi, S., Becker, G., Ashouri, A., & Maréchal, F. (2015). Multi-objective, multi-period optimization of district energy systems: IV–A case study. *Energy. 1*(84), 365-381.

Khalil, I. S., Doyle, J. C., & Glover, K. (1996). *Robust and optimal control*. Prentice hall.

Kumar, D., Sharma, A., & Sharma, S. K. (2012). Developing model for fuel consumption optimization in aviation industry. *Innovative Systems Design and Engineering*, *3*(10), 26-37.

Kwakernaak, H., & Sivan, R. (1972). *Linear optimal control systems*. Wiley-Interscience.

Lewis, F. L., Vrabie, D., & Syrmos, V. L. (2012). *Optimal control*. John Wiley & Sons.

Miettinen, K., Ruiz, F., & Wierzbicki, A. P. (2008). Introduction to multiobjective optimization: Interactive approaches. In *Multiobjective optimization* (pp. 27-57). Springer.

Okello, M. (2020). *Multi-objective optimization concept based on periodical and permanent objective within a process.* Preprints. (doi: 10.20944/preprints202005.0331.v1).

Sayin, S. (2003). Nonlinear multiobjective optimization kluwer academic publishers. *European Journal of Operational Research. 148*(1), 229-230.

Shokoohi, M., Tabesh, M., Nazif, S., & Dini, M. (2017). Water quality based multi-objective optimal design of water distribution systems. *Water Resources Management*, *31*(1), 93-108.

Taboada, H. A., Baheranwala, F., Coit, D. W., & Wattanapongsakorn, N. (2007). Practical solutions for multi-objective optimization: An application to system reliability design problems. *Reliability Engineering & System Safety*, *92*(3), 314-322.

Vinter, R. B., & Vinter, R. B. (2010). *Optimal control*. Birkhäuser.

Wang, R., Lai, S., Wu, G., Xing, L., Wang, L., & Ishibuchi, H. (2018). Multi-clustering via evolutionary multi-objective optimization. *Information Sciences*, *450*, 128-140.

Wang, Y., Lin, X., Pedram, M., Park, S., & Chang, N. (2013, March). Optimal control of a grid-connected hybrid electrical energy storage system for homes. In *2013 Design, Automation & Test in Europe Conference & Exhibition (DATE)* (pp. 881-886). IEEE.

Wrzaczek, S., Kuhn, M., & Frankovic, I. (2020). Using age structure for a multi-stage optimal control model with random switching time. *Journal of Optimization Theory and Applications*, *184*(3), 1065-1082.

Xiao, C., Xiongqing, Y. & Yu, W. (2018). Multipoint optimization on fuel efficiency in conceptual design of wide-body aircraft. *Chinese Journal of Aeronautics*, *31*(1), 99-106.

Yang, X. S. (2012). Flower pollination algorithm for global optimization. In *International conference on unconventional computing and natural computation* (pp. 240-249). Springer.

Zhang, X., Tian, Y., Cheng, R., & Jin, Y. (2016). A decision variable clustering-based evolutionary algorithm for large-scale many-objective optimization. *IEEE Transactions on Evolutionary Computation*, *22*(1), 97-112.

Author Information

Moses Oyaro OKELLO
Address: Jiangsu University of Science and Technology
Gulu, Uganda
Contact e-mail:*mosesokellomoses@gmail.com*

To cite this article:

Okello, M.O. (2021). Time governed multi-objective optimization. *The Eurasia Proceedings of Science, Technology, Engineering & Mathematics (EPSTEM), 16*, 167-181.

The Eurasia Proceedings of Science, Technology, Engineering & Mathematics (EPSTEM)
ISSN: 2602-3199

The Eurasia Proceedings of Science, Technology, Engineering & Mathematics (EPSTEM), 2021

Volume 16, Pages 182-190

IConTES 2021: International Conference on Technology, Engineering and Science

Do API-Migration Changes Introduce New Bugs?

Omar MEQDADI
Jordan University

Shadi ALJAWARNEH
Jordan University

Muneer BANI YASSEIN
Jordan University

Abstract: Software quality is broadly dependent on the use of dependent platforms, compilers, and APIs. This research reports a case study exploring the risk of API-migration activities in the regard of bug-introducing changes and software maintenance quality. The study involves screening tens of thousands of commits for six large C++ open source systems to identify bug-introducing commits caused by undertaking adaptive maintenance tasks through using traditional heuristic approaches. The obtained results show that 14.5% to 22.2% of examined adaptive commits enclose buggy code changes and so developers have to consider the potential risk of introducing new bugs after undertaking API-migration practices. Moreover, from investigating the bug fixing activities made by API-migration tasks, we provide a demonstration that typically these fixing activities do not cause further bugs and hence are safe undertakings. We feel that this work has developed a data set that will be used for constructing approaches to identify, characterize, and minimize potential adaptive maintenance practices that introduce bugs into a software system.

Keywords: Bug-introducing commits, Adaptive maintenance, API migration, Cchange commits

Introduction

When developers evolve software systems, they frequently perform *adaptive maintenance* activities as a process to cope with changes of underlying APIs, compilers, operating systems, and dependent platforms (Swanson,1976; Schach et. al., 2003). Examples of adaptive maintenance comprise of migrating a software system to work on a new version of the underlying API (Meqdadi et. al., 2013; Meqdadi et. al., 2019).

Normally, during the evolution activities, developers perform changes that are clean (e.g., containing no bugs or defects). Unfortunately, developers sometimes unintended make improper code statements that introduce bugs into software systems (Kim et. al., 2008; Śliwerski et. al., 2005). These improper changes are termed *bug-introducing changes*. A bug in the source code negatively impacts the quality of software systems through leading the execution of systems to an undesired external behavior (Kim et. al., 2008). Sometime later, the developer who realize this behavior records the bug in a bug report that be submitted to bug tracking systems.

Recently, a rich number of studies have been undertaken to better understanding the phenomenon of bug-introducing changes by mining history repositories of software systems (Hassan et. al., 2005; Eyolfson et. al., 2011; Posnett et. al., 2013). Kim et.al (Kim et. al., 2008) used repository commits to develop a machine learning classifier that determine whether a new software change is buggy (e.g., cause a new bug) or clean change. Shedding the light on the impact of change-proneness APIs in fault-proneness of software systems have been

made previously. After studying 7,097 Android applications, Linares-Vásquez et.al (Linares-Vásquez et. al., 2013) Found that making use of a change-proneness API would negatively affect the quality of a software system. Zibran et. al. (Zibran et. al., 2011) manually examined 1,513 bug-reports extracted from bug tracking systems of different open-source projects. The study shows that 37.14% of the examined reports were relevant to the issues of API usability. However, there is no general analysis previously made on how potentially bug prone is a system after undertaking necessary adaptive maintenance changes. Unfortunately, there is no attempt in the literature to figure out whether API-migration changes are clean or buggy.

In this regard, we explore whether API-migration changes introduce new bugs into open source systems. The motivation of this work is to gain the attention of developers to take steps to focus on the possibility of introducing further bugs because of API-migration practices. The contribution of our study is to develop a data set that can be used for further investigations that interest in exploring methods to recognize, characterize, and minimize potential bug-introducing changes that might be caused by practicing adaptive maintenance activities. For instance, this study draws observations that directly guide developers involved in quality management and regression testing processes relevant to adaptive maintenance.

Therefore, we performed a case study of six C++ open-source systems that have a long evolutionary history comprises of successful API migration activities. We analyzed the history repositories and bug tracking systems used by our subject systems to determine adaptive commits that introduced bugs after accomplishing API-migration tasks. Next, we followed up our previous work in (Meqdadi et. al., 2019) and discovered whether bug-fixing activities undertaken through API-migration tasks are clean changes or lead to new bugs.

Research Questions

In our previous study undertaken in (Meqdadi et. al., 2019), we discussed the beneficial of undertaking API-migration tasks with respect to bug fixing activities. On the contrast, this study explores the risk of introducing new bugs into software systems after accomplishing demanded adaptive maintenance changes. Our hypothesis is that API-migration tasks can play an important role in the quality of software systems positively through bug fixing and negatively through introducing further bugs. Specifically, we address two main questions concerning bug-introducing changes.

RQ1) - Is there a new bug injected into system as a result of accomplishing an API-migration task?

To answer this question, we need to identify the set of bug-introducing commits of each system. Then, we have to cross intersection the list of bug-introducing commits and the list of recognized adaptive commits. The resultant intersection list with non-zero value of size means that API-migration changes might introduce bugs into systems. We view this question as an important investigation since it can be used to identify potential risks of adaptive maintenance practices. Obtained dataset from this question would serve as a baseline that is of great interest for future work focused on further studying the problematic aspects (e.g., bug-introduction) of API-migrations.

RQ2) - Is a bug fixing change through an API-migration task a clean change?

Clearly, the collection of adaptive commits that are simultaneously identified as a bug fixing and a bug-introducing commit is used to answer this question. Given this trend of adaptive commits means that a specific API-migration change might fix a bug and in conjunction introduce another into a software system. We consider this question as an important demand in order to help developers to realize whether fixing current bugs through API-migration practices is a safe process.

Study Setup

To undertake our case study, we selected diverse open source systems written in C++. The main principle behind electing our subject systems is that they all have active API-migration tasks that were undertaken successfully. In this study, for each subject system, we have identified bug-fixing commits along with relevant bug-introducing changes. Below, we present details behind our study approaches.

Studied Systems

Previously, we have identified and examined the adaptive maintenance tasks in the context of API-migration changes for several open source systems (Meqdadi et. al., 2013; Meqdadi et. al., 2019). In this research, we have chosen our dataset from six open source systems namely: four KDE packages: *KOffice*, *Extragear/graphics*, the KDE editor *Kate*, and the visual database applications creator *Kexi*. Also, we studied the 3D graphics toolkit *OpenSceneGraph (OSG)* and the full text search tool *Recoll*.

The studied systems were elected because of their active evolutionary history that include effective adaptive maintenance tasks in the context of API migrations changes. As well, we have previously inspected the undertaken adaptive maintenance changes of these selected systems in our prior research (Meqdadi et. al., 2013; Meqdadi et. al., 2019; Meqdadi et. al., 2020). For instance, the API-migration tasks of the KOffice, Extragear/graphics, and OSG systems were analyzed in (Meqdadi et. al., 2013), where their adaptive commits had been allocated through the manually reading of messages in the log files. If a message of a commit encloses key terms of API-migration tasks (i.e., APIs interfaces or language features), then the commit is considered as an adaptive commit. Similarly, the adaptive commits of the remaining systems were allocated and examined in (Meqdadi et. al., 2019) and (Meqdadi et. al., 2020), where the study proposed a machine learning classifier to label the commits of an evolution history into either one of two classes, namely adaptive and non-adaptive commits.

Next, to develop our dataset, we have used the *GNU UNIX DIFF* utility to recover the added, modified, and removed source code lines in every adaptive commit of examined projects. Alike, we determined change hunks relevant to each adaptive commit. A change hunk is defined as a continuous set of code lines that are affected by a commit along with contextual unchanged lines (Alali et. al., 2008).

Table 1 has the main information regarding our dataset. For instance, the table demonstrates the undertaken API-migration task, the examination period of time, total number of commits along with the number of adaptive commits, and the number of files and hunks touched by the captured adaptive commits of each subject system.

Identification of Bug Fixing Commits

Similar to our previous work (Meqdadi et. al., 2019), to identify whether a given change commit has fixed a bug, we employed the traditional heuristics approach (Fischer et. al., 2003; Bird et. al., 2009) that successfully and widely used for recognizing the set of bug-fixing commits from a history repository (Kim et. al., 2006). This traditional method is based on searching for valid bug reference IDs and key words (i.e., fixed, crash, or bug) within the messages of the change log file. Next, for each extracted bug's ID, we retrieve the associated bug report from the bug tracking system of the examined system. Although a commit could fix more than one bug, in this study we assume that each bug is only being fixed by one fixing commit. This aforementioned assumption represents one of the threats to validity of this work.

Identification of Bug-Introducing Commits

Our research study aims at understanding whether adaptive changes might introduce new bugs in open source systems. Therefore, we basically need to recognize the set of the adaptive commits that have introduced bugs, and then figure whether these problematic commits also have fixed earlier bugs.

The bug tracking systems are valuable resources regarding bugs. However, the major problem is that these tracking systems have no insight on when and why a bug was introduced into the code, who injected it, and where it occurred (Kim et. al., 2006; Kim et. al., 2008). That is, there is not enough information to identify bug-introducing changes immediately from bug tracking systems. Based on that, we need an approach or a tool that would help us to recognize bug-introducing changes.

Consequently, we have surveyed several valuable prior studies in the literature that have focused on examining bug-introducing commits. We have leveraged the knowledge regarding numerous known recovering methods of such problematic commits. Particularly, for our investigating experiments, we have used the approach that was proposed and effectively evaluated in (Kim et. al., 2006; Kim et. al., 2008). Initially, the approach determines bug-introducing changes from the bug-fixing commits that are recovered using the approach discussed in the prior section. Next, for each recovered fixing commit R, the approach runs the *DIFF* tool to detect all hunks in the preceding commit of R (e.g., R-1) that have been changed to fix the bug.

That is, the approach follows the assumption that deleted or modified statements in each changed hunk represent the candidate source code of relevant bug. After that, the approach tracks down the origins of source code lines in the potential buggy hunks by using the built-in *annotate* command of the version history. This feature returns the most recent commit in which a line was changed, which would be considered as the candidate bug-introducing commit. For accurateness, the approach skips all source code lines that have been changed after the bug has been reported. Furthermore, the approach removes false positives and false negatives by using annotation graphs and also by ignoring non-semantic source code changes and outlier fixes. More details regarding this approach can be regained in (Kim et. al., 2006; Kim et. al., 2008).

Table 1. Subject open-source systems of our study

	KOffice	Extragear / graphics	OSG	Kexi	Kate	QuantLib
Adaptive Maintenance Task	Migrating to Qt4	Migrating to Qt4	Migrating to OpenGL 4.x	Migrating to Qt5.x	Migrating to Qt5.x	Migration to Visual C++ 2017
Time Period	1/1/2006 – 12/31/2010	1/1/2006 – 12/31/2010	1/1/2014 - 1/1/2017	7/7/2014 – 1/1/2018	1/1/2015 – 1/1/2018	1/1/2017– 1/1/2018
# Commits in the Log File	38980	26336	1984	3283	922	628
# Adaptive Commits	131 (0.3%)	219 (0.8%)	126 (6.35%)	161 (4.90%)	54 (5.9%)	59 (9.4%)
# Adaptive Change Files	858	910	491	682	186	206
# Adaptive Change Hunks	1138	1893	1521	2104	571	550

Results and Discussion

Figure 1 illustrates the entire workflow that we performed to achieve our results for each subject system. As shown, we must first collect the set of the adaptive commits that are considered as bug-fixing commits. Then, the set of all bug-fixing commits of each subject system are collected using the identification approach discusses previously. But, this approach retrieves all bug-fixing commits regardless their type (e.g., adaptive or non-adaptive). Therefore, we have categorized retrieved fixing commits as adaptive or non-adaptive using the results of our previous studies (Meqdadi et. al., 2013; Meqdadi et. al., 2019; Meqdadi et. al., 2020). Basically, the outcome of this phase is the extraction of commits that fix bugs by performing API-migration tasks We refer to these interested adaptive commits as "*Adaptive-Bug-Fixing*" ones.

As the next step, we need to know commits that were probably induced bugs into each examined system. We have applied the identification approach of bug-introducing commits that presented previously, which depends on the annotation feature of history repositories. Again, this produces, for each subject system, a set of commits that are likely introduce bugs irrespective their type of maintenance (e.g., adaptive or non-adaptive). Also, it labels, for each bug-introducing commit, the potential buggy hunks that comprise bug-introducing code statements. To be precise, we manually examined all retrieved buggy code changes and we found they were all true candidates. For instance, no returned change was a comment line change, or a cosmetic change.

Essentially, we restricted our attention to buggy changes made by API-migration tasks. Therefore, we reused the categorization of adaptive commits performed in (Meqdadi et. al., 2013; Meqdadi et. al., 2019; Meqdadi et. al., 2020) to mark adaptive commits that would be described as bug-introducing commits. We will call these problematic commits as "*Adaptive-Bug-Introducing*" commits.

For instance, Figure 2 shows the commit #1177459 that was marked as a bug-fixing commit. From the developer message, we would observe that the adaptive maintenance task that ported the file *KoCsvImportDialog.cpp* from Qt3 to Qt4 would be considered as a bug-introducing change. After tracking down the origins of source code lines in the changed hunks of the commit #1177459 using the built-in *annotate* command, we found that the bug was originally injected because of some API incompatibilities resultant from using the modified version of class *QString* in Qt4(e.g., incompatibilities with item-based table view in the case of a default model). This using of modified *QString* was made by the adaptive commit #1132380. Thus, this adaptive commit is considered as a bug-introducing commit. The relevant buggy hunk made by this commit is shown in Figure 3.

Table 2 shows the results achieved after applying the identification approach of bug-introducing commits for each subject system. Also, the table reports the percentages of adaptive commits and change hunks that were recognized as bug-introducing. For instance, the percentages given in the second row were calculated with respect to the total number of adaptive commits while the percentages given in the third row were calculated with respect to the total number of adaptive change hunks given in Table 1.

Thereby, we could realize that *adaptive maintenance tasks (in the context of API-migration changes) might unawares introduce new bugs into open source systems*. For instance, for the OSG system, our observation is that nearly 19.0% of undertaken adaptive commits were buggy commits and caused injection of various bugs into the system. Furthermore, 14.9% of adaptively changed hunks of the OSG system involved buggy code statements.

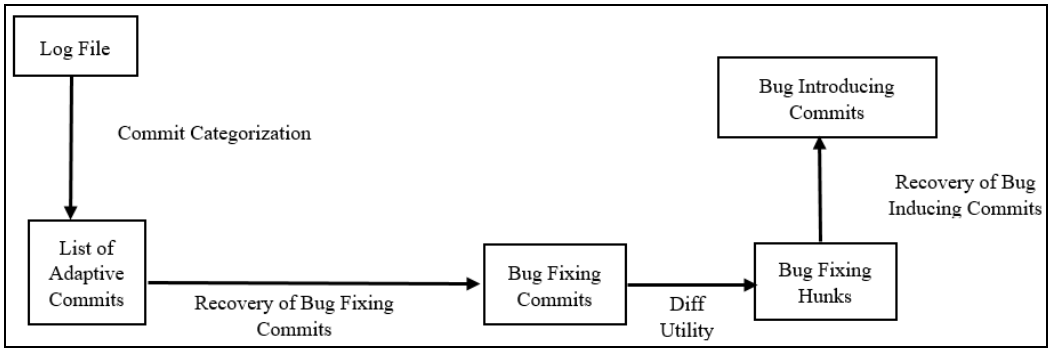

Figure 1. Workflow for study approach

Figure 2. A Snippet of a bug-fixing commit for Koffice

```
< logentry
  revision=" 1177459 ">
<author> mkruisselbrink </author>
<date>2010-09-20 T09:16:49.750410Z</date>
<paths>
<path
  kind=""action="M"> /trunk/koffice/libs/ widgets/
KoCsvImportDialog.cpp </path>
</paths>
<msg> don't crash when trying to change the format
while importing a csv file. This turned out to be both a
qt3->qt4 porting bug, and an if-condition that got
accidentally inverted about 5 years ago :)
BUG: 249773
</msg>
</logentry>
</logentry>
```

Line #	
542:	const QString header = dialog->m_sheet-> model() -> headerData(column, Qt::Horizontal).toString();
543:	if (formatList.contains(header))
544:	dialog->m_sheet->model()-> setHeaderData (column, Qt::Horizontal, i18n("Generic"));

Figure 3. A Snippet of a buggy adaptive code hunk

Table 2. Statistics from identification of bug-introducing commits

	KOffice	Extragear / graphics	OSG	Kexi	Kate	QuantLib
# of Bug-Introducing Commits	6626	4161	409	575	147	130
# of Adaptive- Bug-Introducing Commits	19 (14.5%)	39 (17.8%)	24 (19.0%)	23 (14.3%)	12 (22.2%)	18 (20.3%)
#of Buggy Adaptive Change Hunks	221 (19.4%)	414 (21.9%)	226 (14.9%)	349 (16.6%)	118 (20.7%)	111 (20.2%)

The study performed in (Meqdadi et. al., 2013) uncovered the result that adaptive commits are usually system wide and large. On the other hand, obtained results of (Śliwerski et. al., 2005) show that typically large commits are being bug-introducing commits more than other commits. Given these two studies, we can explain why adaptive commits might introduce bugs into systems. It is hardly surprising that adaptive commits that involved of large changes have a possibility for inducing later fixes.

Although most adaptive commits being clean, this type of maintenance should receive certain attention throughout testing and validation tasks. Importantly, our study uncovered the main result that *it is particularly worthy to spend efforts in quality assurance after accomplishing specific adaptive maintenance task*. For instance, developers have to confirm that adaptive commits are carefully revised and tested since these commits have a potential for introducing later bugs. Essentially, our study is a valuable source of data for further examining of bugs being introduced by adaptive changes. It is of great interest for future work to get a more detailed picture regarding buggy adaptive changes to develop automated methods to characterize, allocate, and hence avoid potential risks from undertaking demanded adaptive maintenance practices.

Our previous work presented in (Meqdadi et. al., 2019) demonstrated that undertaking API-migration tasks are supportive for fixing a set of existing bugs in open source systems. In contrast to the previous study, after answering RQ1, it will be a paramount investigating to figure out whether the adaptive maintenance could be recommended as a safe approach to fix current bugs of a software system. That is, a fair question to ask now is, is a bug fixing change through an API-migration task a clean change? In order to answer this question, we further examined the sets of extracted *Adaptive-Bug-Introducing* and *Adaptive-Bug-Fixing* commits. We have defined a new classification of adaptive commits. The new category involves adaptive commits that had fixed a bug and simultaneously introduced another into a software system. We refer to this category as "*Adaptive-Bug-Fixing-Inducing*".

Certainly, the group of Adaptive-Bug-Fixing-Inducing commits represent the cross intersection between Adaptive-Bug-Fixing and Adaptive-Bug-Introducing sets. Table 3 shows the percentages of adaptive commits that are classified as Adaptive-Bug-Fixing-Inducing for each system. These percentages were calculated with respect to the total number of Adaptive-Bug-Introducing commits given in Table 2. The results are surprising. Although adaptive changes might cause new bugs, the majority of bug fixing activities that undertaken throughout API-migration tasks did not inject new bugs into systems. That is, *fixing bugs through an API-migration task is typically a clean and safe with no risks of bugs*.

Table 3. Adaptive Bug-Fixing-Inducing commits

	KOffice	Extragear/ Graphics	OSG	Kexi	Kate	QuantLib
# of Adaptive Bug-Fixing-Inducing commits	1 (5.3%)	0 (0.0%)	0 (0.0%)	0 (0.0%)	0 (0.0%)	1 (5.6%)

Threats to Validity

A first threat to the validity of our work is that our examined systems may not be representative for all software systems. For instance, our dataset was extracted from open source systems written in C++. Thus, we cannot assume all obtained results have same weight or can be generalized for other systems written in other than C++ or these results are valid for commercial systems.

A construct threat to validity of our study is that there might be adaptive commits that we did not rely on in our case study. The group of adaptive commits that were examined in our study are the outcomes from the manual

identification of adaptive commits performed in (Meqdadi et. al., 2013; Meqdadi et. al., 2019; Meqdadi et. al., 2020) that may comprise false positives and false negatives. Moreover, the presented case study here is based on the assumption that all adaptive commits being used in the undertaken experiments embraces only adaptive changes. However, developers might group both adaptive and non-adaptive changes into one version history commit.

We followed the traditional heuristics approach to identify bug fixing commits. However, we do not argue that this approach is without faults and consequently might affect the accuracy and correctness of our findings. Moreover, there is no standard how developers commit changes. Hence, some bug-fixing tasks might be accomplished through several commits. Another internal threat to validity is that we have depend on the approach proposed in (Kim et. al., 2006; Kim et. al., 2008) to obtain the set of bug-introducing commits. This approach has several limitations and so we believe that the using another accurate approach to find missing bug-introducing commits is essential. This is a one of our future plans.

Related Works

Similar to our study, lots of studies have been proposed to investigate the impact of software maintenance tasks on bug fixing activities. Kim et al. (Kim et. al., 2011) examined the role of API-level refactoring in fixing bugs for several JAVA projects such as Eclipse, JEdit, and Columba systems. They found that there are more bug fixes after finishing API-level refactoring activities. Also their results show that developers need less time to fix a bug after submitting API-level refactoring. The impact of adding new features and other code improvements with respect to bug proneness was reviewed by Posnett et al. (Posnett et. al., 2011). Their results show that code improvements might positively affect bug-fixing activities for some symptoms but could negatively influence fixing activities for other systems.

The influence of underlying API on software quality was investigated through numerous earlier studies. In (Linares-Vásquez et. al., 2013), the authors examined thousands of android applications to analyze the role of underlying API changes on software quality of a software system in terms of fault proneness. The obtained results illustrated that instability of underlying API negatively impact the quality of software projects. Similarly, Zibran et.al (Zibran et.al, 2011) found that a significant portion of reported bugs were originally related to the API usability and correctness. A case study of Apache projects was performed by Mileva et al. (Mileva et. al., 2009) to investigate the role of migration of code libraries on bug fixing efforts. The main finding of the study is that developers usually migrate back to earlier version of a library to ease the fixing efforts. Even though these studies have focused on the role of API correctness on the quality of software systems, the risk of API-migration in terms of bug-introducing changes was not considered in the literature.

There is a rich literature for examining the characteristics of bug-introducing changes using project histories. Kim et al. (Kim et. al., 2008) developed a machine learning classifier to classify whether an undertaking maintenance change is clean or buggy. Their classifier used several features of a committed change to determine if the change might introduce bugs in the future, such as added and deleted delta, author of the change, and the complexity of the modified files. The performance of the classifier was evaluated across 12 open source projects. Tufano et al. (Tufano et. al., 2017) performed an empirical study to characterize fix-inducing commits using several developers related factors. The studied factors are coherence of the commit, the experience level of developers, and the interfering changes made by other developers. The main finding of the study is that bug-introducing changes were made by more experienced developers. Also, the study shows that bug-introducing commits are usually less coherent and have more past interfering changes when compared to other commits. Rahman et. al. (Rahman et. al., 2011) studied version control systems to examine the impact of the developer experience and ownership on the possibility of introducing bugs after committing a maintenance change. The main observation is that specialized experience developers have made less defects in a software system when compared with general experience developers. The main characteristics of fix-inducing changes were investigated for ECLIPSE and MOZILLA projects in (Śliwerski et. al., 2005). The results show that that larger maintenance changes are more likely to induce future fixes. Furthermore, bug fix changes are likely to induce a future change than regular code enhancements. Despite, rather than general examination of fix-inducing changes, our study directly investigates these risky changes relevant to adaptive maintenance activities in the context of API-migration.

To the best of our knowledge, our work is the first study examines the risks of API-migration activities in terms of bug-introducing changes. There is no other work underwent previously had address this research area.

Conclusion

This work presents a case study of several C++ open source systems to determine whether adaptive maintenance changes (e.g., in the context of API-migration practices) lead to introduce new bugs into a software system. The study is based on the data obtained from software repositories of subject systems and through using traditional heuristic approaches to identify bug fixing and introducing code changes relevant to maintenance activities.

The study uncovered the main result that API-migration changes occasionally introduce new bugs into open source systems. For instance, our results show that 14.5% to 22.2% of studied adaptive commits were identified as bug-introducing commits. Thus, the observation that was obtained indicates that developers have to consider the potential risk of introducing new bugs after performing API-migration practices. On the other hand, a set of investigations was made focusing on whether bug fixing activities undertaken through API-migrations introduced new bugs. Our obtained results demonstrated that fixing current bugs by performing a specific API-migration practices is a safe process.

Our study developed a data set that will be used for further investigations of buggy changes relevant to adaptive maintenance. We expect that our future works will center on a deeply understanding of bugs that are being introduced by adaptive changes. We plan for a deep analysis of change features to identify common causality and patterns of adaptive changes that introduce bugs. We would explore the possibility of using machine learning algorithms to develop a model that automatically classify adaptive changes as buggy or clean immediately upon the accomplishment of an API-migration task.

Scientific Ethics Declaration

The authors declare that the scientific ethical and legal responsibility of this article published in EPSTEM journal belongs to the authors.

References

Alali, A., Kagdi, H., & Maletic, J. I. (2008, June). What's a typical commit? a characterization of open source software repositories. In *2008 16th IEEE international conference on program comprehension* (pp. 182-191). IEEE.

Bird, C., Bachmann, A., Aune, E., Duffy, J., Bernstein, A., Filkov, V., & Devanbu, P. (2009, August). Fair and balanced? bias in bug-fix datasets. In *Proceedings of the 7th joint meeting of the European Software Engineering Conference and the ACM SIGSOFT Symposium on the Foundations of Software Engineering* (pp. 121-130).

Eyolfson, J., Tan, L., & Lam, P. (2011, May). Do time of day and developer experience affect commit bugginess?. In *Proceedings of the 8th Working Conference on Mining Software Repositories* (pp. 153-162).

Fischer, M., Pinzger, M., & Gall, H. (2003, September). Populating a release history database from version control and bug tracking systems. In *International Conference on Software Maintenance, 2003. ICSM 2003. Proceedings.* (pp. 23-32). IEEE.

Hassan, A. E., & Holt, R. C. (2005, September). The top ten list: Dynamic fault prediction. In *21st IEEE International Conference on Software Maintenance (ICSM'05)* (pp. 263-272). IEEE.

Kim, M., Cai, D., & Kim, S. (2011, May). An empirical investigation into the role of API-level refactorings during software evolution. In *Proceedings of the 33rd International Conference on Software Engineering* (pp. 151-160).

Kim, S., Whitehead, E. J., & Zhang, Y. (2008). Classifying software changes: clean or buggy?. *IEEE Transactions on Software Engineering*, *34*(2), 181-196.

Kim, S., Zimmermann, T., Pan, K., & James Jr, E. (2006, September). Automatic identification of bug-introducing changes. In *21st IEEE/ACM international conference on automated software engineering (ASE'06)* (pp. 81-90). IEEE.

Linares-Vásquez, M., Bavota, G., Bernal-Cárdenas, C., Di Penta, M., Oliveto, R., & Poshyvanyk, D. (2013, August). Api change and fault proneness: A threat to the success of android apps. In *Proceedings Of The 2013 9th Joint Meeting On Foundations of Software Engineering* (pp. 477-487).

Meqdadi, O., & Aljawarneh, S. (2020). A study of code change patterns for adaptive maintenance with AST analysis. *International Journal of Electrical and Computer Engineering*, *10*(3), 2719-2733.

Meqdadi, O., & Aljawarneh, S. (2019, December). Bug types fixed by api-migration: a case study. In *Proceedings of the Second International Conference on Data Science, E-Learning and Information Systems* (pp. 1-7).

Meqdadi, O., Alhindawi, N., Alsakran, J., Saifan, A., & Migdadi, H. (2019). Mining software repositories for adaptive change commits using machine learning techniques. *Information and Software Technology, 109*, 80-91.

Meqdadi, O., Alhindawi, N., Maletic, J.I., and Collard, M.L. (2013). Understanding large-scale adaptive changes from version histories: a case study. *In Proceedings of the 29th IEEE International Conference on Software Maintenance, ERA Track*, (pp. 22-28).

Mileva, Y. M., Dallmeier, V., Burger, M., & Zeller, A. (2009, August). Mining trends of library usage. In *Proceedings of the joint international and annual ERCIM workshops on Principles of software evolution (IWPSE) and software evolution (Evol) workshops* (pp. 57-62).

Posnett, D., D'Souza, R., Devanbu, P., & Filkov, V. (2013, May). Dual ecological measures of focus in software development. In *2013 35th International Conference on Software Engineering (ICSE)* (pp. 452-461). IEEE.

Posnett, D., Hindle, A., & Devanbu, P. (2011, October). Got issues? do new features and code improvements affect defects?. In *2011 18th Working Conference on Reverse Engineering* (pp. 211-215). IEEE.

Rahman, F., & Devanbu, P. (2011, May). Ownership, experience and defects: a fine-grained study of authorship. In *Proceedings of the 33rd International Conference on Software Engineering* (pp. 491-500).

Schach, S. R., Jin, B. O., Yu, L., Heller, G. Z., & Offutt, J. (2003). Determining the distribution of maintenance categories: Survey versus measurement. *Empirical Software Engineering*, *8*(4), 351-365.

Śliwerski, J., Zimmermann, T., & Zeller, A. (2005). When do changes induce fixes?. *ACM sigsoft software engineering notes*, *30*(4), 1-5.

Swanson, E. B. (1976, October). The dimensions of maintenance. In *Proceedings of the 2nd international conference on Software engineering* (pp. 492-497).

Tufano, M., Bavota, G., Poshyvanyk, D., Di Penta, M., Oliveto, R., & De Lucia, A. (2017). An empirical study on developer- related factors characterizing fix- inducing commits. *Journal of Software: Evolution and Process*, *29*(1), e1797.

Zibran, M. F., Eishita, F. Z., & Roy, C. K. (2011, October). Useful, but usable? factors affecting the usability of APIs. In *2011 18th Working Conference on Reverse Engineering* (pp. 151-155). IEEE.

Author Information

Omar MEQDADI
Jordan University of Science and Technology
Irbid, Jordan
Contact e-mail: *ommeqdadi@just.edu.jo*

Shadi ALJAWARNEH
Jordan University of Science and Technology
Irbid, Jordan

Muneer BANI YASSEIN
Jordan University of Science and Technology
Irbid, Jordan

To cite this article:

Meqdadi, O., Aljawarneh, S., & Bani Yassein, M. (2021). Do API-migration changes introduce new bugs?. *The Eurasia Proceedings of Science, Technology, Engineering & Mathematics (EPSTEM), 16*, 182-190.

The Eurasia Proceedings of Science, Technology, Engineering & Mathematics (EPSTEM)
ISSN: 2602-3199

The Eurasia Proceedings of Science, Technology, Engineering & Mathematics (EPSTEM), 2021

Volume 16, Pages 191-194

IConTES 2021: International Conference on Technology, Engineering and Science

Urinary Stone in Outdoor and Indoor Workers Patients with Family History

Zena A. M. AL-JAWADI
University of Mosul

Abstract: A biochemical study of 365 patients with urinary stones disease according to occupation and family history, and the occupation divided to tow subgroups (outdoor workers (n=183) and indoor workers (n=182)) and evaluated laboratory test was done for each patients included phosphorus, calcium, uric acid, urea and creatinine in serum of patients and control group. The results showed a higher significant difference serum phosphorus, uric acid, urea and creatinine in patients outdoor workers compared with the patients' indoor workers and control group at (P=0.001), and the higher significant difference more obvious in patients with family history, as a higher significant difference serum calcium in patients with family history outdoor workers compared with the patients' indoor workers and control group at (P≤0.05). Finally, this study proved the strong relationship between occupation and urinary stones formation, the epidemiology of stones increases according to the type of occupation. In addition, the study proved that patients' outdoor workers have incidence more than patients' indoor workers, and increase with family history.

Keywords: Urinary Stone, Family History, Outdoor Workers, Indoor Workers

Introduction

Urinary stones can develop when certain chemicals in urine form crystals that stick together. The crystals may grow into a stone ranging in size from a grain of sand to a golf ball (Pearle et. al., 2005; Delvecchio et. al., 2003; Menon et. al., 2002**)**, small stones can pass through the urinary system without causing problems. However, larger stones might block the flow of urine or irritate the lining layer of the urinary tract (Pietrow et. al., 2006; Reungjui et. al., 2002; Segura et. al., 1997).

A consecutive series of patients presenting to institutions in world for the management of proven urinary stones was interviewed by questionnaires designed to obtain data on age, gender, ethnicity, occupation, stone location, a family history of certain medical disease (Lotan et. al., 2004; Anatol et. al., 2003).

Most stones 62.8% contain mainly calcium oxalate crystal, 26.8% contain uric acid stones, 9.9% phosphate stones and 0.5% cystine stones. The incidence of calcium oxalate and phosphate stones is similar to that in other studies from different countries. The incidence of uric acid stone was higher than that reported in western industrialized countries. Therefore, it seems that our stone composition lies between those of the developing and industrialized countries (Al-Jawadi, 2002).

The aim of this study to identify the risk factor of occupation on renal stones formation, to planning treatment and prevention of recurrence of stones.

Method

Our study included (365) patients with urinary stone attending the urological out patient's clinic in Al-Zahrawi Teaching Hospital in Mosul for stone removal. In the collections from North of Iraq, the patient's occupation (outdoor(n=183) and indoor(n=182)) was provided in 365 cases (excluding housewives) every patient was evaluated clinically and by a biochemical laboratory test, and compared with (50) normal subjects as control group. Biochemical analysis was done for phosphorus, calcium, uric acid, urea and creatinine in serum by using commercial kits (BioMerieux Vitek, Inc., UAS).

The statistical methods used to analyse the data include mean, standard deviation, minimum and maximum, while Z-test was used to compare between total control and total patients according to the occupation at $p \leq 0.05$ (Steel & Torrie, 1980).

Results and Discussion

The results in Table (1) showed a higher significant difference serum phosphorus and uric acid in patients' outdoor workers more than patients indoor workers compared with control group at P=0.001, P≤0.05 respectively, may be due to secondary urinary tract infection or/and stone formation (Menon & Resnick, 2002).

In addition, a higher significant difference serum urea in patients' outdoor workers more than patients' indoor workers compared with control group at P=0.001 was noted, Postrenal uraemia occurs due to outflow obstruction, which may occur at different level (i.e., in the ureter, bladder or urethra), due to renal stones. Back-pressure on the renal tubules enhances back-diffusion of urea, so that serum urea rises disproportionately more than serum creatinine (Smith et. al., 1998).

Table 1. Compares between serum phosphorus, calcium, uric acid, urea and creatinine in patients without family history and control groups according to occupation.

Parameters	Patients of urinary stones without family history (n=165)		Control (n=50)
	Outdoor workers (n=83)	Indoor workers (n=82)	
Phosphorus(mg\dl)	4.51± 1.32**	4.39 ± 1.73*	4.03±0.69
Calcium(mg\dl)	9.07 ± 1.09	8.93 ± 1.11	8.99±0.53
Uric acid(mg\dl)	4.95 ± 1.20**	4.88 ± 1.74*	4.40±1.13
Urea(mg\dl)	35.14±11.05**	33.86±10.37*	29.70±5.42
Creatinine(mg\dl)	0.88±0.29	0.84±0.367	0.77±0.12

Significant difference at P≤0.05, **Significant difference at P=0.001

These results increased incidence in individuals living in areas with a hot climate and those with predominantly sedentary work, may be because of inadequate access to bathroom facilities or drinking water, athletic activity, heat and sun exposure (Giovanni et. al., 2006; Borghi et. al., 1993). In Table (2), a higher significant difference serum uric acid and urea in patients' outdoor workers more than patient's indoor worker compared with control group at P=0.001 was noted and this agree with other study (Tosukhowong et. al., 2001).

Also, in the same table showed a significant difference in phosphorus and calcium in patients' outdoor workers more than patients indoor workers compared with control group at (P=0.001, P≤0.05) respectively, and these results agree with Pin et al study who's found the prevalence of urinary stone disease was five times higher in outdoor workers compared to indoor workers (Sharma, 2000; Pin et. al., 1992). Chronic dehydration is likely to be the most important risk factor for the increased risk of urinary stones in outdoor workers in the tropics, and should be easily prevented by increased water intake (Ozmen, 2004). Person with positive family history have a high-risk factor to increase the ratio of renal stones more than person without family history (Thun & Schober, 1991), and this agree with the results in Table (2).

The results showed a higher significant difference between serum phosphorus and calcium in patient worker (indoor and outdoor) with family history compared with patient worker (indoor and outdoor) without family history and this agree with the previous studies (Giovanni et. al., 2006; Lotan et. al., 2004). And in the same table showed a higher significant difference in serum uric acid, urea and creatinine in patient worker (indoor and outdoor) with family history compared with patient worker (indoor and outdoor) without family history may be because indicates a fall in GFR is found in urinary tract obstruction (Smith et. al., 1998), but patients' workers outdoor more than patients' worker indoor as seen in Table (2) and this agree with Krop et al studies 2007 (Krop et. al., 2007).

Table 2. Compares between serum phosphorus, calcium, uric acid, urea and creatinine in patients with family history and control groups according to occupation.

Parameters	Patients of urinary stones with family history (n=200)		Control (n=50)
	Outdoor workers (n=100)	Indoor workers (n=100)	
Phosphorus(mg\dl)	4.78±1.86**	4.51±0.97*	4.03±0.69
Calcium(mg\dl)	9.36±0.87*	9.11± 0.90	8.99±0.53
Uric acid(mg\dl)	5.19±1.08**	4.98±1.08*	4.40±1.13
Urea(mg\dl)	38.27±9.49**	37.13±8.82**	29.70±5.42
Creatinine(mg\dl)	1.21±0.30	1.09±0.39	0.77±0.12

*Significant difference at P≤0.05, **Significant difference at P=0.001

Conclusion

Finally, this study proved the strong relationship between occupation and urinary stones formation, the epidemiology of stones increases according to the type of occupation. In addition, the study proved that patients' outdoor workers have incidence more than patients' indoor workers, and increase with family history.

Acknowledgements or Notes

The researcher is grateful the Mosul University, the management.

Scientific Ethics Declaration

The author declares that the scientific ethical and legal responsibility of this article published in EPSTEM journal belongs to the author.

References

Al-Jawadi, Z. A. M. (2002). *Clinical and biochemical study of urinary stone disease in Ninevah and surrounded province* [Doctoral dissertation, Mosul University].

Anatol, T., Pereira, L. P., Simeon, D., & Sawh, L. (2003). Risk factors for urinary tract calculi in Trinidad. *Tropical medicine & international health*, *8*(4), 348-353.

Borghi, L., Meschi, T., Amato, F., Novarini, A., Romanelli, A., & Cigala, F. (1993). Hot occupation and nephrolithiasis. *The Journal of Urology*, *150*(6), 1757-1760.

Delvecchio, F. C., & Preminger, G. M. (2003). Medical management of stone disease. *Current Opinion in Urology*, *13*(3), 229-233.

Krop, E. J., Doekes, G., Stone, M. J., Aalberse, R. C., & Van der Zee, J. S. (2007). Spreading of occupational allergens: laboratory animal allergens on hair-covering caps and in mattress dust of laboratory animal workers. *Occupational and Environmental Medicine*, *64*(4), 267-272.

Lotan, Y., Cadeddu, J. A., Roerhborn, C. G., Pak, C. Y., & Pearle, M. S. (2004). Cost-effectiveness of medical management strategies for nephrolithiasis. *The Journal of Urology*, *172*(6 Part 1), 2275-2281.

Menon, M., & Resnick, M. I. (2002). Urinary lithiasis: etiology, diagnosis, and medical treatment. In *Campbell's Urology*, (pp. 3287–3289), Saunders Elsevier.

Ozmen, O. (2004). Kidney Pathology in Non- obstructive Urolithiasis in Cattle. *Journal of Veterinary Medicine Series A*, *51*(9- 10), 405-408.

Pearle, M. S., Calhoun, E. A., Curhan, G. C., & Urologic Diseases of America Project. (2005). Urologic diseases in America project: urolithiasis. *The Journal of Urology*, *173*(3), 848-857.

Pietrow, P. K., & Karellas, M. K. (2007). Medical management of common urinary calculi. *South African Family Practice*, *49*(3), 44-48.

Pin, N. T., Ling, N. Y., & Siang, L. H. (1992). Dehydration from outdoor work and urinary stones in a tropical environment. *Occupational Medicine*, *42*(1), 30-32.

Reungjui, S., Prasongwatana, V., Premgamone, A., Tosukhowong, P., Jirakulsomchok, S., & Sriboonlue, P. (2002). Magnesium status of patients with renal stones and its effect on urinary citrate excretion. *BJU İnternational*, *90*(7), 635-639.

Segura, J. W., Preminger, G. M., Assimos, D. G., Dretler, S. P., Kahn, R. I., Lingeman, J. E., & Macaluso, J. N. (1997). Ureteral stones clinical guidelines panel summary report on the management of ureteral calculi. *The Journal of Urology*, *158*(5), 1915-1921.

Sharma, O. P. (2000). Hypercalcemia in granulomatous disorders: a clinical review. *Current Opinion in Pulmonary Medicine*, *6*(5), 442-447.

Smith, A. F., Beckett, G. J., Walker, S. W. & RAE, P. W. H. (1998). *Clinical Biochemistry* (6th ed).,WB Saunders.

Steel, R. G. D., & Torrie, J. H. (1980). *Principles and procedures of statistics a biometrical approach*. (2nd ed.). McGraw-Hill, Inc.

Thun, M. J., & Schober, S. (1991). Urolithiasis in Tennessee: an occupational window into a regional problem. *American Journal of Public Health*, *81*(5), 587-591.

Tosukhowong, P., Sriboonlue, P., Tungsanga, K., Bovornpadungkitti, S., Chatuporn, S., Muktahant, B., ... & Sitprija, V. (2001). Potassium status of Northeast Thai constructors in three different geographic locations. *Journal of the Medical Association of Thailand*, *84*, 163-72.

Author Information

Zena A. M. Al-Jawadi
University of Mosul, College of Science, Department of Chemistry, Mosul, Iraq.
Contact e-mail: *zena_aljawadi@uomosul.edu.iq*

To cite this article:

Al-Jawadi, Z.A.M. (2021). Urinary stone in outdoor and indoor workers patients with family history. *The Eurasia Proceedings of Science, Technology, Engineering & Mathematics (EPSTEM), 16*, 191-194.

The Eurasia Proceedings of Science, Technology, Engineering & Mathematics (EPSTEM)
ISSN: 2602-3199

The Eurasia Proceedings of Science, Technology, Engineering & Mathematics (EPSTEM), 2021

Volume 16, Pages 195-203

IConTES 2021: International Conference on Technology, Engineering and Science

Investigation of the Role of Vitamin C In Enhancing the Activity of Antibacterial Agents and Biofilm Formation

Khansa MOHAMMED YOUNIS
University of Mosul

Ghaydaa M. A. ALI
University of Mosul

Ashwaq Hazem NAJEM
University of Mosul

Abstract: Resistance to antibiotics is rapidly spreading across the globe, posing a new health-care challenge for all countries. Bacterial biofilms are three-dimensional formations made up of cells encased in a matrix of polymeric, making cells resistant to the drugs and the immune system. As a result, new tactics for inhibiting the production of the EPS matrix may lead to more efficient use of already available antibiotics. The mechanism of vitamins C effect on boosting the effectiveness of several anti-bacterial drugs was investigated in this study, the target isolates were obtained from University of Mosul/ Biology department/ bacterial culture collections and evaluated qualitatively and quantitatively. The isolates involved: *Staphylococcus aureus*, *Escherichia coli* ,Klebsiella *sp*., *Serratia marcescens* and *Pseudomonas aeroginosa*. Antibiotic sensitivity tests and biofilm producing assay results revealed that the majority of the isolates were resistant to a range of antibiotics and had a large capacity for biofilm formation when grown on a cover glass surface. Vitamin C is an antioxidant, a scavenger of active metabolites. The Minimum Inhibitory Concentration (MIC) of Vitamin C against selected isolates had been determined, and all further experiments used concentrations below the MIC. Our results showed that Vit.C pre-treatment enhance the bactericidal effect of antibiotic and increases bacterial susceptibility to antibiotics. Using light microscopy, experiments of sub inhibitory doses of Vitamin C revealed good suppression of selected isolates biofilm development on the cover glass surface. Vitamin C can be utilized as an antibiotic adjuvant in combination with antibiotic and has effective biofilm inhibition, caused by multidrug-resistant bacteria, according to evidence.

Keywords: Vitamin C, Antibacterial agents and biofilm formation.

Introduction

Vitamin C has previously been reported for its antibacterial properties towards Mycobacterium TB, the germs that cause tuberculosis in humans, since the 1930s. (Boissevain et. al., 1937). In a 1933 in vivo investigation, Feeding TB sputum to vitamin C-deficient guinea pigs resulted in intestinal tuberculosis, while providing a same guinea pigs vitamin C-rich tomato juice did not produce sickness (McConkey et. al., 1933). Vitamin C, an antioxidant, and N-acetyl cysteine (NAC), an active metabolite scavenger, both prevent hepatotoxicity. Vitamin C's antimicrobial properties were previously assumed to be linked to its pH-lowering properties. In contrast, one study suggests that

vitamin C has potent antimicrobial activity toward group A hemolytic streptococci, even in pH-neutral conditions. (Mehmeti et. al., 2013). Microdilution experiments were employed in other studies to look into the antimicrobial properties of vitamin C against a variety of microbial (opportunistic) illnesses (Holloway et. al., 2011). Vitamin C dosages of 0.31 mg/mL were found to be effective in reducing the growth of Pseudomonas aeruginosa in vitro. Notably, co-administration of vitamin C can significantly boost the antibacterial activity of other drugs like epi-gallocatechin gallate, such as against multi-drug resistant bacteria. (Hatano et al. 2008), this was likewise true for vitamin C combined with deferoxamine in the treatment of Gram-positive cocci., such as *Staphylococcus epidermidis* and *Staphylococcus aureus*, as well as against Gram negative rods, including, *P. mirabilis, K. pneumoniae* and *E. coli*. Vitamin C mixed with quercetin had a synergistic antibacterial effects, and vitamin C combined with extracts such as white tea and pomegranate rind extracts had a synergistic bactericidal activity. (Chen et. al., 2018).

Method

Selection of the Isolates

The isolates were obtained from University of Mosul/ Biology department/ bacterial culture collections, the isolates involved: *Staphylococcus aureus*, *Escherichia coli* ,Klebsiella sp., *Serratia marcescens* and *Pseudomonas aeroginosa*

Morphological Characterisation

In order to confirm the purity and the diagnosis, the morphological and cultural characteristics were conducted for all the pure isolates on prepared medium NA and BHI (Difco). The morphological characteristic include shape, Gram staining. Growth patterns were checked using NA, BHI and Mannitol Salt Agar (MSA) media after incubation at 37 °C for 24 hours.

DNase Activity Assay

DNA extraction: boiling method

Colonies of overnight growth for the selected isolates were used. Briefly, the bacterial pellets were suspended in 200 µl of TE buffer Tris-HCl (10 mM): EDTA (1 mM) and subjected to 15 min of boiling. Immediately after boiling, the tubes were placed in an ice for 15 min and then centrifuged for 5 minutes at 14,000 rpm at room temperature. The supernatant containing DNA (100 µl) was transferred to another clean tube and stored at -20°C.

DNase Tube test

With each isolate, colonies of *Staphylococcus aureus*, *Escherichia coli*, Klebsiella sp., *Serratia marcescens*, and *Pseudomonas aeruginosa* were taken from the pure culture and 0.1 g of DNA was added to 200 l BHI broth in an Eppendorf tube. The DNA and bacteria-containing tubes were incubated at 37°C with shake (150 rpm). Following 24 hours, 20 µl of media was removed and spun for 1 minute at 10,000 g. The supernatants were processed in a 0.9 percent gel electrophoresis device containing EtBr and observed with an Ultraviolet trans illuminator (Gerceker et.al., 2009).

Antibiotic Sensitivity Assay

The isolates were screened for antibiotic sensitivity using disk diffusion (Kirby Bauer's) method on Mueller–Hinton agar (Merck, Germany). The assays to establish the susceptibility of drugs were conducted according to the Clinical and Laboratory Standards Institute (CLSI) (Bayer et. al., 1966). Tetracycline, Ciprofloxacin, Flucloxacillin, Streptomycin, and Ampicillin were among the antibiotics utilized.

Determined Of Minimal Inhibitory Concentration (MIC) Of Sodium Ascorbate Against S. *Aureus* and *Klebsiella* Sp.

A broth dilution assay against chosen isolates was used to identify the minimum dosage of sodium ascorbate that suppressed growth of bacteria (CLSI, 2006). Two-fold serial dilutions of sodium ascorbate (0, 100, 50, 25, 12.5, 6.25, 3.15 mg/ml) were performed in 1 ml LB broth. 0.1 ml of cells were added to each concentration of ascorbate dilutions and incubated at 37°C for 24 hours. The lowest concentration that stopped observable growth of bacteria was referred to as the (MIC). The MIC for *S. aureus* and *Klebsiella* sp. was 12.5 mg/ mL, 25 mg/mL respectively. Depending on pre- treatment cells for the selected isolates in the presence of sub-inhibitory concentrations 6.25 mg/mL of sodium ascorbate, determination of the antibiotic susceptibility and biofilm forming for the selected isolates were done.

Assessment of Antibiotic Susceptibility of *S. Aureus* and *Klebsiella* Sp.

Antibiotic susceptibility of *S. aureus* and *Klebsiella* sp. were assessed Briefly, inoculation of the 0.5 ml (1× 108) CFU/ml of overnight cultures of isolates were done using 5 ml LB broth which contained sub-inhibitory concentrations of sodium ascorbate at 6.25 mg/ml. They were then incubated at 37°C for 16–18 h. The isolates were tested for antibiotic sensitivity using disk diffusion (Kirby Bauer's) technique on Mueller–Hinton agar using the antibiotic that were resistance to it. The results were compared with the untreated cultures. The experiments were done in triplicate and the mean values were utilised.

Biofilm Forming Assay

The study of biofilm using optical microscopy was carried out according to procedures of (Martin-Cereceda et. al., 2001) with little modification. Briefly, in 24-well MTP, 1% of overnight isolate colonies were introduced to 1 ml of fresh growth medium with a 1cm glass cover and cultured for 24 hours. The cover glasses were removed carefully following incubation and rinsed with deionized water to eliminate the planktonic cells. The assumed biofilms on the cover glass were dyed with a 0.4 percent crystal violet solution and then examined under a light microscope.

Effect of Sub Inhibitory Concentrations of Sodium Ascorbate on Biofilm Forming of *S. Aureus* and *Klebsiella* Sp.

Some sub inhibitory concentrations of sodium ascorbate showed no effect on the growth rate, but still were able to significantly inhibit biofilm formation. These concentrations were used for microscopic observation. The microscopical study of the biofilm was conducted using (Musthafa et. al., 2010) methods with minor modifications. Briefly, both overnight cultures that were untreated and treated with sub inhibitory concentrations of sodium ascorbate were mixed with 1 mL of fresh growth medium that had a cover glass of 1 cm and then incubated for 24 h. The cover glasses were removed carefully after incubation and were then rinsed with distilled water in order to remove the planktonic cells. A solution of 0.4% crystal violet was used to stain the presumed biofilms that adhered to the cover glasses before being studied under a light.

Results and Discussion

The diagnosis and purification of bacterial isolates obtained from Biology department/ bacterial culture collections were confirmed based on gram stain and biochemical tests, the results were identical to what was stated in the approved diagnostic systems (Gary, 2017). A DNase tubes testing was carried out for DNase activity for the growing culture of *S. aureus, Klebsiella sp., E. coli, Serratia marcescens and P. aeroginosa* (Figure 1). Only *S. aureus* and *Serratia marcescens* are positive in this test and showed degrade DNA. In a tube containing Klebsiella sp., *E. coli and P. aeruginosa* no DNA damage was observed.

Each of the isolates was subjected to screening for antibiotic susceptibility and the results were compared with the standard protocols produced by CLSI.

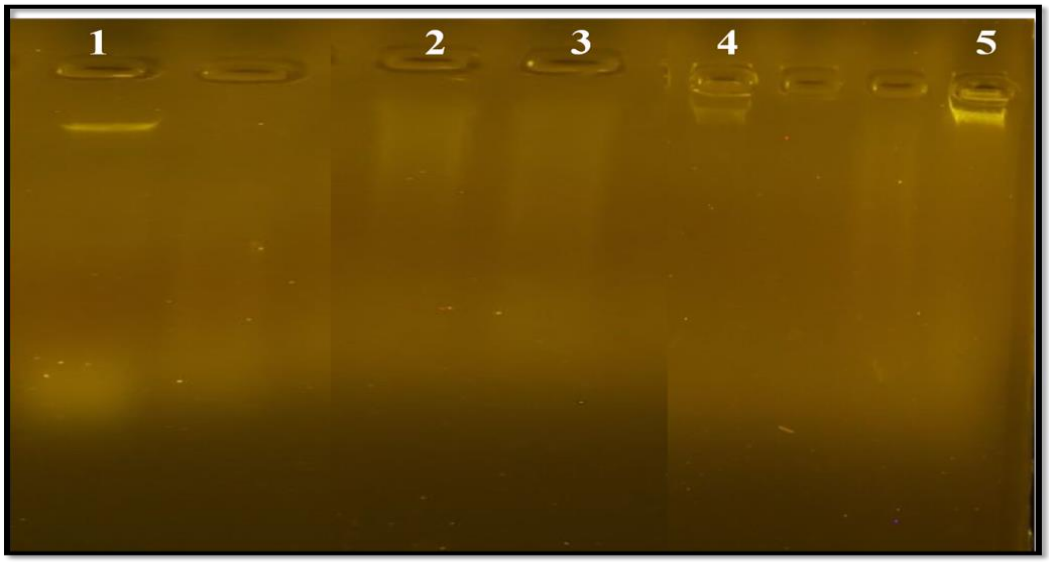

Figure 1. DNase activity of 1: *Escherichia coli ,2*: *Staphylococcus aureus*, 3: *Serratia marcescens*, 4: *Klebsiella sp.* and 5: *Pseudomonas aeroginosa* using the DNase tube test. The dashed band shows the degraded DNA and the vertical band shows the intact DNA.

The results showed that *Psedomonas aeruginosa*, *Serratia marcescens*, were sensitive to Cip. and resistance for the TE., S, F and APX, E. *coli* was sensitive to Cip. and F, while *Klibsiella sp.* and S. *aureus* were resistance to all antibiotic used, therefor *Klibsiella sp.* and S. *aureus* were chosen for study the effect of sodium ascorbate assays (Table 1) (Figure 2).

Table 1. Results of the screening for antibiotic susceptibility assay

Bacteria	Cip	TE	S	F	APX
Pseudomonas aeruginosa	37mm Susceptible	7mm resistant	18mm susceptible	8mm resistant	9mm resistant
Escherichia coli	22mm Susceptible	7mm resistant	10mm resistant	17mm susceptible	8mm resistant
Serratia marcescens	30mm Susceptible	6mm resistant	18mm resistant	13mm resistant	7mm resistant
Klebsiella sp.	6mm resistant	6mm resistant	8mm resistant	7mm resistant	6mm resistant
Staphylococcus aureus	11mm resistant	6mm resistant	10mm resistant	8mm resistant	6mm resistant

Multidrug-resistant bacteria have been a cause of concern, and efforts to find new antibiotics have had mixed results. (Puzari et. al., 2018). As a result, a novel adjuvant to fight infectious disease is required. According to prior research, vitamin C is one such possible adjuvant. The effect of vitamin C sub-MIC concentrations on the development and biofilm generation of certain isolates was investigated in this study. In terms of isolates susceptibility profiling (Figure 2), resistant to a broad range of beta- and non-beta-lactam antibiotic had the largest percentage, and the majority of isolates were multi-drug resistant, which is consistent with prior researches (Guggenbichler et. al., 2011, Mansour et. al., 2009). Nearly half of biofilm producers are resistant to at least three different antibiotic families at the same time, that could be related to the biofilm matrix (Alves et al. 2014) , and the physiological properties of the microbes that make it allow for antibiotic resistance. The antibacterial agent's delayed penetration, a shift in the microbial growth rate, or other physiological modifications linked to the biofilm's formation are generally the mechanisms of resistance(Donlan et. al., 2002). Enterococci, one of the commensal organisms in the genital tracts and intestines, are becoming key pathogenicity sources in hospitals. Because of their own regular resistance to commonly used antibiotics, as well as their ability to obtain additional resistance to other kinds, either through plasmid and transposon elements, as in glycopeptide and aminoglycoside compounds, or via mutations, as in penicillin, they are receiving more attention. (Cohen, 1992). This development is linked to the

dissemination of resistance-bearing plasmid and transposon vectors across a variety of *Enterococcus faecalis* and *Enterococcus faecium* strains, as well as a rise in vancomycin use in medical centres.

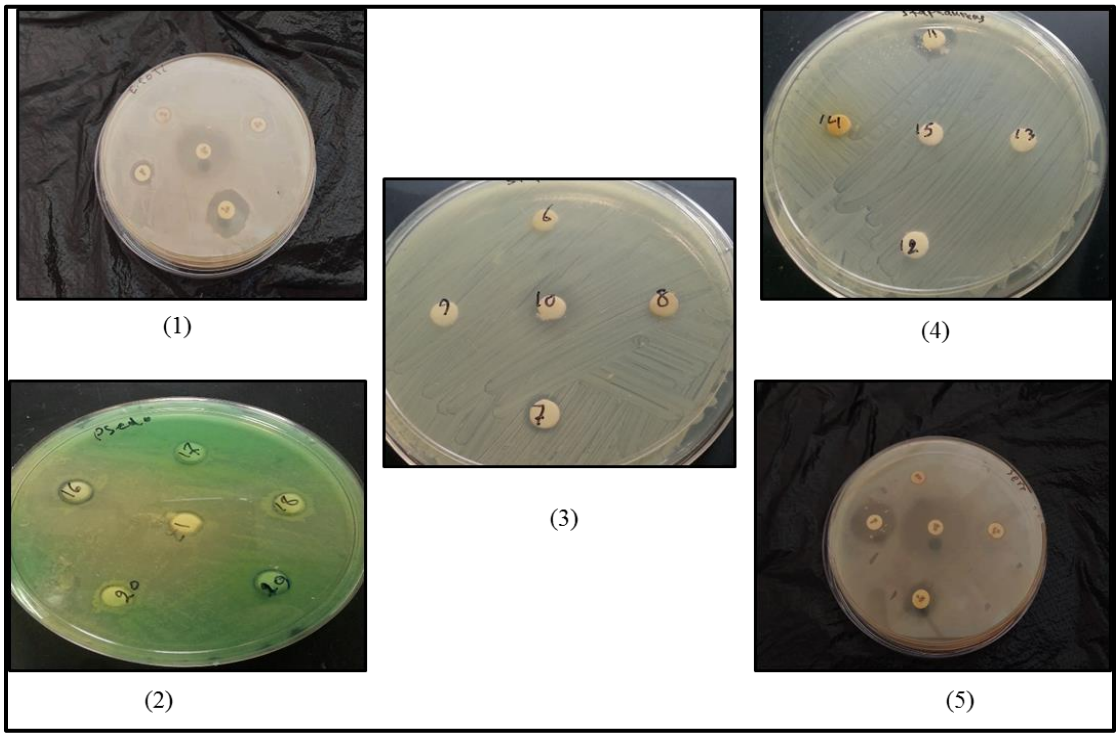

Figure 2. Sscreening for antibiotic susceptibility assay, 1- *Escherichia coli*, 2- *Pseudomonas aeruginosa*, 3- *Klebsiella* sp. 4- *Staphylococcus aureus* and 5- *Serratia marcescens*.

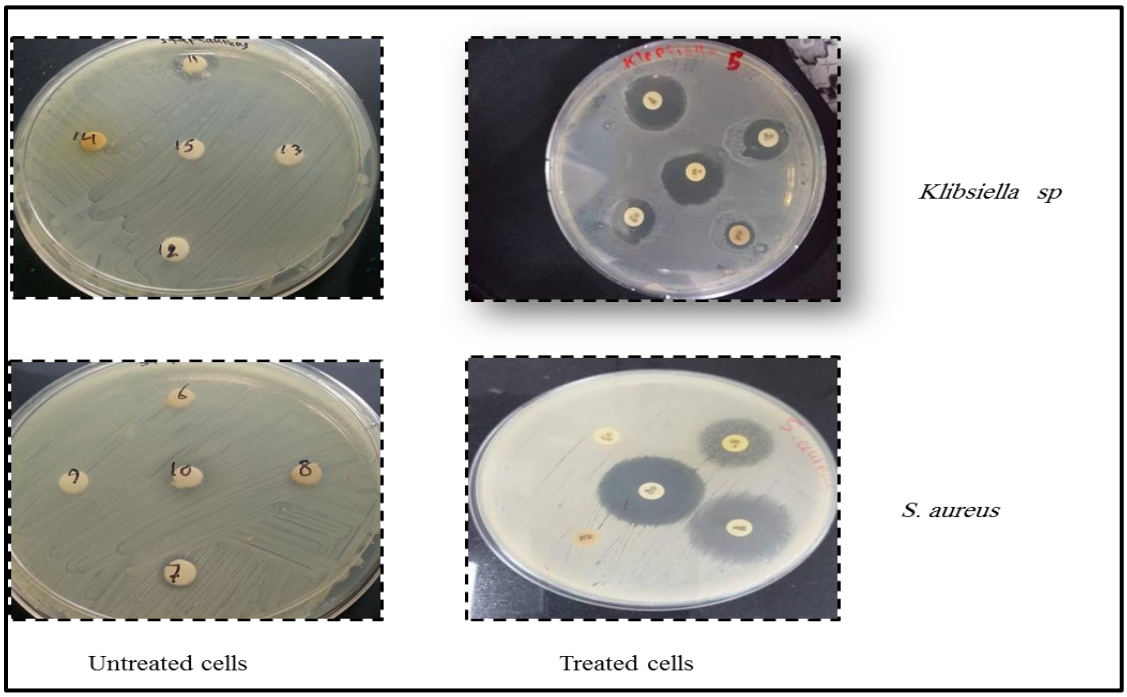

Figure 3. Antibiotic susceptibility test using disk diffusion method of selected bacteria showing the significant change of suseptibility after treated cells with sub inhibitory concentration of sodium ascorbate 6.25 mg/mL.

The survival of *S. aureus* and Klibsiella sp. in the presence of sub-MIC sodium ascorbate is vital to see if any of sodium ascorbate's effect are due to cell functioning changes rather than bactericidal or bacteriostatic actions. The MIC of sodium ascorbate for *S. aureus* and Klibsiella sp. were found to be 12.5 mg/ mL and 25 mg/mL using the broth dilution method, respectively. Sub inhibitory concentration of sodium ascorbate 6.25 mg/mL, where used for antibiotic susceptibility and biofilm forming assays for the selected isolates.

Antibiotic susceptibility assay demonstrated a significant change. The results of *Klibsiella* sp. treated cultures with sodium ascorbate showed the intermediate effect to TE, sensitive effect to S, F, AMP and Cip compared to untreated cultures. For the *S. aureus* treated cultures were intermediate effect to F and sensitive effect for only Cip and S compared to untreated cultures (Figure 3).

In this study, the soluble forms of vitamin C increases bacterial susceptibility to antibiotics, This observation is consistent with the results of (Helgadóttir et al., 2017; Vilchèze et. al., 2013), who stated that drugs that target bacterial growth might work synergistically with some other antibacterial drugs to reduce pathogens resistance.

A known ROS-generator is vitamin C, a natural food additive that can be used safely in medical care. Pretreatment of cells with vitamin C at various intervals with 48 hours of bacterial growth may improve antibacterial activity and eradicate specific bacterial species. (Vilchèze et al. 2013; Foti et. al., 2012).

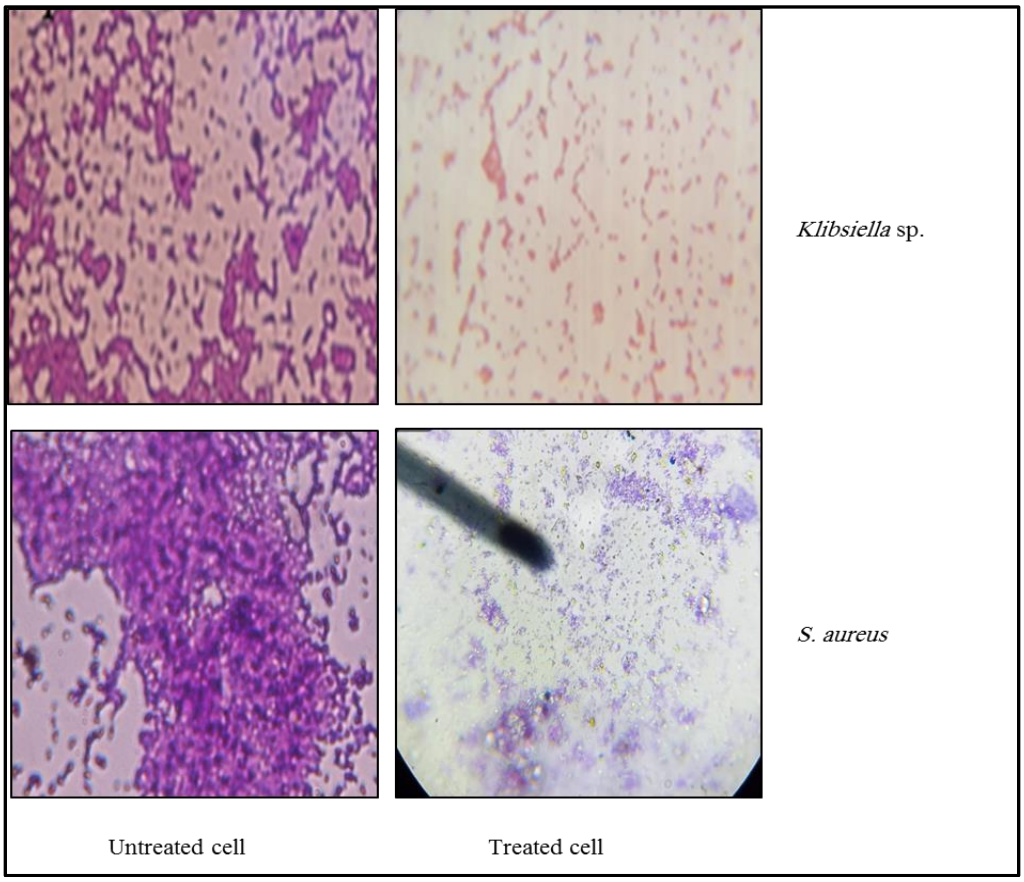

Figure 4. light microscopic images. Biofilm development of the *Klibsiella* sp. and S. *aureus* grown in the absence and presence of sub inhibitory concentration of sodium ascorbate 6.25 mg/mL showing inhibitory activity.

Vit C pre - treatment improves the bactericidal effect of the drug and behaves as just a lipocalin antimicrobials binding inhibitor, increasing the effective concentration of antibiotics around bacterial cells, indicating that Vit C can be used as an antimicrobials adjuvant in combination therapy to treat infections caused by multi drug resistance pathogens. Biofilms are up to 1,000 times more resistant to the antibiotics than bacteria in their planktonic form, and they cause 60% of human infections, with a higher risk of getting antibiotic resistance (Mai-Prochno et. al., 2015).

Interbacterial communication is essential for the production of biofilms by *S. aureus* and Klibsiella sp. The influence of sodium ascorbate on the production of biofilms is depicted in (Figure 4). Biofilm was shown to be significantly reduced in overall when *S. aureus* and Klibsiella sp. was grown with concentration of sub-MIC sodium ascorbate.

Biofilm generation on medical equipment, in wounds, and in immunocompromised people is now recognized as a major cause of chronic infections (Bjarnsholt et. al., 2010). In immunocompromised patients, common pathogens such as *Escherichia coli Pseudomonas aeruginosa* and *Staphylococcus epidermidis*, which are often pathogenic, can cause dangerous long-term infections. Antibiotic overuse can lead to bacterial resistance, resulting in infections caused by antibiotic resistant bacteria, which is a serious increasing issue. (Flores-Encarnación et al., 2018). The global threat of resistance to antibiotics, according to WHO, is going to usher in a post-antibiotic period. (W. H. O., 2014). As a result, in addition to limiting antibiotic dosage, innovative techniques to bacterial infection treatment are urgently needed. Because conventional antibiotic therapies are ineffective in eradicating persistent biofilms, we sought out a combination therapeutic strategy to supplement them. The biofilm matrix's polysaccharides and proteins generate a hydrophobic covering that prevents antimicrobial compounds from penetrating and provides biofilm resistance (Roy et. al., 2018). Fighting bacterial infections by inhibiting EPS generation is a potential method. Antibiotics and other recognized antibacterial treatments are not powerful enough as to entirely eliminate biofilms. In this case, using a combination treatment strategy to achieve a significant bactericidal effect towards bacterial biofilms is indicated. Vitamin C, a vital nutritional supplement for human, has been shown to boost the antibacterial activity of a variety of antimicrobials. (Khameneh et. al., 2016). In most microbial cells, it is also known for producing reactive oxygen species (ROS). Because direct microscopic examination of biofilms following exposure to sodium ascorbate can provide significant data on the activity of sodium ascorbate on biofilms, light microscopy analysis was carried out (Manjunath Mandhira Doss, 2013).

In this study, microscopic analysis was carried out on sub-MIC concentrations that had no effect on the growth rates but inhibited biofilm formation significantly. Results analysis revealed that controls (untreated cells) had thick coating of biofilms while biofilms of treated isolates showed a visible reduction in the numbers of micro colonies. Moreover, the architecture of the biofilm was also deteriorated by sodium ascorbate, as observed with the Light microscopy analysis (Fig. 3). The same observations were also recorded when *P. mirabilis* and *S. marcescens* were administered with p-nitrophenyl glycerol (PNPG) and tannic acid (Jones et. al., 2009; Wei et. al., 2004).

Vit C pretreatment boosts the antimicrobial effect of cold plasma via decreasing survivability from 50 to percent in P. aeruginosa biofilm, 10% to 2% in E. coli biofilm, and 61 to 18 percent in S. epidermidis biofilm (Helgadóttir et al., 2017). Because lengthy CAP treatments are not realistic in clinical practice, we believe that pre-treating infect lesion with vit C before exposing them to CAP could be a valid idea for fast eradication of bacterial biofilms in a variety of applications.

According to our findings Vitamin C can significantly inhibit bacterial biofilms by suppressing EPS synthesis at concentration less than 25 mg/mL. Vitamin C's bactericidal activity towards mycobacteria was previously shown to be primarily connected with oxidative stress. (Pandit et al., 2017). Based on these data, Biofilms was prevented by vit C, which inhibits the quorum sensing and other stationary phase regulatory systems that underpin biofilm growth, resulting in reduced in polysaccharide production. Once EPS content is lowered at vit C concentrations, bacterial cells are totally exposed to the media, as a result, as proven in this research, they are more susceptible to antimicrobial medications or therapies, such as sodium Ascorbate oxidative. (Helgadóttir et al., 2017).

Conclusion

The synergistic effect of antibiotics with sub-MIC doses of Vit C salt was studied in this study. Furthermore, the effect of sub-MIC Vit C salt concentrations on biofilm architecture was explored in this study.

Recommendations

Based on our results, the study recommends using a Vit C- Antibiotic combination treatment strategy to achieve a significant bactericidal effect towards bacterial resistance and biofilms formation.

Acknowledgments

The authors would like to thank the Iraqi Ministry of Higher Education and the Biology department, University of Mosul for supporting this research

Scientific Ethics Declaration

The author declares that the scientific ethical and legal responsibility of this article published in EPSTEM journal belongs to the author.

References

Alves, M. J., Barreira, J. C., Carvalho, I., Trinta, L., Perreira, L., Ferreira, I. C., & Pintado, M. (2014). Propensity for biofilm formation by clinical isolates from urinary tract infections: developing a multifactorial predictive model to improve antibiotherapy. *Journal of Medical Microbiology, 63*(3), 471-477.

Bayer, A., Kirby, W., Sherris, J., & Turck, M. (1966). Antibiotic susceptibility testing by a standardized single disc method. *Am J Clin Pathol, 45*(4), 493-496.

Bjarnsholt, T., Tolker-Nielsen, T., Høiby, N., & Givskov, M. (2010). Interference of Pseudomonas aeruginosa signalling and biofilm formation for infection control. *Expert Reviews in Molecular Medicine, 12*, 1-11. doi:10.1017/S1462399410001420

Boissevain, C. H., & Spillane Jr, J. H. (1937). A note on the effect of synthetic ascorbic acid (vitamin C) on the growth of the tubercle bacillus. *American Review of Tuberculosis, 35*(5), 661-662.

Chen, X., Liu, R., Liu, X., Xu, C., & Wang, X. (2018). L-ascorbic Acid-2-Glucoside inhibits Helicobacter pylori-induced apoptosis through mitochondrial pathway in Gastric Epithelial cells. *Biomedicine & Pharmacotherapy, 97*, 75-81.

Cohen, M. L. (1992). Epidemiology of drug resistance: implications for a post-antimicrobial era. *Science(Washington), 257*(5073), 1050-1055.

Donlan, R. M., & Costerton, J. W. (2002). Biofilms: survival mechanisms of clinically relevant microorganisms. *Clinical microbiology reviews, 15*(2), 167-193.

Flores-Encarnación, M., Nava-Nolazco, R., Aguilar-Gutiérrez, G., Carreño-López, R., Carreno-L, & oopez, R. (2018). The effect of Thymus vulgaris on growth and biofilm formation of uropathogenic Escherichia coli. *African Journal of Microbiology Research, 12*(10), 237-242.

Foti, J. J., Devadoss, B., Winkler, J. A., Collins, J. J., & Walker, G. C. (2012). Oxidation of the guanine nucleotide pool underlies cell death by bactericidal antibiotics. *Science, 336*(6079), 315-319.

Gary, P. W. (2017). Koneman. *Diagnostico Microbiologico/Microbiological diagnosis: Texto Y Atlas En Color/Text and Color Atlas.(Septima Ed.) Wolters Kluwer*.

Gerceker, D., Karasartova, D., Elyürek, E., Barkar, S., KIyan, M., Özsan, T. M. & Sahin, F. (2009). A new, simple, rapid test for detection of DNase activity of microorganisms: DNase Tube test. *The Journal of General and Applied Microbiology, 55*(4), 291-294.

Guggenbichler, J. P., Assadian, O., Boeswald, M., & Kramer, A. (2011). Incidence and clinical implication of nosocomial infections associated with implantable biomaterials-catheters, ventilator-associated pneumonia, urinary tract infections. *GMS Krankenhaushygiene interdisziplinär, 6*(1), 1-19.

Hatano, T., Tsugawa, M., Kusuda, M., Taniguchi, S., Yoshida, T., Shiota, S., & Tsuchiya, T. (2008). Enhancement of antibacterial effects of epigallocatechin gallate, using ascorbic acid. *Phytochemistry, 69*(18), 3111-3116.

Helgadóttir, S., Pandit, S., Mokkapati, V. R., Westerlund, F., Apell, P., & Mijakovic, I. (2017). Vitamin C pretreatment enhances the antibacterial effect of cold atmospheric plasma. *Frontiers in Cellular and Infection Microbiology, 7*, 43.

Holloway, A. C., Gould, S. W., Fielder, M. D., Naughton, D. P., & Kelly, A. F. (2011). Enhancement of antimicrobial activities of whole and sub-fractionated white tea by addition of copper (II) sulphate and vitamin C against Staphylococcus aureus; a mechanistic approach. *BMC Complementary and Alternative Medicine, 11*(1), 1-9.

Jones, S. M., Dang, T. T., & Martinuzzi, R. (2009). Use of quorum sensing antagonists to deter the formation of crystalline Proteus mirabilis biofilms. *International Journal of Antimicrobial Agents, 34*(4), 360-364.

Khameneh, B., Diab, R., Ghazvini, K., & Bazzaz, B. S. F. (2016). Breakthroughs in bacterial resistance mechanisms and the potential ways to combat them. *Microbial Pathogenesis, 95*, 32-42.

Mai-Prochnow, A., Bradbury, M., Ostrikov, K., & Murphy, A. B. (2015). Pseudomonas aeruginosa biofilm response and resistance to cold atmospheric pressure plasma is linked to the redox-active molecule phenazine. *PloS one, 10*(6), e0130373.

Manjunath Mandhira Doss, M. R. (2013). *Comparative evaluation of reversal of shear bond strength on bleached enamel using antioxidants–sodium ascorbate, salicylic acid & N-acetyl cysteine: An in vitro study* (Doctoral dissertation, Tamilnadu Government Dental College and Hospital, Chennai).

Mansour, A., Manijeh, M., & Zohreh, P. (2009). Study of bacteria isolated from urinary tract infections and determination of their susceptibility to antibiotics. *Jundishapur Journal of Microbiology, 2*(3), 118-123.

Martin-Cereceda, M., Alvarez, A. M., Serrano, S., & Guinea, A. (2001). Confocal and light microscope examination of protozoa and other microorganisms in the biofilms from a rotating biological contactor wastewater treatment plant. *Acta Protozoologica, 40*(4), 263-272.

McConkey, M., & Smith, D. T. (1933). The relation of vitamin C deficiency to intestinal tuberculosis in the guinea pig. *The Journal of Experimental Medicine, 58*(4), 503.

Mehmeti, I., Solheim, M., Nes, I. F., & Holo, H. (2013). Enterococcus faecalis grows on ascorbic acid. *Applied and Environmental Microbiology, 79*(15), 4756-4758.

Musthafa, K., Ravi, A., Annapoorani, A., Packiavathy, I. V., & Pandian, S. (2010). Evaluation of anti-quorum-sensing activity of edible plants and fruits through inhibition of the N-acyl-homoserine lactone system in Chromobacterium violaceum and Pseudomonas aeruginosa. *Chemotherapy, 56*(4), 333-339.

W. H. O. (2014). *Global status report on noncommunicable diseases 2014*: World Health Organization.

Pandit, S., Ravikumar, V., Abdel-Haleem, A. M., Derouiche, A., Mokkapati, V., Sihlbom, C., Westerlund, F. (2017). Low concentrations of vitamin C reduce the synthesis of extracellular polymers and destabilize bacterial biofilms. *Frontiers in Microbiology, 8*, 2599.

Puzari, M., Sharma, M., & Chetia, P. (2018). Emergence of antibiotic resistant Shigella species: A matter of concern. *Journal of Infection and Public Health, 11*(4), 451-454.

Roy, R., Tiwari, M., Donelli, G., & Tiwari, V. (2018). Strategies for combating bacterial biofilms: A focus on anti-biofilm agents and their mechanisms of action. *Virulence, 9*(1), 522-554.

Vilchèze, C., Hartman, T., Weinrick, B., & Jacobs, W. R. (2013). Mycobacterium tuberculosis is extraordinarily sensitive to killing by a vitamin C-induced Fenton reaction. *Nature Communications, 4*(1), 1-10.

Wei, J.-R., Horng, Y.-T., Lai, H.-C., Luh, K.-T., & Ho, S.-W. (2004). Effects of PNPG on cell growth cycle, motility machinery and quorum sensing in Serratia marcescens. *Journal of microbiology, immunology, and infection= Wei mian yu gan ran za zhi, 37*(1), 1-7.

Author Information

Khansa MOHAMMED YOUNIS
University of Mosul, Iraq
Mosul city, Iraq
Contact e-mail*:* *kansbio50@uomosul.edu.iq*

Ghaydaa M. A. ALI
University of Mosul, Iraq
Mosul city, Iraq

Ashwaq Hazem NAJEM
University of Mosul, Iraq
Mosul city, Iraq

To cite this article:

Mohammed Younis, K., Ali, G.M.A.& Najem, A.H. (2021). Investigation of the role of Vitamin C in enhancing the activity of antibacterial agents and biofilm formation. *The Eurasia Proceedings of Science, Technology, Engineering & Mathematics (EPSTEM), 16*, 195-203.

The Eurasia Proceedings of Science, Technology, Engineering & Mathematics (EPSTEM)
ISSN: 2602-3199

The Eurasia Proceedings of Science, Technology, Engineering & Mathematics (EPSTEM), 2021

Volume 16, Pages 204-208

IConTES 2021: International Conference on Technology, Engineering and Science

Measuring the Level of Some Trace Elements in the Serum and Placentae of Pregnant Women Infected with *Toxoplasmosis*

Muna ISMAIL IBRAHIM
Office of Agricultural Research

Layla ABDULLAH MUSTAFA
University of Mosul

Abstract: The current study deals with *Toxoplasmosis* and the relation of the parasite causing it *(Toxoplasma gondii)*, its impact on the levels of trace elements in the serum and placentae of some pregnant women infected with compared to non-infected who are considered a control group. Several trace elements, which included the Selenium (Se), Copper (Cu), Zinc (Zn), Ferrous (Fe), Magnesium (Mg) and Manganese (Mn) were measured, the study was conducted on a sample of (450) women, 225 of them were not infected with *Toxoplasmosis* and 225 were infected, 24 placenta of non-infected women and 18 of infected women. Results showed that there was a significant increase in the levels of Se, Cu, Zn and Mg in the pregnant women serum who are infected with *Toxoplasmosis*, while there was an insignificant decrease in the level of Fe throughout the period of pregnancy for the in the serum of the infected pregnant women. The correlation between the infection and the period of pregnancy showed a significant increase in the levels of Se and Zn during the (3-6 months) period of pregnancy, a significant increase in the levels of Cu and Mg and insignificant increase in Mn level during the (6-9 months) period of pregnancy and on the other hand the level of Fe decreased. Moreover, results showed a significant increase in Se, Fe and Mg levels during the (6-9 months) period of pregnancy and insignificant increase in Cu level during the (6-9 months) period of pregnancy. The levels of Zn and Mn decreased during the pregnancy period in the placentas of the infected women.

Keywords: Antioxidants, Placentae, Serum, *Toxoplasmosis*, Trace elements.

Introduction

Toxoplasmosis is a disease caused by *Toxoplasma gondii*, which is considered as Intracellular Parasites and can infect a variety of mid hosts such as rodents, birds and other animals as well as the human (Steven et. al., 2008). *Toxoplasma gondii* are characterized with having several phases responsible for the occurrence of the infection, which are the Alveolar oocyte, Tachyzoites and Bradyzoites located in the tissue cysts (Remington et. al., 2006). Infection with *Toxoplasmosis* for the various types of hosts varies between mild, acute and chronic, where the infection is Asymptomatic for the Immunocompetent host, or similar to flu and could last for few days and most of the persons with natural immunity are healed spontaneously without any diagnosis, unless the relevant blood test is conducted (Lienden, 2005). The immunity system of the host can prevent the multiplication of the parasite and consequently forming the tissue cysts in most of the body tissues, especially the central neural system, skeletal and cordial muscles (Herrmann et al., 2010). From the other hand, symptoms are severe and evident for the patients suffering from immunity deficiency and pregnant. Mothers' infection during the first three months of pregnancy results in abortion, but when infection occurs during the middle months of pregnancy, it results in deformation and jaundice symptoms, liver enlarged and spleen and the infection of the embryo's central neural system resulting to mental retardation, Blindness and Congenital anomalies (Montoya et. al., 2004). Infection during the last three months of pregnancy is not accompanied with clinical symptoms

for the embryo and it might lead to the birth of children who suffer from dysfunctions in the central neural system and these births are subjected to mortality within about one month or suffer from dysfunction in the eyes and it develops with the infant's age and results in Choriorinitis and then to Ocular *Toxoplasmosis* (Oktenli et. al., 2004).

The objective of the study is to determine the change of trace elements levels like the Selenium, Copper, Zinc, Iron, Magnesium and Manganese as antioxidants in serum and placentae of the women infected with the disease (weather aborted or not aborted).

Method

Collecting the Blood Samples

Blood samples were taken for a various group of pregnant women with ages ranged between 20 to 45 years. The number of the sample was (450) samples of pregnant women infected and not infected with *Toxoplasma gondii*, who were diagnosed by specialized physicians, department of consultancies at Al-Khansaa Hospital for Maternity and obstetrics. Ten millimeters of the veins blood were taken from the patients, put in plastic containers, left to for ten minutes coagulate (clot) in a temperature of 37ºC. After that a centrifuge with a speed of 5000 xg was conducted to the blood to obtain serum (Tietz, 1999), for the purpose of measuring the trace elements and then stored at -20ºC.

Collection of Placentae Samples

The number of placentae samples were collected from aborted and unabated women was 24 samples at Al-Khansaa Hospital for Maternity and obstetrics. From the women who suffered repeated abortion with various pregnancy periods (1-3, 3-6 and 6-9 months), 18 placentae sample were collected and put into glass containers which contain Normal Saline (Nacl) with a concentration of (0.9%). To confirm the infection, the direct microscopic test of the placentae extract was performed.

Parasite Isolation

The pure form of the parasite was isolated from the infected placentae using the following procedures (Sharma et. al., 1981; Dubey et. al., 1986**;** Al-Khaffaf, 2001).

Trace Elements

Determining a number of the trace elements represented by Zinc, Copper, Manganese, Magnesium and Iron in the pregnant women serum and placentae extractes using the atomic absorption spectrum (D'Haese et. al., 1992) where the sample were diluted 4 times with the sterilized water that doesn't contain ions (Tietz, 1999), while Selenium was determined by using a modified colorimetric method (Allwsh, 2000).

Results and Discussion

Levels of trace elements in the serum of infected and uninfected pregnant women

Results in table (1) show that there is a significant effect in the levels of Zinc and Magnesium in the serum of pregnant women infected and uninfected with *Toxoplasmosis* during the interrelation cases with pregnancy periods at probability level of $P \leq 0.01$ from the other hand a significant effect of iron was observed at probability level of $P \leq 0.05$. Also, a significant increase was observed in the levels of Selenium, Cooper, Zinc and Magnesium in the serum of the pregnant women infected with *Toxoplasmosis* where the levels values were: 0.24±0.12, 7.10±6.53, 25.06±12.58 and 0.69±0.14 micromole/liter respectively. Also, the results of correlation between the infected cases and pregnancy periods showed increase in the levels of Selenium and Zinc in the serum of pregnant women infected with *Toxoplasmosis* during the pregnancy period (3-6) months as they were: 0.36±0.12 and 30.30±15.77 micromole/liter respectively. The levels of Copper and Magnesium significantly increased during the pregnancy period (6-9) months to be 7.74±8.27 and 0.73±0.152 micromole/liter

respectively. While the level of iron decreased during the pregnancy period (3-6) months to be 1.27±0.57 micromole/liter.

Table 1. The mean ± standard deviation of the trace elements in the serum of the infected and uninfected pregnant women.

Variables	No.	Mean ± SD µmol/L Selinium	Copper	Zinc	Iron	Magnesium	Manganese
Uninfected pregnant women	225	0.07±0.05 B	6.36±1.12A	16.39±3.91B	1.44±0.70A	0.65±0.14B	0.23±0.17 A
infected pregnant women	225	0.24±0.12 A	7.10±6.53A	25.06±12.58 A	1.31±0.67A	0.69±0.20A	0.30±0.58 A
correlation between infection and pregnancy periods							
Uninfected (1-3) months	75	0.13±0.04C	6.16±1.18A B	16.21±3.76C D	1.57±0.63A	0.67±0.10BC	0.13±0.07 A
Uninfected (3-6) months	75	0.05±0.01D	6.98±1.07A B	14.12±3.54D	1.62±0.81A	0.70±0.17AB	0.15±0.03 A
Uninfected (6-9) months	75	0.03±0.01D	5.94±0.82B	18.84±2.86C	1.11±0.54B	0.58±0.11D	0.10±0.05 A
infected (1-3) months	75	0.18±0.04B	6.39±1.40A B	17.62±6.46C	1.18±0.59B	0.70±0.24AB	0.21±0.18 A
infected (3-6) months	75	0.36±0.12A	7.18±7.60A B	30.30±15.77 A	1.27±0.57B	0.63±0.19CD	0.23±0.18 A
infected (6-9) months	75	0.18±0.08B	7.74±8.27A	27.27±10.01 B	1.49±0.80A	0.73±0.15A	0.25±0.16 A

Levels of trace elements in the placentae of infected and uninfected pregnant women

Results in table (2) indicate that there is a significant impact in the concentrations of Selenium, Zinc, Magnesium and Manganese in the placentae of pregnant women who are infected and uninfected with *Toxoplasma gondii*, at probability level of $P \leq 0.01$.

Table 2. shows the mean and the standard deviation of the trace elements in the placentae of the infected and uninfected pregnant women.

Placentae during pregnancy	No.	Mean ± SD µmol/L Selenium	Copper	Zinc	Iron	Magnesium	Manganese
Uninfected placentae	6	0.12±0.03C	6.68±1.70 A	12.01±6.49 A	1.67±0.56A	1.00±0.15B	0.47±0.01 A
Infected (1-3) months	6	0.64±0.01B	6.02±0.01 A	10.01±0.01 A	1.48±0.01A B	0.95±0.01B	0.23±0.01 B
Infected (3-6) months	6	0.63±0.01B	7.34±2.70 A	4.66±1.82B	0.98±0.01B	0.82±0.07C	0.23±0.01 D
Infected (6-9) months	6	0.85±0.16A	5.80±0.88 A	3.33±0.01B	1.67±0.74A	1.14±0.07A	0.23±0.01 C

Within columns, means having the same letters don't differ significantly at $p \leq 0.05$.

Also, the results in table (2) showed that there is a significant increase in the concentration of Selenium in the placentae of the infected pregnant women during the pregnancy period (6-9 months) as the concentration was 0.85±0.16 micromole/liter and there was no significant increase in iron level compared to its level in the

uninfected pregnant women placentae. Also, the level of Magnesium significantly increased in the infected women placentae during the pregnancy period (6-9 months) as it was 1.14±0.07 micromole/liter, while the levels of Zinc and Manganese significantly increased in the infected women placentae to be 3.33±0.01 and 0.23±0.01 micromole/liter respectively.

The results of the current study show that there is a significant increase in the levels of Selenium, Copper, Zinc and Magnesium but Manganese showed no significant effect and a decrease in the level of iron in in the serum of the pregnant women who are infected with *Toxoplasma gondii*, compared to the uninfected women during the various pregnancy periods. From the other hand the levels of Zinc and Manganese decreased significantly in the placentae of the infected women compared to the uninfected women. Iron didn't show a significant effect, but the levels of Selenium and Magnesium increased significantly in the placentae of the infected women, whereas Copper didn't reach a statistical significance. The reason behind the decrease of Iron in the pregnant women serums may be due to its capture by the Albumin as an antioxidant, which captures several metals inside the human body such as the free Iron and free Copper (Iqpal et. al., 2004), in addition to that, the lack of iron ions during pregnancy is due to using large amounts to build the body cells especially red blood cells needed by the pregnant (Choi et. al., 2000) and also the amounts of iron decrease with the period of pregnancy (Tam et. al., 2002). The increase of Copper level in the pregnant serum may be attributed to the disorders between the effectiveness of Sodium ion transferring systems and the level of Copper in the serum, because the decrease in the effectiveness of these systems due to oxidation stress is accompanied with increase in Copper level in the serum (Avkiran, 2001; Bober et. al., 2002**;** Eshratkah et. al., 2008; Seyrek et. al., 2009). An imbalance of other elements (Selenium, Zinc and Manganese) was observed, which ranged between increase and decrease in the serum of pregnant women infected with *Toxoplasma gondii*. The decrease is due to using Zinc ion with high amounts as an escort to the superoxide dismutase enzyme (SOD), which shows its effectiveness with the presence of Zinc, Copper and Manganese and which is used to remove Super oxide anionradced radicals and then it is transformed into hydrogen peroxide which is an oxidant compound free of the free radicals (Saczko et. al., 2002).

Conclusion

The objective of the study is to determine the change of trace elements levels like the Selenium, Copper, Zinc, Iron, Magnesium and Manganese as antioxidants in serum and placentae of the women infected with the disease (weather aborted or not aborted).

Scientific Ethics Declaration

The authors declare that the scientific ethical and legal responsibility of this article published in EPSTEM journal belongs to the authors.

References

Al-Khaffaf, F.H.O. (2001). *Isolation and study of epidemiological seroprevalence of Toxoplasmosis age in Nineveh province* [Master Thesis]. University of Mosul.

Allwsh, T.A. (2000). *Biochemistry study of selenium and its relation with cancer* [Ph.D. Thesis]. Mosul University.

Avkiran, M. (2001). Protection of the ischaemic myocardium by Na+/H+ exchange inhibitors: potential mechanisms of action. *Basic research in cardiology*, *96*(4), 306-311.

Bober, J., Kedzierska, K., Kwiatkowska, E., Ciechanowski, K., Widecka, K., Stachowska, E., ... & Dutkiewicz, G. (2002). The erythrocyte sodium-proton exchanger activity in patient with primary hypertension. *Polskie Archiwum Medycyny Wewnetrznej*, *108*(1), 619-624.

Choi, J.W. & Pai, S.H. (2000). Plasma lipid concentration change with plasma alkaline phosphatase activity during pregnancy. *Ann. Clin.Lab.Sci.*,*30*(4), 422-428.

D'haese, P. C., Lamberts, L. V., Vanheule, A. O., & De Broe, M. E. (1992). Direct determination of zinc in serum by Zeeman atomic absorption spectrometry with a graphite furnace. *Clinical chemistry*, *38*(12), 2439-2443.

Dubey, J. P., & Livingston Jr, C. W. (1986). Sarcocystis capracanis and Toxoplasma gondii infections in range goats from Texas. *American journal of veterinary research*, *47*(3), 523-524.

Eshratkhah, B., Sadaghian, M., Nezhad, M., Sabri, V., & Geyglou, B. F. (2008). Evaluation of electrolytes normal values in blood of Moghani sheep breed. *Journal of Animal and Veterinary Advances*, *7*(4), 437-440.

Herrmann, D. C., Pantchev, N., Vrhovec, M. G., Barutzki, D., Wilking, H., Fröhlich, A., ... & Schares, G. (2010). Atypical Toxoplasma gondii genotypes identified in oocysts shed by cats in Germany. *International journal for parasitology*, *40*(3), 285-292. doi: 10.1016/j.ijpara.08.001.

Iqpal, S. A., Khan, M. A., Khan, M. I. & Fayaz, K. M. (2004). Assessment of renal function during (1st edn). In *Transment of pregnancy*. The PRO.

Lienden, R.V. (2005). *Toxoplasmosis*. Pawprints and purrs, Inc. Cat health care information by condition or disease, Anon-profit 50 c3 organization all donationsare tax deductable. http://www.sinksank.com/cat health/*Toxoplasmosis*.htm.

Montoya, J. G. & Liesenfeld, O. (2004). Toxoplasmosis. *Lancet. ;363*(9425), 1965–1976. doi: 10.1016/S0140-6736(04)16412-X.

Oktenli, C., Doganci, L., Ozgurtas, T., Araz, R. E., Tanyuksel, M., Musabak, U., ... & Inal, A. (2004). Transient hypogonadotrophic hypogonadism in males with acute toxoplasmosis: suppressive effect of interleukin- 1β on the secretion of GnRH. *Human Reproduction*, *19*(4), 859-866. doi: 10.1093/humrep/deh161.

Remington, J. S. (2006). *Infectious diseases of the fetus and newborn infant*. Elsevier Saunders.

Saczko, J., Daczweska, M., Marcinkowska, A., Chwiekowska, A., Aaczko, Z., Ogorzaeek, A. & Bana, T. (2002) Superoxide dismutase activity (SOD) in placentas complicated with pregnancy induced hypertention (PIH). *Zool. Polo*, *47*(3), 75-80.

Seyrek, K., Karagenç, T., Paşa, S., Kıral, F., & Atasoy, A. (2009). Serum zinc, iron and copper concentrations in dogs infected with Hepatozoon canis. *Acta Veterinaria Brno*, *78*(3), 471-475.

Sharma, S. P., & Dubey, J. P. (1981). Quantitative survival of Toxoplasma gondii tachyzoites and bradyzoites in pepsin and in trypsin solutions. *American Journal of Veterinary Research*, *42*(1), 128-130.

Steven, E., Schmitt, B., Golovko, A., Mehdi, E., & Santanu, K. (2008). Toxoplasmosis. In *Terrestrial Manual*. OIE Scientific Publications.

Tam, K.F. & Lao, T.T. (2002) Iron supplementation in pregnancy. *J. Paed. Obst. Gyna*, 24-28.

Tietz NW (1999) *Textbook of Clinical Chemistry.* (3rd edn.) W.B.Saunders Company.

Author Information

Muna ISMAIL IBRAHIM
Office of Agricultural Research / Nineveh
Iraq

Layla ABDULLAH MUSTAFA
Department of Chemistry - College of Science - University of Mosul – Iraq
Contact e-mail: *Layla.abdulla@uomosul.edu.iq*

To cite this article:

Ismail Ibrahim, M. & Abdullah Mustafa, L. (2021). Measuring the level of some trace elements in the serum and placentae of pregnant women infected with *toxoplasmosis*. *The Eurasia Proceedings of Science, Technology, Engineering & Mathematics (EPSTEM), 16*, 204-208.

The Eurasia Proceedings of Science, Technology, Engineering & Mathematics (EPSTEM)
ISSN: 2602-3199

The Eurasia Proceedings of Science, Technology, Engineering & Mathematics (EPSTEM), 2021

Volume 16, Pages 209-218

IConTES 2021: International Conference on Technology, Engineering and Science

Transmission of Secret Information Based on Time Instances

Moses Oyaro OKELLO
Jiangsu University of Science and Technology

Abstract: This Paper presents improvement and extension of previous methodology about timing steganography based on network steganography. The previous article uses time interval between two successive time instances of transmissions mixed with cryptography prior to hiding. However, this improvement tends to extend and provide new methods based on single time instance unlike the previous methodology which depend on two-time instances such as hours, minutes, second, millisecond etc. It further examines how to handle effect of different time zone and high precision timing for ultrafast timing such as millisecond, and many more which human actions is too slow for perfect timing. In addition, the extension based on Transmission Control Protocol and Internet Protocol (TCP-IP) status codes where each element of set of status code are index and the index represents certain numeric of combination for hiding. Finally, the cryptography method is improved and extended to series-based cryptography with any defined number of different cryptography methods combined altogether with multiple keys generated dynamically. The methods for both cryptography and steganography were integrated and each module carefully tested for their feasibility and appropriate analysis, comparisons presented too. A brief discussion of possible extension or application of Time Interval and Instance Steganography from network based to Video and Audio time Steganography are presented which depends on time such as rate of change of features in Video, or in Audio as well. However, these video and audio Time steganography are considered as out of scope for this article which is mainly about network Steganography.

Keywords: Steganography, Cryptography, Cyber Security, Time

Introduction

Information security also known as cyber security by Von et el (2013) is an area that deals with privacy and protection of confidential information. As a result of advancement in cyber security risk, there is need to develop advanced security methods for data protection. This call for improvement of existing security methods and or coming up with novel methods that outsmart advanced technological tools used for penetrating data Security/Privacy. Cyber security sub-divides into several branches such as cryptography by Jonathan et el (2014), steganography and many more. Steganography by Wang et el (2004) is the practice of hiding information inside another information and can be categories into several sub-categories basing on the media use for hiding and transmitting or carrying hidden message. Steganography can be classified into several categories as given below, see figure 1.

Network Steganography: is the practise of concealing information in a network carrier by either modifying inter-arrival time for network data packet to network protocols for embedding secret message see an article by Mazurczyk et el (2016).

Multimedia Steganography: this is another type of steganography which uses Multiemedia such as Images, Text, Audio and Video or motion picture for hidding secret information see paper by Papapanagiotou et el (2005) and Johnri et el (2016).

Text Steganography: this uses text for embedding secret message inside,as presented by Narayana et el (2018) based on method such as text formate modification such that the modification is invisible or by some form of text permutation just to embed the confidential message.

Video Steganograph: Is bassically about hidding secret message in video such as the one by Wang et el (2014) which may include modifying motion picture information etc.

Audio Steganography just as video steganography is about hiding information in audio signal which can be noise signal to many more methods fro example the one presented by Cvejic et el (2002) and Djebbar et el (2011).

Image Steganography. Is mostly about hiding secret information in image format such as jpg, png etc. Using some methods like Least Significant bit (LSB) Methods and many more for instance, by Kadhim el (2019).

Hybrid Steganography: this is when two or more of steganography methods is combine and used altogether for example: Image Steganography mixed with Text Steganography etc.

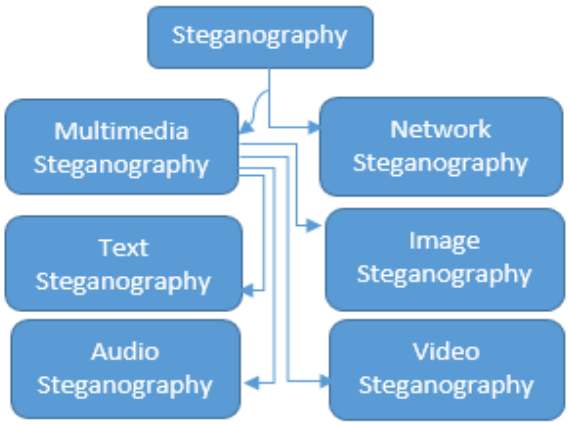

Figur 1. Classification of Stganography

Related Methodology

There are some previously published articles in the area of timing steganography, which deals with concealing information based on time instances especially in network. This initially appeared in preprint Okello (2020). For the previous manuscript by Okello (2018) which hides bits based on time interval (1) of inter-arrival of packets or events triggered in network Subject to $s.t$ (2).

$$\Delta t = t_i - t_{i-j} \tag{1}$$

$$s.t \quad t_i \geq t_{i-j}\,;\ (i-j) \in k_1;\ k_1 \geq 0 \tag{2}$$

Where if $\Delta t \in k_2$ represents bit one else if $\Delta t \notin k_2$ represents bit zero. However, for $(i-j) \in k_1$ must always belong to the set of keys in order to keep track of the previous index of time t_{i-j}. The drawback of the method is that since each interval represents a bit, it is difficult to transmit more bits. For the case of cryptography methods, it only uses two alternating cryptography method i.e., XOR and bitwise shifting i.e. Right shift $(\ll)$ and Left shift $(\gg)$. For cryptography, method presented previous which uses bi-cryptography methods for encrypting a given piece of secret message (c) was mainly to scramble secrets information (c) prior to hiding and scramble (c) it is $e = (c \oplus k_1) \gg k_2$ In addition, to decrypt content in (e), and is $c = (e \ll k_2) \oplus k_1$.

A similar work presented in an article by Liu et el (2012) where they slightly modify inter-arrival time of network packets. Their methods show that the modification is untraceable as slight modification is undetected. However, due to advancement in detectability of covert timing channel it is possible to detect such slight or very small modification.

Improvement of Methodology

This section of the paper discusses and presents new concepts as an improvement of the previous article by Okello (2018) and extension using TCP-IP status code. First, we introduce Unit of Time and the following sub-section after presents the improvement and extension methodology.

Unit of Time

Time units divide into several sub-units such as (3)

$$\infty \leftarrow : \text{hh} : \text{mm} : \text{ss} : \rightarrow \infty^{-1} \tag{3}$$

Smaller Units after Seconds are Millisecond (10^{-3}), Microsecond(10^{-6}), Nanosecond(10^{-9}), Picoseconds(10^{-12}), Femtosecond(10^{-15}), and can further subdivides up to infinitesimal unit (∞^{-1}). In term of seconds, it's express as (10^{-x}) where $x \in \mathbb{N}$ and if $x \to \infty$. Therefore, it is (10^{∞}) of a Second just like in an article by Okello (2018). It should be noted that $\infty = n^{\infty}$ for $n > 1$. Therefore, $\infty^{-1} = 10^{-\infty}$ see (3). However, for larger Units after hours are days, weeks, month, years, Decades, Century, Millennium (Kilo-Year), Mega-Year, Giga-Year, Tera-Year, eon, Supereon up to infinity(∞). Time is a special case where $\infty^{-1} \neq 0$ and $\infty^{-1} \approx 0$ because $\infty = \sum_{i=0}^{\infty} \infty^{-1}$.

The quest of how big is the biggest (∞) or how small is the smallest (∞^{-1}) lies beyond the realm of my understanding.

Time Instance Steganography

Table 1. Shows Alphanumerical (ALP) and Binary Combination (BC) Assigned to Minutes (MM)

MM	ALP	BC	MM	ALP	BC
00	M	00	30	SP	10
01	E	01	31	X	11
02	8	10	32	L	00
03	S	11	33	4	10
04	3	00	34	0	10
05	N	10	35	I	11
06	G	01	36	SP	00
07	SP	11	37	B	01
08	Q	00	38	A	10
09	T	10	39	8	11
10	.ST	01	40	CM	00
11	U	11	41	G	01
12	Y	00	42	W	10
13	B	10	43	V	11
14	H	01	44	3	00
15	D	11	45	?	10
16	J	00	46	A	01
17	P	01	47	CM	11
18	SP	10	48	:	00
19	O	11	49	M	10
20	1	00	50	C	01
21	J	10	51	N	11
22	R	01	52	6	00
23	K	11	53	T	10
24	2	00	54	5	01
25	W	10	55	S	11
26	9	01	56	F	00
27	Z	11	57	E	10
28	7	00	58	5	01
29	C	01	59	B	11

In this improvement of timing using time format such as in (3) instead of using time interval like in the previous article by Okello (2019) using combination from set $V = \{0,1,2,3,4,5,6,7,8,9\}$ of numbers. However, a concept from previous article Okello (2019) where use of Kleen Star $V^* = \{V_0 \cup V_2 \cup \ldots \cup V_n\}$ formulae is applied for generating combination of numbers from set V using relationship($\mapsto$) i.e., $(a \mapsto b)$. For instance, initially $V_0 = \{\emptyset\}$, and $V_1 = V$; so $V_1 = \{0,1,2,3,\ldots\ldots,9\}$. Therefore, possible combination of $V_2 = V_1 \mapsto V$: $V_2 = \{00,01,02,03,\ldots\ldots,99\}$ and for $V_3 = V_2 \mapsto V$: $V_3 = \{000,001,002,003,\ldots\ldots,999\}$. This continues up to a define number of combinations n such that V_n can be express as in (4). Please Table 1 for and reference corresponding characters.

$$V_n = V_{n-1} \mapsto V \quad (4)$$
$$s.t \;\; V_{n-1} = V_{n-2} \mapsto V$$

Hours (hh)

For 12 hrs. System, the following condition must hold $1 \leq hh \leq 12$ where $V_0 = \{0,1,2,3,4,..,9\}$ for both AM and PM and $hh \in V_1$. For 24hrs system, it can be express as$V_2 = \{00,01,02,03,\ldots,99\}$.

Where $00 \leq hh \leq 23$ and $hh \in V_2$

Minutes (mm)

In minutes, it is express numerically as $00 \leq mm \leq 59$ where $V_2 = \{00,01,02,03,04\ldots.,99\}$ $mm \in V_2$ And $mm \leq 59$ please see Table 1 for sample minutes assigned alphanumerical characters ALP and bit combinations as explain in paper by Okello (2019) using two-bit combination. Please note in Table 1, the following means SP (Space), ST (Full Stop), CM (Comma). Here we use only uppercase letter and some few special character and numeric commonly use.

Seconds(ss)

Second is defined as $00 \leq ss \leq 59$ and $SS \in V_2$; $ss \leq 59$ same as minutes.

Millisecond (ms)

Millisecond is measure as $000 \leq ms \leq 999$. Since its maximum value is 999, from combination of set V, such that $V_3 = \{000,001,002,\ldots,999\}$ so $ms \in V_3$; $ms \leq 999$.

Time Numeric Concatenation

Given t_i, its numeric values of combination $n \geq 2$ are consider as concatenation $a||b$ in an article Okello (2019) of set of digits index as $t_i = \{t_{i,0}||t_{i,1}||\ldots||t_{i,k}\}$. Suppose $t_i = V_{n,j}$ so $V_{n,j} = \{V_{n,j,0}||V_{n,j,1}||\ldots||V_{n,j,k}\}$. In addition, $\Delta t'$ is a different between any two or more elements of set t_i or $V_{n,j}$. To find t_{i+1} for any known $\Delta t'$, t_{i+1} is express as in (5) (6) with the aid from (4) where $\Delta t'$ represents hidden contents. Please note $\bowtie$ simply represents any of this operator $+, -, *, /$
Which can be use but because $+, -$ is the only operator that can be easily use, so we omit the rest of operators.

$$t_{i+1} = V_{n,j+l} \quad (5)$$
$$s.t \;\; \Delta t' = V_{n,j+l,k} \bowtie V_{n,j+l,k+1} \quad (6)$$

$(j + l) \geq 0$ In addition, $(j, l) \in \mathbb{N}$ for any given t_i, $\Delta t'$ can be obtain from (7). If $t_i \geq t_{i.+1}$, it means t_{i+1} is in the next cycle of time.

$$\Delta t' = t_{i,k} \bowtie t_{i,k+1} \quad (7)$$

So, by comparing $\Delta t'$ with Table 1, or those presented by Okello (2018) to extract or hid matching content. An example of minute $t_i = 27$. So $t_{i,k} = 2$, $t_{i,k+1} = 7$ then $\Delta t' = 5$. And we take $\bowtie = -$ for the case of $n > 2$, $\Delta t'$ can be from combination of any order example in (8) and (9) or many more. Also $\Delta t' = \Delta V'$

$$\Delta V' = V_{n,j,k} || V_{n,j,k+1} \bowtie V_{n,j,k+2} \tag{8}$$

$$\Delta V' = V_{n,j,k} || V_{n,j,k+1} \bowtie V_{n,j,k} || V_{n,j,k+2} \tag{9}$$

Example is $V_{n,j} = 256$, from (8) $\Delta V' = 19$ and from (9), $\Delta V' = -1$
Further inner layer e.g. $\Delta t''$ can be as in (10). Provided $\Delta t'' \in V_n; n \geq 2$

$$\Delta t'' = \Delta t'_k \bowtie \Delta t'_{k+1} \tag{10}$$

Supposed (w) represents total of $(''')$, so $\Delta t'''$ is Δt^w when $w = 3$. General expression of (10) is in (11)

$$\Delta t^w = \Delta t_k^{w-1} \bowtie \Delta t_{k+1}^{w-1} \tag{11}$$

$s.t\ \Delta t^w \in V_n$, $n \geq 2$. For Δt^* is define in (12) given that $\Delta t^0 = \Delta t;\ w \geq 0$

$$\Delta t^* = \Delta t^w \bowtie \Delta t^{w+1} \tag{12}$$

Additional in-depth layer $\Delta t^{*\prime}$ can be express in many different ways such as in (13)

$$\Delta t^{*\prime} = \Delta t_k^* \bowtie \Delta t_{k+1}^* \tag{13}$$

Note that for values of (t) of the corresponding $\Delta t^*, \Delta t^w$ should be within range of V_n. An example: Supposed Susan sent five digits access code and Mary received $t = 256$, and to decode secrete code; it is known that Mary has to use concatenation of absolute values of $\Delta t' || \Delta t'' || \Delta t^*$. And we take $\bowtie = -$
Solution: from (8) $\Delta t = 19$ and from (10) $\Delta t'' = -8$, and from (12) $\Delta t^* = 27$. Therefore, Secret Access code is 19827

Time Numerical Interval

Time interval Δt also ΔV in term of V since $t_i = V_{n,j}$ (1) and (2) have been previously use for hiding bits in article Okello (2018) by comparing if the interval $\Delta t \in k_1$ then represents bit one else zero. However here, the improvement uses combination technique in (4) since Δt is numeric such that $\Delta t \in \mathbb{N}$ where $\Delta t = \{0,1,2,3, \ldots . n\}$. Therefore, just like in Table 1, these numbers can be compared with alphanumeric values or bit combination. Those numbers are then the interval. In addition, Δt just like in (7), (8), and up to (13) can be as (14). $s.t\ \Delta t \in V_n\ ; n \geq 2$

$$\Delta t' = \Delta t_k \bowtie \Delta t_{k+1} \tag{14}$$

Unlike in time instances, different time zone does not affect time interval.

Time Zone

Different time zone

Across the globe, there is possibility that sender and receiver of secret message/information are located in different time zone(Z). Therefore, if the hidden information is encoded base on sender time zone, therefore for receiver to decode the right time, they must first subtract time zone (Z) from the receiver time (3) to get the sender time T_s. Here sender time zone is defined as Z_s and receiver time zone Z_r . In addition, receiver time as T_r . To find sender time in order to decode the right time from receiver time, see (15).

$$T_s = (T_r + Z_s) - Z_r \tag{15}$$

However, to find receiver time in case when hidden information is to be encoded using receiver time, sender need to use (16) to find the right receiver time for encoding the right information before sending.

$$T_r = (T_s + Z_r) - Z_s \tag{16}$$

For $(T_r, T_s) < 0$ indicate previous day $t_r += 24$ and for $(T_s, T_r) \geq 24$ in 24 hrs system indicates next day $t_r -= 24$. The same applies for t_s

Same Time Zone

For the case when both sender and receiver are located within the same time zone. $Z_s = Z_r$. Therefore, from (15) and (16) $T_r = T_s$. Furthermore, considering non-real-time system with uniform delays δt should abstract from (15) and (16) to get the actual T_r, T_s. However, $\delta t \approx 0$ in real-time transmission system, so there is no need for subtracting anything just like in Okello (2018). For ultrafast timing (3), use of automated devices is highly recommended.

Extension to TCP-IP Status Code

For the use of TCP-IP status code given status code set $S = \{s_1, s_2, s_3, \dots, s_n\}$ where $s_i \in S$ and index i of the status code represents bit combination as shown in example Table 2. Here, combination technique presented in (4) is use. Where combination base value $V = \{0,1\}$ representing binary numbers that is equivalent of bits and for set $V = \{0,1,2,3, \dots 9\}$ represents numeric integers and a set of TCP-IP status codes. For example, see Table 2 where set of status code for hypertext transfer protocol (http) are index numerically up to 16 index from zero to fifteen, and this number of index are assign four bits combination. So to generate a given bit combination of total (n) $V_n = V_{n-1} \mapsto V$ just like in (4) so for instance when $n = 4$. So $V_4 = \{0000, 0001, 0010, \dots \dots 1111\}$ for more details see paper by Okello (2019) on how to generate combination of binary values. Please see Table 2 for sample http status code where each http status code has an index assigned to them and an equivalent bit combination allocated.

Table 2. Sample http status code (SC), index (ID), and bit combination (BC)

ID	BC	http	ID	BC	http
0	0000	301	8	1000	411
1	0001	304	9	1001	503
2	0010	307	10	1010	204
3	0011	400	11	1011	205
4	0100	401	12	1100	302
5	0101	403	13	1101	308
6	0110	404	14	1110	405
7	0111	408	15	1111	410

Improvement of Cryptography

From the previous bi-cryptography methods presented by Okello (2018), multiple cryptography methods is presented called series based cryptography where a given character/information is encrypted up to a defined number of cryptography method with given number of varying keys as per the cryptography method presented. Supposed function $G(c, K)$ represents set of known cryptography methods such that

$\{g_1(c, k_1), g_2(c, k_2), .., g_n(c, k_n)\} \in G(c, K)$ and $k_i \in K$ are set of keys for encrypting. For parameter (c) represents character, or information for encrypting by cryptography methods. $g_i(c, k)$ Moreover, (k_i) is key for encrypting information. To encrypt character (17).

$$e = g_n(g_{n-1}(\dots g_1(c, k_1) \dots, k_{n-1}), k_n) \tag{17}$$

To decrypt encrypted contents in (e), it is the reverse of the formulae in (17) please see (18) for decrypting. We assume that the function for decrypting is $G'(e, K')$ where $\{g'_1(e, k'_1), g'_2(e, k'_2), .. g'_n(e, k'_n)\} \in G'(e, K')$ and $k'_i \in K'$ are sets of keys for decrypting encrypted contents.

$$c = g'_1(g'_2(\dots g'_n(e, k'_n) \dots \dots, k'_2), k'_1) \tag{18}$$

In the functions for decrypting $G'(e, K')$ takes in encrypted contents (e) with keys K' for decrypting and returns decrypted contents c. From the previous methods, $e = (c \oplus k_1) \gg k_2$ can write as $e = g_2(g_1(c, k_1), k_2)$ where $g_2(c, k_2) = (\gg\ll)$ representing the bitwise shift operator and $g_1(c, k_1) = \oplus$ representing XOR operator. To decrypt e, $c = g_1'(g_2'(e, k_2'), k_1')$ the same function can represent any cryptography method known and feasible, so that their combination is use to improve on security strength.

Experimental Results

Results for Timing Steganography

In this to show that this method can work perfectly, it is performed using minutes where records of chart messages and phone time of calls from the sender to receiver located within the same time zone. Figure 2 shows extracted time from calls in a day from sender and decoded as "MEETING 18:18 AT GULU" please see Table I for reference on how to extract the message and in addition, this is an unencrypted hidden message. However, both sender and receiver should know Table I before sending in order to encode and decode the hidden message.

08:49, 08:57, 09:01, 09:09, 09:18, 09:20, 09:39, 09:48, 10:20, 10:39, 11:18, 11:38, 11:53, 12:36, 12:41, 13:11, 13:32, 14:11

Figure 2. Shows extracted time of chart messages.

Results for TCP-IP Status Code

The experimental condition to verify the method base on http status code was perform on Server side and Client side where client received http status code message from server by accessing web services from the server. The status code (S) received is then compare with information in Table II to extract the hidden contents it represents. The following extracted http status code $S = \{404, 403, 400, 503\}$, which indices are ID= {6, 5, 3, 9}. Now converting the numeric in base ten to base two binary. 6 is 110 in base two, 5 is 101 in base two, 3 is, 11 in base two, 9 is 1001 in base two. However, total bit combination is four in each base two, so adding zero in front to make four bit combination and Joining $\{0110 + 0101 + 0011 + 1001\}$, Converting from binary stream to characters ="e9" and decrypting to "Hi".

Results for Cryptography

To demonstrate the feasibility of the cryptography method, see Table 3 where a given text is encrypted using series-based cryptography methods.

Table 3 Shows how to encrypt contents using series Cryptography having three Cryptography methods

Functions	Initial c_0	$g_1(c_0, k_1)$	$g_2(c_1, k_2)$	$g_3(c_2, k_3)$
Cryptography Methods	Plain texts	Blowfish	AES	RSA
Key(s)		654321	65431234okello10	Public key not included here
Text to be encrypted	Hello, how are you doing today?	C2iPxDg9gInP+Pg OFX7DYjXUoWAM 6bPtQGVoFgo/qwY=	F5580164B3908025A CF548DAC94049A1A BABB225C67DE4209 7287E8FC9FB378C87 7C79C7F73DE4B5AE F01C62987BFC99	KFEzHUJ+mHIMfFn0WvfuGj+ VIM75PsVyZIuunEZ+8iRhGVY okchuEq6nyYpzY4zYocSc1MQX VwikBQrEHi9ihjklhqwxom/7clxk Q3w2KhhnIV6wGmzrutsIwOx6T Xorpylb0S6wZLZGnm/gS5ol7IHs 4c8cIYZqOixWRyGvf2g=

To decrypt the contents in Table 3 see Table 4 blow here

Table 4 shows how to decrypt contents using series Cryptography with three Cryptography methods

Functions	Initial $g_3'(c_3, k_3)$	$g_2'(c_2, k_2)$	$g_1'(c_1, k_1)$	Decrypted Text c_0
Cryptography Methods	Encrypted Texts Using RSA	AES	Blowfish	Plain Text
Key(s)	Enter Public key not included	65431234okello10654321	654321	
Text to be decrypted	KFEzHUJ+mHIMfFn0WvfuGj+ VIM75PsVyZIuunEZ+8iRhGV YokchuEq6nyYpzY4zYocSc1 MQXVwikBQrEHi9ihjklhqwx om/7clxkQ3w2KhhnIV6wGmz rutsIwOx6TXorpylb0S6wZLZ Gnm/gS5ol7IHs4c8cIYZqOix WRyGvf2g=	F5580164B39 08025A CF548DAC9 4049A1A BABB225C6 7DE4209 7287E8FC9F B378C87 7C79C7F73D E4B5AE F01C62987B FC99	C2iPxDg9gI nP+Pg OFX7DYjX UoWAM 6bPtQGVoF go/qwY=	Hello, how are you doing today?

Analysis and Comparison

Analysis of Time Instance Steganography and TCP-IP

Let sample space he defines as $n(V_i)$ (4), which is the cardinality of set V_i for both TCP/IP status code and timing steganography such as in (3). Therefore, the probability that a chosen status code or time format is the right one containing hidden information /character combinations can be express as $P = 1/n(V_i)$ and that it's not, can be express as $P' = (1 - P)$. Therefore, this implies that by making $n(V_i)$ big or large enough, it reduces the chances of guessing the hidden content as shown in the probability see (19).

$$P' = (n(V_i) - 1)\big(n(V_i)\big)^{-1} \tag{19}$$

In comparison to previous methods and some existing methods in timing steganography, this method including TCP/IP status code does not modify the code or time for carrying hidden message as it only represents combination of bit/character to be hidden, so it is quite difficult to intercept the hidden information flow.

Analysis of Cryptography

This method is very hard for cryptanalyst to decrypt the encrypted contents. Let probability that $g_i(c, k_i)$ is breakable be p_i' and that it is not be p_i. Therefore, probability that at least one of $g_i(c, k_i)$ in (17) is not breakable is express as in (20).

$$P = 1 - (\prod_{i=0}^{n} p_i') \tag{20}$$

So as n in (20) increases, P approximately equals one, implying strength of cryptography increases with more series. However, a greater number of keys can delay execution for larger strings/text, as more cryptography methods and keys mean more series or repetitive encryption of the same character/information, so it is advisable to use fewer numbers of cryptography methods and keys with larger string where time performance is more important than security. Also repeating character in key will results into decrypting the encrypted contents like for the case of XOR cipher, which means no work done. Therefore, one should take care to avoid repeating keys.

Time performance analysis of formulae (17) and (18). Let total function of $g_n(c, k_n)$ operator in a series cryptography is (n) and time taken for each $g_i(c, k_i)$ in $G(c, K)$ operation be t_i. Therefore, total time T taken to encrypt a character a given number of operations is the summation of all t_i for using mixture of cryptography.

Finally, to encrypt an entire string or text of total character"m", one has to use the formulae below (21) to find total encryption time.

$$T = m(\sum_{i=0}^{n}(t_i)) \tag{21}$$

To have higher security, element of set $G(c,K)$ should be large enough, however making these too large when "m" is large makes T extremely large, hence significantly slowing down execution time. Therefore, to make time of execution T small, for larger value of m total of $G(c,K)$ elements should be as small as possible. However, by making $G(c,K)$ elements small means less keys. Therefore, security strength diminishes too. The equation (21) can embed directly into the algorithm (17) and (18) to calculate total time taken for encrypting a given set of text or string of character.

Discussion of Possible Extension

In this sub-section, further ways of how to encode information based on both video and audio or even text-based steganography.

Video: For video, it is based on the idea that video comprises of moving pictures in which a feature in a recorded video is timed such that the instances or the interval represent the intended message just like in network steganography.

For example, in action movie where background of actors angle/positioning of reference object/Actor or even some tiny feature which is part of the video that keep changing at a varying interval or at given instances. A similar approach can be used in Audio such as timing of sentences construction, tone variation, etc. For text, it's quite difficult. However, the concept of numerical value in Time interval or Time instance steganography can also be applied in text where possible.

Conclusion

This improvement and extension of previous article by Okello (2018), which hides bits or information by using time format such as in (3). Moreover, TCP-IP status code using numeric index and combination technique that is in paper **Hata! Başvuru kaynağı bulunamadı.** has made it possible to hide more bits or information unlike in previous article Okello (2018) where time interval hides a single bit at each interval. In addition, time being very reliable and also status code in TCP is very convenient unlike UDP where packets are delivered without acknowledgements or status updates or no delivery feedback makes TCP very desirable to use in the method due to the prompt status feedback.

The method further encrypts information prior to hiding to improve on un-detectability and making it hard to decrypt by improving the previous encryption methods to series base cryptography where contents to be hidden is first encrypted up to a given number of times with different encryption methods and different keys generated dynamically. The use of $\Delta t^{w}, \Delta t^{*}, \Delta t^{*\prime}$ for $w \gg 1$ remains a theoretical work and its practical application are beyond the scope of this work.

Scientific Ethics Declaration

The author declares that the scientific ethical and legal responsibility of this article published in EPSTEM journal belongs to the author.

References

Cvejic, N., & Seppanen, T. (2002, December). Increasing the capacity of LSB-based audio steganography. In *2002 IEEE Workshop on Multimedia Signal Processing.*

Djebbar, F., Ayad, B., Hamam, H., & Abed-Meraim, K. (2011, April). A view on latest audio steganography techniques. In *2011 International Conference on Innovations in Information Technology* (pp. 409-414). *IEEE Transactions on Information Forensics and Security*, *9*(5), 741-751.

Johri, P., Mishra, A., Das, S., & Kumar, A. (2016, March). Survey on steganography methods (text, image, audio, video, protocol and network steganography). In *2016 3rd International Conference on Computing for Sustainable Global Development (INDIACom)* (pp. 2906-2909).

Jonathan, K., & Yehuda, L. (2015). Introduction to Modern Cryptography.-2nd. http://203.162.10.101/jspui/handle/123456789/723

Kadhim, I. J., Premaratne, P., Vial, P. J., & Halloran, B. (2019). Comprehensive survey of image steganography: Techniques, Evaluations, and trends in future research. *Neurocomputing*, *335*, 299-326.

Liu, G., Zhai, J., & Dai, Y. (2012). Network covert timing channel with distribution matching. *Telecommunication Systems*, *49*(2), 199-205.

Mazurczyk, W., Wendzel, S., Azagra Villares, I., & Szczypiorski, K. (2016). On importance of steganographic cost for network steganography. Security and Communication Networks, 9(8), 781-790.

Narayana, V. L., Gopi, A. P., & Kumar, N. A. (2018). Different techniques for hiding the text information using text steganography techniques. *Neurocomputing*, *335*, 299-326.

Okello, M. (2018, October). A New Timing Steganography Algorithm in Real-Time Transmission Devices. In *2018 IEEE 18th International Conference on Communication Technology (ICCT)* (pp. 880-884).

Okello, M. (2020). A mixture of timing steganography and series. https://www.techrxiv.org/articles/preprint/A_Mixture_of_Timing_Steganography_and_Series_Cryptography/13134992

Okello, M. A (2019). Secure and optimal method of steganography using bit combination and dynamical rotation. Over Addresses. Preprints 2019, 2019020252. https://www.preprints.org/manuscript/201902.0252/v2

Papapanagiotou, K., Kellinis, E., Marias, G. F., & Georgiadis, P. (2005, December). Alternatives for multimedia messaging system steganography. In *International Conference on Computational and Information Science* (pp. 589-596). Springer, Berlin, Heidelberg.

Von Solms, R., & Van Niekerk, J. (2013). From information security to cyber security. *Computers & Security*, *38*, 97-102.

Wang, H., & Wang, S. (2004). Cyber warfare: steganography vs. steganalysis. *Communications of the ACM*, *47*(10), 76-82.

Wang, K., Zhao, H., & Wang, H. (2014). Video steganalysis against motion vector-based steganography by adding or subtracting one motion vector value. *IEEE Transactions on Information Forensics and Security*, *9*(5), 741-751.

Author Information

Moses Oyaro OKELLO
Jiangsu University of Science and Technology Gulu,
Uganda
Contact e-mail: *mosesokellomoses@gmail.com*

To cite this article:

Okello, M.O. (2021). Transmission of secret information based on time instances. *The Eurasia Proceedings of Science, Technology, Engineering & Mathematics (EPSTEM)*, *16*, 209-218.

The Eurasia Proceedings of Science, Technology, Engineering & Mathematics (EPSTEM)
ISSN: 2602-3199

The Eurasia Proceedings of Science, Technology, Engineering & Mathematics (EPSTEM), 2021

Volume 16, Pages 219-224

IConTES 2021: International Conference on Technology, Engineering and Science

600W DC-DC Converter Design Using Flyback, Half Bridge, Full Bridge LLC Topologies and Comparison of Simulation Results

Omer Emre EKICI
Eskisehir Osmangazi University

Atabak NAJAFI
Eskisehir Osmangazi University

Faruk DIRISAGLIK
Eskisehir Osmangazi University

Abstract: This paper presents design and simulation of typical DC-DC converter topologies such as Flyback, half bridge, full bridge LLC, using the PLECS simulation tool. Requirements are chosen to be 600 W power rating and 250 kHz switching frequency with high efficiency and reduced built size. MOSFET is used as the switching element. According to the simulation results, optimum design with the lowest fluctuations in output voltage and current are achieved using the full bridge LLC converter topology. Thanks to the resonant coil and resonant capacitor in its structure, reduced switching losses have been observed in this converter design, which provides soft switching and high switching frequency.

Keywords: DC-DC converter, Switching, Half bridge, FlyBack, Full bridge LLC

Introduction

DC-DC converters are electronic circuits that convert -increase/decrease- a DC voltage level to another level. It accumulates energy in the coil by switching the switching element in its structure at appropriate times. It provides the desired power and voltage level by transferring this energy to the output. They are widely used in variety of applications such portable electronic devices, automotive, military, aerospace, energy and medical systems in which requires continuous and multiple voltage levels. Therefore, they have great importance in the industry. There are many different topologies in DC-DC converters for different purposes such as extra security, control method, desired power, type of load. In industry, the aim is to provide the desired quality at the cheapest cost. Resonance converters transfers power with resonance in contrast to conventional DC-DC converters that operating according to the principle of energy stored in the inductor. DC-DC converters based on resonance power transmission provide soft switching, so switching losses are significantly reduced, efficiency and frequency are increased, thus reducing costs. Hence, resonant converters are common in the industry. (Mohan, 1995; Rashid, 2001).

The key objectives in converter design are high power density, high efficiency, and optimum built size. Switching frequencies are increased in order to provide high power density and optimum size among these. The increase in the switching frequency reduces the size of the elements such as transformers, coils and capacitors in the converter. However, high switching frequency brings high switching losses. Switching losses cause decreased efficiency, shortened life of materials and excessive heat. Therefore, soft switching techniques are

used in high switching frequency converters. Soft switching reduces the switching losses through the components connected to the switching elements. Zero voltage switching (ZVS), zero current switching (ZCS), zero voltage transition (ZVT) and zero current transition (ZCT) are the most common soft switching methods (Çetin, 2017; Kubilay, 2020, İşbilir, 2005; Polat, 2017).

Zero voltage switching reduces the rapid rise in voltage during switching by a capacitor connected in parallel with the switching element. Zero current switching reduces the rapid rise in current during switching, thanks to the coil connected in series with the switching element. Zero-current transition and zero-voltage transition also provide a delay in voltage and current spikes during switching (Mohan, 1995; Rashid, 2001; İşbilir, 2005; Saydı, 2017; Polat, 2017).

DC-DC converters are classified as isolated and non-isolated converters. Transformers provide galvanic isolation between input and output. Hence, converters using a transformer such as full bridge, half bridge, forward, flyback and push-pull converters are called isolated DC-DC converters. Converters without a transformer such as boost, buck, buck-boost, CUK, SEPIC and ZETA are called non-isolated DC-DC converters. In isolated converters, the energy flow is provided through the transformer (Mohan, 1995; Rashid, 2001; İşbilir, 2005; Saydı, 2017; Polat, 2017; Yılmaz, 2020).

DC-DC Converter Design

Flyback Converter Design

Flyback converters are frequently preferred converter topology due to their galvanic isolation and simple design. They can be used where the input voltage is lower or higher than the output voltage. Transformer winding ratio and switching element duty cycle time determine the relationship between input and output voltages. The flyback converter topology is shown in figure 1. When the switch S is on, the input voltage transfers energy to the coil. The load is energized from capacitor. When the S switch goes off, the diode turns on and the energy on the coil is transferred to both the capacitor and the load (Mohan, 1995; Rashid, 2001; İşbilir, 2005; Yılmaz, 2020).

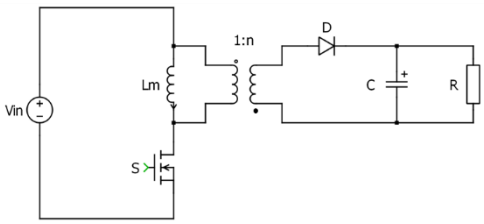

Figure 1. Flyback converter topology

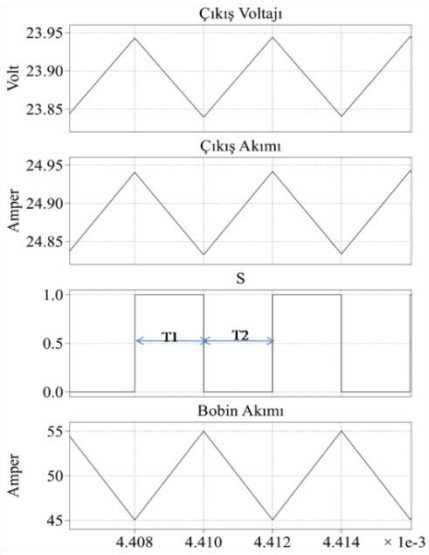

Figure 2. Flyback converter simulation results

A flyback converter with 600 W of power rating was designed. The output voltage is 25 V and output current is 25 Simulations were made using the PLECS tool. Output voltage waveform, output current waveform, current drawn from the primary winding of the transformer and switching are shown in figure 2.

The ratio of the time that the switching element is on to the switching period gives the duty cycle time (*D*). The relationship in between transformer winding ratios (*n*) and input (V_i) and output (V_o) voltages shown below.

$$D = \frac{T1}{T1+T2} \quad (1)$$

$$n = \frac{Seconder\ sarım\ oranı}{Primer\ sarım\ oranı} \quad (2)$$

$$V_o = n \times \frac{D}{1-D} \times V_i \quad (3)$$

The following relationship exists between the input (I_i) and output (I_o) currents in ideal conditions,

$$I_i = n \times \frac{D}{1-D} \times I_o \quad (4)$$

The value of capacitor *C* can be found with the following formula. F_s is the switching frequency. ΔVo is the output voltage fluctuation value.

$$C = \frac{Io\ x\ D}{\Delta Vo\ x\ Fs} \quad (5)$$

Flyback converters are used in low power applications. In high power applications, the transformer must have a large air gap to store energy. Large air gap increases leakage in flux and causes inefficiency.

Half Bridge Converter Design

Half Bridge converters are used at power rating up to 500 W. Since it contains fewer switching elements compared to the full bridge structure, the switching losses are less. Half bridge converter topology is shown in figure 3.

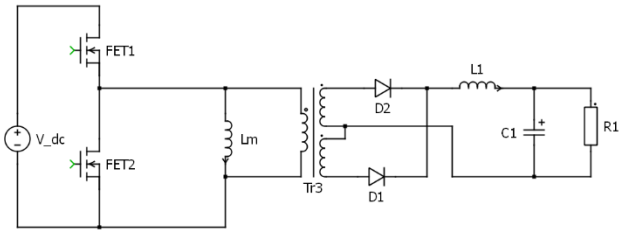

Figure 3. Half Bridge converter topology

Output voltage waveform, output current waveform, L1 coil current waveform and switching are shown in figure 4 for the designed half bridge converter with 600 W power rating.

As seen in Figure 4, there is 0.7 V fluctuation in voltage and 0.7 A in current. When the S switch is on, energy accumulates in the coil, when the S switch is off, the energy in the coil is transferred to the output. The relationship in between input and output voltages and currents is shown below.

$$V_o = n \times D \times V_i \quad (6)$$

$$I_i = n \times D \times I_o \quad (7)$$

L1 and *C1* are used for filtering. It is found with the following equations. ΔIl is the desired current fluctuation value on the *L1* coil. F_s is the switching frequency. ΔVo is the output voltage fluctuation value.

$$L1 = \frac{\left(\frac{Vi}{n} - Vo\right) xD}{\Delta Ilx2xFs} \quad (8)$$

$$C1 = \frac{\Delta Il}{8x\Delta Vox2xFs} \quad (9)$$

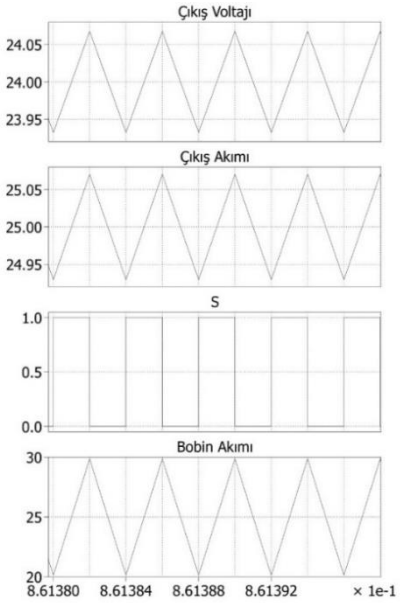

Figure 4. Half Bridge converter simulation results

Full Bridge LLC Converter Design

Full Bridge LLC converters work with the resonant converter principle. The resonant coil and resonant capacitor resonate with the square wave coming from the switching elements and transfer the energy to the transformer. Energy flow is provided through the transformer. Unlike the classical PWM method, the appropriate control signal is provided by the frequency modulation technique. Resonant converters consist of switching network, resonant tank and rectifier network shown in figure 5 (Mohan, 1995; Kubilay, 2020; Seminar Notes, 2018).

Figure 5. Resonant converter structure

The switching network generates a square wave to excite the resonant tank. The resonant tank generates resonance wave according to the appropriate resonance frequency and is transmitted to the rectifier network via transformer. In the rectifier network, the wave is rectified. DC voltage is transmitted to the output by filtering process. Control is provided by changing the switching frequency in full bridge LLC converters. Maximum efficiency and power flow is achieved where the switching frequency and the resonant frequency are equal. The resonance coil and resonance capacitor value are determined according to this principle (Mohan, 1995; Kubilay, 2020; Seminar Notes, 2018).

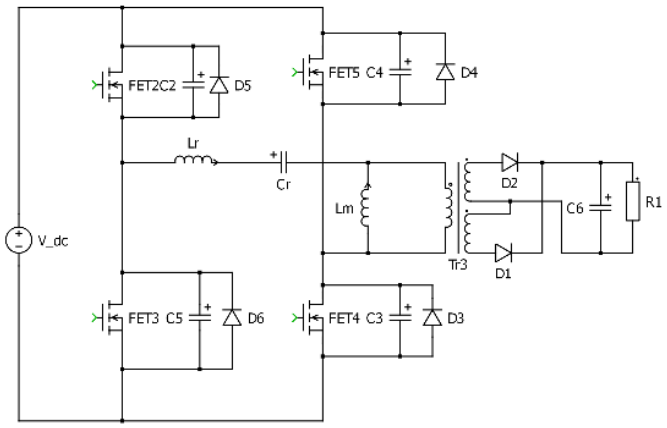

Figure 6. Full Bridge LLC converter topology

The Full Bridge LLC Converter topology is shown in Figure 6. The square wave produced by the switches is transmitted to the transformer by changing the gain with the resonant tank elements.

The output voltage and current waveforms, switching and resonant coil current waveform are as shown in figure 7. Fluctuation in output voltage is seen as 0.05 V in the converter, which has an output voltage of 24 V. In addition, the fluctuation in output current is 0.05 A. Since the current drawn from the coil is close to the full sinus format, it is understood that the resonant frequency is close to or equal to the switching frequency. For this reason, it is observed that there is maximum efficiency and minimum fluctuation.

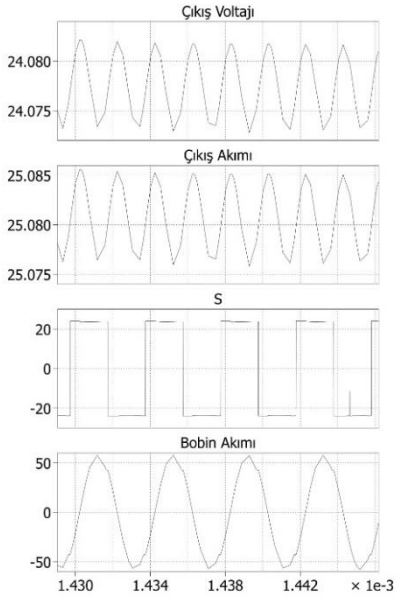

Figure 7**.** Full Bridge LLC converter simulation results

Results

In this paper, 3 DC-DC converter topologies were designed, and simulation results were obtained by using the PLECS tool. Switching frequencies were chosen as 250 kHz. Output voltage fluctuation, output current fluctuation, current drawn from the coils are examined. The lowest fluctuation in output current and voltage is seen in the full bridge LLC converter design. Thanks to the resonance coil and resonance capacitor in its structure, soft switching is provided. Thus, switching losses are reduced. Additional components must be added to provide soft switching to other converter topologies. Considering these reasons, it is seen that the optimum topology for 600 W DC-DC converter design is full bridge LLC structure.

Scientific Ethics Declaration

The authors declare that the scientific ethical and legal responsibility of this article published in EPSTEM journal belongs to the authors.

References

Çetin, S. (2017). Veri merkezi uygulamaları için yüksek verimli bir llc rezonanslı dc-dc dönüştürücü tasarımı. *Gazi Üniversitesi Fen Bilimleri Dergisi Part C: Tasarım ve Teknoloji*, *5*(1), 45-54.

İşbilir, H. (2005). *Yüksek güçlü yumuşak anahtarlamalı tam köprü bir anahtarlamalı güç kaynağı uygulaması* [Yüksek Lisans Tezi]. Yıldız Teknik Üniversitesi.

Kubilay, M., & Aydemir, M. T. (2020) LLC rezonanslı da-da dönüştürücü tasarımında kullanılabilecek bir grafiksel arayüzün geliştirilmesi. *Gazi Üniversitesi Fen Bilimleri Dergisi Part C: Tasarım ve Teknoloji*, *8*(3), 632-643.

Mohan, N., Undeland, T. M., Robbins, W. P. (1995). *Power electronics converters, applications, and design.* John Wiley & Sons Inc.

Polat, A. H. (2015). *Sıfır gerilimde anahtarlamalı, faz kaydırmalı rezonant pwm kontrollü, tam köprü dc-dc dönüştürücü tasarımı ve uygulaması.* (Yüksek Lisans Tezi). İstanbul Teknik Üniversitesi.

Rashid, M. H. (2001). *Power electronics handbook*, Academic Press.

Saydı, A. S. (2017). *DA-DA dönüştürücülerde kullanılan yumuşak anahtarlama tekniklerinin incelenmesi ve simülasyonu.* (Yüksek Lisans Tezi). Kocaeli Üniversitesi.

Seminar Notes, 2. T. (2018). S*urvey of resonant converter topologies. texas instruments incorporated.* https://www.ti.com/seclit/ml/slup376/slup376.pdf

Yılmaz, Ü. (2020). *Investigation of high efficient dc-dc converters for on-board battery charging system in electric vehicles.* (Doktora Tezi). Çukurova Üniversitesi.

Author Information

Omer Emre EKICI
Eskişehir Osmangazi University
Eskişehir, Turkey
Contact e-mail: *emreekici3@gmail.com*

Atabak NAJAFI
Eskişehir Osmangazi University
Eskişehir, Turkey

Faruk DIRISAGLIK
Eskişehir Osmangazi University
Eskişehir, Turkey

To cite this article:

Ekici, O., E., Najafi, A. & Dirisaglik, F. (2021). 600W DC-DC converter design using flyback, half bridge, full bridge LLC topologies and comparison of simulation results. *The Eurasia Proceedings of Science, Technology, Engineering & Mathematics (EPSTEM), 16*, 219-224.

The Eurasia Proceedings of Science, Technology, Engineering & Mathematics (EPSTEM)
ISSN: 2602-3199

The Eurasia Proceedings of Science, Technology, Engineering & Mathematics (EPSTEM), 2021

Volume 16, Pages 225-230

IConTES 2021: International Conference on Technology, Engineering and Science

Measurements the Level of Lipid Peroxidation and Some Antioxidants in Blood Serum of Thalassemia's Patients

Saba Z. AL-ABACHI
University of Mosul

Sameer M. AL-GORANY
Middle Technical University

Abdulrazzaq ALTUWAIJARI
Director of Diyala Haematology Center

Jaafar Ather GHAZY
Philadelphia University

Abstract: Repeated blood transfusion in beta thalassemia patients may lead to peroxidative tissue injury by secondary iron overload. In the present study, (43) patients with beta thalassemia. We have evaluated hemoglobin (Hb), packed cell volume (PCV), red blood cells (RBC), white blood cells (WBC), iron (Fe), ferriten, uric acid, glutathion (GSH), malondialdehyde (MDA), Vitamins C and E and electrolytes as sodium (Na), potassium (K), and chloride (Cl). The findings were compared with (25) age matched healthy individuals were included in this study as a control group. A significant increase in the levels of WBC, Fe, ferritin, MDA and Vit C ($P < 0.001$), whereas significant decrease in the levels of Hb, PCV, RBC, GSH and Vit E ($P < 0.001$) was observed. Uric acid, Na and K were significant increase ($P < 0.05$) in the patients when compared with controls, while there was a non-significant increase in mean value of Cl. These results were suggesting that oxidative stress and reduced antioxidant defense mechanism play an important role in pathogenesis of beta thalassemia major. We can conclude that defective membrane transport is responsible for observed changes of lipid peroxidation and some antioxidants. These results may help to understand the altered electrolyte homeostasis in thalassemia but there is still need of many future studies to clarify their mechanism of generation and pathological significance.

Keywords: Antioxidant, Beta thalassemia, Hemoglobin, Glutathion, Malondialdehyde.

Introduction

Thalassemia is an inherited blood disorders characterized by abnormal hemoglobin production. Symptoms depend on the type and can vary from none too severe. Regularly there is mellow to serious frailty (low red platelets) which can bring about inclination drained and fair skin. There may likewise be bone issues, an expanded spleen, yellowish skin, dull pee, and among kids' moderate development (Rund, 2016; Hashim et. al., 2020).

There are two main types of thalassemia, beta thalassemia, which includes the subtypes major, intermediate. It occurs when the body cannot produce beta globin. Alpha thalassemia occurs when the body cannot make alpha globin. This type of thalassemia also has two serious types hemoglobin H disease and hydrops fetalis. Thalassemia minor, people with this case do not usually have any symptoms. Both α- and β-thalassemia are

- Selection and peer-review under responsibility of the Organizing Committee of the Conference

often inherited in an autosomal recessive manner. For the autosomal recessive forms of the disease, both parents must be carriers for a child to be affected. If both parents carry a hemoglobinopathy trait, the risk is 25% for each pregnancy for an affected child (Kingchaiyaphum et. al., 2020).

Thalassemia is a hereditary blood issue that causes hemoglobin inadequacy and extreme weakness, keeping organs from oxygen, which represses their capacity to work appropriately. The survival of patients with thalassemia has progressively improved with advances in therapy; however, rehashed blood transfusion in beta thalassemia noteworthy patients may provoke peroxidative tissue harm by assistant iron over-load (Antonio et. al., 2019).

Oxidative damage incited by free globin chains has been involved in the pathogenesis of the film varieties from the standard saw in β thalassemia. We decided if thalassemia could represent anomalous cation transport framework. Thalassemia is an innate hemolytic issue caused by a fractional or finish insufficiency of alpha-or beta-globin chain blend. Homozygous bearers of beta-globin quality imperfections experience the ill effects of extreme iron deficiency and different genuine entanglements from adolescence (Srinoun et. al., 2019). The significant irregularity inside red blood cell (RBC) of patient with thalassemia results from the precipitation of unstable hemoglobin chain, which is available in overabundance. The RBC film is to a great degree hurt by the wealth empowering hemoglobin chains. Relatively every part of the thalassemic blood cell layer is changed: lipids, proteins, sialoglycoproteins and glycolipids. This layer harm speaks to a vital instrument prompting pallor in thalassemia (Al- Janabi et. al., 2021).

Method

Patients were enrolled in the present study to the Hematology center in Diyala. Samples of (43) patients were included in this study (22 males and 21 females) ranging in their age between (2-37) years, were collected during the period June to November 2017. They are diagnosed clinically based on serious paleness and hemoglobin electrophoresis. Every one of the patients were analyzed frequently on more than one occasion per month by clinicians. They were consistently accepting erythrocytes transfusions (stuffed RBC) consistently.

The control group include Twenty- five age matched healthy individuals were included in this study (15 males and 10 females) as a control group. None of these group had history of anemia, abnormal complete blood counts and abnormal hemoglobin electrophoresis results.

Hematology measurements were applied by Horiba Medical technology which will provide a significant improvement in differentiating blood cells.

Materials

- The GSH was determined by using modify method of (Sedlak and Lindsay, 1968)
- Serum lipid peroxide was measured by Kei Satoh (Wysocka et. al., 1995).
- Vit C was determined according to (Omaye et. al., 1979) method.
- Serum Vit E was resolute by (Varley et. al., 1979).
- Uric acid level was estimated by Enzymatic methods of (Tietz, 1999).
- For estimation of Iron, serum was deproteinized by Ramsay's Dipyridyl Method (Varley, 1967).
- Ferritin was dictated by using Elecsys technology with cobas instrument (Tietz, 1999).
- The estimation of serum Na and K by using (Annino and Giese, 1976).
- The colorimetric method was used to determine the Cl by (Snell, 1981).

Statistical Analysis

The information was performed utilizing the Statistical bundle for the sociology (SPSS) program. Results were communicated as mean ± standard deviation (SD). The t-test used to analyze the noteworthiness of the mean contrasts between two gatherings. The distinctions were viewed as noteworthy if the acquired p esteem was less or equivalent to 0.05 (Hinton, 2004).

Results and Discussion

In individuals with beta thalassemia, low levels of hemoglobin prompt an absence of oxygen in numerous of parts of the body. Thalassemia upsets the typical creation of hemoglobin and sound red platelets. This causes weakness and, the blood doesn't have enough red platelets to convey oxygen to tissues leaving the exhausted patients (Psatha et. al., 2018). Thalassemia disrupts the normal production of hemoglobin and healthy red blood cells. This causes anemia and, the blood doesn't have enough red blood cells to carry oxygen to tissues leaving the fatigued patients (Wafaa Al-Mosawy, 2017).

Significant lower mean levels of the red cell PCV values in patients were observed ($P < 0.001$), as compared to control group. This might be produced because of low mean corpuscular hemoglobin fixation (MCHC), on the grounds that the absence of typical amounts of intracellular hemoglobin, which fills in as a substrate for the powerful oxygen radicals and could result in an abundance of free radicals which oxidize different film segments prompt layer harm in thalassemia RBCs (Anselmo et. al., 2020) as shown in table (1).

Table 1. The Hb, PCV, RBC and WBC concentration in serum of thalassemia patients and control group.

	Mean ± SD	
Parameters	Control n= 25	Patients n= 43
Hb (g \ L)	14.64 ± 0.42	8.18 ± 1.14***
PCV %	41.07 ± 1.72	19.27 ± 3.14***
RBC $* 10^9$ \ L	4.86 ± 0.17	2.66 ± 0.09***
WBC $* 10^9$ \ L	6.41± 0.52	45.41 ± 7.05***

*** Significant difference between controls at ($P < 0.001$)

A significant increase in serum WBC ($P < 0.001$) of thalassemia patients when compared with control group. Leukocytosis is very common in acutely ill patients. It occurs in response to a wide variety of conditions, including viral, bacterial, fungal, or parasitic infection, hemorrhage, and exposure to certain medications or chemicals including steroids. Leukocytosis can be a reaction to various infectious, inflammatory, and, in certain instances, physiologic processes as stress or exercise (Chen et. al., 2020).

Table 1. The GSH, MDA, Uric acid, Iron and Ferritin concentration in serum of thalassemia patients and control group.

	Mean ± SD	
Parameters	Control n = 25	Patients n= 43
GSH $* 10^{-5}$ (µmole /L)	7.44 ± 0.22	1.56 ± 0.43***
MDA (µmole/L)	0.85 ± 0.13	1.51 ± 0.08***
Uric acid (mg /dl)	389.42 ± 16.81	395.11 ± 17.64**
Iron (µg /dl)	83.97 ± 7.38	379.80 ± 49.96***
Ferritin (ng /ml)	71.73 ± 7.33	3484.21 ± 447.29***

** Significant difference between controls at ($P < 0.01$)
*** Significant difference between controls at ($P < 0.001$)

The GSH level was decreased highly statistically significant, as shown in table (2), The present investigation announced an inadequacy in levels of decreased glutathione, which is 34.4% lower than in controls. These outcomes recommended that GSH is a noteworthy intracellular decreasing specialist, which is extremely touchy to oxidative pressure and has a few essential capacities (Abo-Shanap et. al., 2020).

Marked changes in the antioxidant pattern were also observed in thalassemia patients, the results in table (2) showed that there was a huge increment ($p < 0.001$) in the level of serum MDA in patients with beta thalassemia when contrasted with controls. The strongest predictors of elevated MDA were liver iron concentration. Our outcomes propose that the estimation of peroxidation items, mustached with assessment of cancer prevention agents, might be a basic proportion of iron harmfulness in thalassemia, in addition to the conventional indices of iron status. In thalassemia there is overabundance generation of receptive oxygen intermediates, these occasions prompt oxidative pressure. This oxidative pressure and a conceivable considerable quickened apoptosis may add to abbreviated life expectancy of erythrocytes. MDA a result of lipid peroxidation is produced in abundance sums in supporting the way that huge measure of layer bound iron is available in thalassemic erythrocytes. (Choudhary et. al., 2017).

The results in table (2) showed a significant increase in uric acid concentration. Uric acid formation occurs only in tissues that contain the enzyme xanthine oxidase. The increased body burden of uric acid is a result of increased *de novo* purine synthesis, increased purine nucleotide degradation diminished renal excretion of urate, or a combination of these defects. The increased of uric acid is due to that the uric acid is one of the antioxidant which present in plasma in high concentration. The leakage of substances from damaged cells into the plasma may have increased plasma antioxidants concentrations making changes difficult to detect (Kadiiska et. al., 2015).

A significant increase in serum iron was observed in beta thalassemia major when compared with controls as shown in table (2). Absence of beta globin chains lead to accumulation of unpaired alpha globin chains. Excess presence of the alpha globin chains is a primary reason for the cellular oxidative damage and also iron overload. As a result of high serum iron in beta thalassemia, there is an enhanced generation of reactive oxygen species ROS (Motta et. al., 2020).

Also, there was a significant increase in serum ferritin concentration in thalassemia patients when compared with control group as shown in table (2). Blood transfusion burden is an important measure of total body iron balance. Ferritin is a relatively inexpensive and widely-available measure, useful in monitoring chelation therapy. Liver iron concentration reflects total body iron stores, but incompletely stratifies the risks of iron overload complications (Khoshfetrat et. al., 2014). Ferritin is the iron storage protein serves to store iron in a non-toxic form, to deposit it in a safe form, and to transport it to areas where it is required. A significantly high level of ferritin is found in patients with iron overload and this may help differentiate thalassemia patients from those with iron deficiency, both of which will have a low red blood cell count (Sobhani et al., 2019).

In this study, the results in table (3) showed that there is a significant increase in vitamin C in serum of patients with thalassemia compared with the control group. The increased amount of vitamin C might be to the accumulation of iron in tissues could increase oxidative stress. Until now, some studies have been shown that ascorbic acid acts as an antioxidant in the presence of high level of iron and traps free radicals, and prevents the diffusion of these components to membrane of red blood cells and low density lipoprotein particles (Mohammad et. al., 2014).

Table 3. The Vitamins C and E concentration in serum of thalassemia patients and control group.

	Mean ± SD	
Parameters	Control n= 25	Patients n= 43
Vit C (µmole/L)	27.65 ± 0.87	30.34 ± 1.08***
Vit E (µmole/L)	17.83 ± 0.78	15.68 ± 4. 65***

*** Significant difference between controls at ($P < 0.001$)

Highly significant depletion ($p<0.001$) in serum vitamin E was observed in present study as shown in table (3). Vitamin E plays a key role in protecting cells against oxidative damage. The antioxidant role of Vitamin E is attributed to its ability in quenching highly reactive lipid peroxide intermediate by donating hydrogen and this prevents extraction of hydrogen. This assists in restricting self-perpetuated lipid peroxidation chain reaction (Sandro et. al., 2020).

Table 4. The Na, K and Cl concentration in serum of thalassemia patients and control group.

	Mean ± SD	
Parameters	Control n= 25	Patients n= 43
Na mmol/dl	136.45 ± 12.93	144.25 ± 15.93*
K mmol /dl	4.07 ± 0.47	6.01 ± 0.92*
Cl mmol/dl	95.9 ± 18.07	98.44 ± 19.12 (NS)

* Significant difference between controls at ($P < 0.05$)

There is a significant increase in the mean values of Na and K for patients, more than control. The mean value of Cl concentration in patients were non-significantly raised as compared to control as shown in table (4). The Na concentration in thalassemic patients increased may be due to reduced pump activity (Sirirat et. al., 2019). Impairment of anion and cation transport in thalassemia is very obvious. Thalassemia RBCs particularly from splenectomized patients' loss K because of an increase in selective permeability of the membrane to K, which results in shrinkage of RBCs and increased cellular rigidity. These results may help to understand the altered electrolyte homeostasis in thalassemia but there is still need of many future studies to clarify their mechanism of generation and pathological significance the K-loss in β-thalassemia by increasing the activity of K-Cl cotransport (Bayejid et. al., 2015).

Unusual layer work assumes a significant part in the modification of film cation transport as saw in thalassemia RBCs. Changes in the levels of serum sodium and potassium mirrors the inadequate film transport of the cations in the red cell layer of thalassemia. These outcomes give an affirmation that strange cation homeostasis may add to the pathogenesis of thalassemia (Pinto et. al., 2019).

Conclusion

We can conclude that defective membrane transport is responsible for observed changes of lipid peroxidation and some antioxidants. These results may help to understand the altered electrolyte homeostasis in thalassemia but there is still need of many future studies to clarify their mechanism of generation and pathological significance.

Scientific Ethics Declaration

The authors declare that the scientific ethical and legal responsibility of this article published in EPSTEM journal belongs to the authors.

References

Al- Janabi, G. , Al-Fahham, A. & Mohammed, R. (2021). Pathophysiology of sickle cell anemia: review article. *Indian Journal of Forensic Medicine and Toxicology, 15*(2), 2037-2043.

Piga, A., Perrotta, S., Gamberini, M. R., Voskaridou, E., Melpignano, A., Filosa, A., ... & Attie, K. M. (2019). Luspatercept improves hemoglobin levels and blood transfusion requirements in a study of patients with β-thalassemia. *Blood, The Journal of the American Society of Hematology*, *133*(12), 1279-1289.

Annino, J. S. & Giese, R. W. (1976). *Clinical the chemistry: principles and procedures* (4th ed.). Little Brown and Co.

Abo-Shanab, A. M., Kholoussi, N., Habib, D., Helwa, I. A., Hussin, G., Omar, N., ... & Fahmy, A. (2020). Use of echocardiography and glutathione S-transferase to detect heart complications in β-thalassemic patients. *Egyptian Pharmaceutical Journal*, *19*(3), 244.

Kingchaiyaphum, B., Sanchaisuriya, K., Fucharoen, G., Chaibunruang, A., Hess, S. Y., Hinnouho, G. M., ... & Fucharoen, S. (2020). Hemoglobins F, A2, and E levels in Laotian children aged 6- 23 months with Hb E disorders: Effect of age, sex, and thalassemia types. *International Journal of Laboratory Hematology*, *42*(3), 277-283.

Rund, D. (2016). Thalassemia 2016: modern medicine battles an ancient disease. *American Journal of Hematology*, *91*(1), 15-21.

Anselmo, F. C., Ferreira, N. S., Mota, A. J. D., Gonçalves, M. D. S., Albuquerque, S. R. L., Fraiji, N. A., ... & Moura Neto, J. P. D. (2020). Deletional alpha-thalassemia alleles in amazon blood donors. *Advances in Hematology*, *2020*, 1-6. https://doi.org/10.1155/2020/4170259.

Hinton, P. R. (2004). *Statistical explained* (2nd Edition). Rontledge.

Motta, I., Bou-Fakhredin, R., Taher, A. T., & Cappellini, M. D. (2020). Beta thalassemia: new therapeutic options beyond transfusion and iron chelation. *Drugs*, *80*(11), 1053-1063.

Kadiiska, M. B., Peddada, S., Herbert, R. A., Basu, S., Hensley, K., Jones, D. P., ... & Mason, R. P. (2015). Biomarkers of oxidative stress study VI. Endogenous plasma antioxidants fail as useful biomarkers of endotoxin-induced oxidative stress. *Free Radical Biology and Medicine*, *81*, 100-106.

Srinoun, K., Sathirapongsasuti, N., Paiboonsukwong, K., Sretrirutchai, S., Wongchanchailert, M., & Fucharoen, S. (2019). miR-144 regulates oxidative stress tolerance of thalassemic erythroid cell via targeting NRF2. *Annals of hematology*, *98*(9), 2045-2052.

Sirirat, K., Sriwantana, T., Kaewchuchuen, J., Paiboonsukwong, K., Fucharoen, S., Ritthidej, G., ... & Sibmooh, N. (2019). Pharmacokinetics and pharmacodynamics of single dose of inhaled nebulized sodium nitrite in healthy and hemoglobin E/β-thalassemia subjects. *Nitric Oxide*, *93*, 6-14.

Choudhary, M., Vyas, R. K., & Lahoti, A. (2017). Correlation of oxidative stress with serum antioxidant enzymes level in thalassemia in a tertiary level hospital of western Rajasthan. *International Journal of Biotechnology and Biochemistry*, *13*(2), 155-65.

Khoshfetrat, M. R., Mortazavi, S., Neyestani, T., Mahmoodi, M. R., Zerafati-Shoae, N., & Mohammadi-Nasrabadi, F. (2014). Iron and vitamin C Co-Supplementation increased serum vitamin C without adverse effect on zinc level in iron deficient female youth. *International Journal of Preventive Medicine*, *5*(8), 1037.

Hashim, N. A., Abdullah, Y. J., & Ibadi, H. A. (2020). Evolution of some biochemical and hematological parameters of thalassemia patients in Maysan Governorate, Iraq. *Annals of Tropical Medicine and Public Health*, *23*, 231-238.

Psatha, N., Reik, A., Phelps, S., Zhou, Y., Dalas, D., Yannaki, E., ... & Papayannopoulou, T. (2018). Disruption of the BCL11A erythroid enhancer reactivates fetal hemoglobin in erythroid cells of patients with β-thalassemia major. *Molecular Therapy-Methods & Clinical Development*, *10*, 313-326.

Sandro, A., Naidu, M., Philipp, S., Timm, S., Michaela, A., Axel, W., Katarzyna, O., Lothar, H., Manuela, S., Camilla, L., Cornelia, K., Josef, M., Dirk, J., Frauke, N., Birgit, R., Martin, H., Christian, B., Katja, M., Marcus, C., Tomas, G., Manfred, K., Martina, U. & Georg, W. (2020). Glutathione peroxidase 4 and vitamin E control reticulocyte maturation, stress erythropoiesis and iron homeostasis. *Haematologica*,*105*(4), 937–950.

Sedlak, J. & Lindsay, R. (1968). Estimation of total, protein-bound, and nonprotein sulfhydryl groups in tissue with Ellman's reagent. *Analytical biochemistry*, *25*, 192-205. https://doi.org/10.1016/0003-2697(68)90092-4.

Sobhani, S., Rahmani, F., Rahmani, M., Askari, M., & Kompani, F. (2019). Serum ferritin levels and irregular use of iron chelators predict liver iron load in patients with major beta thalassemia: a cross-sectional study. *Croatian Medical Journal*, *60*(5), 405-413. https://doi.org/10,3325/cmj.2019.60.405

Omaye, S.T., Turnbull, J.D., & Sauberlich, H.E. (1979). Selected methods for the determination of ascorbic acid in animal cells, tissues, and fluids. *Methods in enzymology, 62*, 3-11.

Tietz, N.W. (1999). *Text Book of Clinical Chemistry* (3rd Ed.). Burtis C.A. and Ashwood.

Pinto, V. M., Poggi, M., Russo, R., Giusti, A., & Forni, G. L. (2019). Management of the aging beta-thalassemia transfusion-dependent population–The Italian experience. *Blood reviews*, *38*, 100594.

Varley, H. (1967). Ramasays Dipyridyl method for total ironbinding capacity. In *Practical Clinical Biochemistry*, (pp. 475).

Varley, H., Gowenlock, A. & Bell, M., (1979). *Practical clinical biochemistry: hormones, vitamins, drugs and poisons* (5th ed.). Williams Heinemann Medical Books Ltd.

Al-Mosawy, W. F. (2017). The beta-thalassemia. *Scientific Journal of Medical Research, 1*(1),24-30.

Wierusz-Wysocka, B., Wysocki, H., Byks, H., Zozulińska, D., Wykrętowicz, A., & Kaźmierczak, M. (1995). Metabolic control quality and free radical activity in diabetic patients. *Diabetes Research and Clinical Practice*, *27*(3), 193-197.

Chen, Y., Cai, N., Lai, Y., Xu, W., Li, J., Huang, L., ... & Chen, J. (2020). Thalidomide for the Treatment of Thrombocytopenia and Hypersplenism in Patients With Cirrhosis or Thalassemia. *Frontiers in Pharmacology*, *11*, 1137. https://doi.org/10.3389/fphar.2020.01137

Author Information

Saba AL-ABACHI
University of Mosul
Department of Chemistry - College of Science - Iraq
Contact e-mail:*saba-alabachi@uomosul.edu.iq*

Sameer AL-GORANY
Baʼaquba Medical institute -Middle Technical University – Diyala -Iraq

Abdulrazzaq ALTUWAIJARI
Director of Diyala Haematology center
Diyala - Iraq

Jaafar GHAZY
Philadelphia University, Pharmacy College
Amman - Jordan.

To cite this article:

Al-Abachi, S., Al-Gorany, S., Altuwaijari, A. & Ghazy, J. (2021). Measurements the level of lipid peroxidation and some antioxidants in blood serum of Thalassemia's patients. *The Eurasia Proceedings of Science, Technology, Engineering & Mathematics (EPSTEM), 16*, 225-230.

The Eurasia Proceedings of Science, Technology, Engineering & Mathematics (EPSTEM)
ISSN: 2602-3199

The Eurasia Proceedings of Science, Technology, Engineering & Mathematics (EPSTEM), 2021

Volume 16, Pages 231-239

IConTES 2021: International Conference on Technology, Engineering and Science

Inhibition of the Growth of *Staphylococcus Aureus* by Using Some Antibiotics Produced from *Bacillus Subtilis*

Yusra Yahya AGHA
University of Mosul

Abstract: *Bacillus subtilis* can produce many substances that are considered as a means of defense in addition to being tested and approved as antibiotics. The goal of this study was to see if *Bacillus subtilis* crude bacteriocin had any antibacterial effects on *Staphylococcus aureus* .The peptidic bacteriocin is considered of importance in the industrial and medical fields as an anticancer.We got our bacteria from the Bacterial Bank at the College of Science and the Department of Biology. Identification of the isolates was confirmed by microscopically and biochemical tests which include catalase, oxidase, IMViC, blood hemolysis, starch hydrolysis for *Bacillus*, and growth on Mannitol Salt Agar (MSA), Voges-Jenson agar(V.J), and Coagulase test for *Staphylococcus*. Based on the capacity of bacteriocin to diffuse in agar, the reverse technique, which eliminated the contact between the producers and sensitive strains, was used to detect bacteriocin antibacterial action. Results demonstrate the antibacterial effect of Bacillus *subtilis* bacteriocin by the inhibition of *Staphylococcus aureus* as compared to other indicator isolates.

Keywords: *Bacillus.subtilis*, *Staphylococcus.aureus*, Bacteriocin

Introduction

We had the good fortune of being alive during the Golden Age of Antibiotics, which lasted from the mid-1940s until recently. Antibiotics have been used to treat all major bacterial and fungal infections during this period. Surgery has improved dramatically during this time period, which has transformed medicine and saved countless lives. It's a shame that the golden era of antibiotics is coming to an end because pathogens are becoming increasingly resistant to them. Penicillin resistance was immediately noticed and has only gotten worse in the last half-century. Antibiotic resistance is a particular concern when dealing with MRSA. (Methicillin-Resistant *S. aureus*), which is endemic in most hospitals Worldwide (Boyce, et. al., 2005). It's been known since the 1880s when *S. aureus* was first discovered that it's a potentially pathogenic Gram-positive bacterium, capable of inflicting serious infections like postoperative wounds and minor skin infections. Currently, it's the second most common cause of bloodstream and lower respiratory tract infections. It took two years after the introduction of penicillin for medical use before penicillin-resistant *S. aureus* began to appear in hospitals. Penicillin-resistant strains of *Staphylococcus aureus* appeared in the general population only a few years later. (Croft, et.al., 2007; Deurenberg, 2008).

Penicillin-resistant strains of *Staphylococcus aureus* have been extensively studied in Iraq. To put this into context, (Kareem, *et al*., 2015) reported that Medical City in Baghdad provided 74 isolates. MRSA was found in 61 of the isolates. There was also a study by (Al-Dahbi,2013) that found 106 *S. aureus* isolates were found to be completely resistant to PenicillinG (100 percent) and highly resistant to Cefoxitin in nasal swabs from health care workers and patients at Al-Kadhamia Teaching Hospital in Baghdad and Al-Numan Hospital. (Alternative to Methicillin 94.3%). Antibiotic resistance, on the other hand, will remain a major issue in future medicine. The simplest solution to this problem is to create new antibiotics that target pathogens that haven't yet developed

resistance to existing ones (Mulvey, 2009). After demonstrating significant activity against *S. aureus*, Bacteriocin may be a potential antibiotic for this pathogen (Mulvey, 2009). Antimicrobial peptides, also known as bacteriocins, are one of the most well-studied microbial defense systems, and they can be used to explain microorganism evolution and ecology. Bacteriocins may also serve as a natural alternative to antibiotics in the treatment of bacterial infections and as natural antimicrobials in food preservation (Cleveland, et. al., 2001).

They can inhibit the growth of bacteria of the same species (narrow spectrum) or other genera (broad spectrum), and their range of activity often depends on the mechanisms of action of each Bacteriocin. Bacteriocins are typical alternatives to antibiotics. Their short chains of about 20-60 amino acid residues are usually heat-stable, but longer chains can also be found (Snyder, 2014). As shown in the BACTIBASE dataset, the majority of bacteriocins are derived from Gram-positive bacteria. Because of their broad spectrum antibiofilm activity, Bacteriocins are generally considered to be safe and stable. Bacteriocins from Gram-negative bacteria have been described, but there are none from the Archaea domain. Gram-negative bacteria are rare (Hammami, et. al., 2013).

General Mode of Action

Bacteriocin act as a target by forming membrane pores that disturb the energy potential of sensitive cells. Different bacteria produce different bacteriocins which have their mode of action.

The mode of action of nisin is best studied. These bacteriocins associate electrostatically with phospholipids, which causes the interaction of bacteriocins' hydrophobic residues with the cytoplasmic membrane of target cell (Nicolle & Prunet.,1964). Electrostatic interaction is caused by Lysine (cationic amino acid). Ionic channels are created as a result of the hydrophobic nisin part interacting with the membrane. High transmembrane potentials, anionic lipids, and the absence of cationic lipids favor this theory (O′Sullivan. et. al.,2002). Because divalent cations neutralize the phospholipids' negative charges, the membrane's fluidity is reduced. Pores produced by nisin create passive efflux of K^+ and Mg^{2+}, amino acids, Cell death occurs as a result of ATP and proton-motive-force dissipation. YGNGV, found in the N-terminal region of Class I bacteriocins, makes them highly specific against Listeria monocytogenes (Schwable. et. al.,2007). The current mechanism to explain mode of action antibacterial binding to the target membrane is electrostatic and is caused by a putative membrane-bound receptor molecule, although the need for this particular receptor is still debatable. The YGNGV anti-listerial motif found in these peptides is recognized by an unknown receptor (Cintas, et. al., 1995).

Pathogenic and spoilage microorganisms can be controlled biologically by using antibacterial peptide-producing *Bacillus* species, which is critical for food preservation. Lactic acid bacteria (LAB) found in food and other sources have been the subject of extensive research. Recently, For inhibitory substances, the Bacillus species have also attracted interest because of the large number of antibiotics in the form of peptides they produce, which represent a wide range of chemical structures. Additionally, similar to LAB, some *Bacillus* spp., such as *B. subtilis, B. licheniformis,* and *B. coagulans* are'GRAS' in the food industry and Agriculture. Endospore-forming Gram-positive bacteria make up the family Bacillaceae, which has rod-shaped members. There are two major types of spore-forming bacteria in this family: Clostridium is a genus of anaerobic, spore-forming bacteria.

Bacillus spore-forming bacteria can be aerobic or facultative anaerobic. Bacillus spore bearers are common names for members of the genus Bacillus. They are all around us, in the soil, in the air, and the water. As well as being common pathogens, these bacteria are frequently found to be contaminants in bacterial culture media. It is well-known that *Bacillus* spp. can be used safely in the food industry (Abriouel, et. al., 2011). The US FDA has designated some of the most important Bacillus species, like *B. subtilis* and *B. lichenifornis*, as "generally recognized as safe for sale. (Chopra, et. al., 2015).

Gram-positive Bacillus is widely distributed and has a rod-shaped morphology, making it an endospore-forming bacterium [O'Sullivan,2002]. The bacteria Bacillus can be found in soil and clays as well as rocks, dust, and aquatic environments as well as vegetation, food, and the gastrointestinal tracts of various insects and animals due to endospore formation in adverse conditions. (Nicholson. 2002).

Some Bacillus species have been found to be rich sources of bacteriocins, lipopeptides, and other inhibitory substances that are similar to those found in Bacillus spp. bacteria produce and secrete antimicrobial peptides known as bacteriocins to protect themselves from the growth of other bacterial species that are closely related (Cotter, et. al., 2013). Most bacteriocins work by blocking pore formation on the cell surface or interfering with

cell wall synthesis to slow bacteria's growth. As reported by the (International Nosocomial Infection Control Consortium in 2010), both *Staphylococcus spp*. gram-positive bacteria and *Escherichia coli* gram-negative bacteria can develop resistance to antibiotics (Hashemizadeh , 2011).

A common source of hospital-acquired infection is Gram-positive bacteria. Nosocomial bacteremia has been linked to the bacteria *Staphylococcus epidermidis*. Because of drug resistance, allergic reactions, and other side effects, researchers are now looking into new drugs to combat nosocomial infections in hospitals (Agarwal, et. al., 2016). A class of molecules known as antimicrobial peptides has shown promise as novel therapeutics due to their potency and broad-spectrum. However, a possible role as an alternative antimicrobial agent for infection is being explored for bacterial bacteriocins, which are used in the food industry (Cotter, 2013).

Bacilli are also of major importance in the fermentation industry since they elaborate on a variety of useful enzymes and antibiotics. As a consequence, in this regard, industrial-scale bacilli cultivation techniques have come a long way. Commercial exploitation is particularly interested in the ability of some bacilli to excrete large amounts of specific proteins into extracellular space. It's unfortunate that so little is known about the molecular basis of bacterial protein excretion and whether or not excretion and synthesis are coupled. This, as well as the intriguing issues surrounding growth stage-related regulation, will most likely be the subject of research shortly. To a certain extent, this optimism stems from the discovery of molecular cloning in *Bacillus subtilis* **(**David, 1982).

Bacteriocin production has been detected using a variety of methods. Gratia and Fredricq are the main sources of inspiration for all of the standard techniques. (Agarwal. *et al*.,2016). Bacteriocins can diffuse into solid or semisolid culture media, which are then inoculated with a suitable indicator strain. These techniques take advantage of this fact. Before moving on to the next step, the bacteriocin-producing strain must be removed or killed with chloroform vapors to ensure the agar surface is sterile for inoculating the indicator strain. If the bacteria are still alive and growing on the agar surface, the inhibition areas of the indicator strain may be completely or partially hidden. Plastic Petri dishes cannot be used after the producer strain of bacteria has been killed with chloroform because the vapors attack the plastic. Residual chloroform in the culture medium insufficiently ventilated after exposure to vapors can give erroneous results. (Al-Danbi. *et al*.,2013).

Nicolle and Prunet's approach are described here. not require killing or removing the producer strain, inoculated with a straight wire and incubated for 2 days under the surface of a truncated Agar Slant. The indicator strain is inoculated onto the slant's surface on the third day. the presence or absence of growth of the indicator strain after incubation can be used to record the results. Since each producer or indicator strain requires a separate test tube, this method is impractical for screening. It's based on the fact that bacteriocin diffusion (like that of any other antibiotic) is tridimensional, which is how the new method works. As a result, the substance can be identified on the agar's reverse side. This site will be used as the indicator strain's culture surface. Here's how to do it: Using the standard procedure, the producer strain is inoculated onto nutrient agar's surface (spot inoculation, single colonies, or strip). A sterile spatula is used to remove the agar from the Petri dish's edges after it has been properly incubated. After that, the plate is inverted and the petri dish is thumped hard on the bench to release the agar disc into the top. A new lid places the sterile surface (previously located at bottom of the dish) higher than before, making it possible to inoculate with the indicator strain. Zones of inhibition can clearly be seen after incubation (Nicolle, 1964).

Material and Method

Reagents:

1. Tetramethyl – p- phenylenediamine (DMPD)
2. 3% H_2O_2
3. Plasma

Stains:

1. Gram Stain
2. Malachite green

Media:

1. Nutrient broth
2. Nutrient Agar
3. blood Agar
4. Mannitol salt agar
5. Christensen's urea Agar
6. Voges – Jenson (VJ)

1. Bacterial Isolates:
Two Bacterial Isolates were obtained from the Bacterial bank/college of science / Dept. of Biology. One Isolates of *Bacillus subtilis* and staphylococcus aureus.
2. Identification of bacterial isolates *Bacillus subtilis:* by using the following test:
Gram and spore stain, catalase, oxidase, urease, starch hydrolysis.
3. Identification of *Staphylococcus aureus:* by using the following test
Gram stain, catalase, oxidase, growth on Mannitol salt agar, VJ, and blood agar and Coaulase test.
4. detection of Bacteriocin production:
In this study, the detection of Bacteriocin production was carried out by applying " Reverse agar technic " suggest by (Schwable, 2007).

Procedure

1. Inoculate the petri dish (blood agar) with the culture of (producer strain) *Bacillus subtilis* (a straight-line streak)
2. Inoculate the plate at the optimal temperature for the growth of the Bactria (at 37Cº for 24 hours)
3. A sterile spatula was used to remove the agar from the plate and place it on the cover.
4. Streak a pure culture of the indicator strain (*s. aureus* and *E. coli*) with a line perpendicular to the producer strain on the other side of the agar
5. Inoculate for 24 hours and observe for inhibition of growth on the intersect of cultures (Koneman, 2006)

Results

Identification of Bacteria:

Results of the Identification test of *B. subtilis* and *S. aureus* are shown in tables (1) and (2).

Table 1. Biochemical test of *Bacillus subtilis*

Name of the test	Results
Gram staining	Positive
Catalase	Positive
Oxidase	Variable
Urease	Negative
Spore	Positive
Starch hydrolysis	Positive

Table 2. Biochemical test of *Staphylococcus aureus*

Name of the test	Results
Gram staining	Positive
Catalase	Positive
Oxidase	Negative
Urease	Positive
Coagulase	Positive
Mannitol	Yellow colonies (sugar fermentation)
VJ agar	Black colonies

In addition to figures (10) demonstrate the positive results optioned for each bacteria.

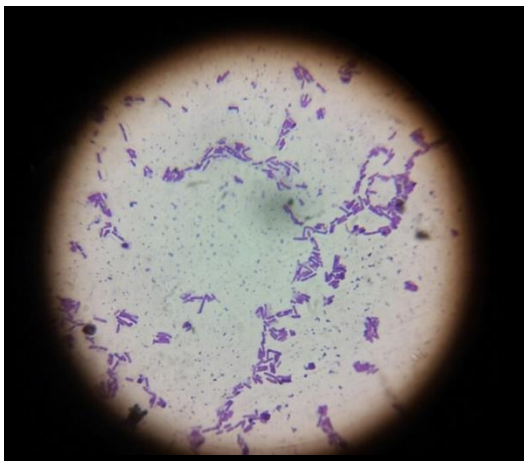

Figure 1. Gram stain of *Bacillus subtilis*

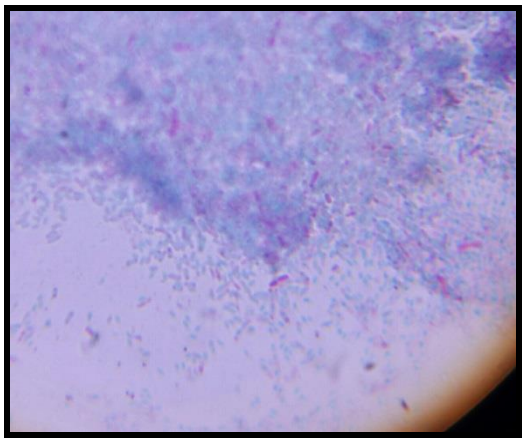

Figure 2. Spore stain of Bacillus subtilis

Figure 3. Catalase test of Bacillus subtilis

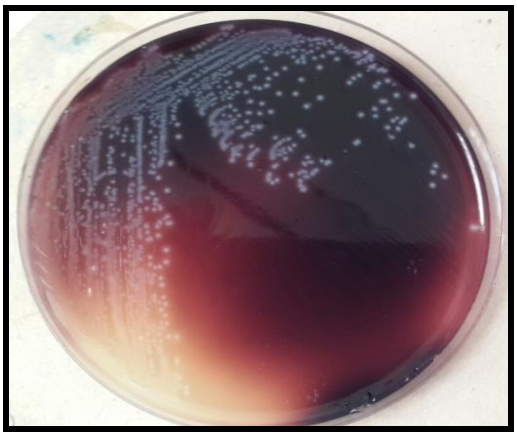

Figure 4. Starch hydrolysis of Bacillus subtilis

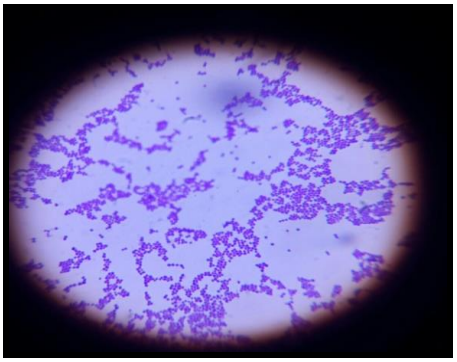

Figure 5. Gram stain of Staphylococcus aureus

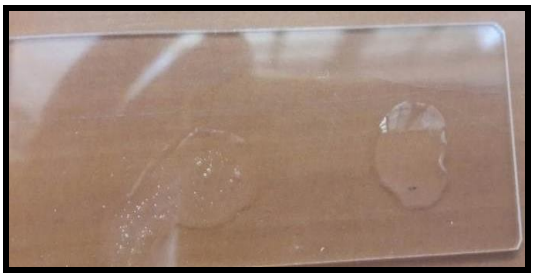

Figure 6. Catalase test of Staphylococcus aureus

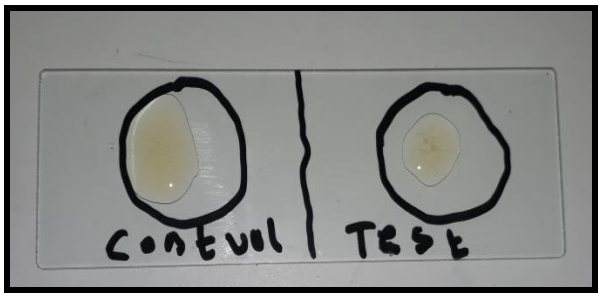

Figure 7. Coagulase test of Staphylococcus aureus

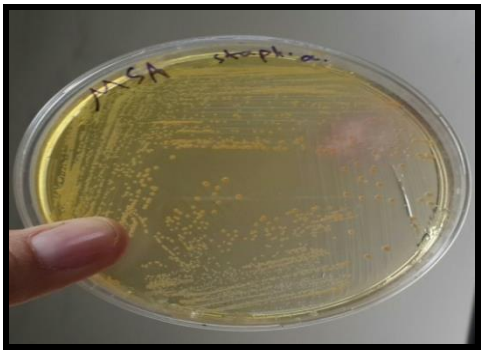

Figure 8. Staphylococcus aureus on Manntiol salt Agar

Detection of Bacteriocin Production:

It was shown that *B. subtilis* is a potent Bacteriocin producer that inhibited *S. aureus* but did not affect the indication strain of *E. Coli*.

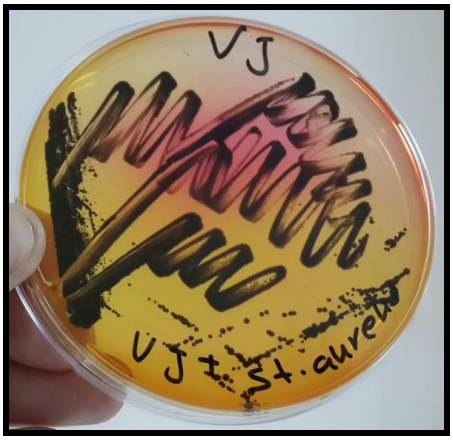

Figure 9. Staphylococcus aureus on V.J.Agar

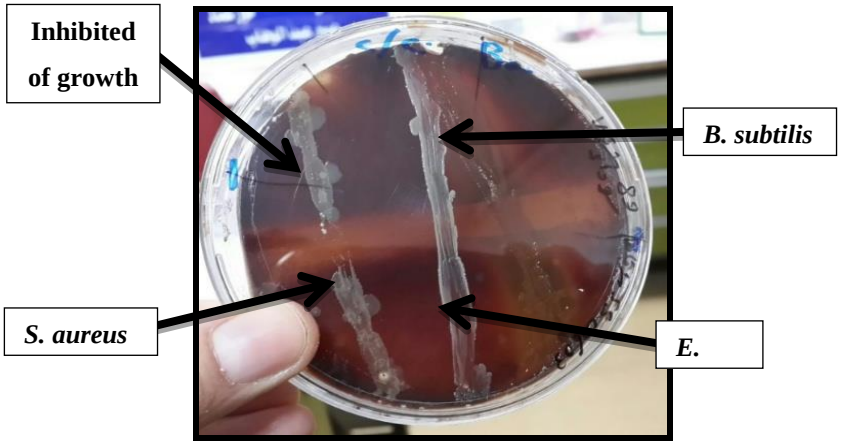

Figure 10. Reverser Agar technic in blood agar

Conclusion

The "reverser Agar Technic" prevents phage particles from reaching the indicator bacteria because there is no direct contact between the producer and the strains being tested. As a result, no inhibition zone due to phages can form, as is often the case with other methods where it is difficult to determine whether a Zone of confluent lysis is caused by phages or bacteriocins.

Resistance to antibiotics is on the rise, posing a therapeutic challenge to the medical community. New approaches and treatment options for infections are therefore becoming increasingly important. Some pathogens would benefit from Bacteriocin instead of the currently prescribed antibiotics. Antibiotic-resistant bacteria like Staphylococcus spp. showed pediculate's resistance to the most widely used antibiotics. Most Bacteriocins have a narrow therapeutic range.

An activator of microorganisms, researchers, on the other hand, believe that bacteriocins' limited antimicrobial activity could be an asset. One of the drawbacks of using throat spectrum antibiotics is that they kill nearly all bacterial species, even those that aren't particularly resistant to ho the one. Because of this, pathogens and commensal bacteria can become resistant to broad-spectrum antibiotics. Due to the relatively narrow spectrum of activity of Bacteriocins, they can be viewed as a specially designed drug that specifically targets a particular pathogen.

Recommendations

Based on our results, the study recommend that Bacteriocic may one day serve as a novel therapeutic agent against pathogens in place of currently used antibiotics.

Acknowledgements or Notes

The authors would like to thank the Iraqi Ministry of Higher Education and the Biology department, University of Mosul for supporting this research .

Scientific Ethics Declaration

The author declares that the scientific ethical and legal responsibility of this article published in EPSTEM journal belongs to the author.

References

Abriouel, H., Franz, C. M., Omar, N. B., & Gálvez, A. (2011). Diversity and applications of Bacillus bacteriocins. *FEMS Microbiology Reviews*, *35*(1), 201-232.

Agarwal, S., Sharma, G., Dang, S., Gupta, S., & Gabrani, R. (2016). Antimicrobial peptides as anti-infectives against Staphylococcus epidermidis. *Medical Principles and Practice*, *25*(4), 301-308.

Al-Dahbi, A. M., & Al-Mathkhury, H. J. (2013). Distribution of methicillin resistant Staphylococcus aureus in Iraqi patients and healthcare workers. *Iraqi Journal of Science*, *54*(2), 293-300.

Bierbaum, G., & Sahl, H. G. (2009). Lantibiotics: mode of action, biosynthesis and bioengineering. *Current Pharmaceutical Biotechnology*, *10*(1), 2-18.

Boyce, J. M., Cookson, B., Christiansen, K., Hori, S., VuopioVarkila, J., Kocagaz, S. Oztop, A. Y., Vandenbroucke-Grauls, C.M.J .E., Harbarth, S., and Pittet, D. (2005). Meticillin-resistant S. aureus. *The Lan. Infect. Disea*, *5*(10), 653-663

Chopra, L., Singh, G., Jena, K. K., & Sahoo, D. K. (2015). Sonorensin: a new bacteriocin with potential of an anti-biofilm agent and a food biopreservative. *Scientific Reports*, *5*(1), 1-13.

Cintas, L. M., Rodriguez, J. M., Fernandez, M. F., Sletten, K., Nes, I. F., Hernandez, P. E., & Holo, H. (1995). Isolation and characterization of pediocin L50, a new bacteriocin from Pediococcus acidilactici with a broad inhibitory spectrum. *Applied and Environmental Microbiology*, *61*(7), 2643-2648.

Cleveland, J., Montville, T. J., Nes, I. F., & Chikindas, M. L. (2001). Bacteriocins: safe, natural antimicrobials for food preservation. *International Journal of Food Microbiology*, *71*(1), 1-20.

Cotter, P. D., Hill, C., & Ross, R. P. (2005). Bacteriocins: developing innate immunity for food. *Nat. R . Microbiol.*, *3*(10), 777-788.

Cotter, P. D., Ross, R. P., & Hill, C. (2013). Bacteriocins—a viable alternative to antibiotics?. *Nature Reviews Microbiology*, *11*(2), 95-105.

Croft, A. C., D'Antoni, A. V., & Terzulli, S. L. (2007). Update on the antibacterial resistance crisis. *Medical Science Monitor*, *13*(6), 103-118.

Dubnau, D. (1982). The *molecular biology, of the bacilli, volume i: bacillus subtilis.* The Public Health Research.

Deurenberg, R. H., & Stobberingh, E. E. (2008). The evolution of Staphylococcus aureus. *Infection, Genetics and Evolution*, *8*(6), 747-763.

Hammami, R., Fernandez, B., Lacroix, C., & Fliss, I. (2013). Anti-infective properties of bacteriocins: an update. *Cellular and Molecular Life Sciences*, *70*(16), 2947-2967.

Hashemizadeh, Z., Bazargani, A., & Davarpanah, M. A. (2011). Blood culture contamination in a neonatal intensive care unit in Shiraz, Southwest-Central Iran. *Medical Principles and Practice*, *20*(2), 133-136.

Kareem, S. M., Al-Jubori, S. S., & Ali, M. R. (2015). Prevalence of erm genes among methicillin resistant Staphylococcus aureus MRSA Iraqi isolates. *Int J Curr Microbiol Appl Sci*, *4*(5), 575-585.

Koneman, E. W., Allen, S. D., Janda, W. M., Schreckenberger, P. C., & Winn, W. C. (1997). Diagnostic microbiology. In *The nonfermentative gram-negative* bacilli (pp. 253-320). Lippincott-Raven Publishers.

Mulvey, M. R., & Simor, A. E. (2009). Antimicrobial resistance in hospitals: how concerned should we be?. *Cmaj*, *180*(4), 408-415.

Nicholson, W. L. (2002). Roles of Bacillus endospores in the environment. *Cellular and Molecular Life Sciences CMLS*, *59*(3), 410-416.

Nicolle, P., & Prunet, J. (1964). La propriete colicinogene dans lespece salmonella typhi. In *Annales De L Institut Pasteur*. Masson Editeur.

O'sullivan, L., Ross, R. P., & Hill, C. (2002). Potential of bacteriocin-producing lactic acid bacteria for improvements in food safety and quality. *Biochimie*, *84*(5-6), 593-604.

Schwalbe, R., Steele-Moore, L., & Goodwin, A. C. (Eds.). (2007). *Antimicrobial susceptibility testing protocols*. Crc Press.

Snyder, A. B., & Worobo, R. W. (2014). Chemical and genetic characterization of bacteriocins: antimicrobial peptides for food safety. *Journal of the Science of Food and Agriculture*, *94*(1), 28-44.

Author Information

Yusra Yahya AGHA
University of Mosul, Iraq
Mosul city, Iraq
Contact e-mail: yossbio56@uomosul.edu.iq

To cite this article:

Agha, Y.Y. (2021). Inhibition of the growth of *staphylococcus aureus* by using some antibiotics produced from *bacillus subtilis*. *The Eurasia Proceedings of Science, Technology, Engineering & Mathematics (EPSTEM), 16*, 231-239.

The Eurasia Proceedings of Science, Technology, Engineering & Mathematics (EPSTEM)
ISSN: 2602-3199

The Eurasia Proceedings of Science, Technology, Engineering & Mathematics (EPSTEM), 2021

Volume 16, Pages 240-247

IConTES 2021: International Conference on Technology, Engineering and Science

The New Designed Mechanical Systems and Protypes for Z-Scan and Nonlinear Measurements

Ferit ARTKIN
Kocaeli University

Abstract: In this study is explained a new mechanical design for z-scanning and nonlinear measurements. Three systems are designed for measurements. The last system has better constructions and design parameters than the other systems designed in 2005 and 2014. The last system has been manufactured from various shafts, roller bearings, mechanical holders, mechanical rails and carrier integrated in these systems and stainless steel mechanical double joint coupling for reducing the workload of the main system and the aluminium alloys used in the system are 6063 and 7075. The z-scan measurement technique is often used for measuring the strength of the magnitude of the nonlinear index n2 of an optical material. Essentially, a sample of the material under investigation is moved through the focus of a laser beam, and the beam radius (or the on-axis intensity) is measured at some point behind the focus as a function of the sample position. These quantities are affected by the self-focusing effect. Various materials in nonlinear optics (liquids, organic structures, semiconductors, thin films…) the nonlinear optical properties used for definning one of the methods the z-scanning techniques for new designed mechanical system is described. The obtained parameters within the measurement will be more accurate and reliable with new designed mechanical system. The system brought into the active mode upon the completion of its design is closed-loop mechanical checking system. It is a control mechanism capable of moving according to the desired display values. Being very important in the industrial and vocational applications, the number of cycles, the speed, direction control of the engine can be done in this system the design of which has been completed. The present academic study in intended to introduce the design and control mechanism of the system and its place in the vocational and technical applications.

Keywords: Mechanical design, Mechanical engineering, Engineering applications, Measurement techniques, protypes.

Introduction

In this study, servo control can be provided at the level of micro signals. It provides great convenience to users in stages such as instant access and intervention to many information, fault detection and commissioning. The system, whose design has been completed and activated, is a closed-loop electromechanical control system. It is a control mechanism that acts according to the desired indicator values. Which is very important in industrial and professional applications; The revolution number, speed and direction control of the servo motor can be done in this system whose design has been completed. In the content of this study; The design of the system, its control mechanism and its importance in professional and technical applications will be explained in detail.

This study is intended to bring together universal 20x20 mm stainless steel mechanical double joint coupling (coupling) used to lower the work load of servo motor, various shafts, mechanical rails and carrier, mini ball bearings, Siemens Simatic S71200, which is a new-generation PLC system, and Siemens AC 1FL6042, 0.4 kW servo motor compatible with this system as well as a variety of mechanical appurtenances; it is also intended to drive a new opto-mechanical system, to control the system with Siemens 6SL3210 Sinamics V-90 servo driver

and to integrate the whole system by using a compatible software with the help of a computer from a single control panel.

The main automation units of the newly designed system; Siemens 6SL3210-5FE10-8UA0 Sinamics V-90 servo motor driver is from Siemens Simatic S71200 CPU1212C PLC, Siemens Simotics S-1F6 series; 1FL6042-1AF61-0AA1 consists of 0.4 kW, servo motor AC (Artkin, 2016; Artkin, 2017).

Figure 1. System components, automation units used in the system; V-90 Servo Driver, S71200 PLC, S-1F6 1FL6042 0.4 Kw Servo Motor.

Z Scan and Non-linear Measurements

The z-scan measurement technique is often applied to size the Kerr nonlinearity's strength (i.e. the magnitude of the nonlinear index n_2) of an optical material. Essentially, a sample of the material under investigation is moved along the laser beam's focus, and the beam radius (or the on-axis intensity) is measured at some point by keeping behind of the focal area to show the function position of sample (Artkin, 2014).

These quantities are affected by the self-focusing effect. If the nonlinear index is positive, and the sample is placed behind the focus (as in Figure 2), self-focusing reduces the beam divergence and thus increases the detector signal. If the sample is put on the left-hand focal point's side, the focus shifts to the left, and the stronger divergence after the focus decreases the detector signal. From the measured dependence of the detector signal on the sample position, the nonlinear index' magnitude can be calculated (E. Van Stryland et. al., 1993).

The refractive index n of nonlinear materials depends on the intensity of light I:

$$n = n_0 + n_2 I \tag{1}$$

where n_2, the nonlinear refraction coefficient, is in proportion with the original part of third order nonlinear sensivity Re $\{\chi^{(3)}\}$. One of the effects of a Third order nonlinearity is so called self-refraction. For the laser beam propagating through a nonlinear material the density of energy in the beam cross-section is altering and the refractive index is changing too. Depending on the nonlinearity the change of refractive index Δn can be positive or negative (Sheik Bahae et. al., 1990; Geoffrey, 2011).

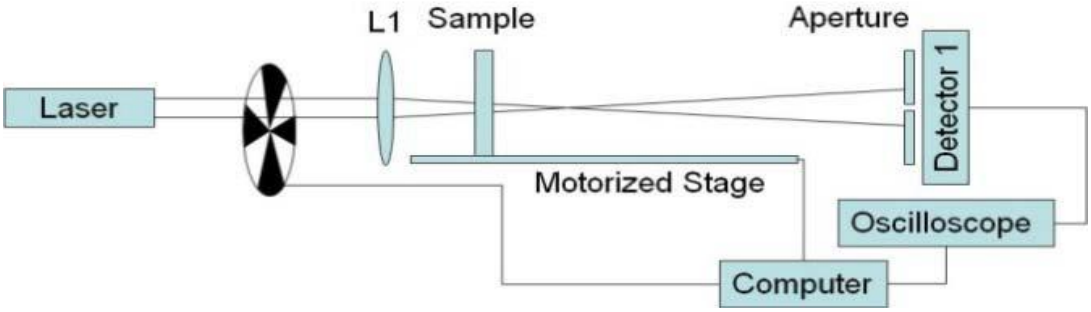

Figure 2. Setup for Z-scan measurements and experimental Z-scan setup units.

If $\Delta n > 0$ the plane wavefront becomes concave along direction of generation while the beam is concentrated on to the axis. This effect is referred to self-focusing if $\Delta n < 0$ the plane wavefront gets convex or the beam gets defocused. Because of diffraction effects a periodic focusing of beam propagating in a nonlinear medium is observed (Sheik-Bahae et.al.,1989). The path length of beam in the medium in which the beam is concentrated is referred to self-focusing length. The self-refraction effect sets basis of one of methods for measurement of cubic nonlinearity of materials -Z-scan method. The sample of thickness L scans the focused light beam alongside the direction of generation and the transmittance as the sample relative' a functional position to the focal plane is measured by a detector with an aperture of radius a in front of it (Artkin, 2014; Artkin, 2017) .

Linear Motion – Leadscrew / Ballscrew Drive

In evaluating a screw drive all of the following must be considered: Screw Inertia (*JS*): This can be determined using the inertia formula for a cylinder. Quite often, for a high pitch screw made of steel, the screw inertia is much larger than the reflected load inertia and the reflected load inertia can be ignored for initial calculations.

Friction Force (*FF*): This is the opposing force composed by the friction between the load and the load bearing surface. Do not confuse the coefficient of friction (μ) with the screw efficiency (*e*).

Nut Preload (*TP*): To eliminate backlash, the drive nut, through which the screw rotates, is sometimes preloaded. This preload composes an additional torque load on the motor.

When performing screw calculations do not confuse the screw pitch (*PS*) which has the units of rev/cm with the screw lead (*LS*) which has the units of cm/rev (See Figure 3).

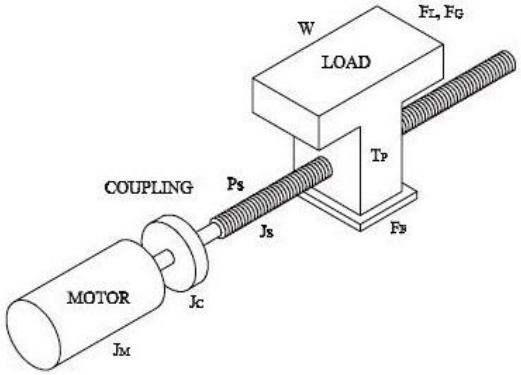

Figure 3. Linear motion; ballscrew drive and system components.

System Data: J_M = motor inertia (g cm s2), J_C = coupling inertia (g cm s2), W = load weight (g), T_P = preload torque (g cm), F_L = load force (g), F_G = gravity force = W (g), F_F = friction force = μW (g), J_S = screw inertia (g cm s^2), T_B = bearing torque (g cm), P_S = screw pitch (rev/cm), e = screw efficiency,μ = friction coefficient can be explained as.

Motion: Position: $\theta_M = (2\pi P_S)(S)$ (rad), Velocity: $\theta'_M = (2\pi P_S)(S^1)$(rad s^{-1}), Acc/Dec: $\theta''_M = (2\pi P_S)(S^{II})$ (rad s^{-2}) can be calculated as (Moritz Frederick G., 2014).

Prototypes

Mechanical parts of the last system; 2 x 800 mm long slide rail linear motion units support shaft diameter Ø2, 150×150 mm sized manufactured with aged aluminum in black color, 2 pcs trapezoidal shafts 800 mm long Chrome plated (0.2-0.33 μm), 1 main shaft 800 mm It is integrated with a 20x20 mm stainless steel mechanical bidirectional coupling coupling with 2 mm pitch in length. Al alloys (alloys) used in the system are 6063 and 7075. All mechanical parts are covered with black static paint because of this; high power laser measurements are color sensitive. The color factor directly affects the optical measurement values. For this reason; All mechanical parts are painted black for more accurate optical measurements. The entire weight of the mechanical system, including the servo motor, is 16.65 kg (Artkin, 2017).

Figure 4. The image of the system in the manufacturing lab. in Hereke V.S. after the assembly is completed.

Prototype 001-2005

The first system produced belongs to 2005. The opto-mechanical system, in which the measurements are taken, consists of the scanner, stepper motor and the mechanical parts that connect them, connected by shafts and bearings. Such assemblies include apparatuses of various types and sizes that are vital in the field of optics.

Opto-mechanical mechanism equipments can be manufactured by various companies, these mechanisms can be used according to their intended use; it is produced in different grades, it is quite expensive to buy directly; The experimental setup we used in the experiment is a completely original system; It is a system that is different from all systems with similar dimensions and connection mechanism. The technical drawings of the opto-mechanical system used in the experimental setup are shown below.

This system can also be used for academic studies, especially in the z-scan experimental setup, which is an experimental application of non-linear optics that enables measurements that require precise position change in optics. Precise position change for this system can be realized thanks to the designed mechanical design.

Motion Basics and Standards is first important parameter for mechanical systems. The function of a stage is to constrain motion to a desired direction. For a linear stage, the desired motion is along an ideal straight line. Prototypes 001-2005 system in total weighs 8,5 kg. Scanning distance of Prototype 001-2005 is 379 mm. and movement resolution of 001-2005 is 2.11×10^{-3} mm.

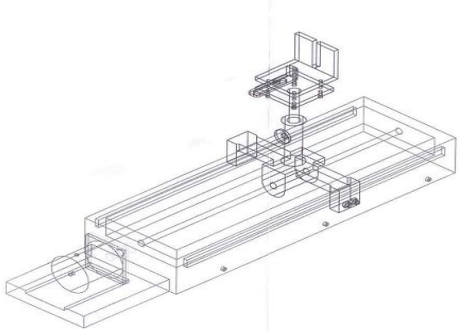

Figure 5. Three Dimensional Technical drawing for the opto-mechanical system designed in 2005, isometric view of the system

Figure 6. Prototype 001-2005 photos from different angles in optical measuremet lab in Gebze Technical University in 2005.

Prototype 002-2014

The system designed in 2014 is as follows. As seen in the technical design; The optical holder is designed for inspecting liquid and transparent materials. The scan distance for the material to be tested is a net 266 mm. The motion resolution for each signal of the system is 1.42×10^{-3} mm. This system includes roller bearings, shafts, aluminum alloy parts, plastic holders and rolling bearings.

As it was seen in technical design; it has been designed for examining optical holder, for liquid and transparent materials. Repeatability is the tolerance to which the controlled mechanical system can be repeatedly positioned to the same point in its travel. Repeatability is generally less than system resolution, but somewhat better than system accuracy. Linear systems are available with resolutions measured in microns (Artkin, 2014).

The 2D and 3D images of the opto-mechanical system, originally designed using solid Works for the 'Z-Scan test apparatus', are as follows. The cost of the system with the optical holder is around 300 Euros, market prices for similar systems vary between 1600 Euros and 3000 Euros.

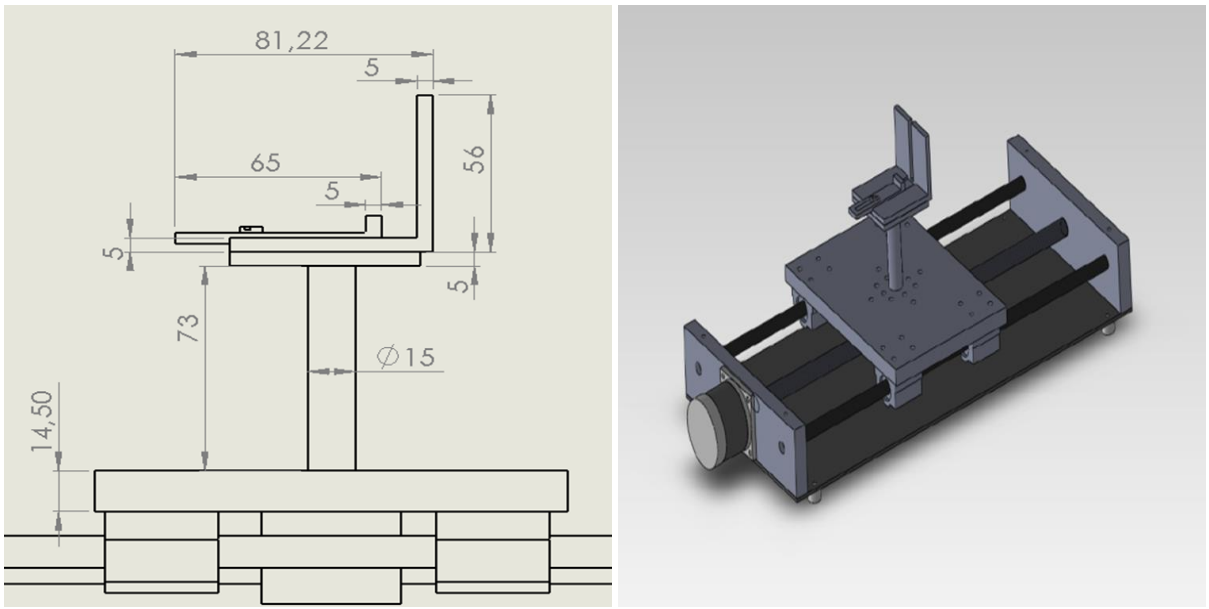

Figure 7. Solid Works isometric picture of opto-mechanical system with optical holder designed in 2014, on the right, detailed dimensioned technical drawing side view of optical holder specially designed for the system and some photos of the Opto-mechanical system designed in 2014.

Table 1. Comparison of some parameters for the designed prototypes of opto-mechanical systems.

Designed Opto-mechanical Systems for Z-Scanning	Weight (kg)	Scanning Distance (mm)	MovementResolution (mm)
The Last System	16.65	650	1.21×10^{-3}
Prototype 002-2014	4.2	266	1.42×10^{-3}
Prototypes 001-2005	8.5	379	2.11×10^{-3}

Result and Conclusion

This system, which includes servo motor and automation units, some of which mechanical parts are processed with CNC Lathe and Universal Milling located in Hereke Asim Kocabiyik Vocational School manufacturing laboratory, is a successful vocational technical application; At the same time, it can be used successfully to determine the optical properties of some materials with precise position control. The designed system is a unique system. High-end applications of this system can be used in Furniture, decoration benches, CNC Router benches (z), mini CNC router (y) workbench, Polyfram cutting machines and similar systems.

All kinds of operations in machinery and automation systems are provided with repetitive circular and linear movements. Whatever the procedure is, it must be in an axial guide and bedding so that the renewed movement can be deployed in a healthy and stable manner. In all kinds of loading and speed applications, there should be no wear in order to maintain the bedding precision and tolerance values. For this reason, the bearing elements must be made of hardened and ground special steel. The bearing surfaces are covered with a felt shield and protective bellows for lubrication purposes, providing long-lasting working quality. Linear motion systems should be designed in accordance with the desired working environments and the loads to be applied. Moment and drive alternatives required in axial movements should be created according to the units they are used in, bedding elements mounted on specially designed aluminum profile bodies are both practical and do not burden the system with unnecessary weights. The channel structures on the existing sections enable all kinds of additional parts to be connected to the process and facilitate adjustment. In linear motion systems, it is possible to control axial coordinate movements according to the desired process by integrating different motors. These systems can offer axial solutions within multi-option classes.

Scientific Ethics Declaration

The author declares that the scientific ethical and legal responsibility of this article published in EPSTEM journal belongs to the author.

References

Artkin, F., (2016) Integration of the new generation plc system and an opto-mechanical system with servo motor. *UMYOS 2016, 3*, 151-155.

Artkin, F., (2017), Yeni nesil plc'lerin meslek yüksekokulları için uygulamaları ve servo-oransal kontrol sistem tasarımı. *UMYOS 2017, 4*, 352-356.

Artkin, F., (2014). *Computer aided z-scan testing apparatus integrated into servo motor and plc for investigation of non-linear materials' permeability* [PhD Thesis]. Technical University of Sofia.

Geoffrey N. (2011). Introduction to nonlinear optics. Cambridge University Press.

Sheik-Bahae, M., Said, A. A., & Van Stryland, E. W. (1989). High-sensitivity, single-beam n 2 measurements. *Optics letters*, *14*(17), 955-957.

Sheik-Bahae, M., Said, A. A., Wei, T. H., Hagan, D. J., & Van Stryland, E. W. (1990). Sensitive measurement of optical nonlinearities using a single beam. *IEEE journal of quantum electronics*, *26*(4), 760-769.

Van Stryland, E. W., Sheik-Bahae, M., Said, A. A., & Hagan, D. J. (1993). Characterization of nonlinear optical absorption and refraction. *Progress in crystal growth and characterization of materials*, *27*(3), 279-311.

Moritz, F. G. (2013). *Electromechanical motion systems: Design and simulation*. John Wiley & Sons.

Author Information

Ferit ARTKIN
Kocaeli University Vocational School of Hereke Asım
Kocabiyik, Department of Machinery and Metal
Technologies, 41800, Korfez, Kocaeli, Turkey
Contact e-mail: *artkinf@kocaeli.edu.tr*

To cite this article:

Artkin, F. (2021). The new designed mechanical systems and protypes for Z-scan and nonlinear measurements. *The Eurasia Proceedings of Science, Technology, Engineering & Mathematics (EPSTEM), 16*, 240-247.